Annual Report
Jahresbericht

2023

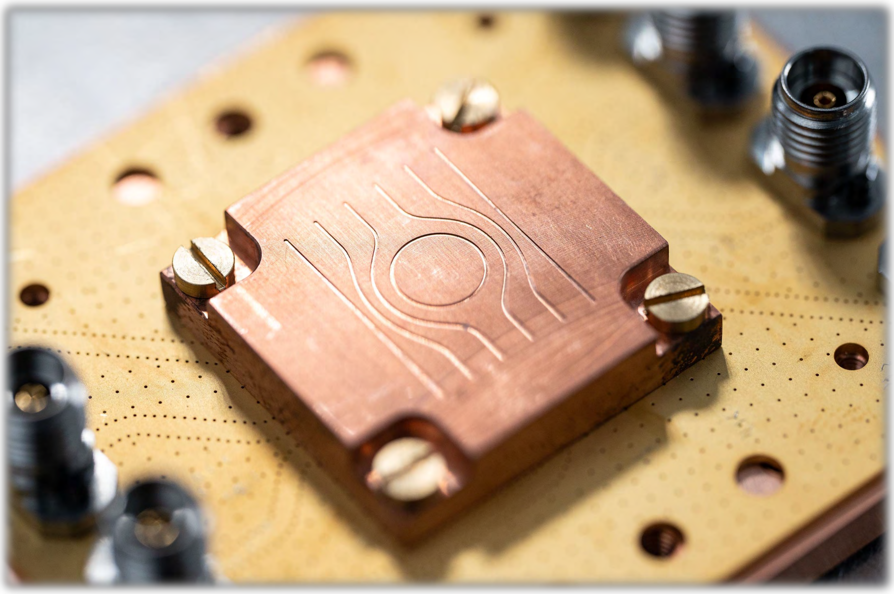

Walther-Meißner-Institut

DER BAYERISCHEN AKADEMIE DER WISSENSCHAFTEN

Cover photo: package of a superconducting qubit chip

Contact:

Prof. Dr. Stefan Filipp, Prof. Dr. Rudolf Gross and **Prof. Dr. Peter Rabl**
Walther–Meißner–Institut für Tieftemperaturforschung
Bayerische Akademie der Wissenschaften

Address:

Walther–Meißner–Str. 8	e–mail:	Stefan.Filipp@wmi.badw.de
D - 85748 Garching	e–mail:	Rudolf.Gross@wmi.badw.de
GERMANY	e–mail:	Peter.Rabl@wmi.badw.de
	www:	https://www.wmi.badw.de

Secretary's Office and Administration:

Emel Dönertas	Phone:	+49 – (0)89 289 14202
	Fax:	+49 – (0)89 289 14206
	e–mail:	Emel.Doenertas@wmi.badw.de
		Sekretariat@wmi.badw.de
Andrea Person	Phone:	+49 – (0)89 289 14442
	Fax:	+49 – (0)89 289 14206
	e–mail:	Andrea.Person@wmi.badw.de
		Verwaltung@wmi.badw.de

Walther-Meißner-Institut
DER BAYERISCHEN AKADEMIE DER WISSENSCHAFTEN

Preface

Dear colleagues, friends, partners, and alumni of the Walther-Meißner-Institute (WMI),

I want to thank everybody who has contributed to the scientific and technological progress of the institute in 2023. I want to express my gratitude to those who have brought in and shared their know-how, their skills and their commitment to shape the present and the future of the Walther-Meißner-Institute. It is indeed the people working together as a team towards the common goal of scientific and technological advances that are the most important asset of the institute.

In particular, I am happy that in the beginning of 2023 Prof. Peter Rabl has joined the institute as a new director. He has established his group working on quantum theoretical concepts and commenced important collaborations with the existing experimental teams at the institute. In 2024 he will take over the management of the institute and guide the institute. As another highlight, Prof. Rudolf Gross has become Scientific Director of Munich Quantum Valley (MQV) and Managing Director of Munich Quantum Valley e.V. starting in August 2023.

I would like to welcome all new people that have joined us to pursue their career as pre- and postdoctoral researchers and scientists at the institute. Moreover, I want to welcome our new staff members Julia Gollasch and Dong Li, who will support us with their expertise in the mechanical workshop and in the administration. Julia Gollasch is replacing Christian Reichlmaier who has left the institute in summer. On behalf of the institute I would like to thank him, and also Georg Nitschke who will retire by the end of 2023, for their year-long commitment to the well-being of the institute.

Throughout 2023, the Walther-Meißner-Institute has achieved several milestones that have opened new scientific perspectives and have brought us closer to harness the full potential of quantum technologies. With the demonstration of quantum key distribution in the microwave domain, the development of concepts on multi-qubit entanglement distribution in quantum networks and the demonstration of quantum links we have made important contributions to the field of quantum communication. We have made fundamental contributions also to basic science with the observation of the nonreciprocal magnon Hanle effect and the demonstration of magnetic levitation of superconducting microspheres. Moreover, the WMI is making excellent progress in the field of quantum technologies and computing with the development of high-quality quantum circuits, the implementation of novel multi-mode superconducting qubits and the realization of an architecture with controllable dissipative and coherent interactions. With the demonstration of first remote-access experiments on its 6-qubit quantum processor the WMI is now in a very good position to become one of the main players in Germany and Europe in this field.

In the past year, we have not only made excellent scientific progress. We have also further expanded the infrastructure to meet the demanding requirements of ongoing and forthcoming projects. Several laboratories have been renovated, the air-conditioning has been upgraded and the process cooling water system has been extended. By installing a new x-ray diffractometer we can bring the quality of the thin-film fabrication of materials to the next level. A new wafer prober will support the reliable fabrication of Josephson junctions. Moreover, we have reduced throughput bottlenecks in fabrication by a new optical lithography machine. We have installed more cryostats ranging from a large-diameter Bluefors cryostat for the planned quantum computer prototype to a rapid-prototyping setup from Kiutra to test microwave properties and DC properties of superconducting quantum circuits. Finally, we have started 3D integration efforts, along the main research direction of the institute to bring together different quantum systems and study coherent quantum interfaces.

On top of the many ongoing projects we have again been successful in acquiring new projects. We are deeply engaged in the OpenSuperQPlus project that aims to build quantum computers for Europe starting from March 2023 as the successor of the OpenSuperQ EU flagship project. The Transregional Collaborative Research Center on Constrained Quanutum Matter (ConQuMat) has started in October 2023 to address questions on magnetic band topology, entangled states of matter, and non-equilibrium dynamics in solid-state systems. In November 2023, the SNSF Sinergia grant on acoustic quantum interfaces for circuits and spins (AcQuaInt) was funded by the Swiss National Science Foundation with the goal to demonstrate a quantum interface between a superconducting qubit and spin qubits.

The institute is also deeply committed to the education and training of the next generation scientists. In this context I would like to congratulate Matthias Althammer and Kirill Fedorov who have received their Venia Legendi in Experimental Physics from the Technical University of Munich.

None of these accomplishments would have been possible without the invaluable support and collaboration from our project partners, funding agencies, industry collaborators, and the broader scientific community. Their shared commitment to the pursuit of scientific excellence and technological progress has been pivotal in our continued progress and success. I also would like to thank our Scientific Advisory Board for their trust and their invaluable guidance.

Reflecting on the achievements of the past year, I feel very optimistic for the future challenges and opportunities that lie ahead. The current structure of the institute foresees up to three scientific directors and we are currently working towards announcing a new director position succeeding Rudolf Gross. We are also working hard to solve the challenge of too little office space. Despite the bureaucratic hurdles that we have encountered in the last two years we are confident that the planned modular office building will finally be ready in 2024 and provide space for new offices and meeting rooms. Besides improving our in-house cleanroom, we are also strengthening our collaboration with the Halbleiterlabor of the Max Planck Society to provide nanofabrication capabilities for the Munich Quantum Valley projects in their newly build facilities. We are confident that the modern cleanroom environment will greatly enhance our capabilities to build state of the art quantum devices.

There are exciting times ahead of us and I am confident that with the groundwork that we have done in the last years in terms of restructuring the governance of the institute, with the infrastructural changes and with the development of all required technologies, we can concentrate even more on research and science, on fruitful discussions and on the development of new ideas. Together, let us continue to explore, innovate, and push the boundaries of science and technology as we strive to unlock the transformative power of quantum physics.

Thank you!

Warm regards,

Garching, December 2023

Contents

The Walther–Meißner–Institute

The ***Walther-Meißner-Institute for Low Temperature Research (WMI)*** was originally operated by the Commission for Low Temperature Research of the ***Bavarian Academy of Sciences and Humanities (BAdW)***. Between 2013 and 2015, the Bavarian Academy of Sciences and Humanities with its more than 300 employees was reorganized. With the passing of the new statutes in October 2015, the 36 Commissions (Research Groups) of the Academy were suspended. The research program of BAdW is now implemented in Academy Institutes, such as the Walther-Meißner-Institute, the ***Leibniz Supercomputing Centre (LRZ)*** or the ***Bavarian Research Institute for Digital Transformation (BIDT)***, and Academy Projects. The Academy Institutes and Projects are managed by the Institute and Project Committees and supervised by the Institute and Project Advisory Boards, respectively. In this way a clear separation between the managing bodies of the institutes/projects (responsible for the implementation of the research programs) and the corresponding supervisory bodies (responsible for the quality control) was established. To this end, also the Commission for Low Temperature Research was dissolved and replaced by the WMI Committee and the WMI Advisory Board in 2015.

The historical roots of WMI go back to ***Walther Meißner***. He founded the Commission for Low Temperature Research in 1946 when he was president of BAdW (1946 – 1950). The first research activities then were started in 1946 in the Herrsching barracks. After the retirement of Walther Meißner in 1952, Heinz Maier-Leibnitz, who followed Walther Meißner on the Chair for Technical Physics of the Technical University of Munich (TUM), became the new head of the Commission for Low Temperature Research. In 1967, the commission moved to the Garching research campus after the construction of the new *Zentralinstitut für Tieftemperaturforschung»* (ZTTF) was completed (director: Prof. Heinz Maier-Leibnitz, technical director: Prof. Franz Xaver Eder). Until 1972, the theory group of the Institute Laue Langevin was hosted at the ZTTF with prominent members such as Peter Fulde. In 1980, Prof. Dr. Klaus Andres became the new director of the ZTTF again associated with the Chair for Technical Physics (E23) at TUM. In 1982, the ZTTF was renamed into Walther-Meißner-Institute for Low Temperature Research (WMI) on the occasion of the 100th anniversary of Walther Meißner's birth.

In 2000, Prof. Dr. Rudolf Gross followed Klaus Andres on the Chair for Technical Physics (E23) at TUM and as the new director of WMI. He extended the scientific focus of WMI by starting new activities in the field of quantum science and technology, as well in magnetism, spin dynamics and spin electronics. Moreover, he established the materials technology for superconducting and magnetic materials (both in form of thin films and single crystals) and a clean room facility, allowing for the fabrication of solid-state nanostructures.

Due to the strong increase of staff, research projects and administrative tasks the governance structure of the WMI was changed in 2019 from a single director to a board of up to three directors headed by a managing director. The implementation of the structural change started in June 2020 with the nomination of Prof. Dr. Stefan Filipp as the second scientific director of the WMI. His research is focused on superconducting quantum circuits and in particular on quantum computing and quantum simulation. In February 2023, Prof. Dr. Peter Rabl started as the third scientific director of the WMI with his group working on applied quantum theory.

The WMI has been playing a leading role in several coordinated research projects in the field of nanosciences with the Cluster of Excellence Nanosystems Initiative Munich from 2006 to 2019 and in the field of quantum science and technology with the Collaborative Research Center 631 on Solid-State Quantum Information Processing (2003-2015), the Cluster of Excellence ***Munich Center for Quantum Science and Technology*** (since 2019) and the EU Quantum Technology Flagship Project QMiCS (2018-2022). The WMI has recently also played a leading role in initiating the ***Munich Quantum Valley*** in 2020 (see strategy paper ***«Munich Quantum Valley Initiative»***). It is now coordinating and participating in several national and European consortia, such as the ***German Quantum Computer based on Superconducting Qubits (GeQCoS)*** and the ***Munich Quantum Valley Superconducting Quantum Computing Demonstrator (MUNIQC-SC)*** projects, to develop quantum computing technologies based on superconducting quantum circuits.

To accommodate the activities, the infrastructure of the WMI has been constantly renewed and upgraded. Starting from 2000 the so far unused basement of the WMI building was made available for technical infrastructure (air conditioning, particulate air filters, pure water system etc. for clean room) and additional laboratory space. Fortunately, in 2008 WMI succeeded in getting extra money from the state government within the so-called *«Konjunkturpaket II»* to establish the new *«WMI Quantum Science Laboratory»* in the basement of the building, providing about 150 m^2 additional laboratory space particularly suited for low-temperature facilities and ultra-sensitive studies on solid-state quantum systems. In 2016, the Bavarian Ministry for Science and Arts granted more than 6 Mio. Euro for redevelopment measures regarding the technical infrastructure, safety requirements and energy efficiency. An important part of the building project implemented in 2017/18 was the reconstruction of the entrance area and the main staircase, providing now direct access to the new WMI Quantum Laboratories in the basement of the WMI building, as well as additional communication areas and meeting rooms in the ground floor. Moreover, it included the replacement of all windows and doors, the upgrade of the technical infrastructure for cooling water, air conditioning, liquid nitrogen and helium storage, as well as the complete redevelopment of the mechanical workshop and various safety measures. With the intense activities in the field of quantum computing and the new groups starting in 2020 and 2023 offices and laboratories have been renovated and repurposed to host the new infrastructure for fabricating and characterizing scalable quantum processors. Aside from the upgrades of the pure water system, the air conditioning system and the cooling units, a new modular office building is planned to provide more office space starting from 2024.

While the WMI traditionally hosts the Chair for Technical Physics (E 23) of the Technical University of Munich (TUM) the WMI has established tight links to research groups of both Munich universities, joining technological and human resources in the fields of experimental and theoretical solid-state and condensed matter physics, quantum technologies, low-temperature techniques, materials science as well as thin film and nanotechnology. Noteworthy is that the WMI supplies liquid helium to more than 25 research groups at both Munich universities and provides the technological basis for low-temperature research.

Important Discoveries

The WMI looks back on a long history of successful research in low-temperature physics. In the following we list some important discoveries as well as experimental and technical developments made at WMI:

- **1961: discovery of flux quantization in multiply connected superconductors**

  (R. Doll, M. Näbauer, *Experimental Proof of Magnetic Flux Quantization in a Superconducting Ring*, Phys. Rev. Lett. **7**, 51-52 (1961)).
- **1986: discovery of an anomalous temperature dependence of the penetration depth in UBe_{13}**

  (F. Gross, B.S. Chandrasekhar, D. Einzel, K. Andres, P.J. Hirschfeld, H.R. Ott, J. Beuers, Z. Fisk, J.L. Smith, *Anomalous Temperature Dependence of the Magnetic Field Penetration Depth in Superconducting* UBe_{13}, Z. Physik B - Condensed Matter **64**, 175-188 (1986)).
- **1992: discovery the intrinsic Josephson effect**

  (R. Kleiner, F. Steinmeyer, G. Kunkel, and P. Müller, *Intrinsic Josephson Effects in* $Bi_2Sr_2CaCu_2O_8$ *Single Crystals*, Phys. Rev. Lett. **68**, 2394-2397 (1992)).
- **2002: development of dilution refrigerators with pulse tube refrigerator precooling**

  (K. Uhlig, *$^3He/^4He$ Dilution Refrigerator with Pulse Tube Precooling*, Cryogenics **42**, 73-77 (2002)).
- **2010: first demonstration of ultrastrong light-matter interaction**

  (T. Niemczyk, F. Deppe, H. Huebl, E. P. Menzel, F. Hocke, M. J. Schwarz, J. J. Garcia-Ripoll, D. Zueco, T. Hümmer, E. Solano, A. Marx, R. Gross, *Circuit Quantum Electrodynamics in the Ultrastrong-Coupling Regime*, Nature Physics **6**, 772-776 (2010)).
- **2010: development of dual path method for state tomography of propagating quantum microwaves**

  (E.P. Menzel, M. Mariantoni, F. Deppe, M.A. Araque Caballero, A. Baust, T. Niemczyk, E. Hoffmann, A. Marx, E. Solano, R. Gross, *Dual-Path State Reconstruction Scheme for Propagating Quantum Microwaves and Detector Noise Tomography* , Phys. Rev. Lett. **105**, 100401 (2010)).
- **2012: first realization of path entanglement of propagating quantum microwaves**

  (E. P. Menzel, R. Di Candia, F. Deppe, P. Eder, L. Zhong, M. Ihmig, M. Haeberlein, A. Baust, E. Hoffmann, D. Ballester, K. Inomata, T. Yamamoto, Y. Nakamura, E. Solano, A. Marx, R. Gross, *Path Entanglement of Continuous-Variable Quantum Microwaves*, Phys. Rev. Lett. **109**, 250502 (2012)).
- **2013: discovery of the spin Hall magnetoresistance** (jointly with partners at Tohoku University and TU Delft)

  (H. Nakayama, M. Althammer, Y.-T. Chen, K. Uchida, Y. Kajiwara, D. Kikuchi, T. Ohtani, S. Geprägs, M. Opel, S. Takahashi, R. Gross, G. E. W. Bauer, S. T. B. Goennenwein, E. Saitoh, *Spin Hall Magnetoresistance Induced by a Non-Equilibrium Proximity Effect*, Phys. Rev. Lett. **110**, 206601 (2013)).
- **2013: first demonstration of strong magnon-photon coupling**

  (H. Huebl, Ch. Zollitsch, J. Lotze, F. Hocke, M. Greifenstein, A. Marx, R. Gross, S.T.B. Goennenwein, *High Cooperativity in Coupled Microwave Resonator Ferrimagnetic Insulator Hybrids*, Phys. Rev. Lett. **111**, 127003 (2013)).
- **2017: first experimental observation of the spin Nernst effect**

  (S. Meyer, Yan-Ting Chen, S. Wimmer, M. Althammer, S. Geprägs, H. Huebl, D. Ködderitzsch, H. Ebert, G.E.W. Bauer, R. Gross, S.T.B. Goennenwein, *Observation of the spin Nernst effect*, Nature Materials **16**, 977-981 (2017)).
- **2019: first demonstration of remote state preparation in the microwave regime**

  (S. Pogorzalek, K. G. Fedorov, M. Xu, A. Parra-Rodriguez, M. Sanz, M. Fischer, E. Xie, K. Inomata, Y. Nakamura, E. Solano, A. Marx, F. Deppe, R. Gross, *Secure Quantum Remote State Preparation of Squeezed Microwave States*, Nature Communications **10**, 2604 (2019)).
- **2021: first demonstration of quantum teleportation in the microwave regime**

  (K. G. Fedorov, M. Renger, S. Pogorzalek, R. Di Candia, Q. Chen, Y. Nojiri, K. Inomata, Y. Nakamura, M. Partanen, A. Marx, R. Gross, F. Deppe, *Experimental quantum teleportation of propagating microwaves*, Science Advances **7**, eabk0891 (2021)).

Present Research Activities

The research activities of the Walther-Meißner-Institute focus on low-temperature condensed matter and quantum physics, as delineated in the reports in the following sections. Broadly speaking, the research program is centered on **fundamental** and **applied research** topics and also addresses **materials science, thin film and nanotechnology** aspects. It conducts research in the field of low and ultra-low-temperature physics with a special focus on quantum systems, quantum computing, superconductivity and correlated electron systems, as well as magnetism and spintronics.

The WMI also develops and operates systems and techniques for low and ultra-low-temperature experiments. A successful development has been dry mK-systems that can be operated without liquid helium by using a pulse-tube refrigerator for pre-cooling. In the early 2000s, these systems have been successfully commercialized by the company VeriCold Technologies GmbH at Ismaning, Germany, which was taken over by Oxford Instruments in 2007. Currently, in a collaboration with Oxford Instruments such dry dilution refrigerators are used to establish a so-called cryolink, allowing for quantum communication in the microwave regime between two superconducting quantum processors over an about 10 m distance. WMI also operates a helium liquifier with an annual capacity of above 180.000 liters and supplies both Munich universities with liquid helium. To optimize the transfer of liquid helium into transport containers, WMI has developed a pumping system for liquid helium which has been commercialized in collaboration with a company.

To a large extent, the research activities of WMI are integrated into national and international research projects such as Clusters of Excellence, Collaborative Research Centers, Research Units, and projects funded by the Federal Ministry of Education and Research (BMBF) as well as the European Union. Moreover, the individual research groups of WMI offer a wide range of attractive research opportunities for bachelor's and master's students, Ph.D. students, and postdoctoral fellows.

Experimental Facilities and Resources

The WMI is equipped with state of the art facilities for the preparation and characterization of superconducting and magnetic materials as well as for various low and ultra–low temperature experiments. The main experimental and technological resources of WMI include infrastructure for **Materials Preparation and Fabrication of Nanostructures** (such as a UHV-cluster cluster deposition system, a UHV electron beam evaporation and sputtering system for qubit fabrication, several sputter deposition systems for superconducting and magnetic heterostructures, a 100 kV electron-beam system as well as optical lithography tools and tools for 3D integration), for **material and system characterization** (e. g. an x–ray diffractometer, a scanning electron microscope, a AFM/STM system, a SQUID magnetometer, several vector network analyzers, and a wafer-prober) and for operating and characterizing systems at low temperatures (several $^3He/^4He$ dilution refrigerators equipped with control electronics). More details can be found on the WMI webpage (www.wmi.badw.de/research/Materials, Methods and Infrastructure.

Building Projects and Reconstruction Measures

Building Projects and New Infrastructure in 2023

A. Marx, S. Geprägs, M. Opel, C.M.F. Schneider, L. Södergren, M. Werninghaus, S. Filipp, R. Gross

Topics in fundamental and applied research and the related experimental methods and techniques are continuously changing. This requires a permanent adjustment of the technical infrastructure to the needs of the ongoing and planned research projects. Therefore, in 2023, several reconstruction measures have been taken to accommodate new equipment and technological infrastructure and warrant the supply of the required resources (electrical power, cooling water, process gases, liquid nitrogen). Moreover, several laboratories and office spaces had to be renovated and reorganized. Due to the substantial increase in heat dissipation from experimental infrastructure, the air conditioning in two laboratories had to be adjusted to the higher demands by installing air coolers with larger cooling capacities. The SQUID laboratory, where the new automatic probe station was installed and put into operation, could subsequently be equipped with one of the lower-capacity air coolers that became available.

To meet the increased demand for cooling capacity from the additional scientific equipment, a new chiller was installed and put into test operation in 2023. The WMI has already been operating two chillers providing a cooling power of 180 kW and 130 kW for different institute sections. The new machine offers an extra cooling capacity of more than 200 kW. Together with the 180 kW machine, it aims to provide stable cooling power for all experimental setups and to stabilize temperatures in all laboratories to guarantee a stable thermal environment for ultrasensitive measurements as well as for sample fabrication technologies. In addition, the new chiller provides a basic level of redundancy in case of failure of one of the two machines. To warrant a reliable supply of electrical power for the increased number of experimental facilities (dilution refrigerators, sample fabrication technology, characterization tools, chillers) as well as for the upcoming temporary office containers (see below), an upgrade of the WMI transformer station with a second transformer is scheduled for 2024, the tender process has already been completed. Installing the second transformer doubles the available maximum electrical power and provides a basic fail-safety of the electricity supply.

In order to meet the demand for the highest level of fabrication quality of superconducting quantum circuits with increasing levels of integration, the grey room area of the WMI has been significantly enlarged. After installing additional doors at both ends of the west side hallway on the ground floor, the complete space between the doors now provides a clean contiguous access area for all fabrication laboratories, the cleanroom, the chemistry laboratory, and the SEM/AFM/profilometer laboratory with grey room quality. This grey room area is expected to significantly improve the reliability of fabrication processes and sample quality by providing a cleaner environment for all fabrication steps.

The change of the governance structure of the WMI from a single director to a board of three directors was accompanied by a substantial increase in research projects, specifically activities on superconducting quantum computing within the Munich Quantum Valley and various BMBF projects entailing a considerable increase both in lab space and staff. WMI has decided to deploy office containers beside the WMI building to accommodate the increase in staff. These temporary office containers will be erected in a modern modular design with air conditioning and complete infrastructure for a scheduled lifetime of 5 years. The two-floor building, with a usable area of around 300 m^2, will provide office space for up to 28 staff members, three meeting rooms, and a mid-size seminar room hosting up to 24 staff members. The container modules have already been ordered by WMI and will be deployed in 2024 as soon as the building permit is available.

In 2023, essential new scientific instrumentation was delivered and installed. In particular, a new reactive ion etcher PlasmaPro 100 Cobra from Oxford Instruments, supporting both Bosch and cryogenic deep silicon etching processes, has been installed in the WMI cleanroom. The numerous external supplies for the Cobra (cooling water, liquid-nitrogen supply, process gases, dedicated BCl_3 safety cabinet, gas monitoring system for BCl_3, vacuum pumping lines, scrubber) have been meanwhile installed. This system is now ready to be put into operation. A maskless aligner MLA150 from Heidelberg Instruments, which provides a minimum resolution of 0.6 µm at a significantly reduced writing time, has been set up in the cleanroom. Another addition to the cleanroom equipment is a flip-chip bonder (Finetech Fineplacer femto 2) delivered in 2023, allowing the bonding of two chips together via Indium bump bonds. These Indium bump bonds with a thickness of several micrometers are deposited in an Indium evaporation system (Plassys ME450S-In), also delivered in 2023, and installed in one of the labs accessible via the extended grey room area (room 004).

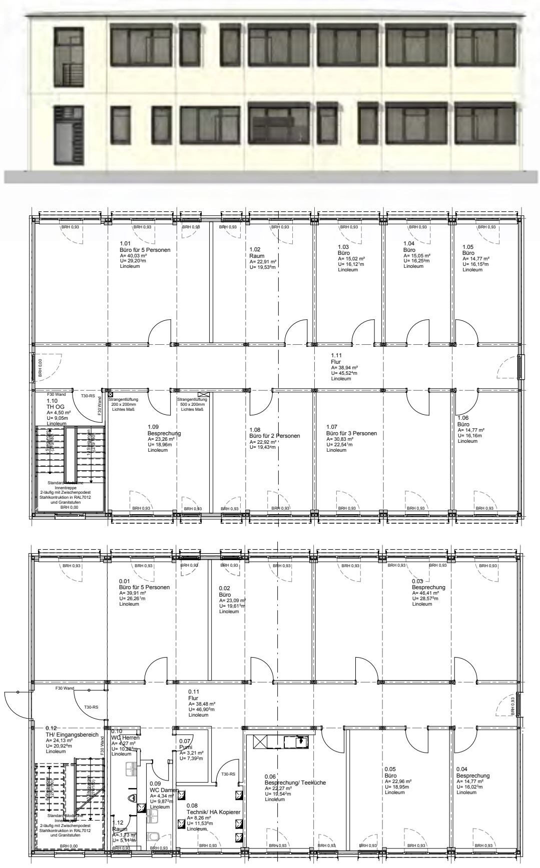

Figure 1: Blueprint of containers.

Further substantial acquisitions to improve sample fabrication technologies in 2023 are

- Profilometer (Bruker DekTak XT), see report on page 92
- Automatic wafer probe station (TS2000-IFE from Automatisierungstechnik Voigt ATV), see report on page 93
- X-ray diffraction (XRD) system from Bruker AXS, see report on page 99
- Automatic wire bonder (5630i from F&S Bondtec), see report on page 101
- Tabletop-PLD system (nanoPVD from Moorfield Nano Techonlogies)

In 2023, two new dry dilution refrigerators from Bluefors Oy company were installed, both Model BF-XLD 1000 (see report on page 97) to support the efforts in the MQV and MUNIQC-SC projects eventually hosting up to 24 and 100 superconducting qubits, respectively. Both refrigerators are equipped with the necessary wiring and measurement electronics. Furthermore, a tabletop rapid-cooldown cryogen-free dilution refrigerator, Sionludi Pro-15 from Qinu company, has been acquired for experiments at millikelvin temperatures with fast characterization time. For even faster sample characterization, an adiabatic demagnetization refrigerator (ADR) L-Type Rapid from Kiutra, allowing sample cooldown to 100 mK within 10 minutes, has been put into operation in 2023 (see report on page 97).

The IT infrastructure at the WMI has been substantially upgraded. To enhance the capability for online streaming, video conferencing, and video recording, professional audio hardware, and new video software was installed in the main seminar room. For better audio quality, the ceiling microphone was replaced in June 2023 by a 2nd generation microphone array (Shure MXA 920) with automatic coverage technology to follow different speakers in designated areas. This upgrade was accompanied by the introduction of an 8-channel digital signal processor (QSC Core Nano) in a Dante network (Audio over IP) with an analog extension (QSC QIO ML2x2) for interoperability with the existing audio receiver and the loudspeakers in the room. In addition, we licensed a Zoom Rooms controller software that can handle three cameras simultaneously for broadcasting lectures and seminars. We have also provided a detailed, written, step-by-step manual ("hitchhiker's guide") on how to correctly operate the new equipment.

For networking and data storage, we have replaced the 6-year-old server hardware. We set up two new physical machines based on Windows Server 2022, each equipped with 256 GB RAM, six network interface cards connected to Gigabit Ethernet, and 6×12 TB hard disk storage. They host two virtual file servers (one operational, one backup) for the home and group directories and seven other virtual servers (DNS server, DHCP server, router, print server, and servers for other particular tasks). They are configured as member servers of the university-wide active directory service (ADS) operated by the Leibniz-Rechenzentrum (LRZ).

In addition, we have set up four Linux servers to support the quantum computing group's growing computational and storage needs. These include two CPU servers for Ansys simulation as well as a GPU server for simulations that can be sped up significantly via a GPU. On the storage front, we have set up a data server with a Proxmox hypervisor containing multiple virtual machines related to storage, mainly raw experimental data via mongo DB and general lab computer backups via rsync.

The most relevant measures implemented in 2023 have been

- renovation two laboratories
- adaption of air conditioning in three laboratories
- installation of contiguous grey room area
- installation of a new chiller
- acquisition of temporary office containers
- completing tender for additional power transformer
- installation of PlasmaPro 100 reactive ion etcher for high and cryogenic etching processes, see report on page 91
- installation of Bruker AXS X-ray diffractometer, see report on page 99
- installation of maskless aligner, see report on page 102
- installation of Indium evaporation system and flip-chip bonder, see report on page 103
- installation of tabletop PLD system
- installation of automatic wire bonder, see report on page 101
- installation of automatic wafer prober, see report on page 93
- installation of 2 BF-XLD 1000 cryogen-free dilution refrigerator, see report on page 97
- installation of Qinu Sionludi Pro-15 cryogen-free dilution refrigerator, see report on page 97
- installation of Kiutra L-Type Rapid ADR, see report on page 97
- installation of new professional audio hardware and video software
- server upgrade
- installation of increased computational and storage capacities

Joint Research Projects

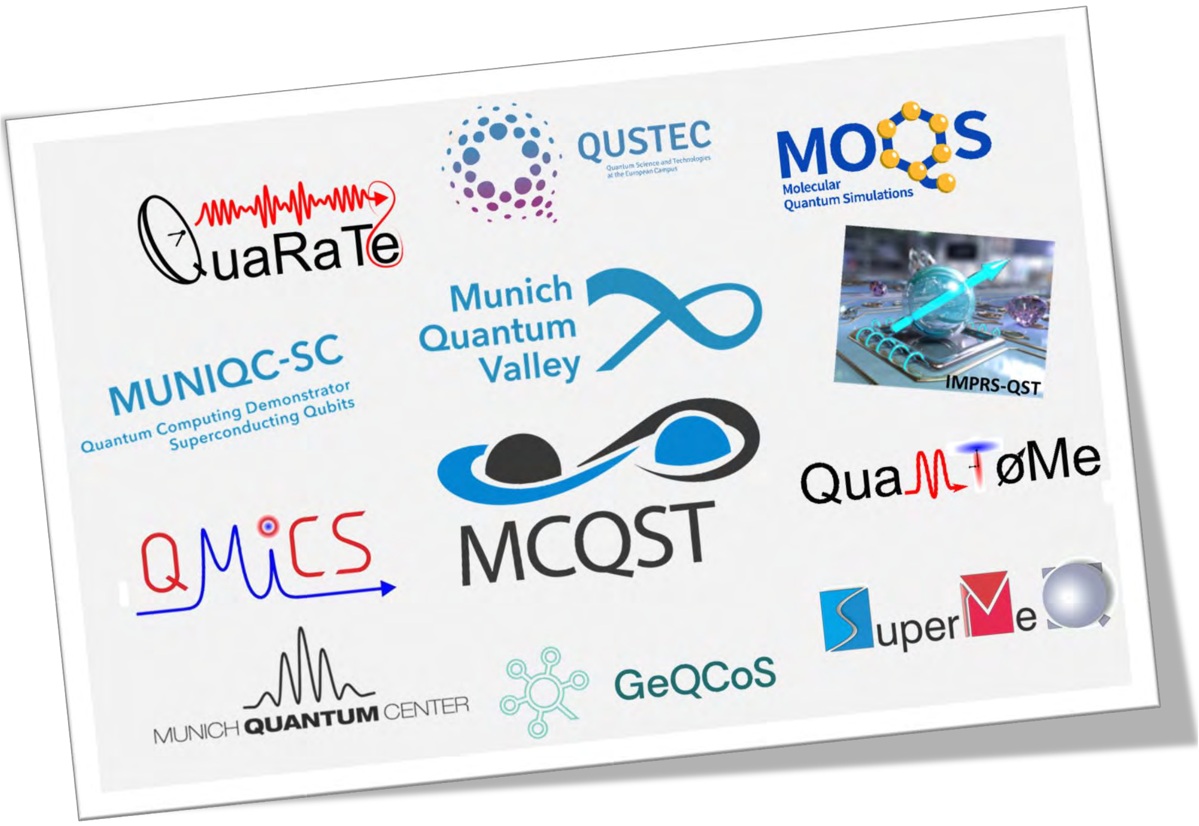

Munich Quantum Valley Takes Off

Rudolf Gross [1]

Munich Quantum Valley (MQV) is one of the flagship projects of the **Hightech Agenda Bavaria**. Munich Quantum Valley is organized as a registered association and combines the research capacities and technology transfer power of three major universities (TUM, LMU, FAU) and key research organizations (BAdW, MPG, FhG, DLR) in Bavaria in an unprecedented intensity of cooperation. As a collaborative project between academia, industry, research, and public organizations, MQV offers state-of-the-art framework conditions for the emergence and further research of quantum technologies and quantum computing throughout Bavaria and forms a crucial part of the Bavarian quantum technology ecosystem.

With the Walther-Meißner-Institute (WMI) and the Leibniz Supercomputing Centre (LRZ) the Bavarian Academy of Sciences and Humanities (BAdW) is one of the key players of MQV. At WMI, the groups of all three Scientific Directors are strongly involved in the R&D program of MQV. In August 2023, Rudolf Gross of WMI became the new Scientific Director of MQV, taking over the coordination of this demanding project from Rainer Blatt, who successfully steered MQV through the starting phase (see press release from 01 August 2023).

With the **Hightech Agenda Bavaria**, Bavaria is rigorously investing in state-of-the-art research and career prospects with regards to innovative future technologies. With an investment of approximately 5.5 billion euros, the Hightech Agenda Bavaria is one-of-a-kind in Germany. The initiative invests in the brightest minds and aims to create and maintain 3,800 positions across Bavarian universities. Among these positions, 1,000 new professorships will be established in key future fields such as artificial intelligence, quantum technology, clean tech, and aerospace.

A. MQV Quantum Mission

A1. Creating a powerful quantum ecosystem in Bavaria

As a hub between research, industry, funding agencies, and the public, MQV establishes a powerful quantum ecosystem in Bavaria to promote efficient knowledge transfer between academia and industry and operates an internationally leading center for developing the full spectrum of quantum technologies. MQV explores novel concepts in QST in focused lighthouse projects, operates a world-class research high-tech infrastructure, offers tailored educational programs for schools, universities, and companies, a platform for international networking, and targeted entrepreneurial support for start-ups.

A2. Developing quantum computing and technologies for real-life applications

Using innovatively engineered superconducting, neutral-atom and trapped-ion platforms, the overarching mission of MQV is to realize full-stack quantum-computer demonstrators, remotely accessible to researchers and industry through seamless integration with local high-performance computing infrastructure. By jointly developing hardware and software, MQV will provide the quantum computing tools allowing to address challenging real-life problems. On a medium-term basis (5–10 years), MQV will focus on noisy intermediate-scale quantum

[1]Munich Quantum Valley is supported by the Bavarian state government with funds from the Hightech Agenda Bavaria.

computers with up to 1000 qubits, while the long-term goal is to develop fault-tolerant quantum computers capable of solving practical problems relevant to the economy and society. Besides an ambitious focus on quantum computing, MQV will create innovation in many related technology fields.

A3. Building on unique Bavarian strengths

MQV builds on its founding members' longstanding tradition and outstanding excellence, covering all fields of QST, and an exceptional industrial high-tech environment. By coordinating efforts of academia, industry, and funding agencies, MQV provides a unique ecosystem, enabling efficient knowledge transfer between research and industry and establishing a network of high international visibility. MQV provides the tools and services to drive the commercialization of quantum technologies and to catalyze their transition from theoretical concepts to tangible real-world applications.

B. MQV Roadmap

Quantum technologies are expected to be era-defining, similar to digital technologies shaping the information age. Therefore, the development of quantum technologies will extend over a longer period and most likely will also be accompanied by technology disruptions. Therefore, the MQV roadmap has been planned for an intermediate to long time scale from the beginning. It is expected that MQV will play a leading role in the long-term development of quantum technologies and enable Bavaria to take a leading role in the industrialization of this important future technology. The world-leading know-how built up and concentrated within MQV will provide industry and start-ups a competitive advantage by having immediate access to this know-how. Moreover, the vibrant MQV quantum ecosystem is expected to be a decisive factor for Bavaria's competitiveness in attracting quantum industry and start-ups, as well as fostering investments.

Within the first funding period (October 2021 to December 2026), MQV aims to

- develop full-stack quantum computers based on different hardware platforms,
- realize high-tech infrastructures and enabling technologies for quantum research within an open-access Quantum Technology Park,
- provide tailored entrepreneurial support for quantum technology start-ups,
- develop targeted programs for educating the next generation of quantum scientists and engineers,
- explore novel concepts and quantum-enabling technologies in focused **Lighthouse Projects** and
- strengthen quantum science at universities by additional MQV professorships.

WMI makes important contributions to the implementation of this ambitious program. In particular, WMI

- coordinates the Superconducting Qubit Quantum Computer (SQQC) consortium of MQV, developing the hardware for superconducting quantum computers,
- coordinates the Quantum Technology Park & Entrepreneurship (QTPE) consortium which aim at realizing an open-access Quantum Technology Park and providing tailored entrepreneurial support for quantum technology start-ups,
- hosts one of the MQV professorships (see below),
- is a key partner in the two MQV Lighthouse Projects NeQuS and IQSense (see below).

C. WMI Contributions to MQV

In the following, we briefly summarize the main contributions of WMI to MQV. We focus on those program parts, which are coordinated or strongly supported by WMI.

C1. Superconducting Qubit Quantum Computer (SQQC)

The Superconducting Qubit Quantum Computer (SQQC) consortium is coordinated by Stefan Filipp of WMI. The SQQC consortium aims to close the gap between hardware developers and end users by realizing a quantum computer demonstrator based on 24 or more superconducting qubits, integrating all relevant components of a full-stack computer in close collaboration with application scientists. The quantum processor will eventually be made available for researchers and industry alike. In close relation to this endeavor, advanced technologies, novel components, and aspects are being developed, putting Germany ahead of the curve of hardware changes during the next decade. Aside from leading the SQQC consortium of MQV, WMI is coordinating the projects **GeQCoS** and **MUNIQC-SC** both funded by the German federal government (see report on page 28).

C2. Quantum Technology Park & Entrepreneurship (QTPE)

The **Quantum Technology Park & Entrepreneurship (QTPE)** consortium was led by Rudolf Gross of WMI until August 2023, when he became MQV Scientific Director, and is now coordinated by Christopher Trummer and Stefan Filipp from TUM. The QTPE consortium provides essential ingredients to the development of a flourishing quantum ecosystem in Bavaria. The Quantum Technology Park drives the coordinated upgrading and extension of critical technology infrastructure and shared access for relevant stakeholders. This creates the basis for state-of-the-art technology development and fosters collaboration and knowledge exchange across institutions and faculties. The entrepreneurial activities and the TUM Venture Lab Quantum are providing a tailored support structure for founders and start-ups, driving quantum technologies and software toward application and commercialization. The TUM Venture Lab Quantum's managing director, Christopher Trummer, is successfully ramping up support for quantum start-ups, supported by Rudolf Gross and Stefan Filipp, who are the Venture Lab Quantum's scientific advisors. Meanwhile, two start-ups have already been spun off, and many more are in the pipeline. The most recent case was **Quantum Diamonds**, which raised 7 million euros from investors and the Bavarian state government via a lighthouse project. Overall, the QTPE consortium plays a crucial role as a connecting link between multiple stakeholder groups for the whole quantum ecosystem in Bavaria.

C3. Promoting the Quantum Ecosystem

A superordinate objective of MQV is to promote quantum science and technology in Bavaria in general and to develop a thriving quantum ecosystem, interlinking academia, established high-tech industry, investors, and start-ups. WMI supports this effort through several collaborations with industry, outreach activities, public talks, newspaper articles, meetings with investors and policymakers, and many more.

C4. Quantum Education in Bavaria

The education and training of the next generation of quantum experts is of utmost importance to position Bavaria as one of the leading international quantum hubs. Therefore, MQV develops and coordinates programs for educating the next generation of scientists, engineers, integrators, and users of quantum technologies, both at the master's and doctoral levels, within its **Quantum Science and Technology Education in Bavaria (QST-EB)** consortium. The approach includes application-oriented internships, an excellence-focused international doctoral fellowship program across the physics, chemistry, computer science, mathematics, and electrical engineering departments open to all Bavarian universities, advanced practical lab experiments at Bavarian universities, and master-level fellowships.

C5. MQV Professsorships

In order to strengthen research and education in the field of quantum science and technology and to attract the best brains to Bavarian universities, MQV promotes so-called research and development professorships. Already internationally recognized as a top location for quantum science and technology, the Free State of Bavaria is further broadening its basis to create expertise and educate future personnel with this program, which is funded by the Hightech Agenda Bavaria. So far, eight R&D professorships have been awarded throughout Bavaria. Peter Rabl, who is Scientific Director at WMI and professor of "Applied Quantum Theory" at TUM since October 2022, is one of them.

The realization of practical quantum technologies still faces many scientific and technological challenges, which arise, loosely speaking, from the incompatibility of fragile quantum states with the surrounding classical world. **Peter Rabl** approaches this challenge from a theoretical perspective and aims to develop novel protocols and control techniques to manipulate quantum systems in a more efficient and robust way. These methods will make it possible to preserve quantum superpositions longer, to build quantum processors with more and more qubits, and to reduce the immense classical control overhead still required to operate such systems. In this context, a specific focus is placed on the theory of hybrid quantum systems, with the long-term goal of integrating quantum systems realized on different physical platforms into a single quantum device or connecting them over long distances via the 'quantum internet'. Beyond this application-oriented research, Rabl's group is also interested in modeling novel quantum phenomena that are not yet accessible in nature but can be observed in artificial quantum devices with specifically designed interactions.

C6. MQV Lighthous Projects

The **Lighthouse Projects** complement the research program of MQV towards the goal of developing, operating, and providing access to quantum computers in Bavaria. They cover a broad range of quantum sciences and technologies. Within the framework of the Lighthouse Projects, Bavarian universities, research institutions, and industry partners are jointly investigating enabling technologies and theoretical foundations in the fields of quantum computing, simulation, communication, sensing, and metrology. In the course of 2023, seven Lighthouse Projects have started their research activities. WMI is actively involved in two of them.

(a) Integrated Spin Systems for Quantum Sensors (IQ-Sense)

Sensors with the highest sensitivity are needed in many fields, especially in the life sciences. The MQV Lighthouse Project IQ-Sense focuses on developing and demonstrating integrated quantum sensors that surpass current sensors in terms of precision. To achieve this goal of tailoring quantum systems for the detection of different quantities to realize sensors with unprecedented sensitivity, researchers from the natural sciences are collaborating with scientists from the life sciences and medicine.

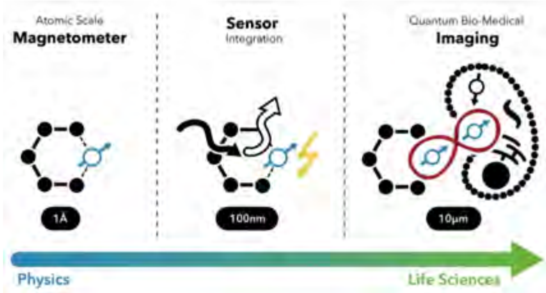

Figure 1: The mission of IQ-Sense is to translate quantum sensing from fundamental physics towards applications in life sciences.

Consortium:

- Würzburg University: V. Dyakonov, B. Hecht, K. Heinze, S. Höfling, M. Sauer
- Walther-Meißner-Institute: R. Gross, H. Hübl
- Technical University of Munich: Ch. Back, M. Brandt, D. Bucher, J. Finley, F. Schilling, G. Westmeyer

(b) Networked Quantum Systems (NeQuS)

The Lighthouse Project NeQuS (for more information, see report on page 24) aims at the development of novel quantum interfaces and transducers needed to connect different quantum systems together and take the first steps towards the quantum internet. Such networks built from interconnected quantum systems will have many advantages, transcending the various sub-fields of quantum information science and technology. Examples include inherently secure quantum communication in which parties can communicate without the risk of eavesdroppers intercepting their messages, linking quantum processors to build more powerful multi-core architectures, and quantum sensors and transducers in which remote systems can be measured with unprecedented sensitivity.

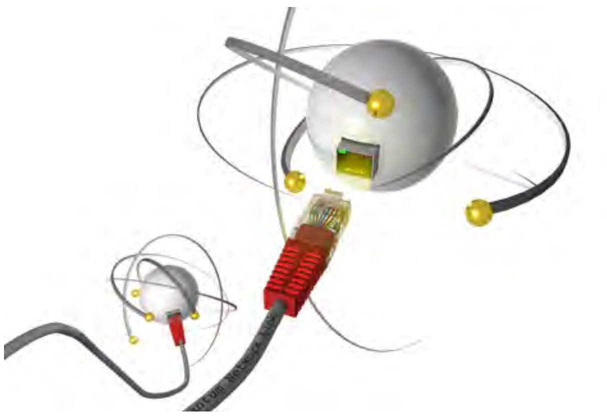

Figure 2: Map of the TUM campus with the institutes contributing to the hybrid quantum network entangling the different partners.

A major goal of NeQuS is to interconnect different quantum systems using photons propagating in glass fiber to build hybrid quantum networks. In the long term, the results of the project will pave the way to a global network of quantum computers that can perform distributed quantum tasks such as computing, communication, and sensing in an efficient, fault-tolerant, and provably secure manner. Such a “quantum internet” will have a similar transformative impact on quantum information science and technology as the development of the internet has had on classical information technology.

Consortium:

- Walther-Meißner-Institute: K. Fedorov, S. Filipp, R. Gross, H. Hübl
- Technical University of Munich: J. Finley, K. Müller, A. Reiserer, P. Rabl, E. Weig
- Ludwig-Maximilians Universität München: H. Weinfurter
- Max Planck Institute of Quantum Optics (MPQ): G. Rempe

MQV Lighthouse Project Networked Quantum Systems (NeQuS)

Kirill G. Fedorov, Hans Huebl, Peter Rabl, Stefan Filipp, Rudolf Gross [1]

Quantum networks are nowadays at the forefront of both fundamental research and industrial applications. Potentially, they enable many groundbreaking paradigms, such as unconditional security of communication or distributed quantum computing. In January 2023, the **MQV Lighthouse Project** Networked Quantum Systems (NeQuS) started. The project brings together ten groups from the Technical University of Munich (TUM), the Ludwig-Maximilians-Universität (LMU), the Walther-Meißner-Institute, and the Max Planck Institute for Quantum Optics (MPQ). NeQuS aims to develop novel quantum interfaces and transducers, operating in both the microwave and optical regimes, needed to connect different quantum systems and take the first steps toward the quantum internet. At WMI, we are focusing on two directions: (1) the development of remote entanglement of superconducting qubits by exploiting propagating squeezed microwaves and (2) the transduction of quantum microwave excitations to optical signals by using magneto-electro-mechanical systems and quantum dot molecules in collaboration with the Walter-Schottky-Institute.

Our first direction is based on superconducting cavity-qubits systems as illustrated in Fig. 1. In this project, we made progress with modeling and fabricating superconducting aluminum cavities coupled to niobium-aluminum transmon qubits. Such systems are known for their long coherence times and reproducibility. In this context, we also focus on preliminary theory simulations of relevant remote entanglement protocols [2, 3] which are based on the illumination of remote qubits with propagating two-mode squeezed microwave signals. Such entangled microwave light enters the remote qubit-cavity systems via a dedicated buffer antenna, coupled to an off-resonant cavity mode, which dispersively steers non-local, entangled qubit states. The results of our theoretical modeling predict that we can reach substantial concurrences, $C \sim$

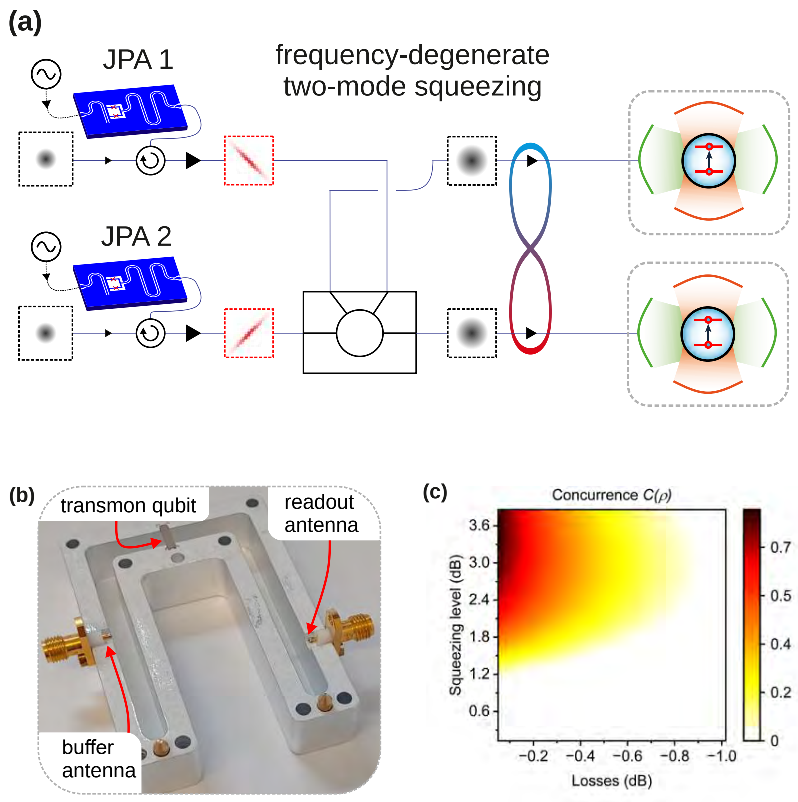

Figure 1: Entanglement of remote superconducting qubits. Panel (a) shows a considered experimental scheme. Here, two Josephson parametric amplifiers (JPAs) are used as sources of squeezed microwaves [1]. Panel (b) shows a photo of a prototype superconducting cavity with a transmon qubit. Panel (c) shows a theory prediction for the entanglement monotone (concurrence, C)) of such superconducting cavity-qubit systems under illumination of two-mode squeezed light.

[1] We acknowledge support by the German Research Foundation via Germany's Excellence Strategy (EXC-2111-390814868). This research is part of the Munich Quantum Valley, which is supported by the Bavarian state government with funds from the Hightech Agenda Bavaria.

0.8, for realistic values of propagating losses and two-mode squeezing, as shown in Fig. 1(c). Related experiments are ongoing and are expected to yield first results early in 2024.

Our second direction is focused on transduction between microwave and optical frequency domains while trying to preserve fragile quantum correlations. Here, we would like to exploit magneto-electro-mechanical nanodevices. These devices rely on a hybrid frequency conversion by combining opto-mechanics and opto-magnonics [4]. In detail, we envisage a device integrating an optical photonic crystal consisting of the ultra-low damping magnetic material YIG placed in a superconducting microwave cavity. This conversion concept uses a combined three-step conversion process, involving the coupling of microwave photons with magnons, the coupling of the magnonic and tailored phononic degrees of freedom harnessing magneto-elasticity, and the opto-mechanical interaction linking the photonic and phononic degree of freedom, as schematically illustrated in Fig 2. In particular, the three-step conversion should allow us to overcome the cooperativity matching criterion of a one-step conversion process and, hereby, will allow for much larger bandwidths. Currently, we are focused on the design and fabrication of suspended magnetic yttrium iron garnet photonic crystals, their integration in on-chip optical and microwave circuits as well as exploring and tailoring the magnetic and optic properties of the mediating magnetic system, e.g. by doping.

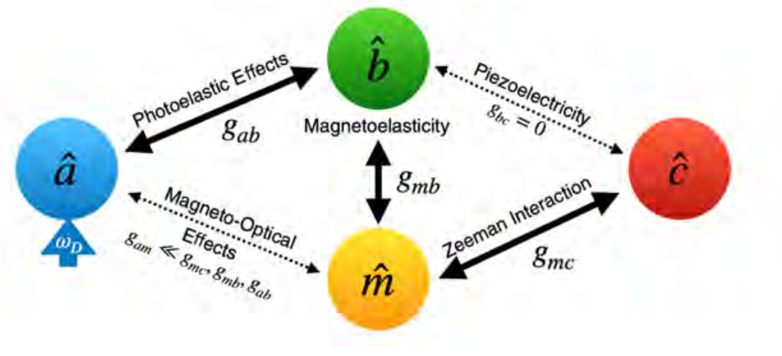

Figure 2: Exploring quantum conversion between microwave and optical frequencies using a hybrid system consisting of a microwave cavity, a microstructure with tailored magnonic and mechanical properties made from yttrium iron garnet and with an optical readout [4].

Along these lines we are also collaborating with the group of Prof. Jonathan Finley towards microwave-to-optical transduction schemes based on quantum dot molecules in semiconductor heterostructures. Coupling quantum dot molecules to microwave photons in superconducting waveguide resonators via the ac-Stark effect leads to sidebands in the optical spectrum, which can be used for coherent transduction. We have fabricated first test devices and successfully tested the dc properties of the diode structures containing the quantum dot molecules in a hybrid semiconductor-superconductor device.

In summary, we are currently in the process of developing two complementary approaches towards distributing quantum correlations over long distances with a final aim to form hybrid, microwave-microwave and microwave-optical, quantum networks. Two prospective Ph.D. students, **Simon Gandorfer** (remote qubit entanglement) and **Matthias Grammer** (magneto-electro-mechanical transducers), have joined the NeQuS project in order to conduct research along the respective experimental directions, along with the theory support from the Ph.D. student **Joan Agustí**.

References

[1] L. Zhong, E. P. Menzel, R. D. Candia, P. Eder, M. Ihmig, A. Baust, M. Haeberlein, E. Hoffmann, K. Inomata, T. Yamamoto, Y. Nakamura, E. Solano, F. Deppe, A. Marx, and R. Gross, New Journal of Physics **15**, 125013 (2013).

[2] N. Didier, J. Guillaud, S. Shankar, and M. Mirrahimi, Phys. Rev. A **98**, 012329 (2018).

[3] J. Agustí, Y. Minoguchi, J. M. Fink, and P. Rabl, Phys. Rev. A **105**, 062454 (2022).

[4] F. Engelhardt, V. Bittencourt, H. Huebl, O. Klein, and S. V. Kusminskiy, Phys. Rev. Appl. **18**, 044059 (2022).

Munich Center for Quantum Science and Technology Prepares for 2nd Funding Period

Rudolf Gross [1]

The **Munich Center for Quantum Science and Technology (MCQST)** plays a key role for the basic research oriented research program of Walther-Meißner-Institute (WMI) in quantum science and technology (QST). Together with the Collaborative Research Center 631 on «Solid-State Quantum Information Processing» it was the long-term basis of WMI's ambitious research program and provided the preliminary work for a large number of BMBF and EU-funded follow-up projects.

MCQST officially started in January 2019. Now, about four years later, the excellence cluster plays a pivotal role in quantum science not only in the Munich area but also on an international scale. Step by step, MCQST is advancing toward the originally envisioned world-leading center in quantum science and technology. All major Munich research institutions being active in fundamental research are involved in MCQST: LMU München, TUM, Max Planck Institute of Quantum Optics (MPQ), Walther-Meißner-Institute (WMI), as well as Deutsches Museum (DM), which serves as an outreach partner. MCQST is a highly interdisciplinary endeavor, bringing together physicists, mathematicians, computer scientists, chemists, and electrical engineers to work jointly on our structured long-term research program covering all quantum science and technology fields.

Figure 1: The MCQST **Mid-Term Report** published in November 2023.

With flexible funding from the German Research Foundation (DFG) we were able to establish MCQST as a strong supporter for curiosity-driven basic research of all quantum researchers in Munich, providing funding, support programs, outreach, and events. An essential aspect of MCQST is the possibility to provide flexible funding of novel ideas, targeted support for talented young researchers, and various internal support programs. Flexible funding allows MCQST to accelerate the scientific innovation process since the research program can be reoriented rapidly when needed to follow new trends and immediately pursue novel research ideas. This clearly contrasts the R&D program of Munich Quantum Valley, which follows a more or less strict road map and is less flexible due to strong interdependencies between different program parts.

The first four years of MCQST have passed by swiftly, taking the cluster from its initial conceptualization on paper to its vibrant existence. Due to the tremendous passion of all the MCQST members, colleagues, and friends, MCQST has become a true success story. MCQST succeeded in creating a vibrant quantum community in Munich, which attracts students and scientists from around the globe. To give a glimpse into MCQST life, the research done within the cluster, and the scientists doing research, MCQST has compiled a **Mid-Term Report**, summarizing the MCQST activities since 2019. The Mid-Term Report documents the broad scientific achievements, the success of the support programs, and the valuable contributions of MCQST to establishing

[1] Munich Quantum Valley is supported by the Bavarian state government with funds from the Hightech Agenda Bavaria.

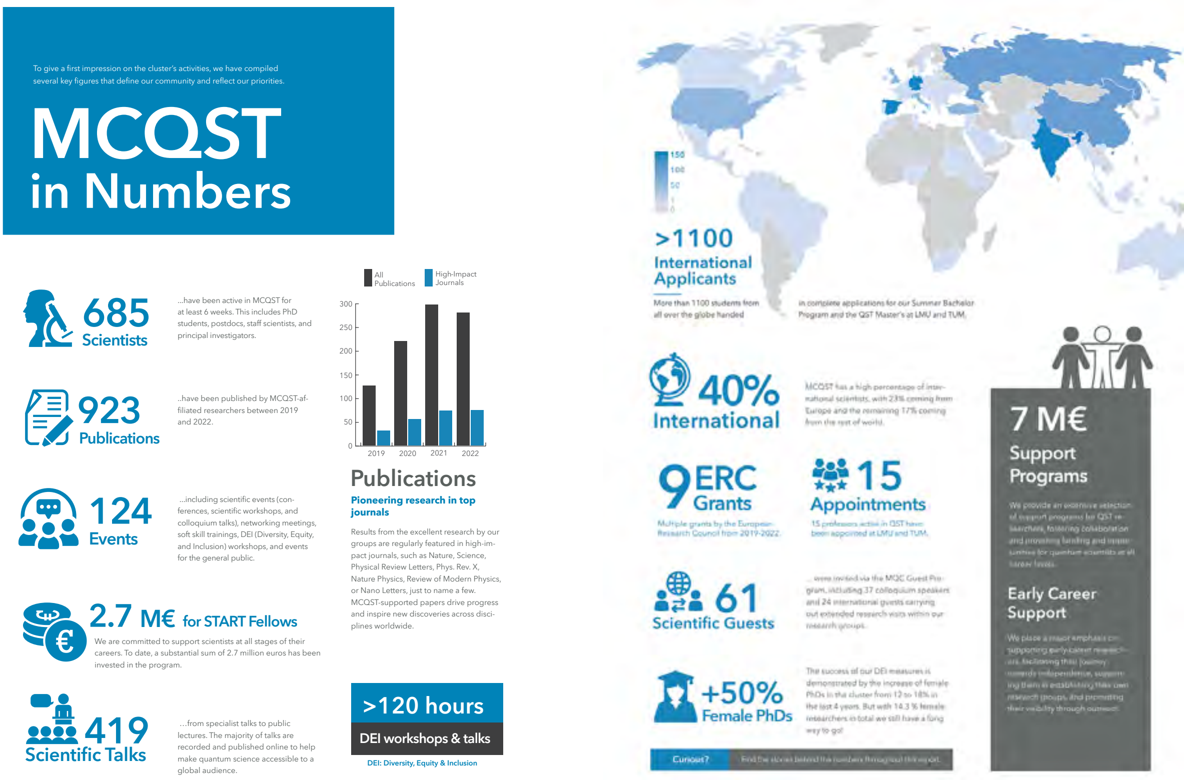

Figure 2: Compilation of several figures and numbers showing the impressive achievements of MCQST in the first four years of its first funding period.

a flourishing quantum ecosystem in Munich. To this end, a major achievement of MCQST was the initiation of Munich Quantum Valley, which was triggered by a strategy paper of the MCQST spokespersons in 2020.

Following the well-known phrase «after the game is before the game» meanwhile, MCQST is already preparing for the German Excellence Strategy's next funding phase (2026–2032). The letter of intent that has to be submitted by the end of January 2024 has already been drafted. For the renewal proposal, the primary objective of MCQST will continue to be focused on discovering and understanding the novel and unifying concepts in the interdisciplinary research fields of QST and making them tangible and practical, as well as on developing extraordinary applications within reach by building next-generation quantum devices. The central focus of MCQST's research remains basic research centered around the concept of entanglement. Given the established scientific surroundings, Munich has never been better suited to address the challenging and highly interdisciplinary scientific objectives of MCQST, emanating from and circulating around quantum entanglement. At the same time, MCQST will broaden and enhance its commitment to nurturing education and providing support for young researchers in QST, building upon the momentum gained in the preceding funding period.

A new focus of MCQST will be on internationalizing its efforts. MCQST plans to foster and enhance interdisciplinary collaborations among the research groups within MCQST and with external partners and offers joint educational programs. Finally, MCQST plans to expand programs that support young scientists at all career stages and actively attract and promote female scientists and other underrepresented groups in the field of QST. The designated spokespersons for the second funding phase are Immanuel Bloch (LMU/MPQ), Ignacio Cirac (MPQ/TUM), and Barbara Kraus (TUM). Rudolf Gross (WMI/TUM) will stay spokesperson until the end of the first funding phase.

Building German Quantum Computing Demonstrators within the BMBF-funded projects MUNIQC-SC and GeQCoS

K. Liegener, S. Filipp [1]

Building quantum computers based on superconducting qubits is an effort that has gained increasing popularity in the recent years and the WMI is actively involved in several projects that investigate the viability and scalability of future quantum devices. Aside from the coordination of the superconducting qubit consortium of the Munich Quantum Valley initiative, the WMI is coordinating two projects, which are supported by the German federal government with the aim to create the first generation of German quantum computing demonstrators.

In the project **"German Quantum Computer based on Superconducting Qubits" (GeQCoS)**, which started in 2021 with a total funding volume of 19 million Euro, the project partners will explore novel ways to realize superconducting qubits and verify their capabilities in a nine qubit demonstrator. The consortium consists of the Forschungszentrum Jülich GmbH, the Karlsruher Institut für Technologie, the Friedrich-Alexander-University, the Fraunhofer Gesellschaft, Infineon Technologies AG, and the WMI (Group S. Filipp), who is coordinating the efforts.

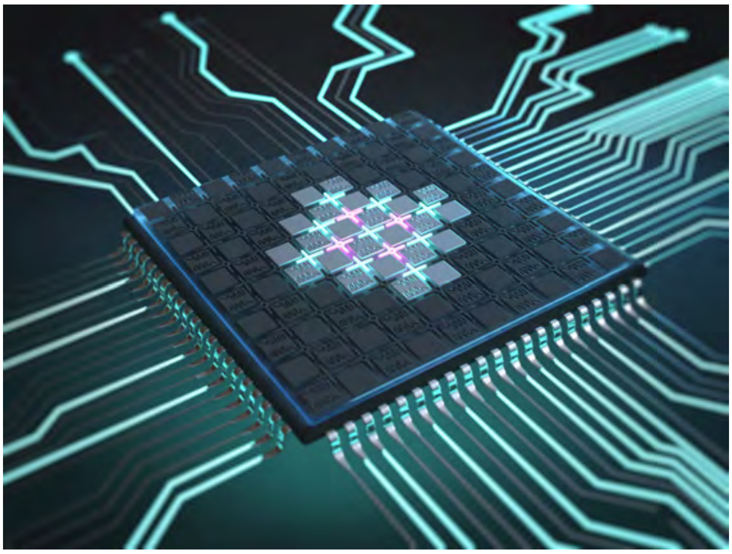

Figure 1: Artistic impression of a quantum processor with improved components developed in the GeQCoS project. (c) C. Hohmann.

Although the complexity and performance of superconducting quantum computers is continuously increasing, an architecture suitable for handling practical problems still requires fundamental improvements. Therefore, the project analyses novel qubit types such as high-frequency qubits and fluxonium qubits, investigates new types of couplers, and aims to enhance the coherence times of qubits by optimizing the fabrication. The key goal is the development of a nine-qubit processor with improved components to be fabricated next year.

The project **"Munich Quantum Valley Quantum Computer demonstrators – Superconducting Qubits" (MUNIQC-SC)** has started in January 2022 with a total budget of 44 million Euro from which 11.5 million Euro go to the TUM Chair of Technical Physics led by Prof. S. Filipp. Its goal is to develop a quantum computing demonstrator with up to a hundred superconducting qubits by the end of 2026. To accomplish this ambitious goal, many crucial challenges related to scaling up quantum computers are addressed by a diverse team of research institutes and industry partners: Friedrich-Alexander University, Fraunhofer-Gesellschaft, Infineon Technologies AG, Leibniz Institute for Innovative Microelectronics, IQM Germany GmbH, Kiutra GmbH, Leibniz Rechenzentrum, Parity Quantum Computing GmbH, TU Munich, and Zürich Instruments.

[1] We acknowledge the funding received for the GeQCoS and MUNIQC-SC initiatives from the Federal Ministry of Education and Research (BMBF) under funding numbers 13N15680 and 13N16188 respectively.

The key innovation directions are the development of a qubit fabrication technology that is suitable for industry, the scaling of a few-qubit devices to larger quantum registers, extended qubit control for high-fidelity operations towards error correction, and the standardization and unification of routine operations. Eventually, it is aimed to make the quantum computing demonstrator available to a broad audience by providing cloud access to quantum computing services via the Leibniz Rechenzentrum high-performance computing center.

Both projects have already reached their first results by fabricating and operating a six-qubit chip at the facilities of the WMI. Its performance excels with properties such as low cross-talk and high single-qubit fidelities. The WMI could recently realize high-quality two-qubit gates with fidelities above 99% (see page 63) and developed improved reset protocols that transfer residual excitations via the couplers (see page 69). Also, investigations on how to enhance qubit read-out via Josephson traveling wave amplifiers as well as improvements on fabrication techniques with qubit coherence now reaching over 500 µs 75 contribute to the efforts of both projects and pave the way towards larger-scale quantum processing units in the upcoming years.

OpenSuperQPlus: Open Superconducting Quantum Computers for Europe

S. Filipp, L. Södergren, M. Werninghaus, Ch. Schneider [1]

Just like its predecessor OpenSuperQ, which was running from 2018 to 2022, the OpenSuperQPlus project is part of the European Quantum Technology Flagship. Lead by the Forschungszentrum Jülich, it brings together in a total of 28 partners from 10 countries. The WMI is contributing with its research on alternative superconducting qubit platforms to test the scalability of fluxonium-based architectures, its expertise in fabricating high coherence qubits, and novel concepts for qubit control.

Figure 1: Logo of the recently started EU flagship project 'OpenSuperQPlus'.

Divided into two 3.5-year project phases, OpenSuperQPlus has an ambitious seven-year agenda with the ultimate goal of a versatile 1,000-qubit quantum-computing system made in Europe. The large-scale consortium anticipates special use cases in quantum simulation for the chemical industry, materials science, or in solving optimization problems and in machine learning. The first phase of the project 'OpenSuperQPlus100', which aims to build and test a 100 superconducting qubit platform, has started in March 2023. In this first 3.5-year phase, a working prototype of a 100-qubit processor, as well as critical components for the next phase aiming towards 1000 qubits, will be developed and evaluated.

The WMI plays a key role in this effort. Its goal is to develop a quantum processor unit based on alternative, fluxonium-type qubits. The WMI focus lies on high-quality operations and on the scalability of the alternative-qubit platform with the main objective to make an informed decision on the platform for the next-generation 1000-qubit QPU. To reach this milestone, the WMI combines basic and exploratory research on novel devices with the technology development required for scalability. It will investigate novel materials and fabrication recipes to reach highest quality superconducting quantum circuits with small footprints. In addition, the WMI will explore ways to optically control qubits, such mitigating the imminent bottleneck created by the large number of individual control and readout lines for thousand and more qubits. Finally, the WMI plans to provide remote access to the QPUs and to develop system integration capabilities in collaboration with the Leibniz Rechenzentrum (LRZ).

In the first project months, WMI has set up collaborations with the project partners. To enhance the scalability of the quantum processors, we are collaborating with our theory partners Mikel Sanz and Pablo Garcia, who visited for a four-week research stay in autumn 2023 at the University of the Basque Country (UPV/EHU) to optimize qubit designs for suppressed crosstalk. We have also started a collaboration with VTT Finland on alternative control methods of qubits with the aim of developing optical control methods and single-flux quantum logic controllers to realize single and two-qubit gates. The first infrastructure for optical measurement and control is currently being built. Moreover, we have successfully characterized the first uncoupled fluxonium chips reaching single qubit gate fidelities of more than 99.9% and readout fidelities above 98% in collaboration with the national research projects described on page 28. Moreover, WMI is exploring flux-pulse-based reset schemes, wherein the fluxonium is pulsed to high frequencies, at which it thermalizes with the environment. With the

[1] We acknowledge the funding received from the European Union via the project 101113946 OpenSuperQPlus100.

flux pulsed reset schemes, WMI has managed to attain very low residual excited state populations which could be further reduced by an active reset approach. In order to provide remote access to our QPUs, the first remote experiments have been carried out on a 6-transmon plus 6-tuneable coupler chip and the software integration into the Leibniz Supercomputing Centre is progressing.

Based on the technologies developed within the national projects and with the large European partner network provided by the OpenSuperQPlus project, we are confident that we can significantly contribute and become a major player not only at the national, but also at the European level.

QuaMToMe: Towards Microwave Quantum Tokens

Nadezhda Kukharchyk, Kirill G. Fedorov, Hans Huebl [1]

The "**Qua**ntum **M**icrowave **To**kens & **Me**mories" (QuaMToMe) project participates in the ***Grand Challenge of Quantum Communications (GCQK)*** organized by BMBF. The Challenge includes 6 experimental projects complemented by one supporting theoretical project. The *'challenge'* aspect of the program implies a competition between the experimental projects with the goal to develop and determine the most reliable quantum token. The QuaMToMe project consists of 3 subprojects led by principal investigators of the WMI and is coordinated by N. Kukharchyk.

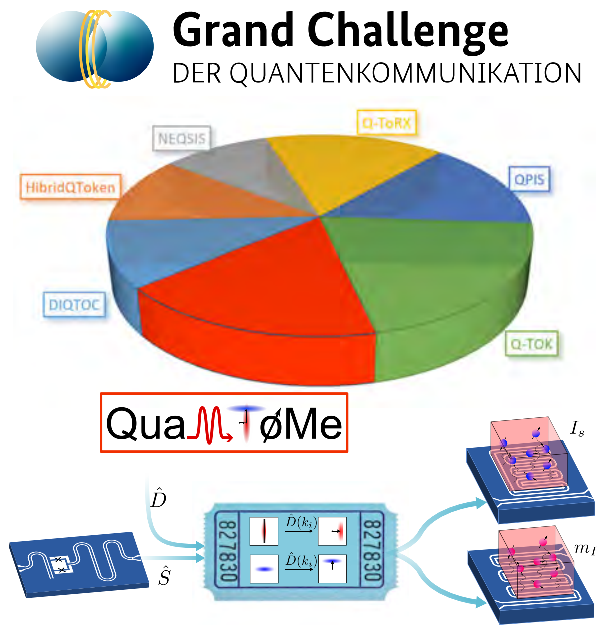

Figure 1: The structure of the "Grand Challenge of Quantum Communications" research program with the QuaMToMe project being one out of seven projects.

Although the experimental challenge has already started, the concept of a reliable quantum token is being actively disputed since it should comply with both, quantum science and IT security requirements. Within the effort of GCQK, the quantum token is understood as a quantum-secure identification key. The simplest classical example is an online banking login procedure. In order to use the online banking account, one should had received a username (ID) and a password (key-token) from a bank and should be able to use it multiple times. High protection levels of such key-tokens are conventionally achieved with modern encryption methods (RSA, ECC, DSA) [1], but are currently being threatened by the advent of quantum computing, capable of efficiently breaking these cryptographic algorithms. This motivated the search for new encryption protocols, which will be robust against quantum computers [2]. One of such approaches is known as *'post-quantum cryptography'* [3], which is looking for new classical mathematical solutions. Another approach is to to make use of quantum technologies, which guarantee unconditional security under certain conditions between classical parties ['quantum-enhanced security', e.g. by quantum key distribution (QKD)] or between quantum parties, such as quantum computers ('quantum-enabled security'). While QKD is one of the most developed methods in quantum communication, approaches based on bypassing the need of key distribution are also being actively studied, with a prominent example being the use of a **quantum token** aiming at multi-usage of once issued secure keys.

The concept of quantum tokens began with the *'Quantum money'* paper by S. Wiesner [4] and has been developed over the years of research beyond the simple 'money' idea towards secure identification tool. In the context of the GCQK projects, a quantum token can be viewed as a quantum memory-based element, which allows for multi-usage of a once issued quantum-secure token and enables quantum physically unclonable functions (qPUF). Details of various qPUF scenarios and their reliability can be found in the overview by the Q.TOK project.

Within the QuaMToMe project, we investigate purely microwave quantum tokens, which can be later implemented in quantum-secure 5/6G communication protocols, directly compatible

[1] This project is part of the "Grand Challenge of Quantum Communication program" of BMBF, grant number 16KISQ036.

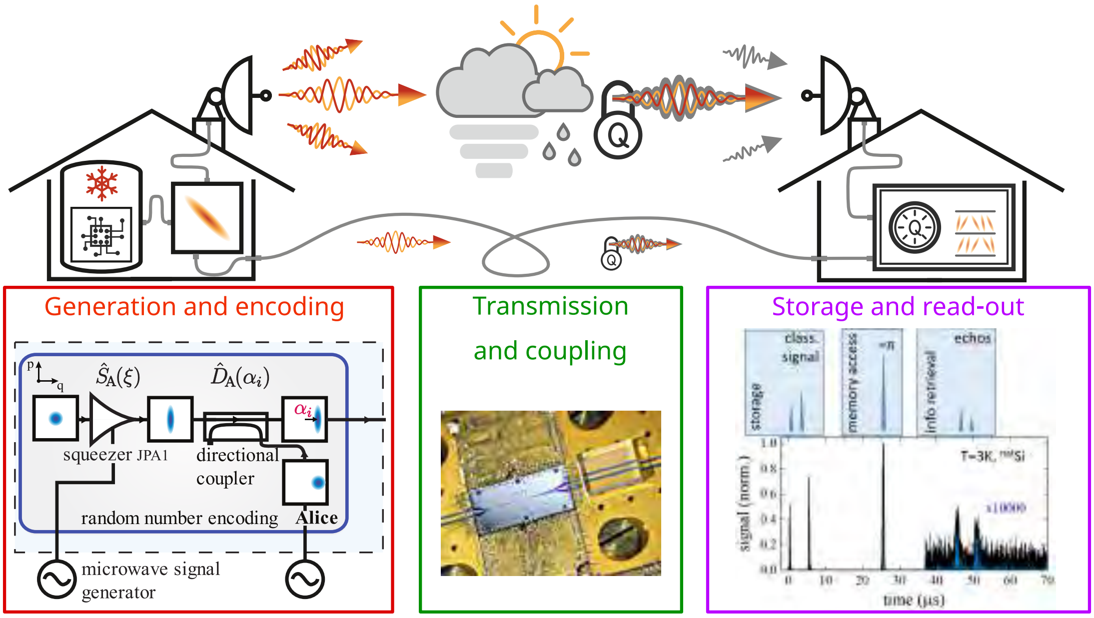

Figure 2: Overview of the QuaMToMe general idea. Generation of quantum token states is performed with superconducting microwave circuits based on JPAs. The token states are then to be stored and read out from the spin quantum memories using the spin echo techniques.

for identification with superconducting quantum systems or feasible for near-distance open-air communication [5]. The quantum token states are generated with superconducting circuits based on Josephson parametric amplifiers (JPAs). The key here is encoded into displacement amplitudes of squeezed microwave states, which can be further stored in quantum memories by using multiplexing in the time or frequency domains. The actual quantum memories are realized by spin ensembles with transition frequencies in the GHz range. At present, we pursue two approaches: the storage of keys in the ^{167}Er rare-earth ion spin ensemble coupled to a broadband transmission line [6] and in the isotopically-engineered ^{28}Si:P donor spin-ensemble coupled to a microwave resonator [7]. We are investigating the coherence times of these spin systems in dependence on the squeezing and displacement amplitudes of the coupled microwave states. Since, the operation of JPAs require a protected magnetic environment, while the spin memories rely on rather strong magnetic fields, we are also developing new ways to isolate superconducting circuits from strong magnetic fields. Here, possible approaches include using complex compensation magnetic coils or multilayer superconducting shields.

References

[1] S. Al Busafi, and B. Kumar. Review and Analysis of Cryptography Techniques. In **2020 9th International Conference System Modeling and Advancement in Research Trends (SMART)**, 323–327 (2020).

[2] P. Wallden, and E. Kashefi, Communications of the ACM **62**, 120 (2019).

[3] R. Bavdekar, and et al. Post Quantum Cryptography: A Review of Techniques, Challenges and Standardizations. In **2023 International Conference on Information Networking (ICOIN)**, 146–151 (2023).

[4] S. Wiesner, SIGACT News **15**, 78–88 (1983).

[5] F. Fesquet, F. Kronowetter, M. Renger, Q. Chen, K. Honasoge, O. Gargiulo, Y. Nojiri, A. Marx, F. Deppe, R. Gross, and K. G. Fedorov, Phys. Rev. A **108**, 032607 (2023).

[6] A. Mladenov, N. Pankratova, D. Sholokhov, V. Manucharyan, R. G. P. A. Bushev, and N. Kukharchyk. Microwave cavity-free hole burning spectroscopy of Er^{3+}:Y_2SiO_5 at millikelvin temperatures. `arXiv:2206.03135 [quant-ph]` (2022).

[7] S. Weichselbaumer, M. Zens, C. W. Zollitsch, M. S. Brandt, S. Rotter, R. Gross, and H. Huebl, Phys. Rev. Lett. **125**, 137701 (2020).

EU Horizon 2020 - Superconducting Quantum Local Area Networks

J. Agusti, S. Gangdorfer, K. Fedorov, R. Gross, P. Rabl

Superconducting quantum circuits are one of the most promising platforms for realizing large-scale quantum computing devices, where in the near future a coherent integration of 100-1000 qubits is feasible. However, the required temperatures of only a few mK currently restrict quantum operations to qubits that are located within a single, heavily shielded dilution refrigerator. This imposes a serious constraint on the realization of even larger quantum processors or the implementation of local- and wide-area quantum networks based on this technology.

The European project **SuperQuLAN** was set out to address this important open problem by developing key network components and quantum communication protocols that will facilitate in the long term the realization of large quantum computing clusters or even city-wide quantum networks using superconducting circuits. The two main objectives are (i) to demonstrate a first operational prototype quantum local area network (QuLAN) of separated superconducting quantum processors and (ii) to realize a quantum-coherent interface between microwave and optical photons for future long-distance quantum communication applications.

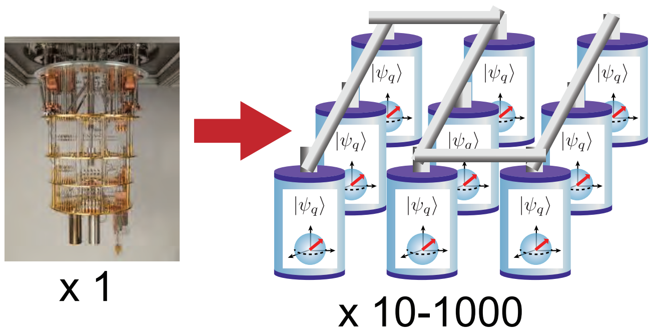

Figure 1: The technological vision behind the SuperQuLAN project. Multiple dilution refrigerators, each hosting a superconducting quantum processor, are coupled in a scalable and modular way into a larger quantum local area network. This can be achieved either via a direct cryogenic quantum link [1, 2] or via a coherent interface to optical photons [3].

The SuperQuLAN project started in September 2020 as a collaboration between TU Wien, CSIC, ETH Zurich, IST Austria, the MPQ in Garching, and Zurich Instruments. With the move of Peter Rabl from Vienna to Munich in the beginning of 2023, the WMI was added as an additional partner to the project. This addition was very beneficial for the project. Apart from a continuation of the theory work on quantum communication schemes, the already existing 6 m long quantum link device [3] developed by the team of Kirill Fedorov and Rudolf Gross is ideally suited to carry out quantum network demonstration experiments. While the SuperQuLAN project ended already in August 2023, this time was used to initiate a new research line on distributed qubit-photon and qubit-qubit entanglement, which is carried out in close collaboration between the Ph.D. students Simon Gangdorfer (experiment) and Joan Agusti (theory).

References

[1] P. Magnard, S. Storz, P. Kurpiers, J. Schär, F. Marxer, J. Lütolf, T. Walter, J.-C. Besse, M. Gabureac, K. Reuer, A. Akin, B. Royer, A. Blais, and A. Wallraff, Phys. Rev. Lett. **125**, 260502 (2020).

[2] M. Renger, S. Gandorfer, W. Yam, F. Fesquet, M. Handschuh, K. E. Honasoge, F. Kronowetter, Y. Nojiri, M. Partanen, M. Pfeiffer, H. van der Vliet, A. J. Matthews, J. Govenius, R. N. Jabdaraghi, M. Prunnila, A. Marx, F. Deppe, R. Gross, and K. G. Fedorov. Cryogenic Microwave Link for Quantum Local Area Networks. arxiv:2308.12398 [cond-mat, physics:physics, physics:quant-ph] (2023).

[3] R. Sahu, L. Qiu, W. Hease, G. Arnold, Y. Minoguchi, P. Rabl, and J. M. Fink, Science **380**, 718–721 (2023).

Interfacing Spins and Superconducting Qubits - A New Collaboration with ETH Zurich

P. Rabl

In November 2023, the **SNSF Sinergia grant** ***«An acoustic quantum interface for circuits and spins»*** (**AcQuaInt**) was funded by the Swiss National Science Foundation (SNSF). This four-year-long research project is led by Prof. Yiwen Chu from ETH Zurich and involves the WMI as an external partner. The overall goal of this project is to demonstrate a quantum interface between a superconducting qubit and spin qubits associated with silicon-vacancy (SiV) color centers in diamond. The coupling between these two very dissimilar systems will be mediated by the quantized phonon modes of a bulk acoustic resonator, which couples to the superconducting qubit via the piezoelectric effect and to the spins via strain. If successful, such an interface can be used to realize a hybrid quantum computing architecture, where quantum information is processed using fast transmon qubits while during idle times the quantum states are stored in long-lived spin degrees of freedom.

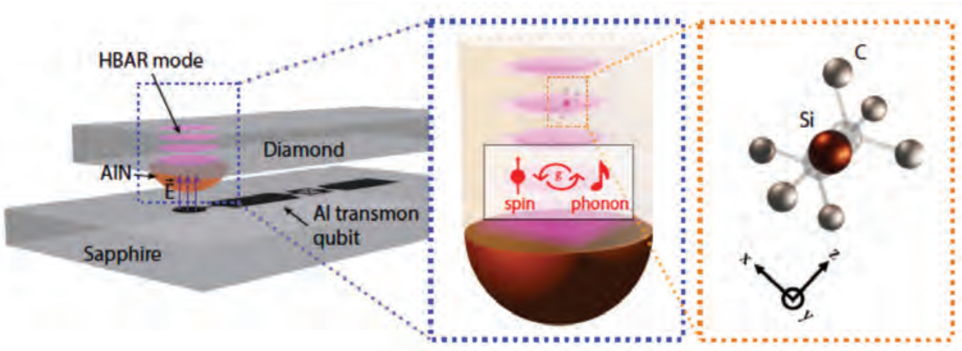

Figure 1: Bulk acoustic wave interface between a SC qubit and a SiV center in diamond. Left: a schematic of the device. A piezoelectric material such as AlN couples the electric field of the transmon superconducting qubit and the strain field of an HBAR mode. Middle: The strain field also deforms the diamond lattice surrounding the SiV center, resulting in a coupling to the spin qubit through the spin-orbit interaction. Right: Structure of the SiV center, showing the substitutional Si atom in a split-vacancy configuration.

While the experimental implementation of the acoustic interface will be mainly carried out by the groups of Prof. Yiwen Chu and Prof. Christian Degen at ETH Zurich, the Theory Division at WMI, led by Peter Rabl, will be responsible for modeling the system and for developing optimized transfer protocols, which are compatible with the weak spin-phonon couplings and relevant decoherence processes in the system. Here, the team can build on the existing expertise in the group on spin-phonon interactions, phononic quantum networks, and noise-mitigation strategies.

New Transregional Collaborative Research Center on Constrained Quantum Matter (ConQuMat)

H. Huebl and S. Geprägs

The Transregional Collaborative Research Center **'Constrained Quanutum Matter (ConQuMat)'** started in October 2023 and brings together researchers at the University of Augsburg, the Technical University of Munich, the Max Planck Institute for Solid State Physics, the University of Leipzig, the University of Tokyo, and the Walther-Meissner-Institute of the Bavarian Academy of Sciences and Humanities. In 18 projects, 32 PhD and postdoctoral researchers will address questions on magnetic band topology, entangled states of matter, and non-equilibrium dynamics in selected solid-state systems.

Figure 1: Logo of the recently started Transregional Collaborative Research Center on 'Constrained Quantum Matter'.

The research center as a whole is based on the recent advances in the understanding of the organizing principles of quantum matter, alongside breakthrough developments of experimental methodology, which provide an excellent starting point for research on the design and control of emergent quantum phases. At the same time, complex quantum materials are developing into a powerful platform for the exploration of conceptual challenges from quantum information theory to non-equilibrium physics. The Transregio on Constrained Quantum Matter (ConQuMat) will address such challenges by creating, detecting, and controlling novel quantum states via carefully chosen constraints, including spin-momentum locking, gauge structures, and kinetic constraints. The basic guiding principle is that a reduction of the degrees of freedom through suitable constraints can yield exciting physical phenomena. Our approach will facilitate the realization as well as detection of quantum entanglement and the exploration of novel quantum effects in solid-state materials with the long-term goal of stabilizing them at practical conditions, thus fostering applications on a broad scale. To reach this goal, ConQuMat will bring together key expertise in three major directions of quantum matter research - magnetic band topology, entangled states of quantum matter, and non-equilibrium dynamics - each of them representing one research area. The individual projects within these three pillars will contribute to the mission by exploring the interplay between the constraints above from different vantage points.

At the Walther-Meissner-Institute, a team around Hans Huebl and Stephan Geprägs will team up with Christian Pfleiderer and Mark Wilde from the Natural School of Sciences of the Technical University of Munich to investigate the properties of quantum materials in non-equilibrium using multiple excitation and detection techniques. For example, we plan to drive low-energy excitations by intense microwave radiation while the response function is probed with a second probe. This approach aims at (i) investigating and understanding the coupling between spin, orbital, lattice or nuclear spin degrees of freedom under intense resonant microwave radiation, (ii) a targeted driving of quantum excitations such as topological magnons, orbitons or topological electronic quasiparticles, (iii) inducing non-thermal melting of long-range order by intense microwave radiation, and (iv) realization of dynamical forms of quantum order in bulk materials such as time crystals or many-body localization.

We are excited to start this project dedicated to exploring quantum physics and signatures in quantum materials.

Basic Research

Autonomous Distribution of Multi-Partite Entanglement

J. Agusti, X. H. H. Zhang, P. Rabl [1]
Y. Minoguchi [2]

As quantum computing and quantum communication systems with an increasing number of coherently integrated components become technologically available, there is a growing demand for efficient schemes to transfer quantum states or distribute entanglement across different parts of such networks. While basic protocols to do so are well-known [1] and have already been successfully implemented in a variety of platforms, it is envisioned that in future quantum devices, entanglement must be generated and interchanged among many thousands of qubits within a limited coherence time. It is currently considered unlikely that a simple serial application of existing protocols can meet these demands, which motivates the continued search for alternative quantum communication strategies that are fast, parallelizable, and, ideally, require a minimal amount of classical control.

In order to address this challenge, we have proposed and analyzed a scalable and fully autonomous scheme for preparing spatially distributed multi-qubit entangled states in a dual-rail waveguide QED setup [2]. In this approach, illustrated in Fig. 1, arrays of qubits located along two separated waveguides are illuminated by correlated photons from the output of a non-degenerate parametric amplifier. Such sources of propagating entangled photonic beams have recently been successfully implemented in the quantum link experiment at the WMI [3]. In our theoretical analysis we have shown that these photons can drive distant qubits into different classes of pure entangled steady states, for which the degree of multipartite entanglement can be conveniently adjusted by the chosen pattern of local qubit-photon detunings.

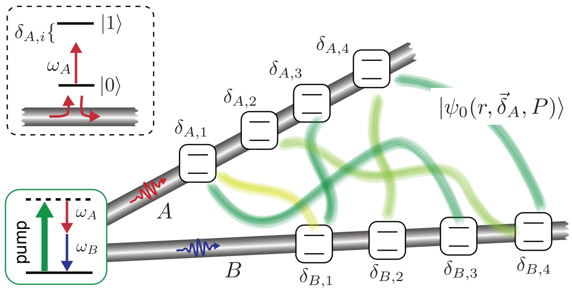

Figure 1: Sketch of a dual-rail quantum network, where qubits along two separated waveguides are driven by the correlated output of a non-degenerate parametric amplifier and relax into a pure steady state $|\psi_0(r,\vec{\delta}_A,P)\rangle$. As shown in the inset, the qubits in waveguide A (B) are detuned from the central photon frequency ω_A (ω_B) by $\delta_{A,i}$ ($\delta_{B,i}$) and the qubit-waveguide coupling is assumed to be fully directional.

More specifically, under ideal conditions this scheme drives an arbitrary number of N qubit pairs into the pure stationary state

$$|\psi_0(r,\vec{\delta}_A,P)\rangle = \prod_{\sigma} U_{i_\sigma,i_\sigma+1} \bigotimes_{i=1}^{N} |\Phi_{i,i}^+\rangle \, , \tag{1}$$

where $|\Phi_{i,i}^+\rangle \simeq (|0_{A,i}\rangle|0_{B,i}\rangle + |1_{A,i}\rangle|1_{B,i}\rangle)/\sqrt{2}$ is close to a maximally entangled Bell state for two qubits in different waveguides. The unitary transformations $U_{i_\sigma,i_\sigma+1}$ depend on the individual detunings $\delta_{A,i}$ and $\delta_{B,i}$ and create additional entanglement along the chain. As a result, one can switch between pair-wise entangled and fully multi-partite entangled states by simply adjusting the qubit frequencies.

[1] We acknowledge support by the German Research Foundation (522216022) and by the European Union's Horizon 2020 research and innovation program under grant agreement No. 899354 (SuperQuLAN). This research is part of the Munich Quantum Valley, which is supported by the Bavarian state government with funds from the Hightech Agenda Bayern Plus.
[2] Vienna Center for Quantum Science and Technology, Atominstitut, TU Wien, 1020 Vienna, Austria

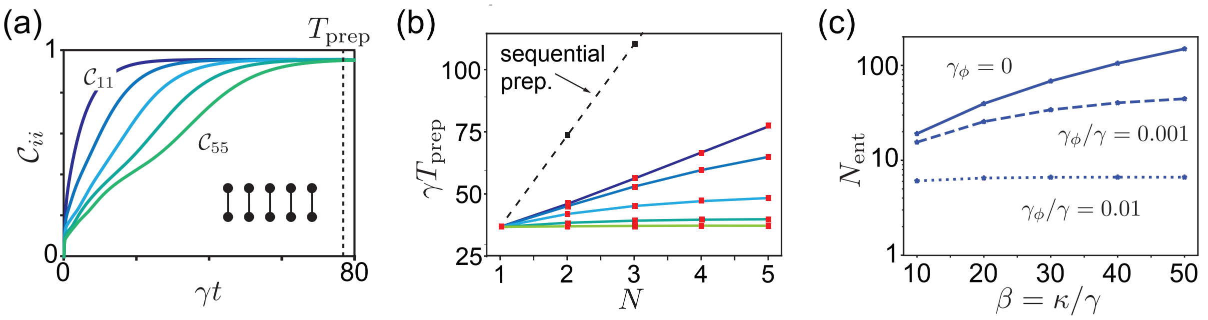

Figure 2: (a) Relaxation dynamics into a bipartite entangled state for $N = 5$ pairs of qubits, where the concurrence $\mathcal{C}_{ii}$ of the reduced two-qubit state $\rho_{A,i;B,i}$ is used as a measure for entanglement. (b) Scaling of the preparation time $T_{\rm prep}$ to reach the stationary state for different detuning patterns. This scaling is compared to the sequential preparation of one entangled pair at a time (dashed line). (c) Maximal number of entangled pairs that can be simultaneously entangled by this scheme, $N_{\rm ent}$, as a function of the amplifier bandwidth κ and the qubit dephasing rate γ_ϕ. Here γ is the rate at which the qubits decay into the waveguide.

While the existence of such highly entangled, but still analytically tractable multi-qubit states is of interest on its own, in the limit of a large amplifier bandwidth we have numerically simulated the build-up of entanglement along the chain [see Fig. 2 (a)] and identified detuning configurations, where the preparation time $T_{\rm prep}$ scales sub-linearly with the number of entangled qubit pairs, N. This behaviour is illustrated in Fig. 2 (b) and shows that under otherwise ideal conditions, this entanglement distribution scheme can be fully parallelized and be used to achieve a significant speed-up compared to sequential preparation of individual pairs [4, 5]. As shown in Fig. 2 (c), even for a finite bandwidth and realistic decoherence processes, one can still benefit from this intrinsic speed up and entangle up to $N_{\rm ent} \sim 10 - 100$ qubit pairs simultaneously.

Conclusion and outlook

In summary, our scheme represents a simple method to distribute multi-partite entanglement in large networks, by making use of a single entangled photon sources only and without relying on any precise time-dependent control pulses. The scheme is completely general and can find applications in optical, microwave or hybrid quantum networks, where such two-mode squeezed photonic sources are currently developed. At the WMI, the quantum link setup [3] developed by the team of K. Fedorov and R. Gross is an ideal setup for testing this scheme with superconducting qubits that are coupled to quantum-correlated microwave channels.

References

[1] J. I. Cirac, P. Zoller, H. J. Kimble, and H. Mabuchi, Phys. Rev. Lett. **78**, 3221–3224 (1997).
[2] J. Agusti, X. H. H. Zhang, Y. Minoguchi, and P. Rabl. Autonomous distribution of programmable multi-qubit entanglement in a dual-rail quantum network. Accepted for publication in Phys. Rev. Lett., `arXiv:2306.16453` (2023).
[3] K. G. Fedorov, M. Renger, S. Pogorzalek, R. D. Candia, Q. Chen, Y. Nojiri, K. Inomata, Y. Nakamura, M. Partanen, A. Marx, R. Gross, and F. Deppe, Sci. Adv. **7**, eabk0891 (2021).
[4] B. Kraus, and J. I. Cirac, Phys. Rev. Lett. **92**, 013602 (2004).
[5] J. Agustí, Y. Minoguchi, J. M. Fink, and P. Rabl, Phys. Rev. A **105**, 062454 (2022).

Dissipative Bosonic Transport

L. Garbe, P. Rabl [1]
Y. Minoguchi, J. Huber [2]

Transport phenomena are of relevance for almost all areas of physics and technology with transport of electric currents and heat conduction in solids being two prototypical examples. However, there is also considerable interest in the analysis of other elementary models, which capture essential aspects of transport in terms of simplified abstractions of broader classes of physical processes. In two recent publications [1, 2], we have analyzed the dissipative transport of bosonic particles along a one-dimensional lattice with asymmetric hopping rates [see Fig. 1 (a)]. This process can be seen as the bosonic counterpart of the celebrated asymmetric simple exclusion process (ASEP) [3], a common model for directed transport of fermions or classical hard-core particles. In stark contrast to fermions, bosonic transport is enhanced by the presence of other particles and one speaks of an asymmetric simple inclusion process (ASIP) instead.

Transport and condensation

In the absence of any coherent interactions, the dissipative transport of bosons is described by a master equation of the form

$$\dot{\rho} = \sum_{i=1}^{L-1} \gamma_- \mathcal{D}[a_i^\dagger a_{i+1}]\rho + \gamma_+ \mathcal{D}[a_{i+1}^\dagger a_i]\rho \quad (1)$$

where a_i are bosonic annihilation operators for the i-th lattice site, γ_- (γ_+) is the hopping rate to the left (right) and $\mathcal{D}[c]\rho = c\rho c^\dagger - \frac{1}{2}\{c^\dagger c, \rho\}_+$. This master equation implies that the rate for a particle to jump from site i to site $i-1$ depends on the occupation number of the target site, i.e, $R_{i\to i-1} = \gamma_-(n_{i-1}+1)n_i$. This is a direct consequence of the bosonic particle statistics and makes the transport nonlinear.

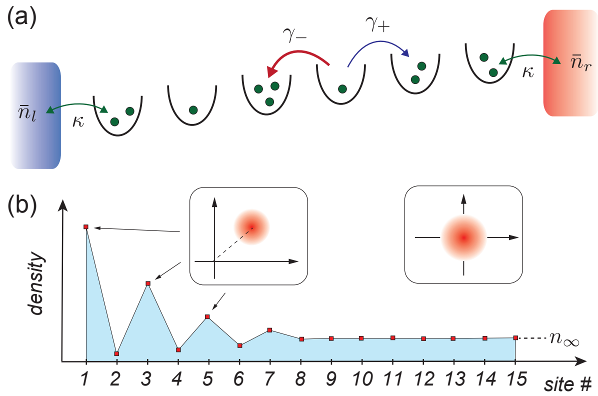

Figure 1: (a) Bosons injected from a thermal particle reservoir on the right can incoherently hop along the lattice with asymmetric rates $\gamma_\pm$, before being emitted into a second reservoir on the left. (b) Under stationary conditions, this hopping asymmetry combined with the bosonic particle statistics results in the formation of a finite boundary region with a staggered density profile. The two insets show sketches of the Wigner function for individual lattice sites, indicating that within this boundary region, the odd sites are in a condensed state with broken $U(1)$ symmetry, while all other lattice sites exhibit a thermal distribution.

When the chain is coupled to two thermal particle reservoirs, a stationary average current $\langle J \rangle$ flows through the lattice, which for symmetric hopping $\gamma_- = \gamma_+$ exhibits the usual Fourier law, $\langle J \rangle \sim 1/L$. For asymmetric hopping, this behavior can change drastically and we find that as the current increases, the system can undergo a transition into a highly unusual transport phase, which is characterized by a staggered density profile near the boundary of the lattice [see Fig. 1

[1] We acknowledge support by the European Union's Horizon 2020 research and innovation program under grant agreement No. 899354 (SuperQuLAN). This research is part of the Munich Quantum Valley, which is supported by the Bavarian state government with funds from the Hightech Agenda Bayern Plus.

[2] Vienna Center for Quantum Science and Technology, Atominstitut, TU Wien, 1020 Vienna, Austria

(b)]. A closer inspection shows [1] that in this region the local particle distribution alternates on every site between a thermal distribution and a Bose-condensed state with broken $U(1)$-symmetry.

Transport fluctuations and KPZ universality

Going beyond average quantities, we have analyzed the full counting statistics of the ASIP [2], starting from a configuration, where one half of the lattice is filled with exactly one particle per site, while the sites $i > 0$ are empty. A quantity of interest is $\mathcal{N}(t) = \sum_{i>0} n_i(t)$, which is the total number of particles transported across the site $i = 0$. Numerical simulations of $\mathcal{N}(t)$ are plotted in Fig. 2 (a) and compared with the cases of fermions and classical particles.

To model the statistics of $\mathcal{N}(t)$, we took the hydrodynamic limit and showed that the particle density $n(x,t)$ is described by a stochastic Burgers equation of the form

$$\partial_t n + \gamma(1+2\sigma n)\partial_x n = \nu\partial_x^2 n - \partial_x \xi, \qquad (2)$$

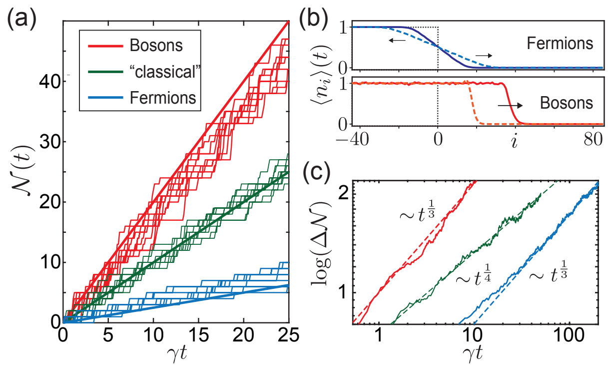

Figure 2: (a) Individual realizations of the total number of transported particles, $\mathcal{N}(t)$, for bosons ($\sigma = 1$), fermions ($\sigma = -1$) and independent classical particles ($\sigma = 0$). (b) Evolution of the average density profiles for bosons and fermions. (c) Scaling of the fluctuations $\Delta\mathcal{N}^2(t) = \langle\mathcal{N}^2(t)\rangle - \langle\mathcal{N}(t)\rangle^2$. For all plots $\gamma_+ = \gamma$ and $\gamma_- = 0$ have been assumed.

where the noise $\xi(x,t)$ is δ-correlated in space and time. By neglecting this noise, the deterministic Burgers equation describes well the average density profiles shown in Fig. 2 (b), with an average bosonic current $j_{\sigma=+1} = 2\gamma$ that is eight times larger than the fermionc current $j_{\sigma=-1} = \gamma/4$.

Taking fluctuations into account, we can use the scaling ansatz $\mathcal{N}(t) = j_\sigma t + (\Gamma_\sigma t)^\beta \eta$, where η is a time-independent random variable. From numerical Monte-Carlo simulations we extracted the scaling exponent β and the full probability distribution $P(\eta)$. Surprisingly, in spite of the drastic difference in the underlying particle statistics, the bosonic currents exhibit the same scaling exponent $\beta = 1/3$ as the ASEP for fermions and therefore belong to the Kadar-Parisi-Zhang (KPZ) [4] universality class. However, crucial differences between the two processes emerge when focusing on the full counting statistics, $P(\eta)$. By mapping both models to the physics of fluctuating interfaces, we found that dissipative transport of bosons and fermions can be understood as surface growth and erosion processes, respectively. Within this unified description, both the similarities and discrepancies between the full counting statistics of the transport are reconciled [2]. Beyond purely theoretical interest, these findings are relevant for experiments with cold atoms or long-lived quasi-particles in nanophotonic lattices, where such transport scenarios can be realized.

References

[1] L. Garbe, Y. Minoguchi, J. Huber, and P. Rabl. The bosonic skin effect: boundary condensation in asymmetric transport. Accepted for publication in SciPost Phys., arXiv:2301.11339 (2023).
[2] Y. Minoguchi, J. Huber, L. Garb, A. Gambassi, and P. Rabl. A Unified Interface Model for Dissipative Transport of Bosons and Fermions. arXiv:2311.10138 (2023).
[3] T. Kriecherbauer, and J. Krug, J. Phys. A Math. Theor. **43**, 403001 (2010).
[4] M. Kardar, G. Parisi, and Y.-C. Zhang, Phys. Rev. Lett. **56**, 889–892 (1986).

Fast and Robust Quantum State Transfer

P. Zielinski, A. Batool, J. Agusti, P. Rabl [1]
Y. Minoguchi [2], *I. Arrazola* [3]

The transfer of quantum states between two distant nodes of a quantum network is an essential task for many quantum communication applications. As first discussed by Cirac *et al.* [1], this task can be implemented in a fully deterministic manner by mapping the local quantum state onto a 'flying' photonic qubit, which can travel over long distances before being coherently reabsorbed at the receiving node. However, there are still many open questions about how to realize such state transfer schemes most efficiently, in particular when going from the optical regime to microwave [2] or phononic [3] quantum networks.

Ultrafast quantum communication

Quantum interfaces are usually discussed under the premise that the coupling between the stationary qubits and the propagating photons is weak compared to the absolute energy scales. In microwave quantum networks, where the so-called ultrastrong-coupling regime of cavity QED can be reached [4], this is not necessarily the case anymore and gives rise to intriguing questions about the ultimate speed limit for quantum communication.

The theory group at the WMI has developed a numerical framework to study quantum communication protocols in the ultrastrong-coupling regime. Under these conditions, conventional quantum state transfer protocols are no longer applicable and effects beyond the rotating wave approximation must be fully taken into account. In our numerical simulations we are able to simulate long chains of coupled oscillators, representing the waveguide, and find optimized control pulses that implement a faithful transfer of quantum states between the first and the last site. Importantly, as shown in Fig. 1, this transfer can happen on a timescale $t_f \approx \omega_0^{-1}$, where $\omega_0 \approx 5\,\mathrm{GHz}$ is the typical oscillation frequency. Although detailed investigations are still ongoing, this result already implies that the transfer can be about 100 times faster than the current state of the art in the field of superconducting circuits.

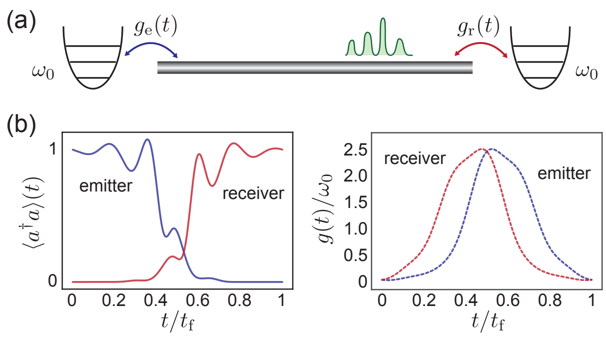

Figure 1: (a) Sketch of a quantum network with an emitting and a receiving node connected by a transmission line. At the two ends, the time-dependent couplings $g_e(t)$ and $g_r(t)$ enable a controlled emission and reabsorption of an arbitrary quantum state. (b) Illustrative example for the numerically optimized transfer of a state with one excitation from the emitting node to the receiving node. The plot on the right shows the corresponding control pulses. For this example, the waveguide is represented by $N = 100$ oscillator modes and the total transfer time is about $t_f \simeq 2\pi/\omega_0$.

[1] We acknowledge support by the German Research Foundation (522216022) and by the European Union's Horizon 2020 research and innovation program under grant agreement No. 899354 (SuperQuLAN). This research is part of the Munich Quantum Valley, which is supported by the Bavarian state government with funds from the Hightech Agenda Bayern Plus.

[2] Vienna Center for Quantum Science and Technology, Atominstitut, TU Wien, 1020 Vienna, Austria
[3] Instituto de Física Teórica, UAM-CSIC, Universidad Autónoma de Madrid, Cantoblanco, 28049 Madrid, Spain

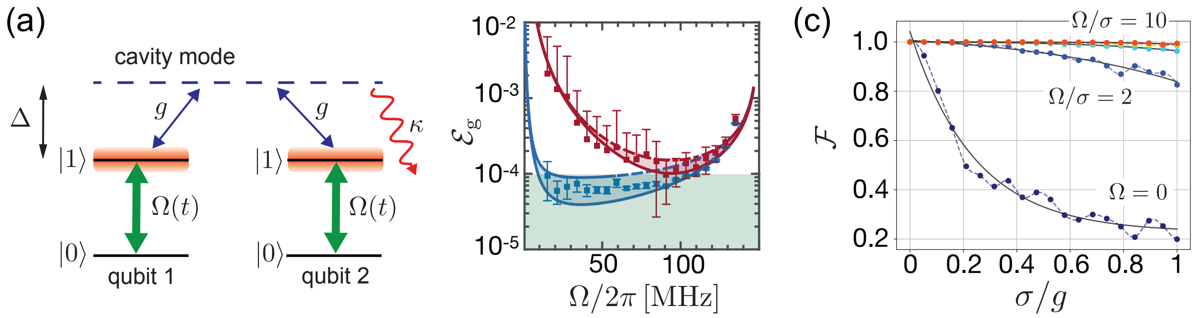

Figure 2: (a) Continuous dynamical protection of a cavity-mediated two-qubit gate. The right plot shows the expected reduction in the gate error $\mathcal{E}_g$ as a function of the Rabi-frequency for a specific application of this scheme. (b) Plot of the average fidelity $\mathcal{F}$ of a dynamically protected quantum state transfer protocol over long distances. Here, σ characterizes the strength of the random fluctuations of the qubit frequencies in both nodes. We see a drastic improvement of the fidelity compared to the unprotected case, $\Omega = 0$.

Dynamically protected qubit-photon interfaces

In solid-state systems, ubiquitous low-frequency noise or slow parameter drifts represent a major source of decoherence, which often requires the application of dynamical decoupling schemes, such as spin echo. However, the decoupling of the qubits from the environment will also affect interactions with neighboring qubits or photon-mediated couplings. To overcome this problem, we analyzed the implementation of *continuous dynamical decoupling* strategies for protecting qubit-photon interfaces from low-frequency noise. In this approach, the qubits are driven by a strong continuous microwave field with Rabi frequency Ω. This maps the original qubit states $|0\rangle$ and $|1\rangle$ onto dressed states $|\tilde{0}\rangle = (|0\rangle + |1\rangle)/\sqrt{2}$ and $|\tilde{1}\rangle = (|0\rangle - |1\rangle)/\sqrt{2}$, which are insensitive to slowly fluctuating frequency shifts $\xi(t)$. As a result the effective qubit Hamiltonian can be written as

$$H = \frac{\Omega}{2}\,\sigma_x + \frac{\xi(t)}{2}\sigma_z \simeq \frac{\Omega}{2}\tilde{\sigma}_z + \frac{\xi^2(t)}{2\Omega}\,\tilde{\sigma}_z\,, \tag{1}$$

where residual second-order effects are systematically suppressed with increasing driving strength. Importantly, while being protected, the dressed qubits can still couple to photonic or phononic cavity modes for realizing photon-mediated interactions and quantum communication schemes. This is illustrated in the two examples shown in Fig. 2, where the scheme is applied for the implementation of a cavity-mediated gate between two nearby qubits as well as for a photon-mediated quantum state transfer protocol over long distances.

References

[1] J. I. Cirac, P. Zoller, H. J. Kimble, and H. Mabuchi, Phys. Rev. Lett. **78**, 3221–3224 (1997).

[2] P. Kurpiers, P. Magnard, T. Walter, B. Royer, M. Pechal, J. Heinsoo, Y. Salathé, A. Akin, S. Storz, J.-C. Besse, S. Gasparinetti, A. Blais, and A. Wallraff, Nature **558**, 264–267 (2018).

[3] S. J. M. Habraken, K. Stannigel, M. D. Lukin, P. Zoller, and P. Rabl, New J. Phys. **14**, 115004 (2012).

[4] T. Niemczyk, F. Deppe, H. Huebl, E. P. Menzel, F. Hocke, M. J. Schwarz, J. J. Garcia-Ripoll, D. Zueco, T. Hümmer, E. Solano, A. Marx, and R. Gross, Nat. Phys **6**, 772–776 (2010).

Observation of the Nonreciprocal Magnon Hanle Effect

J. Gückelhorn, M. Scheufele, M. Grammer, M. Opel, S. Geprägs, R. Gross, H. Huebl, M. Althammer [1]
S. de-la-Peña, J.C. Cuevas, A. Kamra [2]

A core research activity at WMI is the investigation of angular momentum transport in solid-state systems. Magnons, the quantized excitations in magnetically ordered systems, provide a unique way of transporting spin information without requiring mobile charge carriers. Due to the two magnetic sublattice nature of antiferromagnets (AFs), one obtains two degenerate magnon modes with opposite spin chirality, similar to the two spin states for electrons. In 2020, we reported the first experimental observation of the magnon Hanle effect [1] in thin films of the antiferromagnetic insulator (AFI) hematite (α-Fe_2O_3) and established the concept of pseudospin [2] to describe the complex interplay and evolution of magnon modes and their superpositions in AFs. Over the last three years we studied this effect in more detail [3] and observed for the first time a nonreciprocal response in hematite thin films, as a direction-dependent magnon Hanle effect, published this year in Physical Review Letters [4].

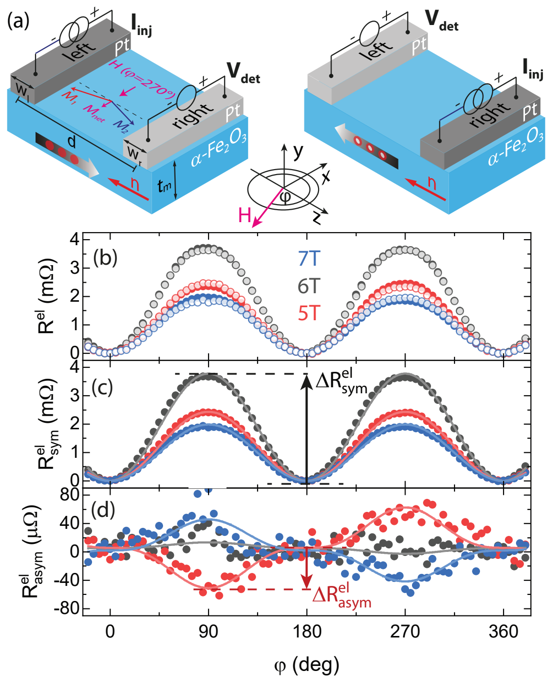

Figure 1: (a) Sketch of the sample configuration for the forward (left panel) and backward (right panel) transport directions. The corresponding net magnetization $\boldsymbol{M}_{net}$ is aligned along the applied magnetic field $\mu_0\boldsymbol{H}$, while the Néel order parameter $\boldsymbol{n} \perp \boldsymbol{H}$. (b) Angle dependence of the electrically induced magnon spin signal R^{el} measured at $T = 250\,\mathrm{K}$ for a center-to-center distance of $d = 1.2\,\mu\mathrm{m}$ and different magnetic field magnitudes. (c) Symmetric part of the two measurement configurations for the same magnetic fields as in panel (b). The lines are fits to the expected $\Delta R^{el}_{sym}\sin^2(\varphi)$ function. (d) Antisymmetric part of the respective curves in panel (b). The lines represent a $\Delta R^{el}_{asym}\sin^3(\varphi)$ fit.

In our experiments, we use a $t_m = 89\,\mathrm{nm}$ thick epitaxial film of hematite (α-Fe_2O_3) in the easy-plane phase at $T = 250\,\mathrm{K}$. To characterize the sample we perform angle-dependent electrical transport measurements by changing the orientation of the external magnetic field $\boldsymbol{H}$ within the xz-plane [see Fig. 1(a)]. A DC charge current with the magnitude of $|I_{inj}| = 500\,\mu\mathrm{A}$ is applied first to the left electrode, leading to spin injection into the hematite film via the spin Hall effect (SHE). The resulting diffusive pseudospin magnon current is detected electrically as a voltage signal V_{det} at the right electrode [left panel, Fig. 1(a)]. In a second step, we interchange the injector and detector electrode, i.e. I_{inj} is injected at the right electrode and the voltage V_{det} is detected at the left Pt strip [right panel, Fig. 1(a)]. The measured magnon spin signal $R^{el} = V^{el}/I_{inj}$ is plotted in Fig. 1(b) versus the angle φ of the applied in-plane magnetic field for three different magnitudes $\mu_0 H$ for both configurations. The full circles correspond to the forward transport direction [$+d$, left panel of Fig. 1(a)], while open circles represent the backward direction [$-d$, right panel of Fig. 1(a)]. We observe differences between the two propagation directions for $\mu_0 H = 5\,\mathrm{T}$ and $7\,\mathrm{T}$. To quantify this observation, we plot the symmetric $R^{el}_{sym} = [R^{el}(+d) + R^{el}(-d)]/2$ and antisymmetric

[1] We gratefully acknowledge financial support from the German Research Foundation under Germany's Excellence Strategy – EXC-2111 – 390814868 and project AL2110/2-1.

[2] Condensed Matter Physics Center (IFIMAC) and Departamento de Física Teórica de la Materia Condensada, Universidad Autónoma de Madrid, Madrid, Spain

$R^{\mathrm{el}}_{\mathrm{asym}} = [R^{\mathrm{el}}(+d) - R^{\mathrm{el}}(-d)]/2$ components of the magnon spin signal in Fig. 1(c) and (d), respectively. The angle dependence in Fig. 1(c) follows the expected $\Delta R^{\mathrm{el}}_{\mathrm{sym}} \sin^2(\varphi)$ behavior with $\Delta R^{\mathrm{el}}_{\mathrm{sym}}$ the amplitude of the symmetric magnon spin signal. Fig. 1(d) shows that $R^{\mathrm{el}}_{\mathrm{asym}}$ is vanishingly small at $\mu_0 H = 6\,\mathrm{T}$ over the whole angle range, while we observe a clear angle-dependence for $\mu_0 H = 5\,\mathrm{T}$ and $7\,\mathrm{T}$. It follows a $\Delta R^{\mathrm{el}}_{\mathrm{asym}} \sin^3(\varphi)$ dependence, with $\Delta R^{\mathrm{el}}_{\mathrm{asym}}$ denoting the amplitude [cf. Fig. 1(d)].

The quantities $\Delta R^{\mathrm{el}}_{\mathrm{sym}}$ and $\Delta R^{\mathrm{el}}_{\mathrm{asym}}$ are extracted and plotted in Fig. 2(a) as a function of the magnetic field magnitude $\mu_0 H$. For $\Delta R^{\mathrm{el}}_{\mathrm{sym}}$ we obtain a maximum at the compensation field of $\mu_0 H_c = 6.2\,\mathrm{T}$ consistent with the magnon Hanle effect [1, 3]. Moreover, $\Delta R^{\mathrm{el}}_{\mathrm{asym}}$ (red dots) approaches zero at $\mu_0 H_c$ and then changes sign for $\mu_0 H > \mu_0 H_c$.

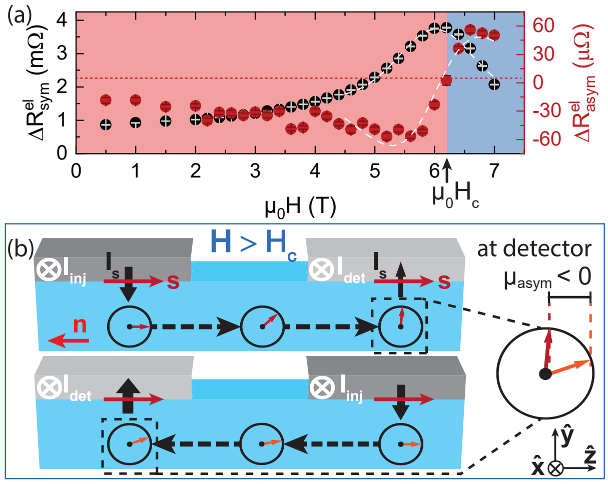

Figure 2: (a) Magnetic field dependence of the symmetric and antisymmetric magnon spin signal $\Delta R^{\mathrm{el}}_{\mathrm{sym}}$ (black dots) and $\Delta R^{\mathrm{el}}_{\mathrm{asym}}$ (red dots), extracted from the data shown in Figs. 1 (c) and (d), respectively. (b) Schematic depiction of magnon spin and pseudospin transport in an AFI (blue) [1, 2]. Two normal metal (NM) strips act as injector (dark gray) and detector (light gray) of magnonic spin current, which corresponds to the pseudospin z-component in the AFI. Due to slightly different pseudofields in the forward (upper panels) and backward (lower panels) propagation directions, there is a difference μ_{asym} in the observed magnon signal.

We can qualitatively describe the observed phenomenon as illustrated in Fig. 2(b). In the upper panel, the left NM electrode injects a magnonic spin current into the AFI, which corresponds to injecting a z-polarized pseudospin current. The AFI under consideration bears an easy-plane anisotropy, which harbors x-directed pseudofield. The spin-1 magnons injected by the NM are not the eigenmodes and start to transmute into other kinds of magnons with varying spin. This process is represented by pseudospin precession about the pseudofield. Consequently, the magnon spin, given by the pseudospin z-component, detected by the right NM depends on the pseudofield. The latter can further be controlled via an applied magnetic field [1] and vanishes at a specific value denoted as H_c. If we interchange the two NM electrodes' roles injecting spin with the right and detecting it using the left, magnons may experience a slightly different pseudofield due to inversion symmetry breaking. Consequently, the magnon spin signal detected in this configuration is slightly different. This difference changes sign at H_c due to a corresponding reversal of the pseudospin precession sense.

In summary, we demonstrate nonreciprocal magnon spin transport in the most widely used antiferromagnetic insulator - hematite. We attribute it to an antisymmetric pseudofield along the spin transport direction. This antisymmetric pseudofield constitutes an observation of emergent pseudospin-orbit interaction. Hence, our work establishes nonlocal magnon transport as a powerful probe for underlying spin interactions in antiferromagnetic insulators.

References

[1] T. Wimmer, A. Kamra, J. Gückelhorn, M. Opel, S. Geprägs, R. Gross, H. Huebl, and M. Althammer, Phys. Rev. Lett. **125**, 247204 (2020).
[2] A. Kamra, T. Wimmer, H. Huebl, and M. Althammer, Phys. Rev. B **102**, 174445 (2020).
[3] J. Gückelhorn, A. Kamra, T. Wimmer, M. Opel, S. Geprägs, R. Gross, H. Huebl, and M. Althammer, Phys. Rev. B **105**, 094440 (2022).
[4] J. Gückelhorn, S. de-la Peña, M. Scheufele, M. Grammer, M. Opel, S. Geprägs, J. C. Cuevas, R. Gross, H. Huebl, A. Kamra, and M. Althammer, Phys. Rev. Lett. **130**, 216703 (2023).

Influence of the Anion Substitution on Electronic Correlations in κ-(BEDT-TTF)$_2$Cu[N(CN)$_2$]Y (Y = Cl, Br)

S. Erkenov, W. Biberacher, R. Gross, M. V. Kartsovnik [1]
I. Sheikin [2]

The layered organic conductors κ-(BEDT-TTF)$_2$X have been extensively employed for studying the bandwidth-controlled Mott metal-insulator transition (MIT) and closely related fascinating phenomena such as unconventional superconductivity, quantum spin-liquid or valence-bond-solid states [1, 2]. In these materials one can easily tune the electronic ground state by applying a moderate pressure $P \lesssim 10$ kbar or tiny chemical modifications. For example, the salt with anion X = Cu[N(CN)$_2$]Cl (referred to as κ-Cl in the following) is an archetypal quasi-two-dimensional antiferromagnetic Mott insulator but becomes metallic under a very moderate pressure of ≈ 0.4 kbar. At the same time, the κ-Br salt, which differs from κ-Cl by just a single atom Br replacing Cl in the complex anion, is metallic already at ambient pressure.

The κ-Cl and κ-Br salts along with the third, even more metallic sibling with X = Cu(NCS)$_2$ (κ-NCS) are commonly put on a generalized phase diagram, where the anion replacement and a change in pressure are both supposed to affect the correlation-strength ratio U/t (U is the onsite Coulomb repulsion and t the effective transfer integral) [3]. Thus, the anion substitution has been considered in terms of "chemical pressure" [2, 3]. An argument in favor of this interpretation was given by optical conductivity studies of "mixed" salts κ-Br$_x$Cl$_{1-x}$ [4] reporting a dramatic, 3-fold increase of the quasiparticle effective mass upon a small reduction of Br content x from 0.85 to 0.73. Ascribing this change to the enhancement of the many-body renormalization, which is largely determined by electron-electron correlations near the MIT, would imply a strong increase in U/t [5]. On the other hand, our recent comparative studies of Shubnikov-de Haas (SdH) oscillations in the pressurized κ-Cl and κ-NCS salts [6] showed nearly identical effective masses. Taking into account that κ-NCS is even more metallic than κ-Br, this result casts doubt on the chemical pressure scenario. To clarify the situation, we have simultaneously measured the SdH oscillations in two selected κ-Cl and κ-Br crystals under pressure.

In magnetic fields of $25 - 30$ T both samples showed sizeable β oscillations (originating from the cyclotron orbit encompassing the entire 2D Fermi surface [7]) at pressures up to 6 kbar. Examples are shown in Fig. 1(a). The effective cyclotron mass was evaluated by fitting the T-dependence of the SdH amplitude by the standard Lifshitz-Kosevich (LK) formula [8], as illustrated in Fig. 1(b). The results are summarized in Fig. 1(c).

One immediately sees that at all pressures the masses in κ-Br and κ-Cl are quite similar to each other. Our finding is in stark contrast to that reported in Ref. [4]. A possible reason for the discrepancy is that the optical properties can be sensitive to spurious surface effects, whereas magnetic quantum oscillations probe the bulk properties and are, therefore, more relevant. Further on, the applicability of the extended Drude model for evaluating the effective mass renormalization from optical conductivity in a strongly correlated system is not obvious [9], whereas the LK theory is more robust in this respect. It may be instructive to compare both methods by applying them on one and the same sample near and away from the MIT.

All in all, the data in Fig. 1(c) is consistent with the earlier study [7] but, being much more precise, allows for a more detailed analysis. At lowest pressures, $P < 0.4$ kbar, where κ-Cl is in the metal/insulator phase-coexistence state, it shows an effective mass m_c^{Cl} notably,

[1] The work was supported by the German Research Foundation, grants KA 1652/5-1 and GR 1132/19-1. High-field measurements were supported by LNCMI-CNRS, a member of the European Magnetic Field Laboratory.
[2] Laboratoire National des Champs Magnétiques Intenses LNCMI, CNRS, F-38042 Grenoble Cedex 9, France

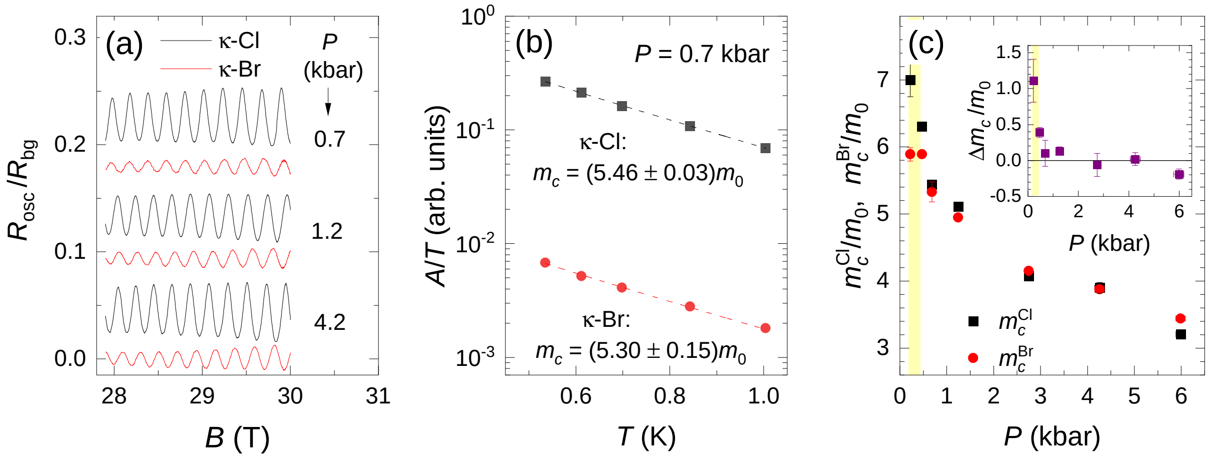

Figure 1: (a) Examples of SdH oscillations in κ-Cl and κ-Br at different pressures, $T = 0.7\,$K. The oscillating component of the interlayer resistance is normalized to the classical background resistance R_{bg}. The curves are vertically shifted for clarity. (b) Examples of LK plots of the SdH amplitudes. Dashed lines are fits by the LK formula, yielding the effective cyclotron mass. (c) Pressure-dependent effective masses of κ-Cl and κ-Br (main panel) and their difference, $\Delta m_c \equiv m_c^{Cl} - m_c^{Br}$, (inset) in units of the free electron mass. The yellow rectangle indicates the metal/insulator phase-coexistence range at the first-order MIT for the κ-Cl salt.

$10 - 20\%$, higher than the fully metallic κ-Br salt. This difference is likely a manifestation of recently proposed heavy "resilient" quasiparticles in thick domain walls emerging in the phase-coexistence region [10]. Right outside this range the difference between the masses rapidly drops, however, remains positive, $\approx 0.1m_0$, and can be attributed to a weak "chemical pressure" effect equivalent to $P \simeq 100\,$bar.

At pressurizing to $\sim 3\,$kbar, Δm_c virtually vanishes. One might interpret this as an indication of vanishing electronic correlations in both compounds and saturation of the effective mass at the level of the one-electron band mass $m_{c,\mathrm{band}}$. However, the $m_c(P)$ dependence does not saturate, showing, instead, a significant negative slope at increasing pressure beyond 3 kbar. Moreover, at 6 kbar m_c^{Cl} becomes smaller than m_c^{Br}. The difference, $|\Delta m_c| \approx 0.2m_0$, is small but exceeds the error bar of our evaluation. Assuming that it originates from the difference in the band masses of the two salts, one has to take it into account when evaluating the mass renormalization factor $m_c/m_{c,\mathrm{band}}$. This would affect our estimation of the "chemical pressure" at the border of the MIT, increasing it to an equivalent of $\simeq 0.7\,$kbar. One should, however, not disregard the possibility that the two salts have slightly different compressibilities, which would lead to different slopes of the $U/t(P)$, hence $m_c(P)$ dependence. Further studies are needed for clarifying this question.

References

[1] B. Miksch, A. Pustogow, M. J. Rahim, A. A. Bardin, K. Kanoda, J. A. Schlueter, R. Hübner, M. Scheffler, and M. Dressel, Science **372**, 276 (2021).
[2] B. J. Powell, and R. H. McKenzie, Rep. Prog, Phys. **74**, 056501 (2011).
[3] K. Kanoda, J. Phys. Soc. Jpn. **75**, 051007 (2006).
[4] J. Merino, M. Dumm, N. Drichko, M. Dressel, and R. H. McKenzie, Phys. Rev. Lett. **100**, 086404 (2008).
[5] W. F. Brinkman, and T. M. Rice, Phys. Rev. B **2**, 4302 (1970).
[6] S. Oberbauer, S. Erkenov, W. Biberacher, N. D. Kushch, R. Gross, and M. V. Kartsovnik, Phys. Rev. B **107**, 075139 (2023).
[7] H. Weiss, M. V. Kartsovnik, W. Biberacher, E. Steep, E. Balthes, A. Jansen, K. Andres, and N. Kushch, Phys. Rev. B **59**, 12370 (1999).
[8] D. Shoenberg. Magnetic Oscillations in Metals (Cambridge University Press, Cambridge, 1984).
[9] A. V. Chubukov, and D. L. Maslov, Phys. Rev. B **96**, 205136 (2017).
[10] T.-H. Lee, J. Vučičević, D. Tanasković, E. Miranda, and V. Dobrosavljević, Phys. Rev. B **106**, L161102 (2022).

Effect of Thermal History on Electronic Properties of κ-(BEDT-TTF)$_2$Cu[N(CN)$_2$]Br at the Border of the Mott-Insulating State

S. Erkenov, F. Kollmannsberger, W. Biberacher, R. Gross, M. V. Kartsovnik [1]
T. Helm [2]

In the charge-transfer salts κ-(BEDT-TTF)$_2$Cu[N(CN)$_2$]Y the organic donor BEDT-TTF [standing for bis(ethylenedithio)tetrathiafulvalene] builds conducting layers, which are alternated with insulating layers of the monovalent anion Cu[N(CN)$_2$]Y$^-$, where Y = Cl or Br. These materials possess a quasi-two-dimensional electronic system with a narrow, effectively half-filled conduction band and, therefore, exhibit a strong Mott-insulating instability of the metallic state. Taking, for instance, the ambient-pressure superconductor κ-(BEDT-TTF)$_2$Cu[N(CN)$_2$]Br (henceforth referred to as κ-Br), a change in the orientation of just a few percent of the terminal ethylene groups (TEG) of BEDT-TTF molecules considerably shifts it towards the Mott metal-insulator transition (MIT) or even drives it into the insulating state. This can be achieved by a rapid cooling of the sample through the temperature interval $80 - 60\,\mathrm{K}$ where the TEG undergo a glassy ordering transition [1]. Based on the band structure calculations [2] and the low-temperature resistivity behavior, it was argued that the glass transition, besides introducing some disorder, affects the Mottness ratio U/t (where U and t are the on-site Coulomb repulsion and the nearest-neighbour transfer integral, respectively). Thus, the effect of TEG conformational ordering is supposed to be analogous to the pressure effect on the Mott-insulating sibling salt with Y = Cl [2, 3]. However, an unequivocal experimental test of this scenario has been lacking.

To clarify this issue, we have measured Shubnikov-de Haas (SdH) oscillations of the interlayer resistance of κ-Br in several states having different thermal histories. To this end, we have adopted and further optimized the annealing/quenching protocol developed originally by B. Hartmann et al. [4]. The state with the highest TEG order, $\geq 98\%$ of TEG ordered in the stable eclipsed conformation, was prepared by holding the samples at a constant temperature $T \approx 68\,\mathrm{K}$ for 50 hours. We will refer to this state as “annealed state” (A-state). A slightly increased disorder, with the occupation probability for the metastable staggered occupation $p_S \approx 3\%$, was obtained by cooling the samples through the glass transition at a rate of $2\,\mathrm{K/min}$ (normally-cooled, NC-state). Finally, the strongest disorder was achieved by applying a rectangular voltage pulse, $V = 6 - 8\,\mathrm{V}$, $t = 2\,\mathrm{s}$, through the sample in the interlayer direction. Thereby the sample was heated up to $100 - 150\,\mathrm{K}$, depending on the exact voltage, and subsequently cooled through the glass transition down to the environment temperature (typically $35\,\mathrm{K}$) within $\approx 0.5\,\mathrm{s}$. This procedure yielded a quenched state (Q-state) with $p_S > 10\%$.

The thermal history is clearly reflected in transport properties of the samples, see Fig. 1(a). Freezing a higher fraction of TEG in the staggered conformation obviously results in stronger scattering, hence higher residual resistance. Further on, the superconducting transition is shifted to lower temperatures. Finally, the quenched state exhibits a prominent upturn of the $R(T)$ dependence at $T < 20\,\mathrm{K}$. The accompanying hysteresis [see inset in Fig. 1(a)] indicates the first-order MIT. Thus, our thermal treatment indeed shifts the material in the phase diagram, effectively enhancing the insulating instability. We note that the difference between the A- and Q-states obtained in our experiment significantly exceeds that reported thus far. Importantly, the applied heat pulses, as cruel as they may look with respect to our brittle sam-

[1] The work was supported by the German Research Foundation, grants KA 1652/5-1 and GR 1132/19-1. Pulsed-field measurements were supported by HLD at HZDR, a member of the European Magnetic Field Laboratory.

[2] Helmholtz Zentrum Dresden Rossendorf, Hochfeld Magnetlabor Dresden HLD, 01328 Dresden, Germany

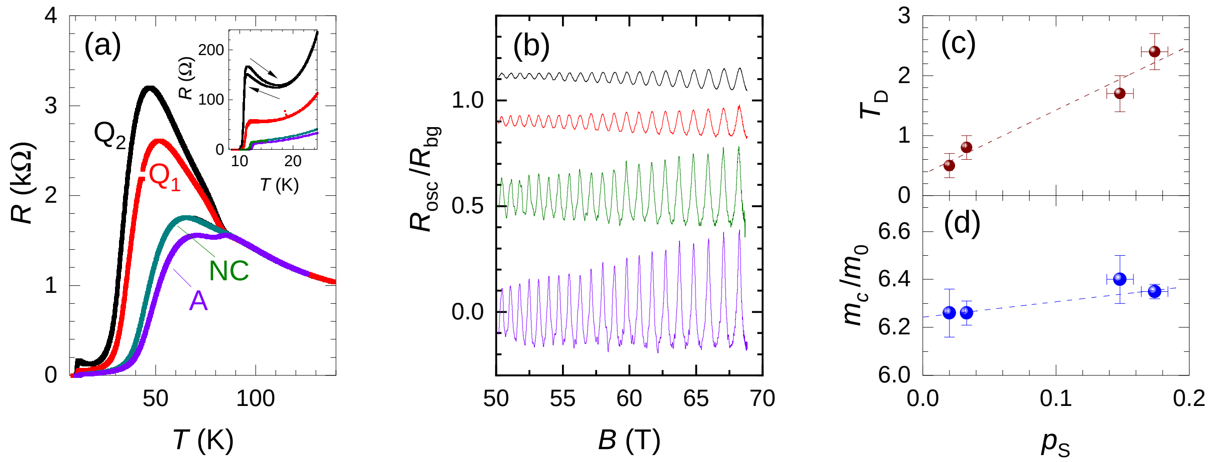

Figure 1: (a) Temperature dependence of the interlayer resistance of a κ-Br sample in the A-, NC-, Q1-, and Q2-states, see text. Inset: expanded low-T part of the same data. The arrows indicate the up and down T-sweep directions for the Q2-state, revealing a hysteresis in the $R(T)$ dependence. (b) Examples of the SdH oscillations in the different states; the color code is the same as in (a). The oscillating signal is normalized to the B-dependent non-oscillating background resistance. The curves are vertically shifted for clarity. (c) Dingle temperature and (d) effective cyclotron mass in units of the free electron mass m_0 plotted against the fraction p_S of staggered TEG.

ples, do not introduce irreversible damage to them. The characteristics of the original A-state are perfectly reproduced after the quenched sample is re-annealed.

Fig. 1(b) shows examples of SdH oscillations recorded in pulsed magnetic fields on a κ-Br sample in the A-, NC-, Q1-, Q2-states (the latter two differ by the maximum temperature reached during the heat pulse, ≈ 120 and $\approx 135\,$K, respectively). As expected, the states with higher staggered TEG occupation numbers exhibit lower oscillation amplitudes and higher Dingle temperatures T_D, see Fig. 1(c). The latter may be related to the scattering rate $1/\tau = 2\pi k_B T_D/\hbar$ [5]. The T_D values in the (best ordered) A- and (most disordered) Q2-states differ by a factor of five, which compares well with the difference in the residual resistances. This is also consistent with the estimated change of the staggered TEG occupation, see Fig. 1(c).

In Fig. 1(d) we plot the effective cyclotron mass obtained from the SdH oscillations, following the standard procedure [5], against p_S estimated according to [4]. Unlike the scattering rate, the mass shows no significant dependence on the thermal history. This breaks the proposed [2, 3] simple analogy of the TEG ordering with pressure. Indeed, comparing our data with that in Refs. [3, 4], one would estimate the difference in the location of our A- and Q-states on the phase diagram to be equivalent to a pressure difference of $\gtrsim 500\,$bar. However, the difference in the U/t ratio, inferred from the effective masses in Fig. 1(d) in the same way as it was done for the sibling κ-Cl salt [6], corresponds to no more than 70 bar of pressure difference. Therefore, we conclude that interpretation of the TEG ordering in terms of "chemical pressure", affecting mainly the Mottness ratio U/t, is incomplete. One has to look for another mechanism, possibly associated with scattering on the TEG disorder potential, which ultimately determines the ground state in κ-Br.

References

[1] J. Müller, M. Lang, F. Steglich, J. A. Schlueter, A. M. Kini, and T. Sasaki, Phys. Rev. B **65**, 144521 (2002).
[2] D. Guterding, R. Valentí, and H. O. Jeschke, Phys. Rev. B **92**, 081109 (2015).
[3] J. Müller, B. Hartmann, and T. Sasaki, Philos. Mag. **97**, 3477 (2017).
[4] B. Hartmann, J. Müller, and T. Sasaki, Phys. Rev. B **90**, 195150 (2014).
[5] D. Shoenberg. Magnetic Oscillations in Metals (Cambridge University Press, Cambridge, 1984).
[6] S. Oberbauer, S. Erkenov, W. Biberacher, N. D. Kushch, R. Gross, and M. V. Kartsovnik, Phys. Rev. B **107**, 075139 (2023).

Application–Oriented Research

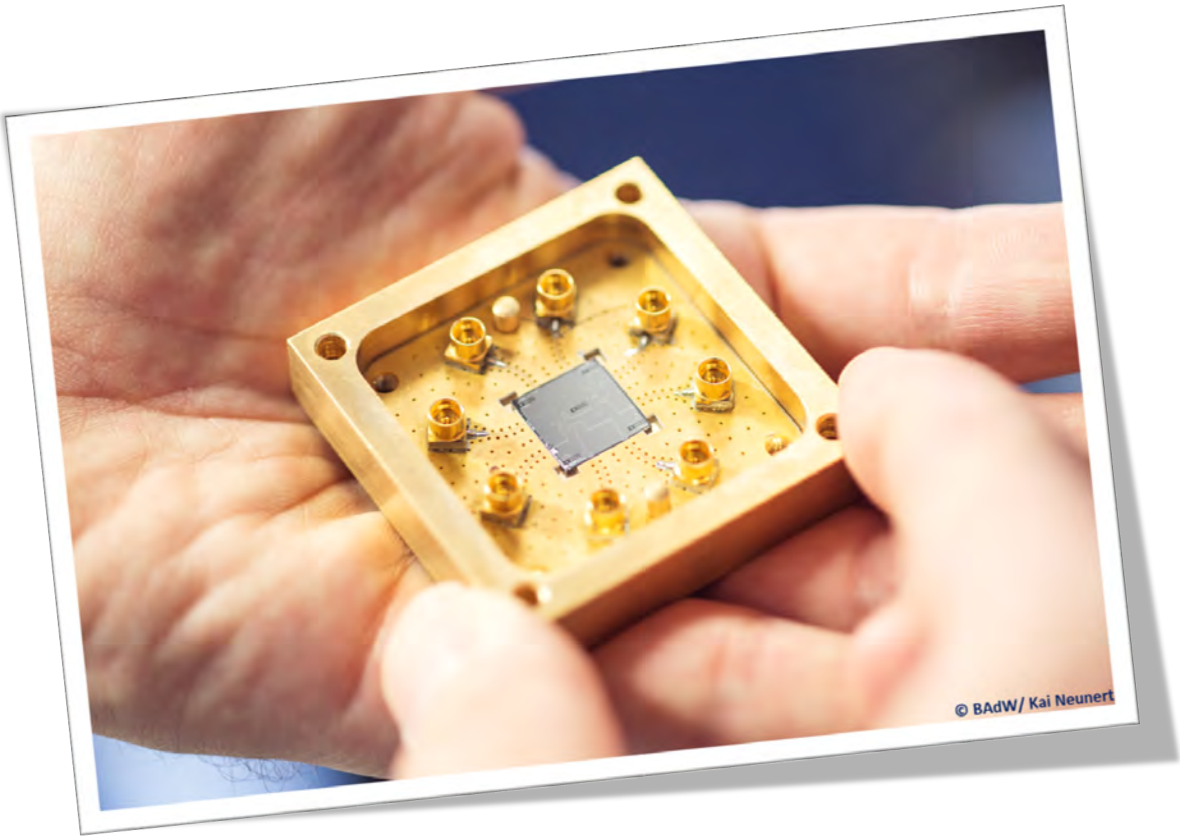

Quantum Microwave Parametric Interferometer

F. Kronowetter, F. Fesquet, M. Renger, K. Honasoge, Y. Nojiri, A. Marx, R. Gross, K. G. Fedorov [1]

In metrology, interferometric techniques have been widely explored in terms of fundamental physics and resulted in a variety of technical breakthroughs [1–3]. Classical interferometers, such as the Mach-Zehnder interferometer, typically rely on the injection of coherent states into one port of a balanced beam splitter, while only vacuum fluctuations enter the second port [4]. Their phase sensitivity is limited by shot noise, also known as the standard quantum limit (SQL). The SQL can be overcome by making use of nonlinear elements, such as parametric amplifiers, leading to interactions between photons [5–7]. In principle, exploiting quantum correlations between photons in these states allows one to improve measurement precision towards the Heisenberg limit (HL). While nonlinear interferometers have been actively investigated at optical frequencies, the microwave domain so far remained unexplored due to relatively small energies of microwave photons at frequencies in the 1–10 GHz range and an associated difficulty of single-photon detection [4, 7, 8]. Here, we present an experimental realization of a nonlinear microwave interferometer making use of Josephson-junction-based superconducting quantum circuits (see Fig. 1) [9].

A quantum microwave parametric interferometer (QUMPI) consists of two linear balanced microwave beam splitters and two nonlinear quantum devices in the form of flux-driven Josephson parametric amplifiers[2] (JPAs). First, we evaluate the interferometric power (IP) of the QUMPI. For a bipartite quantum probe state, the IP defines the worst-case precision of a parameter estimation, where the corresponding parameter experiences unitary dynamics in one of the two subsystems (e.g., a phase shift of the signal in one interferometer arm) [10]. The respective IP is defined as

$$\mathcal{P}\left(\rho_{\mathrm{AB}}\right) = \frac{1}{4} \inf_{\hat{U}_{\mathrm{A}}} \mathcal{F}\left(\rho_{\mathrm{AB}}^{\Phi,\hat{U}_{\mathrm{A}}}\right), \qquad (1)$$

where ρ_{AB} is the two-mode probe state, $\hat{U}_{\mathrm{A}}$ is an arbitrary unitary transformation of the subsystem A, $\mathcal{F}$ is the quantum Fisher information, and Φ is the corresponding estimator [10]. We observe that the interferometric power of the QUMPI clearly exceeds the SQL in experiment, $\mathcal{P}_{\mathrm{exp}}/\mathcal{P}_{\mathrm{SQL}} = 1.70$, which highlights the potential of our scheme in precision metrology [9].

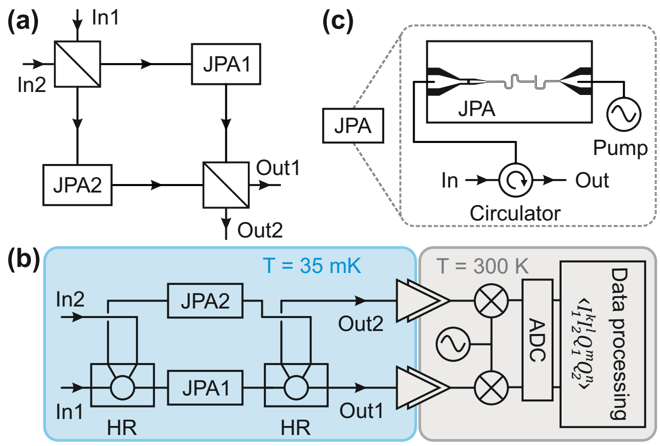

Figure 1: (a) General scheme of the QUMPI. (b) Details of the experimental setup consisting of a 180° hybrid ring (HR), which splits and symmetrically superimposes two incoming signals from ports In1 and In2, two JPAs for phase-sensitive amplification, and a second 180° HR, which completes the nonlinear interferometer. Output two-mode signals are detected with a heterodyne microwave receiver and digitally processed to extract statistical signal moments. The latter enable a full quantum state tomography. (c) A circulator separates incoming and outgoing signals for each JPA.

[1] We acknowledge support by the German Research Foundation via Germany's Excellence Strategy (EXC-2111-390814868) and the German Federal Ministry of Education and Research via the project QUARATE (Grant No. 13N15380). This research is part of the Munich Quantum Valley, which is supported by the Bavarian state government with funds from the Hightech Agenda Bayern Plus.

[2] The JPAs used in these studies were provided by `K. Inomata` and `Y. Nakamura` from RIKEN Center for Quantum Computing, Japan.

In a second step, we experimentally investigate the second-order cross-correlation function, $g_C^{(2)}(0)$, as a function of the displacement amplitude of the incident coherent states. We observe that for sufficiently large displacement amplitudes, $|\alpha_1|$ and $|\alpha_2|$, and equal displacement angles, $\theta_1 = \theta_2$, $g_C^{(2)}(0)$ indicates anti-bunching between the interferometer outputs, providing evidence for non-classical correlations between them [7]. In Fig. 2(a), we show $g_C^{(2)}(0)$ predicted by our theoretical model. For the experimentally relevant model parameters, such as the average JPA gain $\overline{G}_{1,2} = 4.06\,\mathrm{dB}$, Fig. 2(a) shows that $|\alpha_1|^2, |\alpha_2|^2 > 5$ is required to realize non-local photon anti-bunching, $g_C^{(2)}(0) < 1$. Figure 2(b) shows the experimental data of $g_C^{(2)}(0)$ as a function of $|\alpha|^2 = |\alpha_1|^2 = |\alpha_2|^2$. The blue line is a cut along the main diagonal of Fig. 2(a). The inset shows an expanded view of the region, where $g_C^{(2)}(0)$ drops below the classical limit.

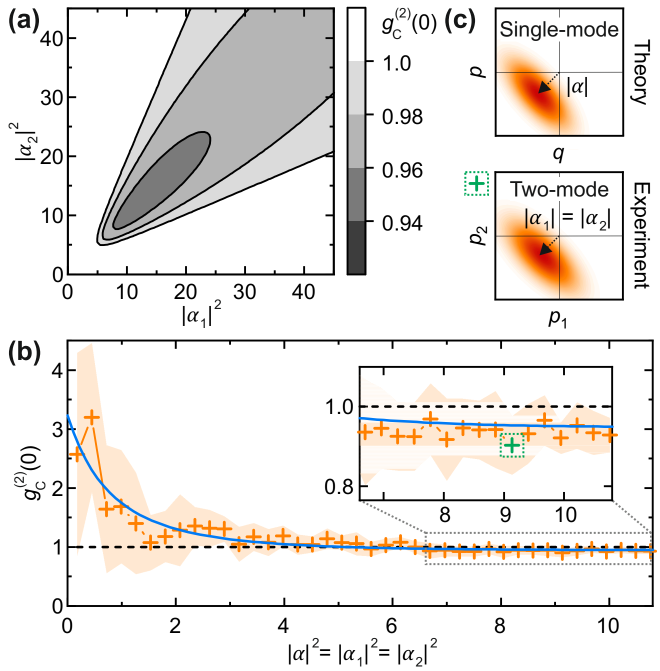

Figure 2: Intensity cross-correlations, $g_C^{(2)}(0)$, of the interferometer output fields for variable displacement amplitudes of coherent input signals. (a) Model predictions as a function of the number of coherent photons $|\alpha_1|^2$ and $|\alpha_2|^2$ ($\theta_1 = \theta_2 = 0.81\pi$) entering the circuit at In1 and In2, respectively. (b) Experimental results for $g_C^{(2)}(0)$ (orange crosses with standard deviation shown in shaded orange) as a function of the symmetrically varied displacement amplitudes. The blue line depicts the theoretical prediction. The black dashed line illustrates the classical limit of $g_C^{(2)}(0) = 1$. (c) Analogy between Wigner functions of single-mode (theory) and two-mode [experiment, green cross from (b)] displaced squeezed states exhibiting $g^{(2)}(0) < 1$ ($g_C^{(2)}(0) < 1$).

In conclusion, the investigated QUMPI circuit is expected to be useful in many applications ranging from quantum-enhanced interferometry to mode-mixing, as part of a joint quantum receiver in quantum sensing experiments [11]. Furthermore, our findings open a new avenue towards quantum-enhanced nonlinear interferometers in the fast-evolving field of superconducting circuits operating in the microwave regime. For more details on these studies, we refer the reader to Ref. [9].

References

[1] M. Xiao, L.-A. Wu, and H. J. Kimble, Phys. Rev. Lett. **59**, 278–281 (1987).
[2] R. Schnabel, Phys. Rep. **684**, 1–51 (2017).
[3] J. Abadie, B. P. Abbott, R. Abbott, T. D. Abbott, M. Abernathy, C. Adams, R. Adhikari, C. Affeldt, P. Ajith, and B. Allen *et al.*, Nat. Phys. **7**, 962–965 (2011).
[4] Z. Y. Ou, and X. Li, APL Photonics **5**, 080902 (2020).
[5] V. Giovannetti, S. Lloyd, and L. Maccone, Nat. Photonics **5**, 222–229 (2011).
[6] M. Napolitano, M. Koschorreck, B. Dubost, N. Behbood, R. J. Sewell, and M. W. Mitchell, Nature **471**, 486–489 (2011).
[7] B. Yurke, S. L. McCall, and J. R. Klauder, Phys. Rev. A **33**, 4033–4054 (1986).
[8] F. Hudelist, J. Kong, C. Liu, J. Jing, Z. Y. Ou, and W. Zhang, Nat. Comm. **5**, 3049 (2014).
[9] F. Kronowetter, F. Fesquet, M. Renger, K. Honasoge, Y. Nojiri, K. Inomata, Y. Nakamura, A. Marx, R. Gross, and K. Fedorov, Phys. Rev. Appl. **20**, 024049 (2023).
[10] G. Adesso, Phys. Rev. A **90**, 022321 (2014).
[11] F. Kronowetter, M. Würth, W. Utschick, R. Gross, and K. G. Fedorov. Imperfect photon detection in quantum illumination. `arXiv:2308.02343 [quant-ph]` (2023).

Microwave Quantum Cryptography with Time Multiplexing

F. Fesquet, V. Weidemann, F. Kronowetter, M. Renger, W. K. Yam, S. Gandorfer, K. Honasoge, M. Handschuh, A. Marx, R. Gross, K. G. Fedorov [1]

Quantum key distribution (QKD) holds the promise of delivering unconditionally secure distribution of classical keys between remote parties, offering a remedy to potential threats to communication security posed by future quantum computers. Recently, we have demonstrated a continuous-variable (CV) QKD protocol in the microwave regime, frequency-compatible with superconducting quantum circuits [1]. In this context, improvement in secret key rates is of particularly great interest. A common approach is to exploit fast time-domain multiplexing.

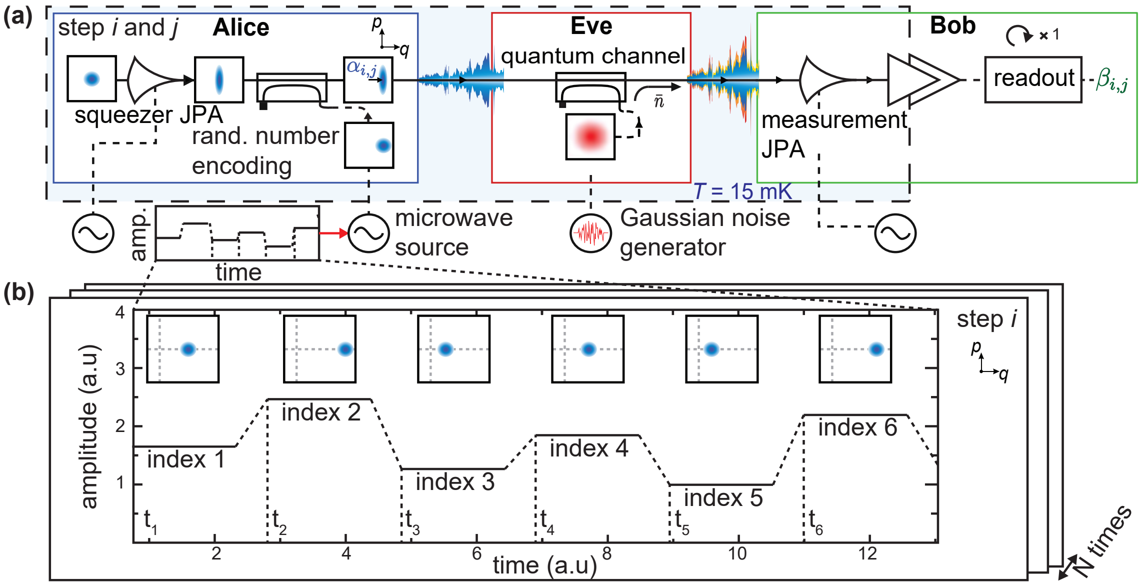

Figure 1: Experimental implementation of a microwave QM with propagating displaced squeezed microwave states. **(a)** Schemes of the experimental setup. Color plots in black boxes represent quantum states in quasi-probability Wigner phase space spanned by field quadratures q and p. **(b)** Displacement amplitude as a function of time for $M = 4$. At a time t_j, a displacement amplitude is drawn from a Gaussian distribution with associated fixed variance σ_j^2, with a corresponding index as shown in Fig. 2. Color plots are illustration of the displacement in phase space, here along the q axis.

In our CV-QKD implementation, a sender (Alice) encodes M Gaussian-distributed keys, each of length N, in displaced q- or p-squeezed states before sending them to a receiver (Bob). Alice chooses M different fixed variances σ_j^2, with $j \in \{1, \ldots, M\}$. As illustrated in Fig. 1(b), for each step $i \in \{1, \ldots, N\}$, Alice encodes M displacements $\alpha_{i,j}$ into displaced squeezed states. Each displacement amplitude $\alpha_{i,j}$ is drawn from a zero-mean Gaussian distribution with the corresponding variance σ_j^2. Bob, after local single-shot quadrature measurements (SQMs) of each individual displaced squeezed states, obtains an estimation of all of Alice's keys. Each key element, or symbol, propagates through a lossy thermal quantum channel, assumed to be under the control of a malicious eavesdropper (Eve). We analyze the measured data by computing the mutual information (MI) between Alice's keys $\{\mathcal{K}_{A,j} = \{\alpha_{i,j}\}_{i\in\{1,\ldots,N\}}\}_{j\in\{1,\ldots,M\}}$ and Bob's keys $\{\mathcal{K}_{B,j} = \{\beta_{i,j}\}_{i\in\{1,\ldots,N\}}\}_{j\in\{1,\ldots,M\}}$.

[1] We acknowledge support by the German Research Foundation via Germany's Excellence Strategy (EXC-2111-390814868) and the BMBF via the projects QUARATE (Grant No. 13N15380) and QuaMToMe (Grant No. 16KISQ036). This research is part of the Munich Quantum Valley, which is supported by the Bavarian state government with funds from the Hightech Agenda Bayern Plus.

Our experimental implementation, shown in Fig. 1(a), relies on superconducting flux-tunable JPAs for generation of squeezed microwave states [2]. The latter are displaced by a complex displacement amplitude $\alpha_{i,j}$ with a cryogenic directional coupler [3]. A second directional coupler emulates the quantum channel by adding a controlled noise photon number $\bar{n}$ to incoming signals. Subsequently, a second JPA, operated in the degenerate regime, enables SQMs by strongly amplifying the to-be-measured quadrature, resulting in a measured symbol $\beta_{i,j}$. Here, we use $M = 6$ different displacement variances σ_j^2. In Fig. 2(a), we shown the variance ratios $\sigma_j^2/\sigma_{\text{ind}}^2$, with σ_{ind}^2 denoting the largest displacement variance. We note that these ratios are insensitive to rescaling of measured data. We plot in Fig. 2(b) the associated experimental MI from which we directly extract the variance ratios. We note that the ensemble variance σ_{e}^2, obtained by combining all of Bob's keys, is in particular smaller than the largest displacement variance σ_{ind}^2. One can show that, by construction, we have

$$\sigma_{\text{e}}^2 = \frac{1}{M}\sum_j^M \sigma_j^2 < \sigma_{\text{ind}}^2. \tag{1}$$

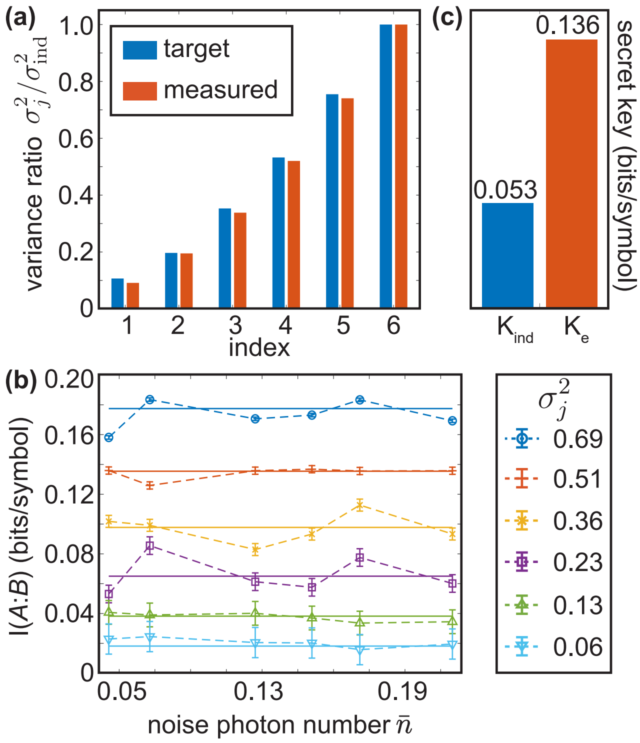

Figure 2: Measurement results. **(a)** Measured variance ratios $\sigma_j^2/\sigma_{\text{ind}}^2$ as compared to target values, in ascending order. **(b)** MI between Alice's and Bob's keys as a function of coupled noise. Solid lines shows corresponding theory predictions. **(c)** Extrapolated maximal secret key K_{ind} from MI with the displacement variance σ_{ind}^2 as compared to the same secret key K_{e} based on the combined ensemble of Bob's keys.

However, by taking advantage of the fact that multiple keys are sent, we observe an increase in the effective ensemble MI, $I(A\colon B)_{\text{e}}$, as compared to the highest individual one, $I(A\colon B)_{\text{ind}}$, i.e.,

$$I(A\colon B)_{\text{e}} = \frac{M}{2}\log_2\left(1+\frac{\sigma_{\text{e}}^2}{\sigma_{\text{n}}^2}\right) > I(A\colon B)_{\text{ind}} = \frac{1}{2}\log_2\left(1+\frac{\sigma_{\text{ind}}^2}{\sigma_{\text{n}}^2}\right), \tag{2}$$

where σ_{n}^2 is the noise variance in the measured signals. The rate of secure information during the communication is bounded by the secret key $K_{\text{e/ind}} = I(A\colon B)_{\text{e/ind}} - \chi_{\text{E}}^{\text{e/ind}}$, where $\chi_{\text{E}}^{\text{e/ind}}$ represents an upper bound on the information leaked to Eve. As shown in Fig. 2(c), we extrapolate, from our measured data, the maximal secret key achievable for our time multiplexing implementation and obtain an increase as high as $K_{\text{e}}/K_{\text{ind}} \simeq 2.6$.

Our preliminary results demonstrate that the time-domain multiplexing approach can be used to improve secure key rates for the CV-QKD protocol in the microwave regime.

References

[1] F. Fesquet, F. Kronowetter, M. Renger, W. K. Yam, S. Gandorfer, K. Inomata, Y. Nakamura, A. Marx, R. Gross, and K. G. Fedorov. Demonstration of microwave single-shot quantum key distribution. arXiv:2311.11069 (2023).

[2] L. Zhong, E. P. Menzel, R. Di Candia, P. Eder, M. Ihmig, A. Baust, M. Haeberlein, E. Hoffmann, K. Inomata, T. Yamamoto, Y. Nakamura, E. Solano, F. Deppe, A. Marx, and R. Gross, New J. Phys. **15**, 125013 (2013).

[3] K. G. Fedorov, L. Zhong, S. Pogorzalek, P. Eder, M. Fischer, J. Goetz, E. Xie, F. Wulschner, K. Inomata, T. Yamamoto, Y. Nakamura, R. Di Candia, U. Las Heras, M. Sanz, E. Solano, E. P. Menzel, F. Deppe, A. Marx, and R. Gross, Phys. Rev. Lett. **117**, 020502 (2016).

Frequency-Targeting and Geometric Effects in the Fabrication of Superconducting Tunable Resonators

M. Handschuh, K. E. Honasoge, W. Yam, F. Fesquet, R. Gross, K. Fedorov [1]

Achieving a high-volume and high-quality fabrication of uniform nonlinear resonators based on Josephson junctions is one of the central challenges of applied quantum information processing with superconductors. In this context, we thoroughly examine a reliable fabrication process tailored for Nb resonators featuring Al/AlOx/Al Josephson junctions. These circuits are implemented on 4-inch high-resistivity silicon wafers. Our primary goal is to establish a manufacturing approach that guarantees precise control over geometric effects, particularly those that emerge during a large-scale fabrication. Additionally, fabricating identical devices on a single wafer facilitates investigations of geometric variations and ensures minimal chip-to-chip variations. The resonance frequencies of our flux-tunable resonator devices are particularly dependent on the critical current of the implemented Josephson junction. This dependence is influenced by both the oxide thickness and the area of Josephson junctions. In order to achieve precise frequency targeting, we need to take in account large scale effects during fabrication and include an analysis of critical currents and inductances based on flux measurements.

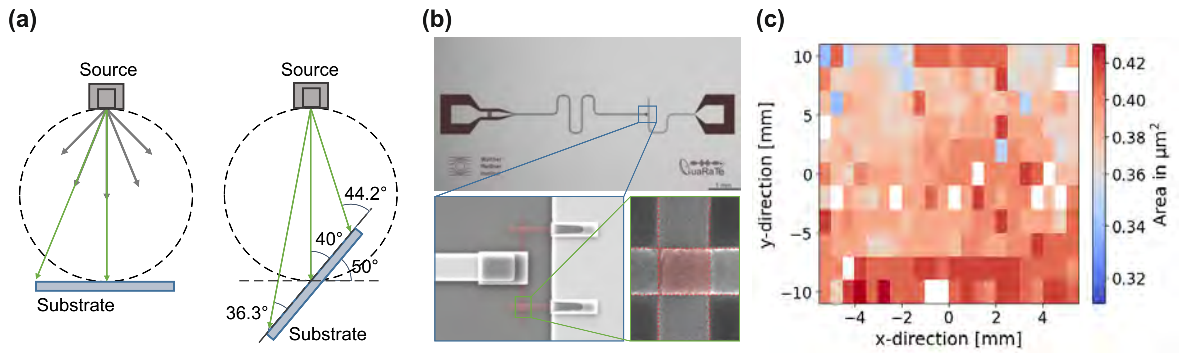

Figure 1: Geometric effects during Al evaporation on a 4-inch wafer for (a) x-direction and y-direction during the double-angle shadow evaporation. (b) Overview of the flux-pumped JPA sample with a scanning electron microscopy (SEM) close-up of the dc-SQUID area and another SEM close-up in the Josephson junction area. The Josephson junction area is falsely colored red. (c) Distribution of the Josephson junction areas as a function of their location on the wafer.

For studying potential variations of the junction area on the junction position on the wafer resulting from the oblique evaporation, we employ the geometric resist-shadowing model [1]. Fig. 1 (a) provides insight into the angle dependence observed during the evaporation from the center to the edge of the substrate, both in a planar and tilted configuration. The angle variation in the planar direction displaces the evaporated structures and the tilt influences the dimensions of the structures, because for a 4-inch substrate and a distance of 55.5 cm between the substrate and crucible the incident angle difference is up to 8.0°. The resulting variation in structure size was investigated for various Josephson junction structures. Our experimental layout comprises approximately 240 individual resonator devices, each containing a Josephson parametric amplifier with a dc-SQUID, along with three additional test structures. Our fabrication process involves a dry-etched Nb coplanar waveguide resonator and Manhattan-style

[1] We acknowledge support by the German Research Foundation via Germany's Excellence Strategy (EXC-2111-390814868), and the BNBF via the project QUARATE (Grant No. 13N15380). This research is part of the Munich Quantum Valley, which is supported by the Bavarian state government with funds from the Hightech Agenda Bayern Plus

Al Josephson junctions. Additionally, we perform ex-situ galvanic contacts between Al and Nb via a bandaging process [2]. Fig. 1 (b) shows a typical device together with SEM images of the dc-SQUID and the junction in the Manhattan-style geometry. Consequently, the junction non-uniformity (see 1 (c)) appears as the result of the geometric angle dependence. Additionally, we suspect an inhomogeneous chemical treatment of our samples during development to contribute to the observed junction area inhomogeneity.

We measure 13 JPA chips with tunable resonators for a more comprehensive analysis and compare their properties with simulations of electromagnetic eigenmodes (see Fig. 2). In Fig. 2 (b), the histogram illustrates frequency variations across three different wafers and 13 JPAs in total, indicating a frequency standard deviation of around $\sigma_1 \simeq 288\,\text{MHz}$, $\sigma_2 \simeq 300\,\text{MHz}$, $\sigma_3 \simeq 171\,\text{MHz}$ for wafers W001, W002, W003, respectively. These significant variations can be explained by the divergence of the junction areas, which are on the order of 16% across the wafers. Additionally, we measure a JPA frequency mismatch at zero flux for all three wafers, $i = 1, 2, 3$ respectively, defined as a $\Delta_i = f_{\text{JPA}}(\Phi = 0) - f_0$, where f_0 is the targeted frequency based on our simulations in dependency of the junction inductance (also see Fig. 2(c)). The different mean frequencies result from thickness variations of the oxide barrier of the Josephson junctions on each wafer. The calculated junction inductance is related to the critical current I_c, extracted from our measurements, and depicted in Fig. 2 (c) for the wafers W001, W002, W003. Compared with the simulation, the corresponding frequency mismatches are $\Delta_1 \simeq 376\,\text{MHz}$, $\Delta_2 \simeq 299\,\text{MHz}$, $\Delta_3 \simeq 314\,\text{MHz}$. In order to reduce these frequency variations and mismatches, one needs to take into account the above-mentioned geometric effects and stabilize the oxidation process. These efforts are currently ongoing.

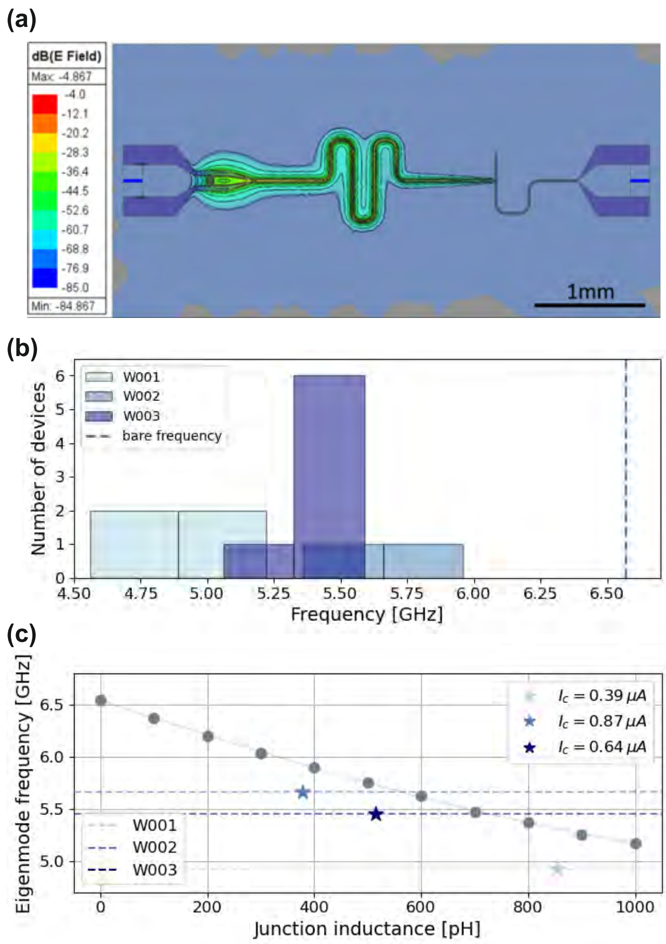

Figure 2: (a) JPA eigenmode simulation pattern. (b) Measured JPA frequency histograms. Dashed line denotes the bare resonance frequency at 6.54 GHz. (c) Simulation results of the JPA eigenfrequency versus the junction inductance and measurement results for each wafer.

References

[1] J. Kreikebaum, K. O'Brien, A. Morvan, and I. Siddiqi, Supercond. Sci. Technol. **33**, 06LT02 (2020).

[2] A. Dunsworth, A. Megrant, C. Quintana, Z. Chen, R. Barends, B. Burkett, B. Foxen, Y. Chen, B. Chiaro, A. Fowler et al., Appl. Phys. Lett. **111**, 022601 (2017).

Two-Dimensional Planck Spectroscopy

S. Gandorfer, M. Renger, W. K. Yam, F. Fesquet, A. Marx, R. Gross, K. G. Fedorov [1]

Detection and analysis of microwave quantum signals belong to fundamental tasks in the modern field of superconducting quantum technology. In order to experimentally extract information from weak microwave quantum signals, one has to apply sophisticated amplification and detection schemes for quantum state tomography [1]. A well-established approach to creating a connection between classical quantities (voltages, currents, etc.) measured at room temperature with conventional receivers to their quantum counterparts (photon numbers, probability amplitudes, etc.) is to embed a reference photon source in the experimental set-up. Here, many existing calibration techniques rely on black-body sources emitting well-defined thermal radiation following Planck's law [2].

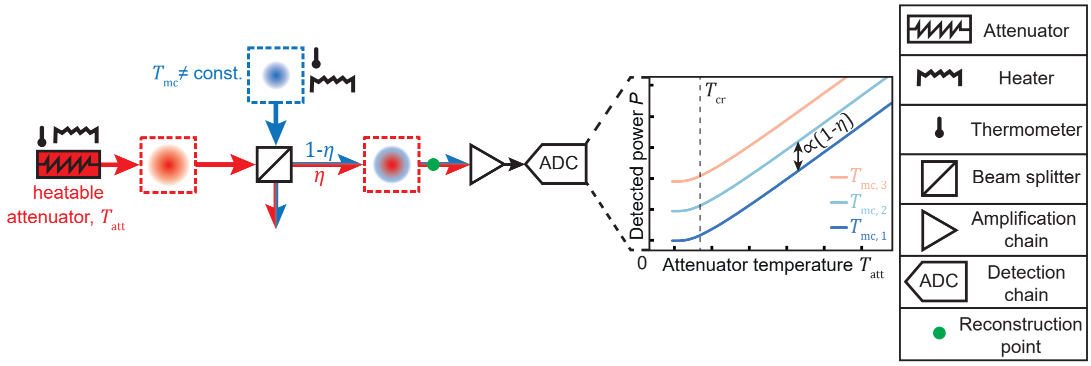

Figure 1: Schematic illustration of the two-dimensional Planck spectroscopy. Thermal noise at the respective mixing chamber temperature T_{mc} couples to a signal channel via unknown losses, $1-\eta$. These losses are modelled by an asymmetric beam splitter with transmissivity η. Next, the signal is amplified by a cryogenic HEMT amplifier and detected at room temperature using an analog-to-digital converter (ADC). The spacing between individual Planck curves, recorded for different $T_{\mathrm{mc},i}$, allows one to extract the unknown transmissivity η. The mixing chamber temperatures are chosen such that $T_{\mathrm{mc},1} < T_{\mathrm{mc},2} < T_{\mathrm{mc},3}$.

Here, we report on two-dimensional Planck spectroscopy as a new experimental approach allowing us to get rid of the loss estimation step, which is usually closely tied to the quantum state tomography procedure. In this way, we can achieve a fully self-consistent photon number calibration procedure. To experimentally determine the transmissivity η between the reference signal source and the reconstruction point, we introduce the two-dimensional Planck spectroscopy by sweeping two independent temperatures, namely the environmental temperature, which is provided by the mixing chamber temperature T_{mc} of the dilution cryostat housing the experiment, and the heatable attenuator temperature T_{att}. The corresponding experimental scheme is shown in Fig. 1. Here, we consider the lossy microwave components as 4-port devices and describe signal losses using a single, asymmetric beam splitter with associated power transmissivity η. Thus, signals incident at the input of this fictitious beam splitter are attenuated and a thermal state, with a mean photon number corresponding to the environmental temperature T_{mc}, couples to the microwave channel. Respectively, the microwave power measured at room temperature at the end of the amplification chain is given by

$$P = \frac{\kappa}{Z_0}\left[\frac{\eta}{2}\coth\left(\frac{hf_0}{2k_{\mathrm{B}}T_{\mathrm{att}}}\right) + \frac{1-\eta}{2}\coth\left(\frac{hf_0}{2k_{\mathrm{B}}T_{\mathrm{mc}}}\right) + n_{\mathrm{H}}\right], \qquad (1)$$

[1] We acknowledge support by the German Research Foundation via Germany's Excellence Strategy (EXC2111-390814868) and the BMBF via the project QUARATE (Grant No.13N15380). This research is part of the Munich Quantum Valley, which is supported by the Bavarian state government with funds from the Hightech Agenda Bayern Plus.

where κ is the photon number conversion factor (PNCF), h Planck's constant, k_B Boltzmann's constant, f_0 the carrier frequency, n_H the noise photon number added by the HEMT amplifier, and $Z_0 = 50\,\Omega$. We first analyze the power difference, ΔP, measured at room temperature at the end of the amplification chain for two different temperature values of the mixing chamber, $T_{mc} = T_{mc,1}, T_{mc,2}$, while we stabilize the heatable attenuator at a constant temperature. For environment temperatures well above the crossover temperature $T_{cr} = hf_0/2k_B$ [2], the noise power can be substituted, in good approximation, with the linear Johnson-Nyquist dependence. In this case, we find

$$\Delta P = (1-\eta)\left[P\left(T_{mc,2}\right) - P\left(T_{mc,1}\right)\right] \simeq \frac{\kappa}{Z_0}(1-\eta)\frac{k_B \Delta T}{hf_0}, \tag{2}$$

where $\Delta T \equiv T_{mc,2} - T_{mc,1}$. Equation (2) illustrates the fact that we can accurately estimate the unknown transmissivity η by measuring the vertical spacing between different conventional Planck spectroscopy curves shown in Fig. 1. By extending this method to at least three different mixing chamber temperatures, we can additionally investigate a potential temperature dependence of η.

For our experimental test of the two-dimensional Planck spectroscopy we perform six consecutive T_{att} sweeps, while increasing the mixing chamber temperature in steps of 50 mK, starting from $T_{mc} = 100$ mK. Figure 2 shows the resulting experimental data. All six Planck curves are simultaneously fitted with a weighted least-square fit according to Eq. (1). The weights for each Planck curve are chosen inversely proportional to the respective number of data points. For this fit, we employ κ, n_H, and η as fit parameters and observe a good agreement between the measured and fitted data for $\kappa_{2D} = 1.15\,(\mathrm{mV})^2$, $n_{H,2D} = 6.83$, and microwave losses $L_{2D} = -10\log\eta = 2.79$ dB. The measured number of noise photons the HEMT amplifier adds is in good agreement with the datasheet value of $n_H = 6.20$. At the carrier frequency of 5.5 GHz, we can also estimate the signal losses based on the datasheet values of individual components. Here, we obtain $L_{datasheet} = 2.18$ dB. We observe that the path loss obtained with the two-dimensional Planck spectroscopy is roughly 0.6 dB larger than the value estimated from the datasheet numbers. Moreover, we employ a Josephson metamaterial sample as a flux-tunable attenuator to benchmark the accuracy of the two-dimensional Planck spectroscopy and demonstrate that we are able to resolve microwave loss changes down to 0.1 dB [3].

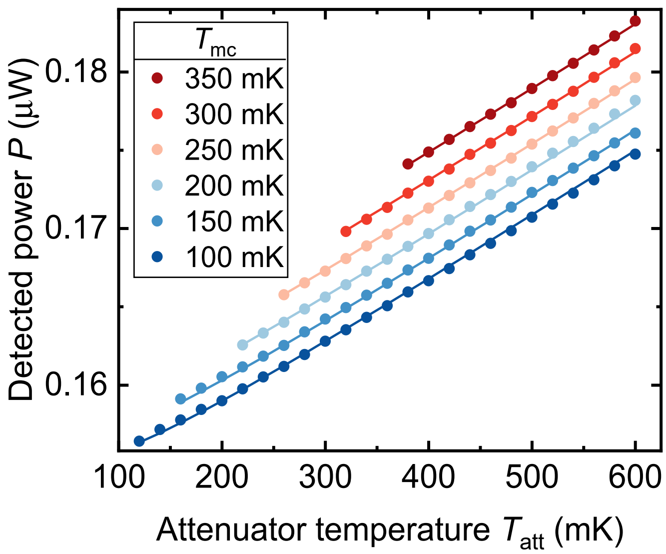

Figure 2: The experimental two-dimensional Planck spectroscopy of a microwave channel. Symbols represent experimental data while solid lines are fits according to Eq. (1). The losses extracted by using this procedure, $L_{2D} = 2.79$ dB, are higher than expected from the datasheet values.

References

[1] E. P. Menzel et al., Phys. Rev. Lett. **109**, 250502 (2012).
[2] M. Mariantoni, E. P. Menzel, F. Deppe, M. A. Araque Caballero, A. Baust, T. Niemczyk, E. Hoffmann, E. Solano, A. Marx, and R. Gross, Phys. Rev. Lett. **105**, 133601 (2010).
[3] S. Gandorfer, M. Renger, W. K. Yam, F. Fesquet, A. Marx, R. Gross, and K. G. Fedorov. Two-Dimensional Planck Spectroscopy. arXiv:2308.02389 (2023).

Optimization of the Microwave Cryogenic Link

W. K. Yam, M. Renger, S. Gandorfer, F. Fesquet, K. Honasoge, M. Handschuh, F. Kronowetter, Y. Nojiri, A. Marx, R. Gross, K. G. Fedorov [1]

The realization of quantum networks is a major step toward improving the capabilities of quantum information processing. In this context, superconducting quantum circuits represent one of the leading platforms. These circuits are operated at microwave frequencies and, therefore, require millikelvin temperatures to preserve their quantum properties. To avoid frequency conversion, it is advantageous to implement microwave quantum local area networks (QLANs) to interconnect remote superconducting nodes. At WMI, we have already realized a prototype microwave QLAN between two dilution cryostats, spatially separated by 6.6 m, connected via a cryogenic link. We reach a base temperature of 52 mK at the cryolink center and successfully demonstrate microwave entanglement distribution over the cryolink [1]. Here, we report further improvements in the cryolink performance.

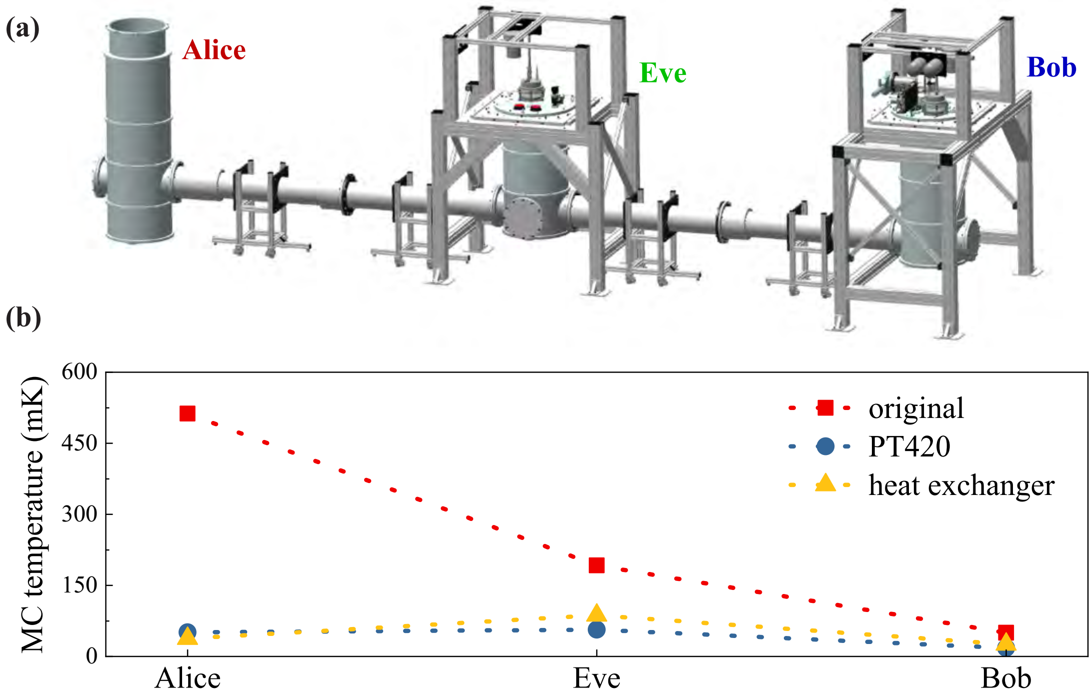

Figure 1: (a) Illustration of the cryolink with its three modules labeled Alice, Bob, and Eve. (b) Base temperatures at the mixing chamber (MC) stages of the cryolink modules after subsequent upgrades.

As illustrated in Fig. 1(a), our QLAN consists of three modules: a home-built dry dilution cryostat (Alice), an Oxford Instruments commercial dilution cryostat (Bob), and a cold network node (Eve). Over time, we have made several upgrades to the cryolink to improve its performance. In the Alice cryostat, we have first replaced its original Cryomech PT 410 cryocooler with a more powerful Cryomech PT 420 model. Second, we installed a counterflow heat exchanger in the mixture circuit to make the precooling of the circulating ^{3}He/^{4}He mixture more efficient. Figures 1(b) and 2 show an impact of these two modifications on the performance of the Alice cryostat. After upgrading the pulse tube cryocooler, we obtained more cooling power at the PT2 stage and, therefore, observed lower steady-state temperatures at various cryostat stages, such as the mixing chamber, the 1K pot, and the PT2 itself. After

[1] We acknowledge support by the German Research Foundation via Germany's Excellence Strategy (EXC-2111-390814868) and the EU Flagship project QMiCS (Grant No. 820505). This research is part of the Munich Quantum Valley, which is supported by the Bavarian state government with funds from the Hightech Agenda Bayern Plus.

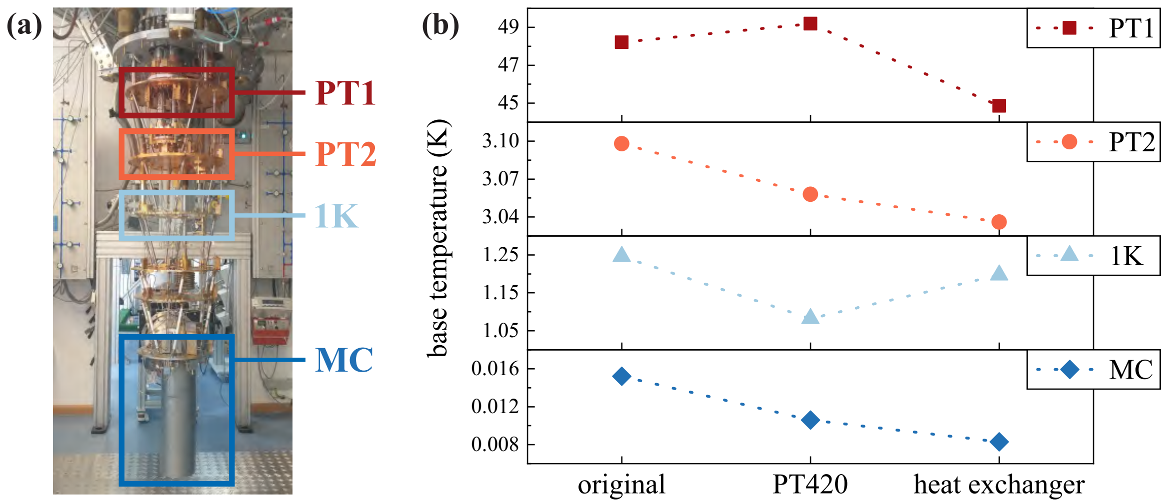

Figure 2: (a) Photo of the Alice cryostat with temperature stages of interest. (b) Base temperatures of these various stages of the Alice cryostat after subsequent upgrades (details are explained in the main text).

installing the counterflow heat exchanger, we observe a larger heat load at the 1K stage, which raises its base temperature to 1.2 K. Simultaneously, the MC base temperature decreases further to 8 mK. These upgrades in the Alice cryostat lead to considerable improvements in the cryolink performance and its operation time. Figure 1(b) shows changes in the base temperatures of the cryolink modules after each upgrade modification. We see a dramatic decrease in the Alice MC temperature from 512 mK to 51 mK after exchanging the pulse tube cryocooler, because it allows for a stable operation of the 1K pot under the cryolink heat load, which has not been possible with the old pulse tube cryocooler. This improvement is crucial, because it allows the QLAN to reach temperatures of around 100 mK, which is essential for transferring microwave quantum signals over it. Installing the counterflow heat exchanger does not aim to significantly decrease the cryolink base temperature, but rather to sustain the dilution cooling process over long periods of time. Previously, the cooldown period of the cryolink has been limited to around three weeks, since the ^{3}He/^{4}He mixing process eventually breaks down due to a gradually increasing heat load from the accumulation of leaked gases into the Alice internal vacuum chamber. The counterflow heat exchanger has notably improved the stability of the Alice cryostat by allowing it to operate at higher heat loads and extending the cryolink lifetime, provisionally, to several months.

Meanwhile, the upgraded cryolink is a powerful system that can be used to test various microwave quantum communication protocols in a QLAN setting. Our current experiments include performing microwave quantum teleportation and microwave quantum key distribution between spatially separated quantum nodes, and we have future plans to demonstrate remote entanglement of superconducting qubits across the cryolink. These efforts bring us closer to realizing distributed quantum computing with superconducting quantum circuits and serve as a foundation for integrating quantum microwaves into larger quantum networks.

References

[1] M. Renger, S. Gandorfer, W. Yam, F. Fesquet, M. Handschuh, K. E. Honasoge, F. Kronowetter, Y. Nojiri, M. Partanen, M. Pfeiffer, H. van der Vliet, A. J. Matthews, J. Govenius, R. N. Jabdaraghi, M. Prunnila, A. Marx, F. Deppe, R. Gross, and K. G. Fedorov. Cryogenic microwave link for quantum local area networks. arXiv:2308.12398 (2023).

High Fidelity Two-Qubit Gates in Superconducting Qubits with Closed-Loop Optimization

N. J. Glaser, M. Werninghaus, F. Roy, I. Tsitsilin, L. Koch, N. Bruckmoser, J. Romeiro, S. Filipp [1]

Realizing reliable and fast qubit operations is a critical challenge to realizing the potential of quantum computing. We investigate the performance of single- and two-qubit operations using coupler-assisted entangling via controlled-phase (CPHASE) gates in a system consisting of two fixed-frequency transmon-type qubits [1], see Fig. 1 (a). Our qubits are strongly coupled to a flux tunable coupling element [2]. The frequency of the coupler can be tuned by threading an external magnetic flux Φ_{ext} through the SQUID loop of the coupler, which is controlled via a flux current inducing a local magnetic field.

In this system, we realize single-qubit gates with $99.93(1)\,\%$ fidelity on qubit 1 and $99.7(1)\,\%$ on qubit 2, where the limits are set by the qubit dephasing and negligible effects from qubit crosstalk. To realize controlled-phase gates, we use the ZZ-type frequency shift

$$\chi = \tilde{\omega}_{11} - \tilde{\omega}_{01} - \tilde{\omega}_{10} + \tilde{\omega}_{00}, \qquad (1)$$

which arises from state hybridizations in the diagonalized Hamiltonian

$$\tilde{H}_{\text{comp}} = \sum_{n_1,n_2\in\{0,1\}} \tilde{\omega}_{n_1n_2} \left|n_1n_2\right\rangle \left\langle n_1n_2\right|, \qquad (2)$$

with the eigenstates $|n_1n_2\rangle$, and eigenfrequencies of the system $\tilde{\omega}_{n_1n_2}$. For a coupler frequency tuned far above the qubit frequency, this coupling element contributes only marginally to the dressed qubit states, and the qubits interact only by the finite residual direct coupling. The residual coupling can be further suppressed by choosing a coupler frequency, where the coupling with opposite signs cancels the interactions.

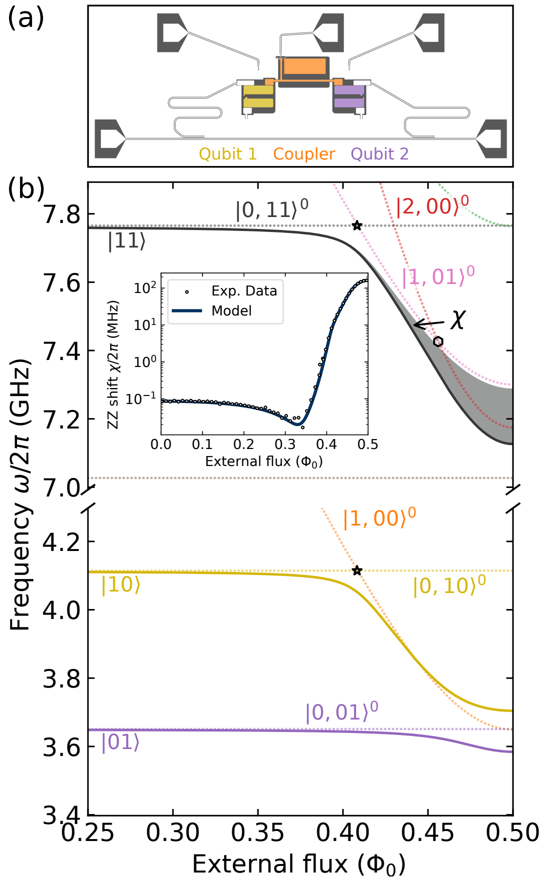

Figure 1: Experimental setup. (a) Layout of investigated two-qubit superconducting circuit sample. Two fixed-frequency parallel plate qubits are coupled via a tunable coupling element. Each qubit is coupled to a dedicated readout resonator coupled to a joined feedline. Dedicated microwave drive lines are used to drive the qubit, and a flux line is used to bias the frequency of the tunable coupling element. (b) Energy-level diagram. The computational adiabatic states $|n_1n_2\rangle$ (solid lines) and the bare states $|n_c, n_1n_2\rangle^0$ (dotted lines) are shown in the single- and two-excitation manifolds as a function of the external flux Φ_{ext} applied to the coupler. The transition frequencies ω are relative to the $|0,00\rangle^0$ state. The gray area indicates the shift χ of $|11\rangle$ respective to the sum of single-excitation frequencies, also depicted in the inset. The data points show experimentally measured χ.

[1] We acknowledge financial support from the German Federal Ministry of Education and Research via the funding program "Quantum technologies - from basic research to the market" under contract number 13N15680 "GeQCoS" and under contract number 13N16188 “MUNIQC-SC” as well as by the Deutsche Forschungsgemeinschaft (DFG, German Research Foundation) via project number FI2549/1-1 and the Germany’s Excellence Strategy EXC-2111-390814868 ‘MCQST’. The research is part of the Munich Quantum Valley, which is supported by the Bavarian state government with funds from the Hightech Agenda Bayern Plus.

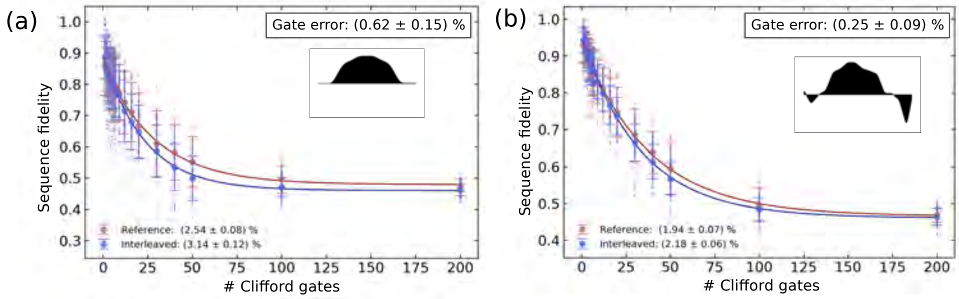

Figure 2: Interleaved randomized benchmarking of controlled-phase gates. We can extract the gate error of the CPHASE gate by comparing a pseudo-identity sequence consisting of two-qubit Clifford gates, with sequences interleaved with a CPHASE gate between every Clifford gate. We compare the results from a pulse based on (a) a Fourier series with five components and (b) 17 linearly interpolated points. The insets show the pulse shape, with features filtered according to the AWG response.

By adiabatically tuning the coupler frequency below the qubit frequency ($\star$ in Fig. 1(b)) we obtain strong frequency shifts χ, as the $|11\rangle$ state exclusively hybridizes with the bare second excited state of the coupler. To realize the CPHASE gate, we use a flux pulse to accumulate the entangling phase of π at elevated χ values and move back afterward. The fidelity of the CPHASE operation is strongly dependent on the pulse trajectory. We thus calibrate the acquired entangling phase and the single-qubit phase corrections while mitigating population loss [3] and reduced coherence during the interaction. We examine the performance of various pulse shape parametrizations, including Fourier series and piecewise constant parametrizations. We require the pulse shape to accommodate solutions to all error sources simultaneously, some of which show substantially correlated effects. Therefore, a certain complexity of the pulse shape is necessary and calibration sequences sensitive to individual parameters are less likely to exist.

We rely, therefore, on a joint optimization of all gate parameters by a multi-dimensional optimization routine based on the CMA-ES algorithm [4]. As a cost function, we use randomized benchmarking sequences with fixed-length evaluations [5]. We further exploit the cost scaling invariance between evolutions of the optimization to gradually adapt the error sensitivity. Using a Fourier series parametrization with a gate length of 60 ns, we reach CPHASE gate fidelities of 99.38(15) %, in interleaved randomized benchmarking experiments, see Fig. 2(a). We observe, however, that our system suffers from flux distortions in the flux control lines. By increasing the available degrees of freedom for the pulse shape, we further improve the gate fidelity and correct for distortions. Using linearly interpolated pulses consisting of 17 points, we decrease the error by roughly a factor of 2.5, resulting in a gate fidelity of 99.75(9) % and reduced leakage contributions, see Fig. 2(b). In combination with real-time flux distortion pre-compensation, with which we remove long-term memory effects, we plan to pursue using this gate within larger qubit systems.

References

[1] J. Koch, T. M. Yu, J. Gambetta, A. A. Houck, D. I. Schuster, J. Majer, A. Blais, M. H. Devoret, S. M. Girvin, and R. J. Schoelkopf, Physical Review A **76**, 042319 (2007).
[2] D. C. McKay, S. Filipp, A. Mezzacapo, E. Magesan, J. M. Chow, and J. M. Gambetta, Physical Review Applied **6**, 064007 (2016).
[3] M. C. Collodo, J. Herrmann, N. Lacroix, C. K. Andersen, A. Remm, S. Lazar, J.-C. Besse, T. Walter, A. Wallraff, and C. Eichler, Physical Review Letters **125**, 240502 (2020).
[4] N. Hansen, arXiv preprint arXiv:1604.00772 (2016).
[5] J. Kelly, R. Barends, B. Campbell, Y. Chen, Z. Chen, B. Chiaro, A. Dunsworth, A. G. Fowler, I.-C. Hoi, E. Jeffrey et al., Physical review letters **112**, 240504 (2014).

Enabling Remote Access to the First German Six-Qubit Quantum Processor

M. Knudsen, N. Glaser, J. Romeiro, M. Singh, G. Krylov, M. Werninghaus , S. Filipp [1]

In the pioneering effort of the superconducting qubit research within the Munich Quantum Valley, the Walther-Meissner-Institute (WMI) and the Technical University of Munich (TUM) have recently demonstrated remote access to its quantum processors. For the first time, a quantum computer fully developed within Germany will be available for collaborators and registered users to program quantum experiments and execute them live on six superconducting qubits.

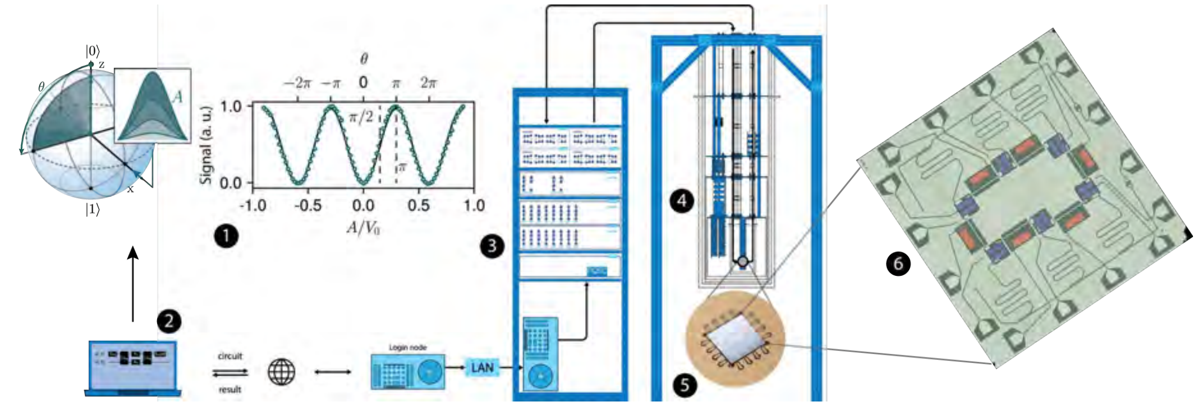

Figure 1: Schematic of the full remote quantum computing stack. The user can create quantum experiments (1) by programming a sequence of operations on a personal laptop (2) which are then sent to the WMI over the web. The local control stack of the WMI (3) interprets the sequence and converts them into microwave signals. These signals pass through the dilution refrigerator (4) and finally reach the quantum chip (5), where they are routed via the on-chip wires (6) to the qubits and coupling mediators (depicted in (6) in blue and red, respectively).

The different stages of a cloud-based quantum experiment are shown in Fig. 1. In the WMI-built quantum processor, the six Transmon qubits [1] are arranged in a ring-shaped connectivity architecture. To control interactions between neighboring qubits, tunable coupling elements that can be modulated or shifted in frequency are used to mediate the interaction strength and to realize two-qubit operations [2]. On the current device, single-qubit gates can be operated at 99.8% fidelity and two-qubit gates at 94% fidelity. The average qubit lifetime amounts to 36 microseconds, which would in theory allow to perform about a hundred qubit operations. By carefully characterizing operations on the qubits, the researchers at WMI can provide a set of operations - which act as logical quantum gates - and can be pieced together into a full-fledged quantum algorithm. While such operations are very similar to fundamental logical operations on classical computers, classical computers hide this layer of access from the user by translating the actual program code, through several compiler stages to this fundamental logic language. When working on currently available quantum computers, however, users can directly apply sequences of fundamental logical operations, the qubit gates, by applying microwave pulse signals to individual qubit units in order to manipulate the quantum state and observe its dynamics in real-time. The resulting measurements trace of such an experiment is shown in Fig. 1 (1). For application-oriented researchers, it is highly interesting to get their hands on quantum hardware and instead of doing numerical simulations directly test how an actual quantum system behaves. With direct access to quantum

[1]We acknowledge financial support by the BMBF within the program "Quantum technologies - from basic research to the market" via the projects "GeQCoS" (grant No. 13N15680) and "MUNIQC-SC" (grant No. 13N16188) as well as by the German Research Foundation (grant No. FI2549/1-1) and Germany's Excellence Strategy via 'MCQST' (EXC-2111-390814868). The research is part of the MQV, which is supported by the Bavarian state government with funds from the Hightech Agenda Bayern Plus.

computing hardware, problems such as the influence of noise on quantum computation or how certain implementation details need to be taken into account can be investigated, solved and improved.

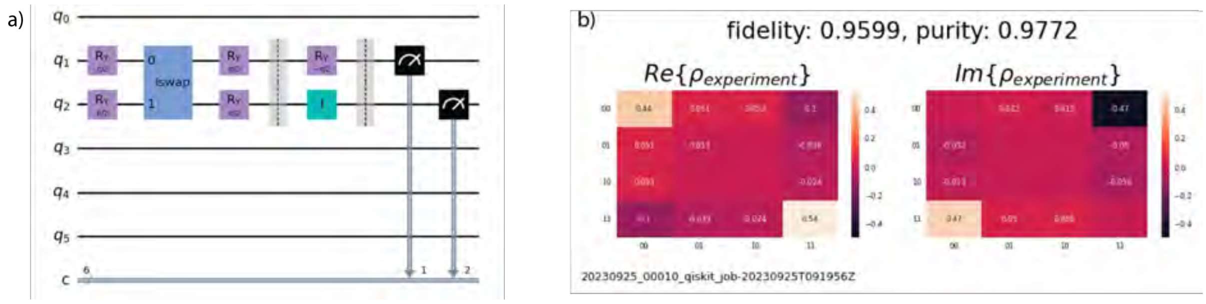

Figure 2: The pulse sequence (a) to prepare and measure a tomographic characterization of an entangled two-qubit state (b). Both figures are provided to the user via the interface of the remote access platform connecting to the WMI quantum computer.

The access to the hardware can vary in its level of abstraction. As the currently available quantum hardware is not able to run practical algorithms yet, the WMI cloud interface allows to conduct more fundamental quantum experiments. To guide users in this process, the WMI has created a collection of pre-designed experiments which offer an introduction and explanation of the experiments that users can execute on the quantum hardware. A well-known example are Rabi experiments: By incrementally increasing the amount of energy that is sent to the qubit by varying the amplitude of a microwave control pulse, one can cause the quantum state to evolve. This can be observed in Fig. 1 via the oscillating signal that is plotted as a function of the signal amplitude, and depicts the probability of the qubit being prepared in the excited state. This level of control is crucial to prepare one of the key capabilities of the quantum computer, namely to prepare quantum bits in a state of superposition, meaning that the qubit exists simultaneously in the logical state 0 and 1. The second unique feature of a quantum computer is its ability to create entangled states which can only be witnessed when using more than one qubit. Entangled qubits are no longer viewed as separate units, but rather host a joined quantum state, with exponentially enlarged information content.

To create entanglement in the system precise control over the interaction between two or more qubits is needed. With another experiment laid out in the cloud environment of the WMI a so-called Bell state - a state with a particularly high entanglement value - can be created. By using quantum tomography methods, as shown in Fig. 2, the creation of this Bell state could be verified with an accuracy of 96%, which showcases the entangling capabilities of the quantum computer at the WMI. Based on these experimental templates, users can design their own experiments and quantum algorithms to gain insights into the workings of quantum algorithms on superconducting qubits. Currently, access to the device is prioritized to realize experiments inside the Munich Quantum Valley. Over the course of the following years, the researchers at the WMI plan a gradual increase of the number and the performance of quantum processors that will become available to the public. Together with the Partners of the MQV, including the LRZ, the computer science departments of TUM and the theory collaborations within the MQV, this cloud access demonstrator will be used as a learning device for all partners to align on interfaces, standards and methodology.

References

[1] J. Koch, T. M. Yu, J. Gambetta, A. A. Houck, D. I. Schuster, J. Majer, A. Blais, M. H. Devoret, S. M. Girvin, and R. J. Schoelkopf, Phys. Rev. A **76**, 042319 (2007).

[2] D. C. McKay, S. Filipp, A. Mezzacapo, E. Magesan, J. M. Chow, and J. M. Gambetta, Phys. Rev. Applied **6**, 064007 (2016).

State Transfer and Entanglement Generation on a Chain of Six Superconducting Qubits

F. Roy, J. Romeiro*, N. Bruckmoser, N. Glaser, G. Huber, L. Koch, G. Krylov, J. Schirk, M. Singh, I. Tsitsilin, M. Werninghaus, S Filipp* [1] **contributed equally*

Superconducting qubit devices have recently demonstrated high-fidelity operations, high coherence times and improved scalability, making them a leading platform for quantum computing. However, practical applications require the efficient generation of many-qubit entangled states, incurring large overheads in single- and two-qubit gates, as qubit connectivity is generally limited to nearest-neighbour pairs. Nonetheless, by evolving the system under simultaneous local interactions, one can realise effective non-local multi-qubit operations and efficiently generate entanglement.

Here, we operate a circuit of six fixed-frequency transmons in a ring-like layout, shown in Fig. 1(a), where couplings are mediated by tunable couplers with individual flux line control. Individual readout resonators, coupled to two separate feed lines, are used to measure the qubit state with an average fidelity of $81.9 \pm 1.3\,\%$. The qubits are controlled via individual microwave lines, enabling 50 ns single-qubit gates with an average fidelity of $99.76 \pm 0.12\,\%$. These fidelities are mostly limited by the coherence times of the qubits, which have an average relaxation time of $45.47 \pm 6.35\,\mu s$ and an average dephasing time of $10.98 \pm 3.33\,\mu s$. During simultaneous operation, the average single-qubit fidelity is reduced to $98.92 \pm 0.53\,\%$, due to microwave crosstalk which averages to 22.18 % for neighbour qubits. Spurious ZZ-coupling also contributes to the reduction in fidelity. However, couplers can be biased to achieve $\leq$ 100 kHz ZZ for all qubit pairs. Biasing requires the effect of flux crosstalk to be taken into account, which is on average 7.19 % for all tunable couplers. We parametrically drive the couplers to activate two-qubit interactions [1] and implement iSWAP gates between neighbour qubits with an average fidelity of $97.28 \pm 0.98\,\%$ and an average length of 269.5 ns. Fig. 1(b) shows exemplary interleaved randomized benchmarking data used to calculate the quoted fidelities.

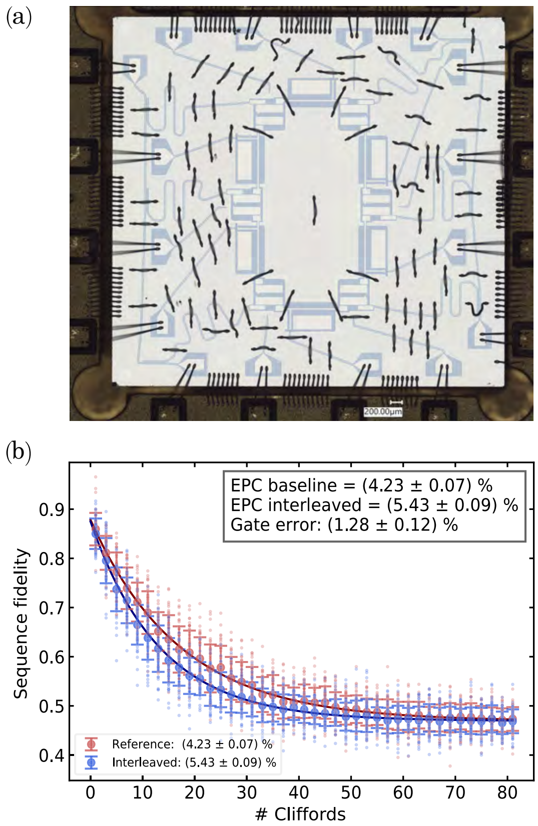

Figure 1: (a) Microscope image of a six-qubits device. Qubits are arranged in a ring with tunable elements between them to mediate couplings. Individual coupler flux lines and qubit drive lines enable full control of the system. Individual readout resonators coupled to feed lines on either side of the chip are used to measure the qubits. Wire bonds connect all ground planes and the PCB lines to lines on the chip. (b) Interleaved randomized benchmarking curve for an iSWAP gate between Q_2 and Q_3. Clifford gates are decomposed using DRAG-pulse for single qubit X-axis π and $\pm\pi/2$ rotations, phase increments for virtual-Z operations and square parametric pulse for iSWAP gates.

[1] We acknowledge financial support by the German Research Foundation via Germany's Excellence Strategy "EXC-2111-390814868", the Munich Quantum Valley, which is supported by the Bavarian state government with funds from the Hightech Agenda Bayern Plus, and the BMBF project GeQCoS (grant No. 13N15680

By driving the couplers simultaneously we activate couplings in a chain of qubits, as shown in Fig. 2(a). The Hamiltonian for the N qubits system is then given by

$$H_{\text{chain}} = \sum_{n=1}^{N} \Delta_n \sigma_n^+ \sigma_n^- + \sum_{n=1}^{N-1} J_n (\sigma_n^- \sigma_{n+1}^+ + h.c.)$$

where $\sigma_n^\pm$ are the raising (lowering) operators for qubit n, Δ_n are the qubit frequencies and J_n are the coupling strengths between qubit n and qubit $n+1$. By tuning the drive amplitudes and frequencies, we set $\Delta_n = 0 \ \forall n$ and $J_n = \frac{\pi}{2\tau}\sqrt{n(N-n)}$. Then, at integer multiples of the transfer time τ the system is effectively described by the non-local Hamiltonian

$$H_{\text{ST}} = \frac{\pi}{\tau} \sum_{n=1}^{\lfloor \frac{N-1}{2} \rfloor} \left(\prod_{k=n+1}^{N-n} \sigma_k^z \right) (\sigma_n^- \sigma_{N+1-n}^+ + h.c.).$$

Fig. 2(b),(c) show the transfer dynamics in the single-excitation manifold for a chain of six qubits, when preparing an excited state in the edge qubit (b) or an intermediate qubit (c). At multiples of the transfer time $\tau = 640\,\text{ns}$ the excitation is fully transferred between mirror-symmetric sites. Therefore, harnessing simultaneous local interactions, we obtain coherent state transfers between distant qubits along the chain.

In addition, the product term in H_{ST} describes the parity-dependent sign of the rotation, meaning that the number of excitations within the chain controls the phase of the transferred state, as described in [2]. This parity-dependent phase can be used to generate multi-qubit entanglement. To do this we prepare an equal superposition of all computational basis states by applying Hadamard gates on all qubits. Then, we apply a state transfer which imparts the parity-dependent phases. Finally, we use single qubit gates to map the obtained phases to a Greenberger-Horne-Zeilinger (GHZ) state, $(|000\rangle + |111\rangle)/\sqrt{2}$. Doing so we prepare a three-qubit GHZ state with a fidelity of 88.08 %, shown in Fig. 2(d), demonstrating that the state transfer generates entanglement. The method generalizes and can be used to demonstrate genuine entanglement in longer chains. However, it requires precise calibration of pulse parameters in order to maximise the fidelity of the transfer operation and of the obtained GHZ state.

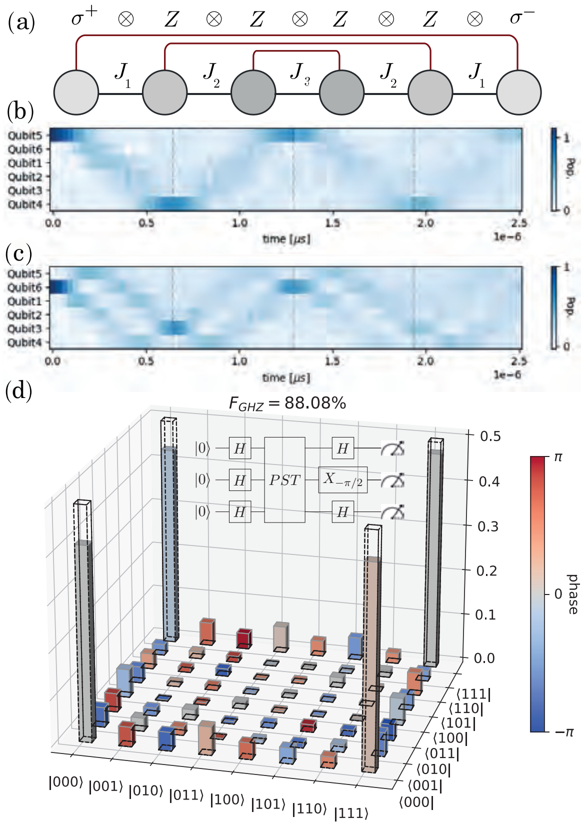

Figure 2: State transfer and entanglement generation. (a) Coupling schematic for the state transfer protocol. Qubits (circles) are connected in a chain of six by nearest-neighbour couplings (black lines). Evolving the system under symmetric analytically determined coupling strengths (J_i) implements a state transfer between mirror symmetric sites (red lines). The operation is equivalent to evolving under a hopping Hamiltonian with parity Z-operators for all intermediate qubit. Single excitation dynamics are shown for excitations starting on an edge qubit (b) and an intermediate qubit (c). In both cases the excitation refocuses at the mirror symmetric qubit after $\tau = 640\,\text{ns}$. (d) State tomography of a three-qubit GHZ state, prepared as shown in the inset circuit. Tomography is performed by measuring in the generalized Pauli basis and performing a physically-constrained maximum likelihood estimation to approximate the state which results in the measured outcomes.

References

[1] D. C. McKay, S. Filipp, A. Mezzacapo, E. Magesan, J. M. Chow, and J. M. Gambetta, Phys. Rev. Applied **6**, 064007 (2016).

[2] M. Nägele, C. Schweizer, F. Roy, and S. Filipp, Phys. Rev. Res. **4**, 033166 (2022).

Parametric Coupler Used for On-demand Reset, Readout and Leakage Recovery of Superconducting Qubits

G. Huber, F. Roy, M Werninghaus, N. Bruckmoser, N Glaser, L Koch, G Krylov, J Romeiro, M Singh, I Tsitsilin, S Filipp [1]

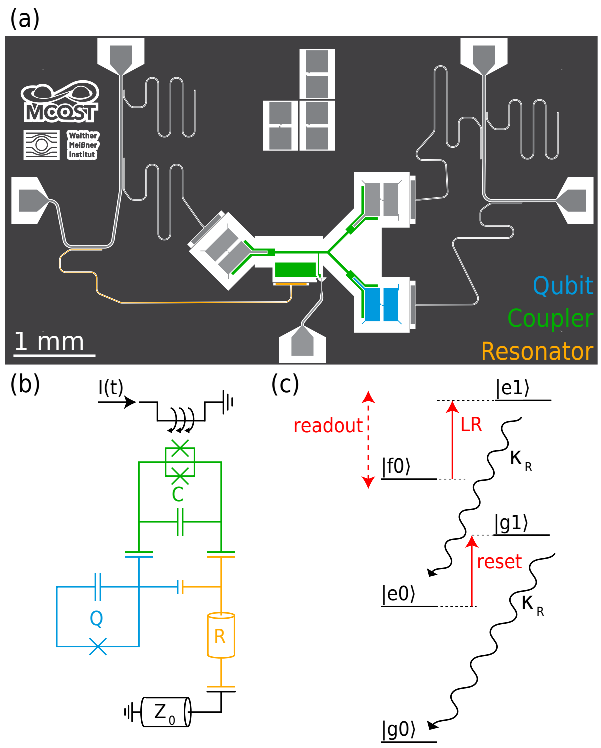

Figure 1: (a) Schematic of the chip design used in this work, with a qubit (blue), a coupler (green), and a resonator (yellow). (b) Simplified circuit of the qubit-coupler-resonator unit used for parametric interactions. Both qubit and resonator are strongly capacitively connected to the coupler. Stray capacitances lead to a small direct qubit-resonator capacitive coupling. The resonator is connected to the $50\,\Omega$ waveguide impedance via an on-chip feedline. (c) Energy diagram of the qubit and resonator with states labeled by $|QR\rangle$. The red arrows represent the used transitions for reset, leakage recovery operation and readout. Resonator relaxation at a rate κ_R is indicated by the black arrows.

To ensure a consistent bring-up of superconducting qubit processors, typical devices rely on passive initialization by relaxation. This progressively limits their effective operation rate as lifetimes and coherence times improve [1, 2] and is limited by unwanted residual excitation of qubits due to the finite temperature of their environment [3, 4]. Another source of error during operation comes from leakage to non-computational basis states introduced by the application of single- and two-qubit gates [5, 6]. Furthermore, in typical dispersive readout architectures the qubit coherence times are decreased due to interactions with the strongly coupled resonator used for readout [7–9]. Here, we present an architecture based on flux-tunable couplers, to remedy these problems. The chip design of the sample used is shown in Fig. 1(a) and a simplified circuit in Fig. 1(b). The design consists of a flux-tunable coupler (green) capacitively connected to a fixed frequency transmon (blue) and a superconducting coplanar resonator (orange). The resonator couples to the $50\,\Omega$ environment via a microwave feedline. The qubit and resonator couple strongly to the coupler and weakly to each other due to stray capacitances. Couplings between eigenstates of the system are activated by applying a resonant flux pulse on the coupler [10, 11]. We use the parametric drive to selectively couple two states $|A\rangle$ and $|B\rangle$ of the qubit and resonator, respectively, as indicated by the red arrows in the level diagram in Fig. 1(c). We perform the qubit reset operation by driving the transition $|\mathrm{A}\rangle = |e0\rangle$, $|\mathrm{B}\rangle = |g1\rangle$. By driving this reset transition for one oscillation period, the qubit excitation is swapped to the resonator, where it decays with the rate κ_R, see black arrows in Fig. 1(c). The effect of the reset pulse is shown in Fig. 2(a). The application of the reset pulse reduces the population in the excited state to $\mathrm{P}^{\mathrm{r}}_{\pi} = 0.33(0.03)\%$, outperforming the passive T_1 reset. Furthermore, the parametric flux pulse for the reset operation is 150 ns long, much shorter than the natural qubit lifetime $T_1 = 32(15)\,\mu\mathrm{s}$.

[1] We acknowledge financial support by the German Research Foundation via Germany's Excellence Strategy "EXC-2111-390814868", the Munich Quantum Valley, which is supported by the Bavarian state government with funds from the Hightech Agenda Bayern Plus and the BMBF program GeQCoS "No 13N15680"

The leakage recovery (LR) is performed by driving the transition $|A\rangle = |f0\rangle$, $|B\rangle = |e1\rangle$. We test the performance of the LR by performing randomized benchmarking (RB) with artificial leakage injection interleaved between Clifford-gates. We characterize the performance of the leakage recovery by measuring the steady state leakage population for different amounts of injected leakage, see Fig. 2(b). The introduction of the LR reduces the buildup of leakage by two orders of magnitude, compared to the case of un-mitigated leakage injection. For the readout operation we off-resonantly drive the $|A\rangle = |e, n\rangle$, $|B\rangle = |f, n-1\rangle$ transition, while simultaneously probing the resonator. In the frame of the drive, the qubit and resonator transition are now coupled by g_{eff} and detuned by Δ, leading to a shift in the resonator given by $\chi/2\pi \approx g^2/\Delta$. We measure this qubit state depended shift of the resonator to be $\chi/2\pi = -0.53\,\mathrm{MHz}$. Fig. 2(c) shows the single-shot readout of the qubit ground and excited state. We obtain clearly distinct measurement outcomes for the two qubit states, resulting in a measurement fidelity of $88(0.4)\%$. This set of operations is enabled using the same coupling element, reducing the system complexity and helping to mitigate challenges faced on the way to large-scale quantum processors.

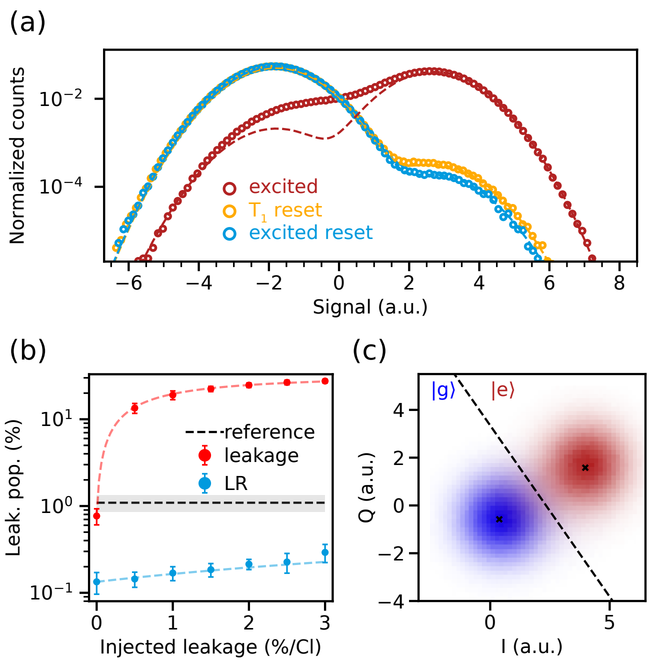

Figure 2: (a) Histogram of projected IQ data for different pulse sequences: T_1 reset performed, letting the qubit naturally decay (orange), excited state prepared by applying a π pulse (red), π pulse followed by a reset pulse (blue). (b) Equilibrium leakage population against the induced leakage for no injected leakage (black line), injected leakage (red points) and injected leakage plus the leakage recovery (red points). Red and blue dashed lines are predictions from rate equations. (c) IQ plot of the parametric measurement of the qubit ground state (blue) and the qubit excited state (red).

References

[1] A. P. M. Place, L. V. H. Rodgers, P. Mundada, B. M. Smitham, M. Fitzpatrick, Z. Leng, A. Premkumar, J. Bryon, A. Vrajitoarea, S. Sussman et al., Nat. Comm. **12**, 1779 (2021).

[2] C. Wang, X. Li, H. Xu, Z. Li, J. Wang, Z. Yang, Z. Mi, X. Liang, T. Su, C. Yang et al., npj Quantum Inf. **8**, 1–6 (2022).

[3] X. Y. Jin, A. Kamal, A. P. Sears, T. Gudmundsen, D. Hover, J. Miloshi, R. Slattery, F. Yan, J. Yoder, T. P. Orlando et al., Phys. Rev. Lett. **114**, 240501 (2015).

[4] A. Sultanov, M. Kuzmanović, A. V. Lebedev, and G. S. Paraoanu, Appl. Phys. Let. **119**, 144002 (2021).

[5] C. C. Bultink, T. E. O'Brien, R. Vollmer, N. Muthusubramanian, M. W. Beekman, M. A. Rol, X. Fu, B. Tarasinski, V. Ostroukh, B. Varbanov, A. Bruno et al., Sci. Adv. **6** (2020).

[6] B. M. Varbanov, F. Battistel, B. M. Tarasinski, V. P. Ostroukh, T. E. O'Brien, L. DiCarlo, and B. M. Terhal, npj Quantum Inf. **6**, 1–13 (2020).

[7] J. Gambetta, A. Blais, D. I. Schuster, A. Wallraff, L. Frunzio, J. Majer, M. H. Devoret, S. M. Girvin, and R. J. Schoelkopf, Phys. Rev. A **74**, 042318 (2006).

[8] C. Rigetti, J. M. Gambetta, S. Poletto, B. L. T. Plourde, J. M. Chow, A. D. Córcoles, J. A. Smolin, S. T. Merkel, J. R. Rozen, G. A. Keefe, M. B. Rothwell, M. B. Ketchen et al., Phys. Rev. B **86**, 100506 (2012).

[9] J. E. Johnson, C. Macklin, D. H. Slichter, R. Vijay, E. B. Weingarten, J. Clarke, and I. Siddiqi, Phys. Rev. Lett. **109**, 050506 (2012).

[10] D. C. McKay, S. Filipp, A. Mezzacapo, E. Magesan, J. M. Chow, and J. M. Gambetta, Phys. Rev. Applied **6**, 064007 (2016).

[11] M. Roth, M. Ganzhorn, N. Moll, S. Filipp, G. Salis, and S. Schmidt, Phys. Rev. A **96**, 062323 (2017).

Efficient Decoupling of a Non-linear Qubit Mode from its Environment

F. Pfeiffer, M. Werninghaus, L. Koch, N. Bruckmoser, N. Glaser, S. Filipp [1]
C. Schweizer [2,3] *C. A. Riofrio* [4]

As the coherence times of superconducting qubits continue to improve through advances in fabrication and qubit design [1, 2], understanding and circumventing the limits imposed by control and readout circuits becomes increasingly important. In particular, qubit readout typically relies on a dispersive coupling to a readout cavity in the form of a transmission line resonator and measuring the qubit-state dependent shift of the resonator frequency. The interaction with the resonator leads to a loss of coherence time of the qubit if the resonator is subject to residual excitations, e.g., caused by thermal noise or by unfiltered noise from the control electronics [3, 4]. In addition, the coupling to the readout mode increases the spontaneous emission rate of the qubit due to the Purcell effect [5]. To mitigate these effects, we design and characterize a three-mode circuit which exhibits a qubit mode with simultaneous protection from Purcell decay and residual photon-induced dephasing. The underlying idea is to generate a flux-insensitive qubit mode and a tunable mediator mode. By coupling two superconducting islands 1 and 2 to a middle island via Josephson junctions, the qubit mode $\mathcal{A}$ is realized as charge oscillations between the outer islands 1 and 2, with the middle island remaining charge neutral. Connecting a fourth island to the middle island via a superconducting interference device (SQUID) introduces two additional flux-tunable modes $\mathcal{B}$ and $\mathcal{C}$, while mode $\mathcal{A}$ remains unchanged and flux-insensitive. Mode $\mathcal{B}$ exhibits charge oscillations from islands 1 and 2 to island 3 and will be used as a tunable mediator. The remaining mode $\mathcal{C}$, in which charges oscillate between the three outer islands and the center island, can be shifted to high frequencies with a suitable choice of parameters. This results in a four-island device that forms a star-like pattern with the electrical circuit diagram shown in

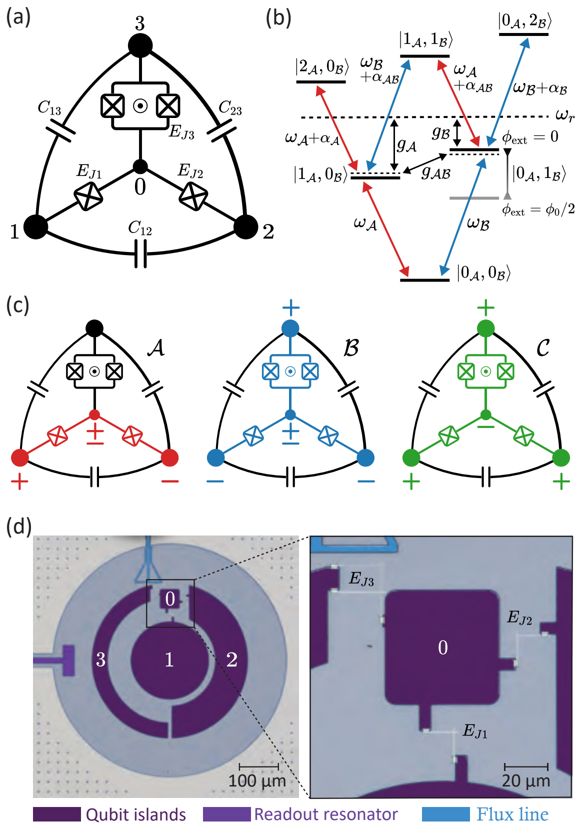

Figure 1: (a) Circuit diagram with outer nodes 1, 2, 3 and middle node 0. The most relevant capacitances are C_{12}, C_{13}, C_{23}. The Josephson energies between the outer nodes and the center node are labeled by E_{Ji}, with $E_{J3}(\phi_{\text{ext}})$ denoting the flux-dependent Josephson energy of the SQUID loop. (b) Energy level diagram restricted to the two-excitation subspace of modes $\mathcal{A}$ and $\mathcal{B}$ relative to the frequency of the readout resonator ω_r. (c) Normal modes under symmetry constraints $C_{13} = C_{23} \neq C_{12}$ and $E_{J1} = E_{J2} = E_{J3}$. Fixed frequency mode $\mathcal{A}$ (red) and frequency tunable modes $\mathcal{B}$ (blue) and $\mathcal{C}$ (green). The oscillating charge distributions are indicated by the (+) and (-) charges. (d) False-color microscope image of the qubit sample with the readout resonator coupler (left) and the flux line (top).

[1]This work is funded by the BMW Group, the DFG (FI 2549/1-1 and EXC-2111-390814868), the BMBF via projects GeCQoS (Grant No. 13N15680) and MUNIQC-SC (Grant No. 13N16188), and the Munich Quantum Valley.
[2]Fakultät für Physik, LMU München, Schellingstraße 4, D-80799 München, Germany
[3]C.S. acknowledges support by the European Union agreement No. 754388 (LMUResearchFellows)
[4]BMW Group, Munich, Germany

Fig. 1(a) and the described circuit modes are illustrated in Fig. 1(c). The nonlinearity of the Josephson junctions leads to non-linear cross-Kerr couplings between the modes, which are the crucial element for mediating interactions between the qubit mode $\mathcal{A}$ and its environment via the mediator mode $\mathcal{B}$.

In particular, when coupled capacitively to a readout resonator, mode $\mathcal{B}$ is used to mediate an indirect dispersive coupling through the non-linear cross-Kerr coupling $\alpha_{\mathcal{AB}}$ between the modes. This indirect coupling can be dynamically controlled by detuning mode $\mathcal{B}$ with respect to the readout resonator. We refer to the point of maximal dispersive interaction (minimal detuning $\Delta_{\mathcal{B}}$) as the readout point, while the point where the dispersive coupling is suppressed (maximal detuning $\Delta_{\mathcal{B}}$) is referred to as control point. We realize the three-mode qubit in a circular design as shown in Fig. 1(d). To demonstrate the Purcell protection we measure the T_1 time of modes $\tilde{\mathcal{A}}$ and $\tilde{\mathcal{B}}$ around the readout point for different values of the detuning $\Delta_{\tilde{\mathcal{B}}}$ of $\tilde{\mathcal{B}}$ set by an applied flux bias, see Fig. 2(a). Several T_1 measurements are performed at each value of $\Delta_{\tilde{\mathcal{B}}}$ to capture fluctuations in T_1. Mode $\tilde{\mathcal{B}}$ is strongly Purcell-limited at the readout point, with increasing detuning the T_1 time increases according to the Purcell limit. In contrast, mode $\tilde{\mathcal{A}}$ maintains a constant T_1-time, indicating that Purcell decay into the readout mode is strongly suppressed. For the demonstration of the protection against photon-induced dephasing, we use a broadband noise source to artificially inject photons into the resonator and track the T_2-time of the qubit mode $\tilde{\mathcal{A}}$, both at the readout point and the control point. At the readout point, the T_2-time decreases rapidly with the photon number. In contrast, when the dispersive shift $\chi_{\tilde{\mathcal{A}}}/2\pi = 19(4)$ kHz is strongly suppressed at the control point, T_2 remains constant over all measured noise photon numbers, thus showcasing the protection against photon-induced dephasing. The resulting highly protected qubit with tunable interactions may serve as a basic building block of a scalable quantum processor architecture, in which qubit decoherence and unwanted coherent interactions are strongly suppressed. More details can be found in [6].

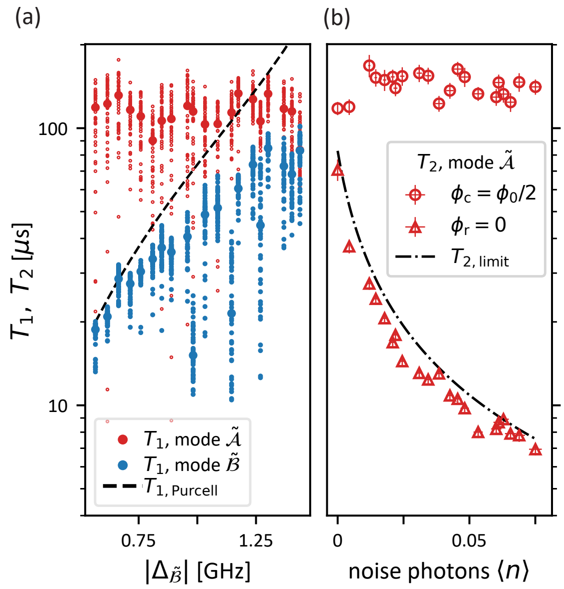

Figure 2: (a) T_1 of both modes vs. resonator detuning $\Delta_{\tilde{\mathcal{B}}}$ of mode $\tilde{\mathcal{B}}$ and comparison with the corresponding Purcell limit (dashed). (b) T_2 of mode $\tilde{\mathcal{A}}$ vs. noise photon number at the readout and control points.

References

[1] A. P. Place, L. V. Rodgers, P. Mundada, B. M. Smitham, M. Fitzpatrick, Z. Leng, A. Premkumar, J. Bryon, A. Vrajitoarea, S. Sussman, G. Cheng, T. Madhavan, H. K. Babla, X. H. Le, Y. Gang, B. Jäck, A. Gyenis, N. Yao, R. J. Cava, N. P. de Leon, and A. A. Houck, Nat. Commun. **12** (2021).

[2] A. Somoroff, Q. Ficheux, R. A. Mencia, H. Xiong, R. Kuzmin, and V. E. Manucharyan, Phys. Rev. Lett. **130** (2023).

[3] C. Rigetti, J. M. Gambetta, S. Poletto, B. L. Plourde, J. M. Chow, A. D. Córcoles, J. A. Smolin, S. T. Merkel, J. R. Rozen, G. A. Keefe, M. B. Rothwell, M. B. Ketchen, and M. Steffen, Phys. Rev. B **86** (2012).

[4] F. Yan, D. Campbell, P. Krantz, M. Kjaergaard, D. Kim, J. L. Yoder, D. Hover, A. Sears, A. J. Kerman, T. P. Orlando, S. Gustavsson, and W. D. Oliver, Phys. Rev. Lett. **120** (2018).

[5] A. A. Houck, J. A. Schreier, B. R. Johnson, J. M. Chow, J. Koch, J. M. Gambetta, D. I. Schuster, L. Frunzio, M. H. Devoret, S. M. Girvin, and R. J. Schoelkopf, Phys. Rev. Lett. **101** (2008).

[6] F. Pfeiffer, M. Werninghaus, C. Schweizer, N. Bruckmoser, L. Koch, N. J. Glaser, G. Huber, D. Bunch, F. X. Haslbeck, M. Knudsen, G. Krylov, K. Liegener, A. Marx, L. Richard, J. H. Romeiro, F. Roy, J. Schirk, C. Schneider, M. Singh, L. Södergren, I. Tsitsilin, F. Wallner, C. A. Riofrío, and S. Filipp, arXiv:2312.16988 (2023).

Development and Characterization of Josephson Traveling Wave Parametric Amplifiers

D.E. Bazulin, K.E. Honasoge, L. Koch, N. Bruckmoser, J. Schirk, T. Luschmann, A. Marx, S. Filipp, and K.G. Fedorov [1]

Large-scale superconducting quantum processors impose stringent requirements on the amplification of qubit readout signals in order to ensure a high signal-to-noise ratio. Typically, one would like to achieve an amplification gain in excess of 20 dB over a bandwidth > 1 GHz, while operating as close as possible to the standard quantum limit. In principle, superconducting Josephson traveling wave parametric amplifiers (JTWPAs) are capable of satisfying these requirements. JTWPAs exploit wave-mixing processes occurring across an extended nonlinear medium, formed by Josephson junctions or various types of SQUIDs connected in series. Here, we report on the development of a flux-pumped JTWPA based on superconducting nonlinear asymmetric inductive elements (SNAILs) [1], with a pump signal propagating through a separate line that is inductively coupled to a SNAIL array. The main advantages of flux-pumping are increased 1 dB compression powers and suppression of the signal back-action on the pump [2].

We fabricate JTWPAs at the WMI using the three-step fabrication process analogous to the WMI qubit process. A ground plane, pump line, and fishbone capacitors are made of niobium using the optical lithography at the first step. Then, SNAILs are fabricated using the aluminum-based double-angle evaporation process with e-beam lithography. In the last step, we implement aluminum bandages. We rely on symmetric fishbone capacitors to provide the JTWPA characteristic impedance of 50 Ω [3].

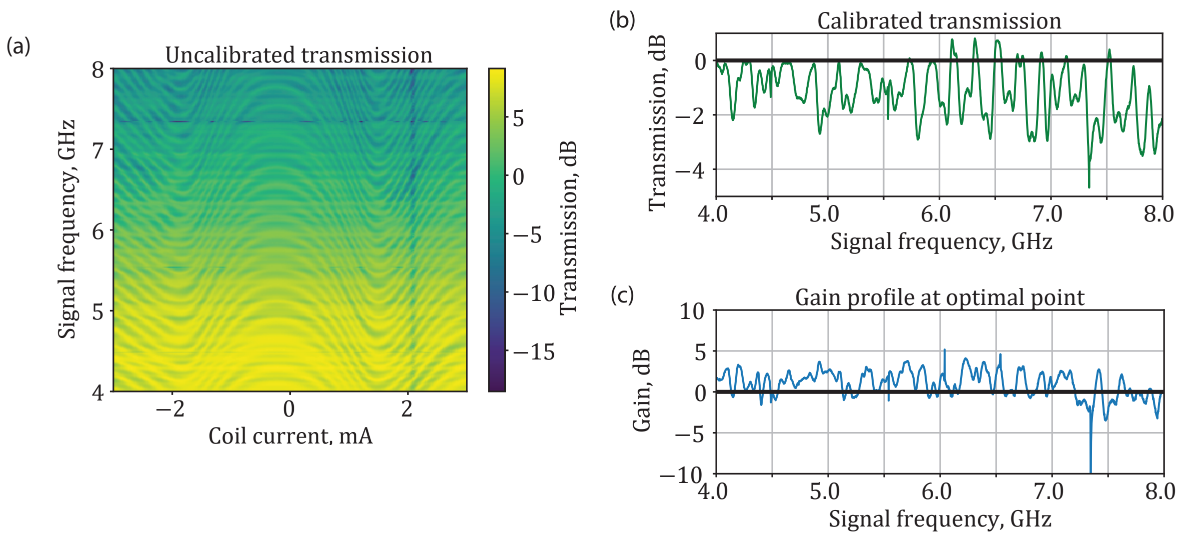

Figure 1: (a) Characterization measurements of the flux-pumped JTWPA. Uncalibrated transmission through the JTWPA signal line in the absence of a pump tone. (b) JTWPA insertion losses at zero magnetic flux bias, calibrated with a bypass cryogenic switch through an SMA barrel. (c) JTWPA calibrated gain at the sweet spot of $\Phi = 0.38\,\Phi_0$.

Using SNAILs as a basic cell of the JTWPA enables operation in a pure three-wave mixing regime with complete suppression of the four-wave mixing processes at a specific point of

[1] We acknowledge support by the German Research Foundation via Germany's Excellence Strategy (EXC-2111-390814868) and the BMBF via the projects GeCQoS (grant No. 13N15680) and QUARATE (grant No. 13N15380). This research is part of the Munich Quantum Valley, which is supported by the Bavarian state government with funds from the Hightech Agenda Bayern Plus.

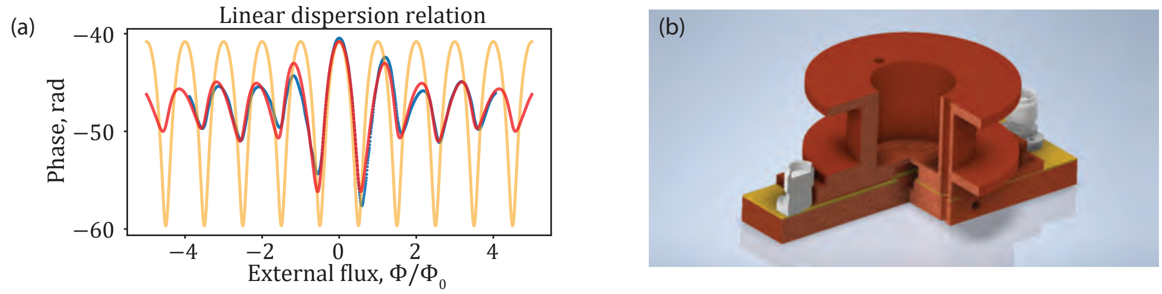

Figure 2: (a) Magnetic field inhomogeneity in the JTWPA. Phase response of the JTWPA at the signal frequency of 4 GHz for different values of external magnetic flux in the case of an ideal homogeneous field (orange line) and parabolic inhomogeneity with the field difference of 30 % between the center and edges of the chip (red line). Blue dots represent the experimental data. (b) 3D model of a new JWTPA sample holder compatible with a larger magnetic coil, aimed at providing the inhomogeneity around 1 % across the chip.

an external magnetic flux bias. We characterize several JTWPAs at 30 mK using an external superconducting magnetic coil for flux biasing. As a calibration reference, we use transmission measurements through an SMA barrel connected in parallel to the JTWPA between two microwave switches. This calibration provides an estimation of frequency-dependent JTWPA insertion losses over the 4-8 GHz bandwidth (see Fig.1(b)). In order to characterize the gain, we conduct a fine sweep of magnetic flux around the sweet-spot $0.38\,\Phi_0$ with the applied pump drive at 12 GHz. By varying the pump power and current through the magnetic coil, we can determine optimal working parameters corresponding to the highest JTWPA gain. We estimate the gain by dividing the measured transmission of the pumped JTWPA by the calibration data. Fig.1(c) shows a respective gain profile of the JTWPA consisting of 371 SNAILs. We observe a small average gain around 2-3 dB with strong ripples over a large spectral bandwidth. The ripples come from an imperfect impedance matching due to the sub-optimal Josephson critical currents and inhomogeneities of the external magnetic field.

The magnetic field inhomogeneity is one of the current bottlenecks in the operation of our flux-pumped JTWPAs. It arises due to the small geometric size of the magnetic coil and results in biasing each of the SNAILs differently, causing higher-order nonlinearities to appear and disturbing the impedance and phase matching of the JTWPA. As a consequence of this inhomogeneity, the JTWPA phase response at a fixed signal frequency as a function of magnetic flux resembles the Fraunhofer pattern, as shown in Fig.2(a). By comparing the experimental data with our model, we infer that the existing coil has the field inhomogeneity around 30 %. In order to resolve this issue, we have developed a new coil design aiming for the field inhomogeneity of <1 % (see Fig.2(b)). By employing the new coil design in conjunction with better critical current targeting, we aim to reach gain values of around 15-20 dB in the bandwidth 4-8 GHz with the next generation of the flux-pumped JTWPAs.

References

[1] N. E. Frattini, U. Vool, S. Shankar, A. Narla, K. M. Sliwa, and M. H. Devoret, Appl. Physics Letters **110**, 222603 (2017).
[2] A. Zorin, Phys. Rev. Applied **12**, 044051 (2019).
[3] Y. Lu, W. Xu, Q. Zuo, J. Pan, X. Wei, J. Jiang, Z. Li, K. Zhang, T. Guo, S. Wang, C. Cao, H. Wang, W. Xu, G. Sun, and P. Wu, Appl. Physics Letters **120**, 082601 (2022).

Progress in High-Coherence Transmon Qubit Fabrication

D. Bunch, L. Koch, N. Bruckmoser, L. Södergren, S. Filipp [1]

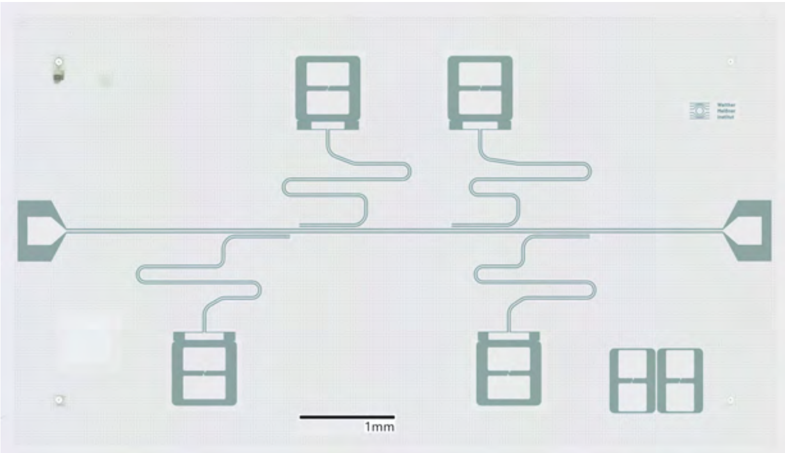

Figure 1: Micrograph of a 2-port $6 \times 10\,\mathrm{mm}^2$ transmon test chip. Four qubits are coupled to the transmission lines with coplanar waveguide resonators. Two additional isolated qubits are available for testing junction critical current. The scale bar is 1 mm.

A fault-tolerant quantum computer relies upon high-fidelity gate operations on qubits with long coherence times. On the superconducting qubit platform, these qubit coherence times are typically limited by material losses, so efforts to extend coherence are focused on improving chip fabrication methods. The majority of losses in state-of-the-art superconducting circuits originate from two-level systems (TLS) which interact via their dipole moments with the qubit. [1] During fabrication, special attention goes to the interfaces between metal, air, and substrate, since they host a high density of TLSs, often in oxides at the surface. [2]

In 2023, the TLS density at interfaces has been drastically reduced by optimizing cleaning procedures and applying a buffered oxide etch (BOE) cleaning wherever possible. This procedure is based on a hydrofluoric acid solution which removes lossy oxides on the Si substrate and Nb ground plane surfaces. Utilizing the BOE at key steps during fabrication allows us to control many of the important interfaces in our qubit chips.

To further increase qubit coherence times, much work has gone into optimizing our reactive ion etching (RIE) parameters. The quality of the RIE process depends heavily on the proportion of the RF power between the main parallel-plate etch chamber and the inductively coupled plasma (ICP) unit. Incorporating the ICP unit into our etch recipes increases the density of the reactive ions that etch the niobium and silicon. By fine-tuning this proportion, we have achieved a highly anisotropic etch profile that results in straight, smooth sidewalls. The combination of the above-mentioned methods has led to a reduction in dielectric losses.

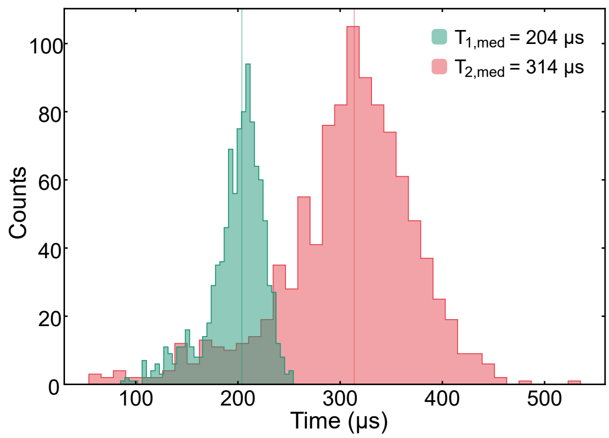

Figure 2: Histogram of qubit coherences. Reported statistics are averages over many T_1 and T_2 measurements on the same qubits.

These investigations and optimizations in the last project year have led to improvements in qubit lifetimes. Our transmon qubits now

[1]This project has received support from the BMBF program No. 13N15680 (GeCQoS), the Munich Quantum Valley Quantum Computer Demonstrators - Superconducting Qubits (MUNIQC-SC; project number: 13N16188), and the Munich Quantum Valley, which is supported by the Bavarian state government with funds from the Hightech Agenda Bayern Plus.

exhibit a median lifetime T_1 of (204 ± 28) μs and a median dephasing time T_2 of (314 ± 66) μs, as shown in Fig. 2. The redesign of the junction array as well as improved niobium etching conditions have also resulted in higher yield and higher quality qubits. Work continues on optimizing the junction fabrication process in order to increase qubit lifetimes further.

References

[1] C. R. H. McRae, H. Wang, J. Gao, M. R. Vissers, T. Brecht, A. Dunsworth, D. P. Pappas, and J. Mutus, Rev. Sci. Instr. **91**, 091101 (2020).

[2] M. V. P. Altoé, A. Banerjee, C. Berk, A. Hajr, A. Schwartzberg, C. Song, M. Alghadeer, S. Aloni, M. J. Elowson, J. M. Kreikebaum, E. K. Wong, S. M. Griffin, S. Rao, A. Weber-Bargioni, A. M. Minor, D. I. Santiago, S. Cabrini, I. Siddiqi, and D. F. Ogletree, PRX Quantum **3**, 020312 (2022).

Development and Characterization of Fluxonium Qubits

C.M.F. Schneider, J. Schirk, F. Wallner, I. Tsitsilin, N. Bruckmoser, L. Koch, V. Koch, L. Huang, N. Glaser, M. Singh, G. Krylov, K. Liegener, M. Werninghaus, S. Filipp [1]

In the realm of superconducting qubits, the Transmon has emerged as a cornerstone, demonstrating high coherence times [1], high-fidelity control [2, 3], and fast and high-fidelity readout capabilities [4, 5] in isolated single or two-qubit samples. However, challenges arise when scaling up to processor-level configurations. Each additional element, be it control lines, flux lines, or tunable couplers, tends to diminish the coherence time. Additionally, defects randomly distributed in frequency space can collide with qubit frequencies [6] and gate fidelities can suffer due to crosstalk and leakage, due to the inherently low anharmonicity of Transmons [2]. While these challenges may be resolvable, they demand increasingly extensive efforts, emphasizing the importance of exploring possible alternative qubit designs.

In pursuit of this goal, we are investigating the potential of Fluxonium qubits, which have demonstrated very promising results in terms of coherence times and gate fidelities [7, 8]. These circuits, however, possess increased complexity due to their requirement for a larger number of Josephson Junctions (JJs). Unlike Transmons, which require just a single or, at maximum, two JJs, Fluxoniums necessitate an array of at least 80 JJs, serving as a very high linear inductance called superinductance, in addition to the single junction. Fig. 1 displays a SEM image alongside a Fluxonium's corresponding electrical circuit diagram. The large number of identical junctions demands highly reliable nanofabrication and careful design studies. Moreover, Fluxoniums require an applied magnetic field for operation that creates half a flux quantum in the loop formed by the superinductance and the single junction. The associated additional flux bias line and the sensitivity of the loop to flux noise require extensive characterization and optimization of the setup, highlighting the intricate balance between innovative design and practical implementations of novel qubit designs.

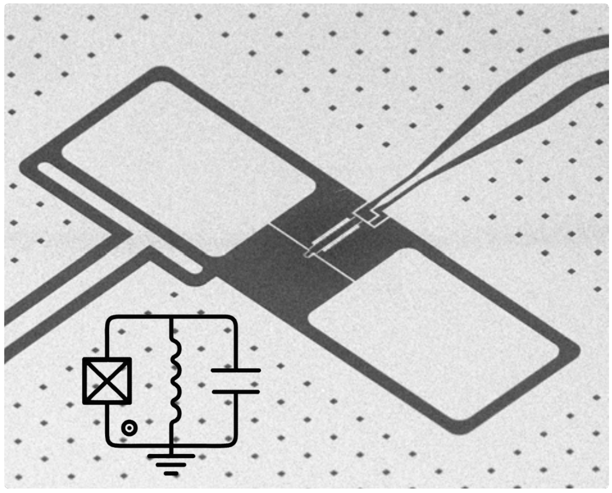

Figure 1: Scanning electron image (SEM) and circuit diagram of a first Fluxonium qubit. Two capacitive pads are linked by a parallel arrangement consisting of a single JJ with a low critical current and a series of JJs, each having a high critical current. These collectively act as a high linear inductance, also known as superinductance. Also displayed at the bottom left is the coupled readout resonator and the necessary flux bias line at the top right.

Over the past year, we have successfully designed, fabricated, and characterized three generations of Fluxonium qubits, achieving average lifetimes around 80 µs and Ramsey coherence times around 50 µs. Fig. 2 presents the main results from one of our best-performing Fluxoniums with promising first life and coherence times [Fig. 2(a)]. We also achieved high-fidelity ($> 98\,\%$) and fast (600 ns) readout without parametric amplifiers as characterized in Fig. 2(b). Furthermore, by employing straightforward optimization routines that utilize error amplification, we have attained single qubit gate fidelities above 99.9 %, as presented in Fig. 2(c).

[1] This project is part of the Munich Quantum Valley, which is supported by the Bavarian state government with funds from the Hightech Agenda Bayern Plus and has received support by the Munich Quantum Valley Quantum Computer Demonstrators - Superconducting Qubits (MUNIQC-SC; project number: 13N16188) as well as the EU project OpenSuperQPlus.

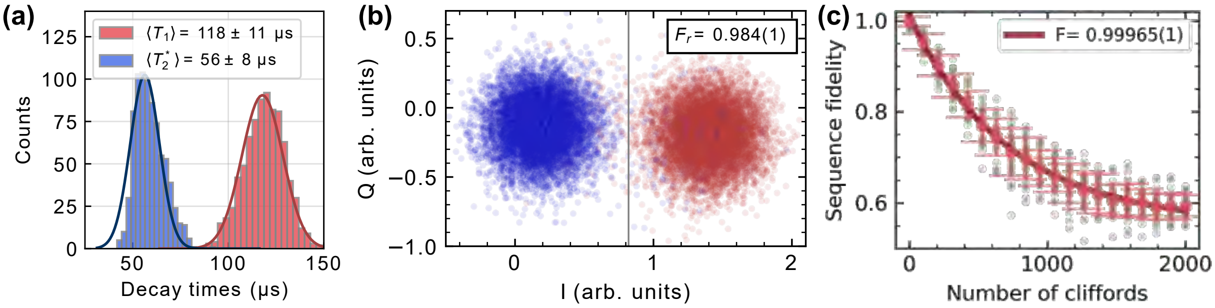

Figure 2: Characterization of Fluxonium1. (a) Histogram displaying lifetimes (red) and coherence times (blue) for a single qubit. (b) *IQ* plot for ground (blue) and excited (red) state. Each point in this plot represents a single-shot measurement of the in-phase (I) and out-of-phase (Q) amplitudes of the acquired voltages at the digitizer relative to the applied measurement pulse. The qubit is assigned to the ground state when the I value falls below a threshold, here set at 0.82 as indicated by the gray vertical line. Incorrect assignments, indicating a discrepancy between the qubit's prepared and measured states, determine the readout fidelity F_r, which, in our case, is primarily limited by state preparation. (c) Randomized benchmarking results for a 15 ns single-qubit gate for Fluxonium1. This experiment involves a sequence of numerous Clifford operations, followed by an inverse gate to reverse all preceding operations. The y-axis indicates the probability of the qubit returning to the ground state. The gate fidelity is determined by fitting this probability as a function of the number of applied Clifford operations (x-axis).

Measurements varying the gate length have revealed that we were coherence-limited. To enhance qubit performance, especially coherence, we have developed comprehensive noise models to identify current limitations and optimize future designs accordingly. Moreover, we have optimized the experimental setup in an iterative process, identifying optimal filter, attenuation, and wiring configurations.

Looking ahead, our primary objectives are enhancing single-qubit performance and progressing towards coupled Fluxonium setups. We are also committed to developing innovative control and readout schemes. Through these advancements, we aim to pave the way for constructing a small-scale quantum processing unit based on Fluxonium qubits.

References

[1] C. Wang, X. Li, H. Xu, Z. Li, J. Wang, Z. Yang, Z. Mi, X. Liang, T. Su, C. Yang, G. Wang, W. Wang, Y. Li, M. Chen, C. Li, K. Linghu, J. Han, Y. Zhang, Y. Feng, Y. Song, T. Ma, J. Zhang, R. Wang, P. Zhao, W. Liu, G. Xue, Y. Jin, and H. Yu, npj Quantum Information **8**, 1–6 (2022).

[2] M. Werninghaus, D. J. Egger, F. Roy, S. Machnes, F. K. Wilhelm, and S. Filipp, npj Quantum Information **7**, 1–6 (2021).

[3] J. Stehlik, D. M. Zajac, D. L. Underwood, T. Phung, J. Blair, S. Carnevale, D. Klaus, G. A. Keefe, A. Carniol, M. Kumph, M. Steffen, and O. E. Dial, Phys. Rev. Lett. **127**, 080505 (2021).

[4] F. Swiadek, R. Shillito, P. Magnard, A. Remm, C. Hellings, N. Lacroix, Q. Ficheux, D. C. Zanuz, G. J. Norris, A. Blais, S. Krinner, and A. Wallraff. Enhancing Dispersive Readout of Superconducting Qubits Through Dynamic Control of the Dispersive Shift: Experiment and Theory. `arxiv:2307.07765 [quant-ph]` (2023).

[5] E. I. Rosenthal, C. M. F. Schneider, M. Malnou, Z. Zhao, F. Leditzky, B. J. Chapman, W. Wustmann, X. Ma, D. A. Palken, M. F. Zanner, L. R. Vale, G. C. Hilton, J. Gao, G. Smith, G. Kirchmair, and K. W. Lehnert, Phys. Rev. Lett. **126**, 090503 (2021).

[6] S. Krinner, N. Lacroix, A. Remm, A. Di Paolo, E. Genois, C. Leroux, C. Hellings, S. Lazar, F. Swiadek, J. Herrmann, G. J. Norris, C. K. Andersen, M. Müller, A. Blais, C. Eichler, and A. Wallraff, Nature **605**, 669–674 (2022).

[7] A. Somoroff, Q. Ficheux, R. A. Mencia, H. Xiong, R. Kuzmin, and V. E. Manucharyan, Phys. Rev. Lett. **130**, 267001 (2023).

[8] I. N. Moskalenko, I. A. Simakov, N. N. Abramov, A. A. Grigorev, D. O. Moskalev, A. A. Pishchimova, N. S. Smirnov, E. V. Zikiy, I. A. Rodionov, and I. S. Besedin, npj Quantum Information **8**, 1–10 (2022).

Materials, Thin Film and Nanotechnology, Experimental Techniques

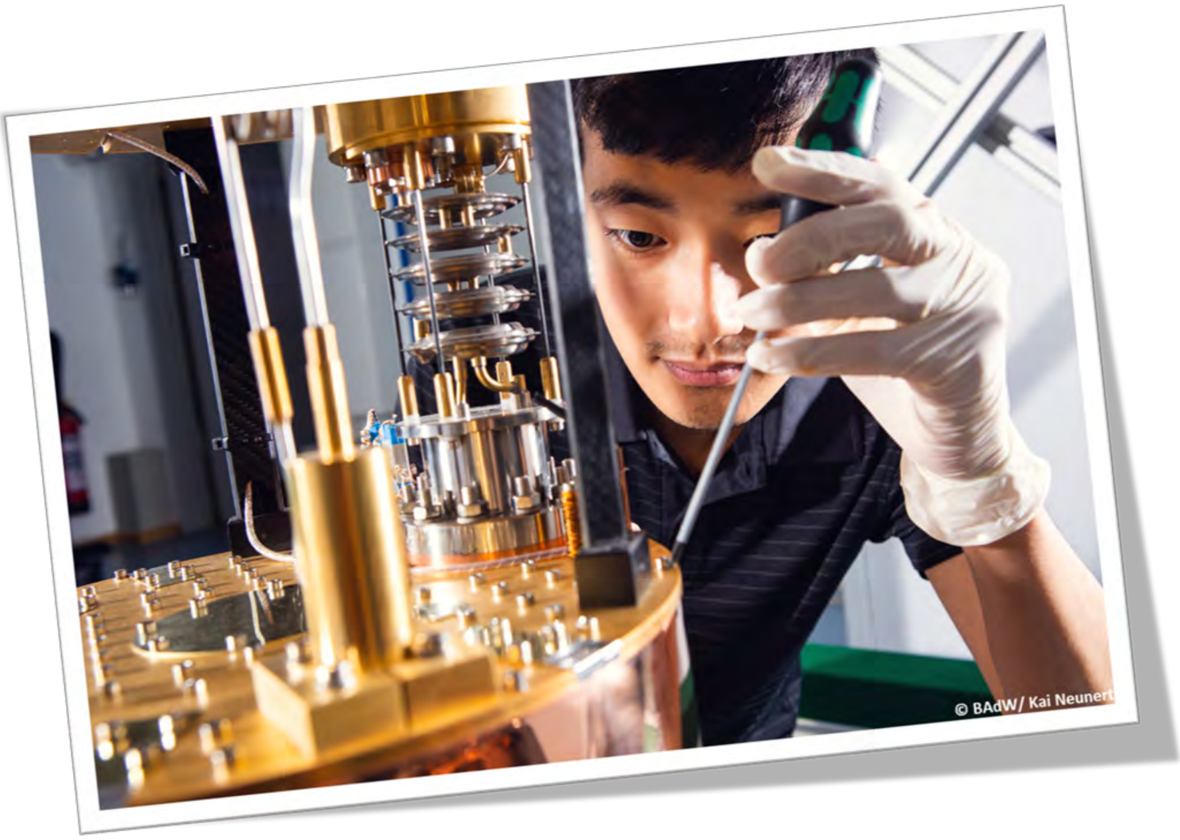

Broadband Electron Spin Resonance Spectroscopy of Rare-Earth Spin Ensembles at mK Temperatures

A. Strinic, P. Oehrl, O. Huisman, H. Huebl, R. Gross, N. Kukharchyk [1]

Hybrid systems that combine a superconducting quantum processor and a quantum memory unit are expected to improve the functionalities and performance of existing quantum computing architectures [1]. To this end, quantum memories operating at microwave frequencies are considered optimal due to their natural frequency compatibility with superconducting quantum processors. A potential platform are rare-earth spin ensembles, since they exhibit exceptionally long coherence times when exploiting their zero first-order Zeeman (ZEFOZ) transitions [2], which originate from hyperfine interactions in the GHz frequency range. In order to identify and model the spin resonance transitions relevant for quantum memory applications, the detailed knowledge of the spin Hamiltonian parameters is essential. In this work, we determine the parameters of the spin Hamiltonian for ^{167}Er defects in a ^{7}LiYF$_4$ host using broadband electron spin resonance (ESR) spectroscopy. This spin system is described by the effective spin Hamiltonian

$$H_{\text{eff}} = H_Z + H_{\text{HF}} + H_Q = \mu_B \boldsymbol{g} \cdot \boldsymbol{B} \cdot \boldsymbol{S} + \boldsymbol{S} \cdot \boldsymbol{A} \cdot \boldsymbol{I} + \boldsymbol{I} \cdot \boldsymbol{Q} \cdot \boldsymbol{I} \tag{1}$$

describing the energy level structure of the ^{167}Er^{3+} ground state ($^4I_{15/2}$, with $S = 1/2, I = 7/2$) with the electron Zeeman (H_Z), the hyperfine (H_{HF}) and the nuclear quadrupole (H_Q) interactions, with the characteristic interaction tensors $\boldsymbol{g}$, $\boldsymbol{A}$ and $\boldsymbol{Q}$, respectively. Furthermore, μ_B is Bohr's magneton, $\boldsymbol{B}$ the magnetic field, and $\boldsymbol{S}$ and $\boldsymbol{I}$ refer to the electron and nuclear spin operators, respectively. Assuming an axial symmetry, the components of $\boldsymbol{g}$, $\boldsymbol{A}$ and $\boldsymbol{Q}$ can be expressed as $g_\parallel$, $g_\perp$, $A_\parallel$, $A_\perp$, when presented in the diagonal form. This corresponds to the representation of the defects parallel and perpendicular to the symmetry axis. Since $\boldsymbol{Q}$ is traceless, it can be described by a parameter P, with $Q_\perp = -P/2$ and $Q_\parallel = P$.

The tetragonal crystal structure of the host crystal (^{7}LiYF$_4$) with four-fold symmetric c-axis is shown in Fig. 1 (a). The ^{167}Er^{3+}-ions substitute the Y^{3+}-ions. We utilize a crystal[2] with a doping concentration of 25 ppm. In contrast to the more common cavity- or resonator-based ESR techniques, broadband ESR spectroscopy probes the absorption of the spin transitions in a waveguide arrangement. Thus, by varying the strength and direction of the external magnetic field $\boldsymbol{B}$, all transitions are probed in a broadband fashion. In our setup, the sample crystal is placed on top of a superconducting coplanar waveguide (CPW) transmission line (Nb on Si) as indicated in Fig. 1 (b) and mounted within a home-built solenoid magnet within a dilution refrigerator with a base temperature of 10 mK. The spin ensemble couples inductively to the CPW, which has a meander-shaped design to maximize the number of probed spins. A vector network analyzer records the transmission amplitude ($|S_{21}|^2$), which contains information about the absorption by the spin ensemble and by the microwave circuit. To disentangle the two, we construct a reference background ($|S_{21,\text{ref}}|^2$),

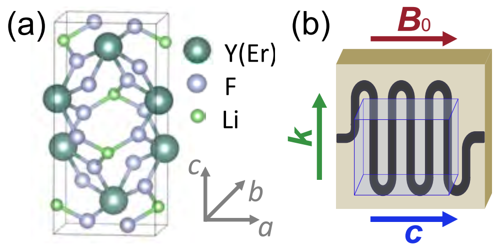

Figure 1: (a) Crystal structure of ^{167}Er:^{7}LiYF$_4$ [3, 4]. (b) Sample crystal on top of a meander-shaped CPW. The arrows indicate the alignment of $\boldsymbol{B}_0$, $\boldsymbol{k}$ and $\boldsymbol{c}$ in the experiment.

[1] We acknowledge support by the German Research Foundation via Germany's Excellence Strategy (EXC-2111-390814868) and the BMBF program "Grand Challenge of Quantum Communication" (project QuaMToMe, grant No. 16KISQ036).

[2] The crystal was grown in 2016 by O. A. Morozov and S. L. Korableva, Kazan Federal University (RU).

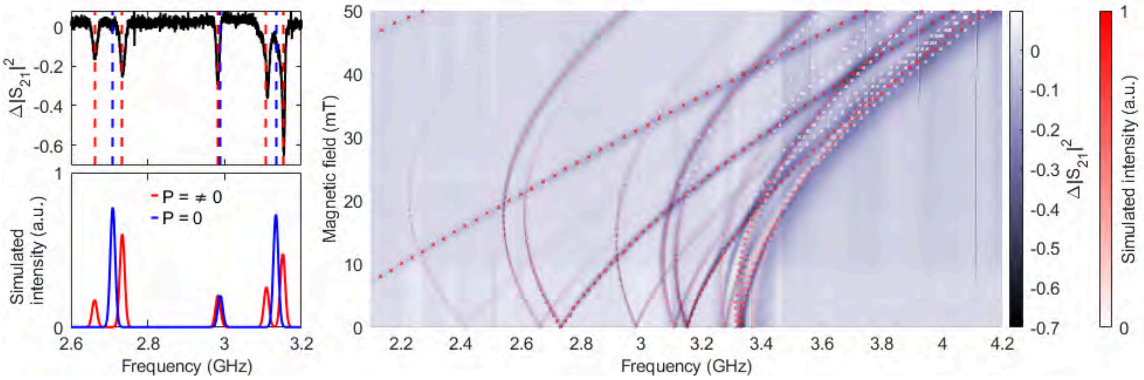

Figure 2: (a) Measured spectrum at $B_0 = 0\,\mathrm{mT}$ from 2.6 GHz to 3.2 GHz (black). The dashed lines indicate the simulated transition frequency for the absence of a quadrupole interaction ($P = 0$, blue) and including the quadrupole interaction ($P \neq 0$, red) matching the experimental data. The simulated spectra are plotted below. (b) Measured broadband ESR spectroscopy data for $\boldsymbol{B}_0 \parallel \boldsymbol{c}$ and $\boldsymbol{k} \perp \boldsymbol{c}$. The simulated hyperfine splitting is plotted on top of the measured ESR data.

which is free from ESR transitions and uses this for subtraction from the individual measured field-dependent spectra. Fig. 2 (b) shows the background-subtracted spectrum given by $\Delta|S_{21}|^2 = |S_{21,B}|^2 - |S_{21,\mathrm{ref}}|^2$ for $\boldsymbol{B}_0 \parallel \boldsymbol{c} \perp \boldsymbol{k}$ from 2.1 GHz to 4.2 GHz in the magnetic field range from 0 mT to 50 mT.

To quantify the parameters of the spin Hamiltonian, we numerically calculate the corresponding ESR transitions using EasySpin [5] and compare those with our spectroscopy data. In addition to the spectral locations indicated by the cross symbols [see Fig. 2 (b)], these calculations also yield the spectral weight of the envisaged transitions, which is encoded in the color of these markers. We find that our parameters are in agreement with previously determined values obtained using cavity-based X-band ESR [6, 7] and polarized excitations spectra [8]. However, we observe an inconsistency of the sign of the hyperfine parameters, which, in our case, are negative. Notably, those authors did not consider the quadrupole interaction, which plays a significant role in our data, especially at low magnetic fields. The contribution of the quadrupole interaction at $B_0 = 0\,\mathrm{mT}$ is highlighted in Fig. 2 (a), where some transitions (blue spectrum for $P = 0$) split into doublets for $P \neq 0$ (red spectrum). Both spectra were simulated with our refined parameters, while the red one includes the quadrupole interaction [9].

In conclusion, we characterize the spin Hamiltonian parameters of ^{167}Er:^{7}LiYF$_4$ from broadband ESR spectroscopy data measured at a temperature of 10 mK. The high resolution spectra allow for the determination of refined hyperfine and quadrupole parameters. Moreover, this technique allows to directly address various hyperfine transitions at their ZEFOZ points, which is essential for the implementation of microwave quantum memory schemes compatible with the working environment of superconducting qubits.

References

[1] Élie Gouzien, and N. Sangouard, Phys. Rev. Lett. **127**, 140503 (2021).
[2] M. Zhong, M. P. Hedges, R. L. Ahlefeldt, J. G. Bartholomew, S. E. Beavan, S. M. Wittig, J. J. Longdell, and M. J. Sellars, Nature **517**, 177–180 (2015).
[3] K. Momma, and F. Izumi, J. Appl. Crystallogr. **44**, 1272–1276 (2011).
[4] A. Goryunov, A. Popov, N. Khajdukov, and P. Fedorov, Mater. Res. Bull. **27**, 213–220 (1992).
[5] S. Stoll, and A. Schweiger, J. Magn. Reson. **178**, 42–55 (2006).
[6] J. P. Sattler, and J. Nemarich, Phys. Rev. B **4**, 1–5 (1971).
[7] K. Guedes, K. Krambrock, and J. Gesland, J. Alloys Compd. **344**, 251–254 (2002).
[8] R. M. Macfarlane, A. Cassanho, and R. S. Meltzer, Phys. Rev. Lett. **69**, 542–545 (1992).
[9] A. Strinic, P. Oehrl, O. Huisman, H. Huebl, O. Morozov, S. Korableva, P. Bushev, R. Gross, and N. Kukharchyk (in preparation).

Faithful Extraction of Internal Quality Factors in Overcoupled Tunable Superconducting Resonators

K.E. Honasoge, Y. Nojiri, D.E. Bazulin, M.T. Handschuh, A. Marx, R. Gross, K.G. Fedorov [1]

In quantum information processing, advancing superconducting circuits to reach ever-higher coherence times and internal quality factors is a key focus. Superconducting resonator measurements underpin these efforts by studying various loss channels, such as dielectric, inductive, or quasiparticle-induced losses. Typically, these losses are determined by extracting the internal quality factor, $Q_{\rm int}$, as a function of parameters used in the fabrication processes, circuit design, flux bias, or drive tones. However, accurately extracting the resonator $Q_{\rm int}$ can be challenging. Transmission measurements lack a reference baseline, hindering direct $Q_{\rm int}$ determination [1]. Reflection measurements are often plagued by Fano interferences, which introduce large uncertainties for $Q_{\rm int}$ fitting in overcoupled resonators [2].

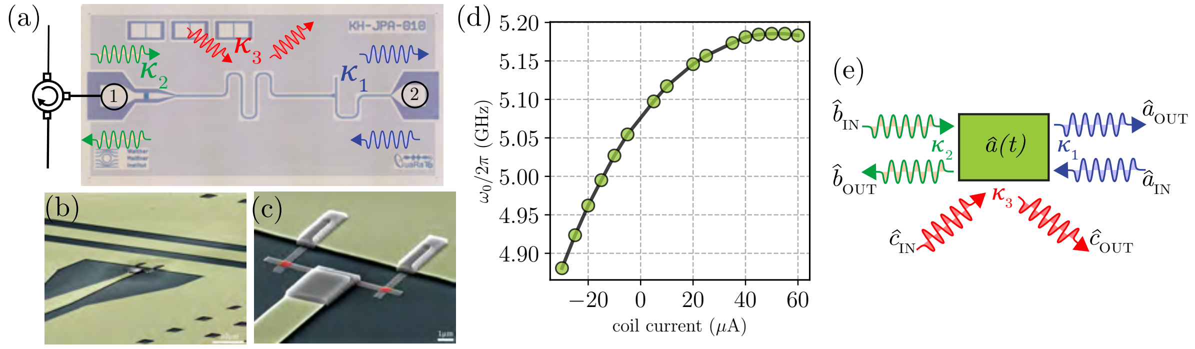

Figure 1: (a) Optical image of the $\lambda/4$-resonator coupled to the antenna circuit. (b) SEM image of the antenna coupling area to the dc-SQUID. (c) SEM image of the dc-SQUID area. (d) The resonance frequency of the tunable resonator as a function of the coil current. (e) Illustration of our input-output model describing the resonator losses.

Here, we study a particular approach for $Q_{\rm int}$ determination based on a tunable superconducting resonator coupled to an antenna line (see Fig. 1). The device fabrication involves a 3-step process with intermediate surface treatment steps. The resonator and antenna circuits are patterned onto a niobium (Nb) base layer with optical lithography. Fabrication of the dc-SQUID involves double-angle aluminum (Al) evaporation with intermediate oxidation post electron beam lithography to form Al/$\mathrm{AlO_x}$/Al Josephson junctions. Finally, the dc-SQUID is galvanically connected to the Nb resonator via an Al bandaging process, forming a tunable resonator. We experimentally investigate the tunable resonator response with VNA reflection and transmission measurements at millikelvin temperatures.

We model our system as a 3-port device with a resonance frequency ω_0. We describe it using the input-output approach for an internal mode $\hat{a}(t)$, as shown in Fig. 1(e). The coupling to the antenna is modeled with a coupling rate κ_1 and a respective quality factor, $Q_{\rm pump} = \omega_0/\kappa_1$. Similarly, the input capacitive coupling is modeled with κ_2 and a respective coupling quality factor, $Q_{\rm c}$. The intrinsic system losses are modeled with κ_3, which yields the internal quality factor, $Q_{\rm int} = \omega_0/\kappa_3$. Corresponding complex reflection (Eq. (1)) and transmission (Eq. (2)) coefficients read as:

[1] We acknowledge support by the German Research Foundation via Germany's Excellence Strategy (EXC – 2111 – 390814868) and the BMBF via the project QUARATE (Grant No. 13N15380). This research is part of the Munich Quantum Valley, which is supported by the Bavarian state government with funds from the Hightech Agenda Bayern Plus.

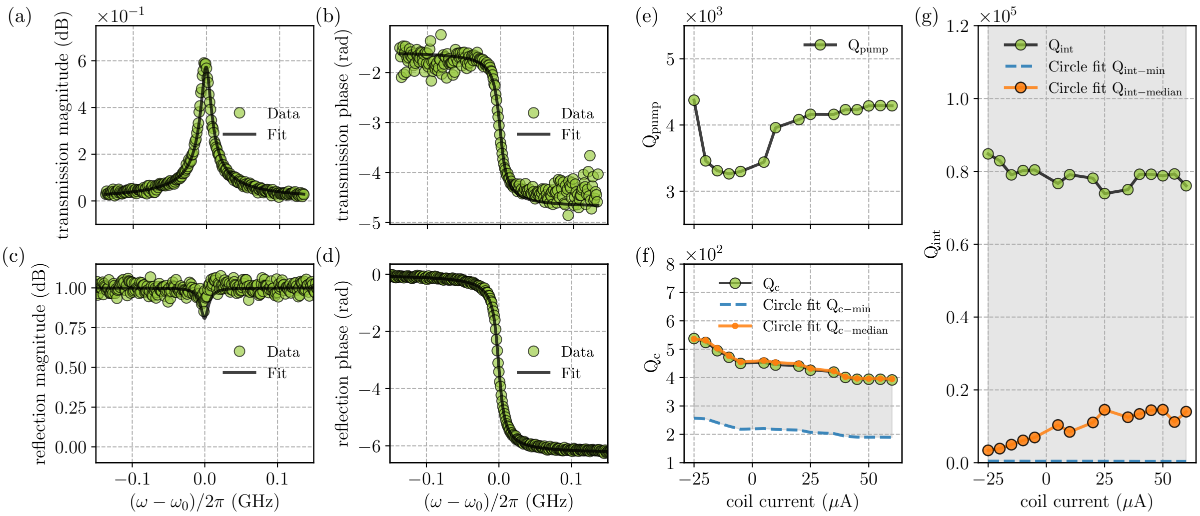

Figure 2: Input-output model fits of the transmission (panels (a) and (b)) and reflection (panels (c) and (d)) data. (e) Coil current dependence of estimated Q_{pump}. (f),(g) Coil current dependence of fitted Q_{c} and Q_{int}, as compared to estimates of a conventional circle fit procedure using the reflection data. Grey shaded area denotes uncertainty of Q_{c} and Q_{int} from the circle fit procedure due to the Fano interference.

$$\frac{\hat{b}_{\mathrm{out}}}{\hat{b}_{\mathrm{in}}} = \frac{i(\omega' - \omega_0) + \frac{\kappa_2 - \kappa_1 - \kappa_3}{2}}{i(\omega' - \omega_0) - \frac{\kappa_1 + \kappa_2 + \kappa_3}{2}}, \tag{1}$$

$$\frac{\hat{b}_{\mathrm{out}}}{\hat{a}_{\mathrm{in}}} = \frac{\sqrt{\kappa_1 \kappa_2}}{i(\omega' - \omega_0) - \frac{1}{2}(\kappa_1 + \kappa_2 + \kappa_3)}. \tag{2}$$

We employ a global minimization procedure to fit our experimental data with Eq. (1) and Eq. (2). This method simultaneously fits the reflection and transmission resonator responses, as illustrated in Fig. 2. We find that this approach is significantly less susceptible to the Fano interference effects and allows for more faithful extraction of Q_{int}, as shown in Fig. 2. Specifically, in Fig. 2 (f), we observe that Q_{c} extracted from our model lies within the uncertainty bounds ($Q_{\mathrm{c-min}} - Q_{\mathrm{c-median}}$) from conventional circle fits, given the Fano interference. As our model accounts for both transmission and reflection, it is less influenced by the Fano interference. Thus, the Q_{c} estimates become more faithful. Additionally, our model provides accurate estimates for Q_{pump}. This enables an even more accurate assessment of Q_{int}, as we decouple decay into the antenna circuit from the internal losses. The extracted Q_{int} from our model is $> 7 \times 10^5$ for all coil current points and lies within the Fano uncertainty from the conventional fits of $Q_{\mathrm{int-min}} - Q_{\mathrm{int-max}}$.

In conclusion, we have demonstrated that, by combining reflection and transmission measurements in overcoupled tunable resonators, it is possible to significantly improve the accuracy of internal loss estimation. The developed approach can be applied to a variety of tunable superconducting resonators, such as flux-driven Josephson parametric amplifiers.

References

[1] S. Probst, F. B. Song, P. A. Bushev, A. V. Ustinov, and M. Weides, Rev. Sci. Instrum. **86**, 024706 (2015).
[2] D. Rieger, S. Günzler, M. Spiecker, A. Nambisan, W. Wernsdorfer, and I. Pop, Phys. Rev. Appl. **20**, 014059 (2023).

Ultra-Low Magnetic Damping in 3*d* Transition-Metal Thin Films

M. Scheufele, O. Graf, M. Althammer, S. Geprägs, R. Gross [1]

Spintronic devices exploiting both the electronic and spin degrees of freedom are by now well established and offer a promising alternative to CMOS-based devices. In this field, an important material parameter determining the magnetization dynamics and therefore the efficiency of spintronic devices is the Gilbert damping parameter, which phenomenologically describes the relaxation rate to equilibrium of an excited magnetic system. Low Gilbert damping can be achieved in magnetic insulators such as yttrium iron garnet. However, for this material class, the lack of electronic conductivity, as well as the demanding fabrication processes, represent major challenges for application. Therefore, there is an increasing interest in the understanding and tuning of magnetic damping in thin films of transition-metal alloys, as their fabrication and patterning is less demanding. In particular, low damping was predicted in Co_xFe_{1-x} alloys [2], which was then explored experimentally by Schoen and coworkers [3]. They found ultra-low damping in $Co_{25}Fe_{75}$ thin films, which was explained by a low density of states at the Fermi level and therefore a reduced intra-band scattering.

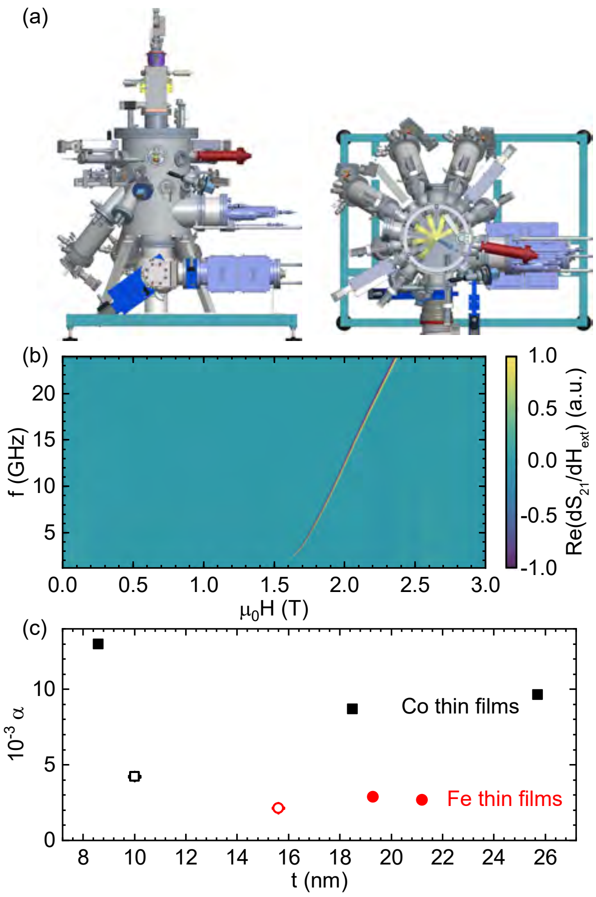

Figure 1: (a) Technical drawing of the recently installed molecular beam epitaxy system used for the fabrication of 3*d* transition-metal thin films [1]. (b) Background corrected real part of the complex transmission parameter S_{21} as a function of the frequency f and the external magnetic field $\mu_0 H_{ext}$ applied perpendicular to the film plane of a 10 nm thick Co thin film sample placed on a coplanar waveguide. (c) From these measurements the phenomenological Gilbert damping parameter α of Co (black symbols) and Fe (red symbols) thin films with different thicknesses t is determined. Two samples with an Al capping layer have been fabricated to investigate the oxidation effects of the Co and Fe thin films. The lower Gilbert damping of these samples (see open black and red symbols) demonstrates that Al capping layers are mandatory to prevent the thin films from oxidation.

To further investigate the compositional dependence of magnetic damping in Co_xFe_{1-x} (CoFe), we fabricated CoFe thin films on (100)-oriented Si substrate using the recently installed molecular beam epitaxy (MBE) system (see Fig. 1(a)) [1, 4]. As a first step, we fabricated thin film layers of Co and Fe with different thicknesses. To determine the magnetic damping of these thin films, we performed broadband ferromagnetic resonance (bbFMR) spectroscopy at room temperature using a coplanar waveguide connected to a vector network analyzer. Exemplarily, Fig. 1(b) shows the background corrected real part of the complex transmission parameter S_{21} as a function of the microwave frequency f and the external magnetic field $\mu_0 H_{ext}$ applied out of the film plane of a 10 nm thick Co thin film sample. The distinct line reveals where the ferromagnetic resonance condition is fulfilled. We extracted the resonance field and line width of the ferromagnetic resonance

[1]Supported by the German Research Foundation under Germany's Excellence Strategy "EXC-2111-390814868".

from these measurements by fitting the data with Lorentzian functions and determining the phenomenological Gilbert damping α. The thus obtained damping parameters of Co and Fe thin films with different thicknesses t are displayed in Fig. 1(c). While the Co thin films exhibit magnetic damping between 8×10^{-3} and 13×10^{-3}, a much lower damping $<4 \times 10^{-3}$ has been found for our Fe thin films.

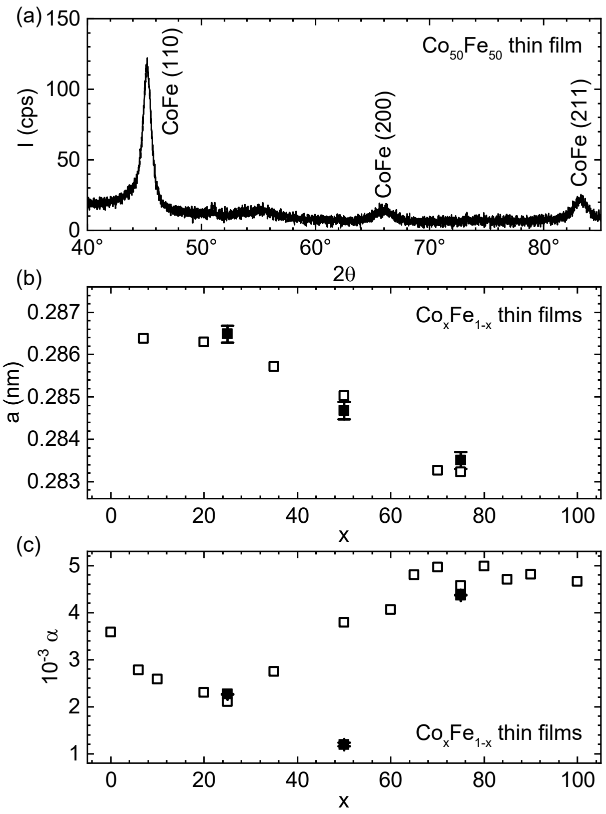

Figure 2: (a) Gracing-incidence diffraction (GID) of a 18 nm thick $Co_{50}Fe_{50}$ thin film fabricated on a Pt/Cu bilayer. The reflections are indexed using a body-centered cubic symmetry. (b) Calculated lattice constants a and (c) extracted Gilbert damping parameters α of Co_xFe_{1-x} thin films as a function of the Co concentration x (solid symbols). The open symbols in (b) and (c) represent data reported by Schoen *et al.* [3].

It is well known that seed layers consisting of a heavy metal (e.g. Pt) together with a metallic spacer layer with vanishing spin-orbit coupling (e.g. Cu) can significantly reduce the Gilbert damping of 3d transition-metal thin films. We, therefore, fabricated CoFe thin films with different Co concentrations on Pt/Cu bilayers capped with Cu/Al to prevent the CoFe thin films from oxidation. To investigate the structural properties of the CoFe thin films, we performed X-ray diffraction (XRD) measurements in grazing-incidence geometry, taking advantage of the new XRD setup. Figure 2(a) shows a 2θ-scan of a 18 nm thick $Co_{50}Fe_{50}$ thin film. The CoFe reflections of this composition can be indexed using a body-centered cubic symmetry. From the 2θ-angle of the CoFe (110) reflection we calculated the lattice constant a of the CoFe thin films (see solid symbols in Fig. 2(b)). The obtained values are in good agreement with the data reported by Schoen *et al.* (open symbols in Fig. 2(b)) [3]. To investigate the magnetic damping of the CoFe thin films, we have performed bbFMR experiments at room temperature. As shown in Fig. 2(c), the obtained Gilbert damping parameter α fits nicely with literature values for a Co concentration of $x = 25\%$ and 75%, while a much lower damping was found for the $Co_{50}Fe_{50}$ thin film sample. This calls into question the result obtained by Schoen *et al.*, but needs to be verified in more detail in the future.

In summary, we were able to fabricate state-of-the-art Co, Fe, and Co_xFe_{1-x} thin films with good structural and magnetic properties using the recently installed MBE system. In particular, we found an ultra-low magnetic damping in our $Co_{50}Fe_{50}$ thin films, demonstrating that Co_xFe_{1-x} is a promising materials platform for a new generation of spintronic applications.

References

[1] S. Geprägs, and R. Gross, WMI Ann. Rep. **2022**, 25–26 (2022).
[2] S. Mankovsky, D. Ködderitzsch, G. Woltersdorf, and H. Ebert, Phys. Rev. B **87**, 014430 (2013).
[3] M. A. W. Schoen, D. Thonig, M. L. Schneider, T. J. Silva, H. T. Nembach, O. Eriksson, O. Karis, and J. M. Shaw, Nat. Phys. **12**, 839 (2016).
[4] O. Graf. Co_xFe_{1-x} thin films for future magnonic devices. Bachelor's thesis, Technische Universität München (2023).

Surface Acoustic Wave Resonators on Thin Film Piezoelectric Substrates in the Quantum Regime

T. Luschmann, A. Jung, S. Geprägs, F.X. Haslbeck, A. Marx, S. Filipp, R. Gross, H. Huebl [1]

Lithium Niobate (LNO) is a well-established material for Surface Acoustic Wave (SAW) devices operating in the MHz and GHz frequency range, including resonators, delay lines, and filters. Recently, multi-layer substrates based on LNO thin films have become commercially available, which offers new opportunities for combining optical circuits with GHz electronics. Here, we present a systematic low-temperature study of the performance of SAW devices fabricated on LNO-on-Insulator (LNOI) and LNO-on-Silicon substrates and compare them to bulk LNO devices. Our study aims at assessing the performance of these substrates for quantum acoustics, i.e. the integration with superconducting circuits operating in the quantum regime [1]. To this end, we designed SAW resonators with GHz frequencies and performed experiments at millikelvin temperatures and microwave power levels corresponding to single excitations. The devices are investigated regarding their internal quality factors, which allows us to quantify losses and identify the dominating loss mechanism.

SAW resonators can be understood as the elastic-wave analog of an optical Fabry-Perot cavity, where a standing wave is confined between two highly reflective mirrors. The SAW resonators investigated in this study are designed for a center frequency of $f_0 \approx 5\,\mathrm{GHz}$ and use a standard, single-port resonator design [see Fig. 1 (a) and (b)]. The transducer in the center consists of alternating signal and ground aluminum electrodes with a pitch of $p = 0.4\,\mu\mathrm{m}$. For the mirrors, we use 500 electrically floating aluminum strips with the same pitch. All aluminum structures have a thickness of 20 nm and are patterned in a single-step process using electron beam lithography and electron beam evaporation, followed by a lift-off process. A false-color optical micrograph of a fabricated structure is displayed in Fig. 1 (b). To compare the properties of SAW resonators fabricated on standard bulk LNO with devices based on multi-layer substrates, we use three different sample types A, B, and C [see Fig. 1 (c)]: (A) a 128°-rotated Y-X-cut bulk lithium niobate (LNO) crystal - the standard material for SAW resonators and filters, (B) a thin film lithium niobate on insulator (LNOI) stack composed of a 500 nm thin 128°-rotated Y-cut LNO thin film on a 2 µm thick SiO_x buffer layer on a 350 µm thick Si(100) substrate, and (C) a 300 nm thin Y-X cut LNO thin film on a 500 µm thick Si(111) substrate.

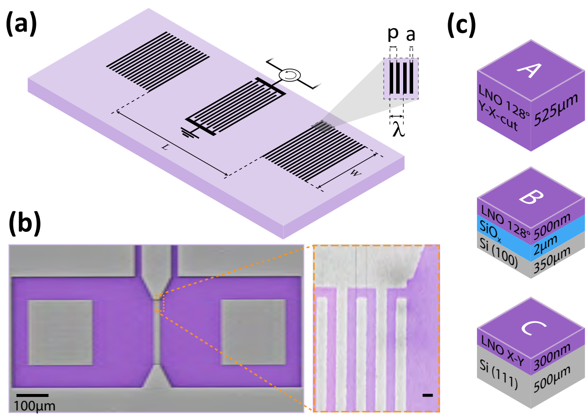

Figure 1: (a) Illustration of the SAW resonator and the relevant geometric parameters. (b) False color optical micrograph of a SAW resonator structure. Aluminium is shown as gray, while LNO is colored violet. The zoom-in shows a scanning electron micrograph (SEM) highlighting the individual strips of the transducer. The black scale bar corresponds to 200 nm, the nominal width of the strips. (c) Illustration of the composition of the sample types A, B, and C studied in this work.

The SAW resonators are investigated by microwave spectroscopy in a dilution refrigerator with a base temperature of $T_{\mathrm{base}} \approx 20\,\mathrm{mK}$. We measure the microwave reflection response

[1] We acknowledge funding from the EU 2020 Research and Innovation Programme under grant agreement No. 736943 and from the German Research Foundation under Germany's Excellence Strategy—EXC-2111-390814868. Further, this work was supported in part by the Horizon Europe 2021-2027 Framework Programme under the grant agreement No. 101080143 (SuperMeQ).

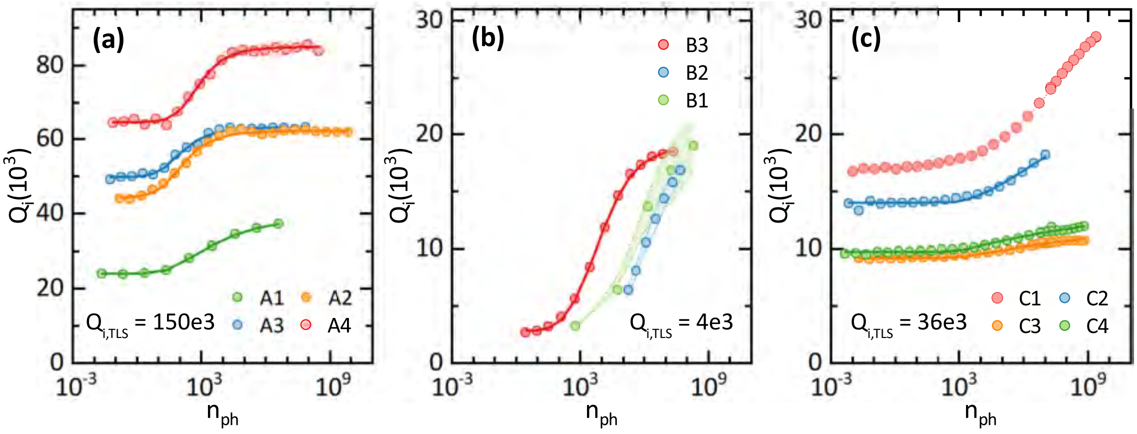

Figure 2: Internal quality factors Q_i as a function of the average phonon number n_{ph} in the resonator mode for various samples of types A (bulk LNO), B (LNOI), and C (thin film LNO). Uncertainties are derived from the fitting model and are illustrated as shaded areas around the data points. Where possible, the power-dependency of Q_i has been fitted to a TLS-based model (solid lines) and the corresponding TLS contribution $Q_{i,TLS}$ was extracted.

and extract from it the characteristic parameters of the resonance, specifically the resonance frequency f_r and the internal quality factor Q_i. One contribution to the intrinsic losses of solid-state based resonators, which are considered to be of high relevance for the low power limit and hence of importance to quantum applications, are the losses due to two-level-systems (TLS) [2]. The experiments addressing this issue examine the internal quality factor Q as a function of microwave power, which we express as the average phonon occupation n_{ph} of the resonator mode (see Fig. 2). We observe an increase in Q_i with increasing the drive power for all investigated devices, which is expected where TLS losses dominate: As the drive power is increased, the TLS saturate and thereby suppress this loss channel. Many of our devices indeed show this characteristic behavior [see Fig. 2 (a) and (b)]. In addition, we find for the SAW resonators fabricated using LNO thin films on Si (sample type C) a qualitatively different behavior, where saturation is not apparent for n_{ph} up to 10^9. Such behavior is commonly associated with off-resonant TLS, which, due to their large detuning from the resonator frequency, do not saturate even at high drive powers.

From the quality factor studies, we discern $Q_{i,TLS} \gg Q_i$ for devices fabricated on bulk LNO, suggesting that TLS are not dominating the losses of these devices and other mechanisms, e.g. acoustic losses to bulk waves, play a more dominant role. Conversely, for the devices fabricated on LNO thin films, we observe $Q_{i,TLS} \approx Q_i$, which is consistent with TLS currently limiting the performance of these devices. This underscores the dominating effect of TLS losses for this type of device when operating in the quantum regime. However, based on the overall magnitude of the measured quality factors, our results suggest that SAW devices on thin film LNO on silicon have comparable performance to devices on bulk LNO and are thus viable for use in SAW-based quantum acoustic devices. For more details, we refer the reader to Ref. [3], where we detail the analysis procedure and present additional measurement data.

References

[1] R. Manenti, A. F. Kockum, A. Patterson, T. Behrle, J. Rahamim, G. Tancredi, F. Nori, and P. J. Leek, Nat Commun **8**, 975 (2017).

[2] D. P. Pappas, M. R. Vissers, D. S. Wisbey, J. S. Kline, and J. Gao, IEEE Transactions on Applied Superconductivity **21**, 871–874 (2011).

[3] T. Luschmann, A. Jung, S. Geprägs, F. X. Haslbeck, A. Marx, S. Filipp, S. Gröblacher, R. Gross, and H. Huebl, Mater. Quantum. Technol. **3**, 021001 (2023).

Experimental Facilities

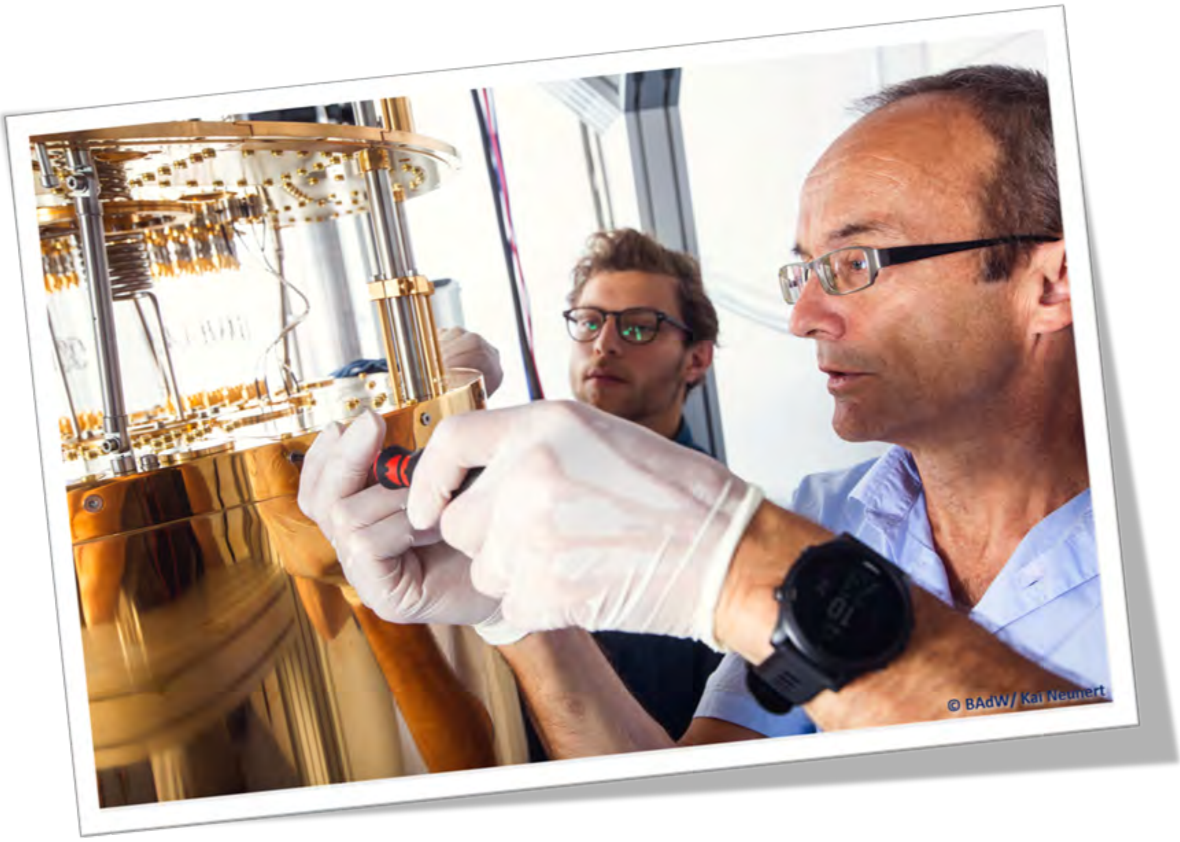

Reactive ion etcher PlasmaPro 100 Cobra

L. Koch, T. Luschmann, N. Bruckmoser, L. Södergren, T. Brenninger, H. Hübl, A. Marx, S. Filipp [1]

In order to explore new circuit topologies and scale up superconducting circuits, advanced structuring of silicon on large substrates is needed. For this purpose, an Oxford PlasmaPro 100 Cobra reactive ion etching tool, shown in Fig. 1, has been set up in the WMI cleanroom. The tool reaches excellent uniformity on wafer scale and accurate etch depth control utilizing laser and plasma colour based end-point detection. A good process repeatability is ensured by the load lock and a wide process window is ensured by an inductively coupled plasma source. The stage of the system can be cooled by liquid nitrogen down to −150 °C and heated up to 400 °C. Additionally a variety of gases ranging from C_4F_8, CHF_3, SF_6, BCl_3, O_2 and Ar extend the number of materials that can be dry etched at the WMI. Furthermore, especially C_4F_8 and SF_6 can be used for the so called Bosch process. This process allows deep reactive ion etching with high-aspect ratios into silicon substrates by alternating the following process steps

1. In the first step a nearly isotropic plasma etch step with SF_6 is used to attack the silicon and etch a nearly vertical trench into the substrate.
2. In a second step a chemically inert passivation layer is deposited by C_4F_8. This layer is similar to teflon.
3. The two steps are repeated for 100 to 1000 times until the desired etch depth is achieved. In the subsequent etch steps the passivation layer avoids a lateral etching. Therefore, deep trenches can be achieved.

Figure 1: Photograph of the reactive ion etching tool PlasmaPro 100 Cobra from Oxford.

[1] This project has received support by the Munich Quantum Valley, which is supported by the Bavarian state government with funds from the Hightech Agenda Bayern Plus.

Profilometer Bruker Dektak XT

L. Koch, N. Bruckmoser, L. Södergren, A. Marx, S. Filipp [1]

For wafer scale metrology a Dektak XT from Bruker has been installed. A photograph of the device is shown in Fig. 1. By scanning along a surface and comparing its height to an optically smooth reference surface this device can measure the topology of wafers with steps of up to 1 mm. The profilometer has a repeatability of 4 Å and allows high scanning speeds. Wafers with a size of up to 150 mm can be measured. Additionally, the fully motorized X and Y stage allows 3D maps of wafers. A motorized Θ stage is implemented to be able to determine the stress of a thin film. For this measurement, the bow of a wafer before and after thin film deposition is measured. Afterwards, the stress of the thin film can be determined from the additional bow induced by the film. The measurement of soft surfaces is enabled by very low contact forces of 1 to 15 mg. The available radii of the scanning tips range from 2 µm to 12.5 µm to also allow for measurements of narrow channels with high aspect ratios.

Figure 1: Photograph of the Dektak XT from Bruker.

[1] This project has received support by the Munich Quantum Valley, which is supported by the Bavarian state government with funds from the Hightech Agenda Bayern Plus.

MPI TS2000-IFE automated probe station

D.E. Bazulin, J. Feigl, L. Koch, N. Bruckmoser, A. Marx and S. Filipp [1]

The performance of a superconducting circuits based quantum processor relies heavily on the precision of Josephson junction fabrication, specifically in achieving precise critical current targeting. Imprecise junction fabrication leads to imperfections in qubit frequency targeting, resulting in a decrease of gate fidelities due to frequency crowding. This becomes a growing challenge when scaling up the number of qubits to build larger processors.

Via the Ambegaokar-Baratoff formula, the room temperature resistance of Josephson junctions gives a straightforward estimate of critical current and, consequently, the qubit frequency. We use the results from room temperature resistance measurements with large statistics to optimize oxidation parameters and improve the yield of the Josephson junction.

The TS2000-IFE automated probestation from MPI offers rapid, semi-automated process of room-temperature characterization of wafers up to 200 mm, both for DC and RF applications. The influence of external noise on measurement results is minimized by electromagnetic interference- and light-shielded test environment. The shielding capabilities surpass 30 dB for electromagnetic interference, and exceeds 130 dB for light attenuation. Other properties include active vibration isolation, two fully motorized probing arms, a moving stage with 0.2 µm resolution in X,Y and Z axes, and a moving microscope with 1 µm movement resolution. Together, these features allow reliable estimation of Josephson junction parameters, yield and spread on a single-chip and wafer scales.

Figure 1: Installed MPI TS2000-IFE automated probe station.

Additionally, the probe station has been upgraded with a laser annealing setup. This setup allows local heating of a Josephson junction with a laser spot, resulting in increase of the tunneling barrier thickness and, consequently, normal state resistance. This shift can be controlled by precise measurements of the junction resistance between the laser pulses. As the normal state resistance of the Josephson junction and the qubit's frequency are closely related, the qubit frequency can be adjusted in post-processing.

Overall, the MPI TS2000-IFE probe station helps to scale to better and larger processors by introducing a crucial technology for frequency targeting. It also helps to deepen the understanding of fabrication steps vital for building many-qubit quantum processors.

[1] This project has received support by the BMBF program No. 13N15680 (GeCQoS).

Finetech FINEPLACER femto 2 die bonder

L. Richard L. Koch, N. Bruckmoser, L. Södergren, A. Marx, S. Filipp [1]

To address traditionally challenging problems using quantum computing, it is essential for quantum processors to scale up significantly. However, the current superconducting planar geometry makes it impossible to route the numerous control and readout lines required for a larger number of qubits. 3D-integration techniques play an essential role in mitigating this issue. With this need for larger-scale quantum platforms in mind, we are now developing a flip-chip bump bonding process towards 3D-integrated quantum circuits at the WMI. One necessary tool to implement this new technology is a flip-chip bonder, to compress the indium bumps and bond the two chips with accurate alignment and controllable force. For this reason, an advanced sub-micron bonder was acquired and installed in the institute's clean room.

The bonder is equipped with chip holders of standard sizes of 6 mm×10 mm, 12 mm×12 mm, 14 mm×14 mm and 30 mm×30 mm. Nonetheless, it can ultimately handle substrates up to 300 mm×300 mm in size with a maximum thickness of 10 mm and top chips up to 100 mm×100 mm with a maximum thickness of 4 mm. Such flexibility in dimensions will enable flip-chip bonding on larger-scale chips in the future. Additionally, the bonding arm, with a force ranging from 0.05 N to 1000 N, can bond structures with numbers of indium bumps varying from several hundred to several hundred thousand. Bump compression can also be performed at room or high temperatures thanks to a heating plate and a heating tool base that can reach up to 500 °C and 450 °C, respectively.

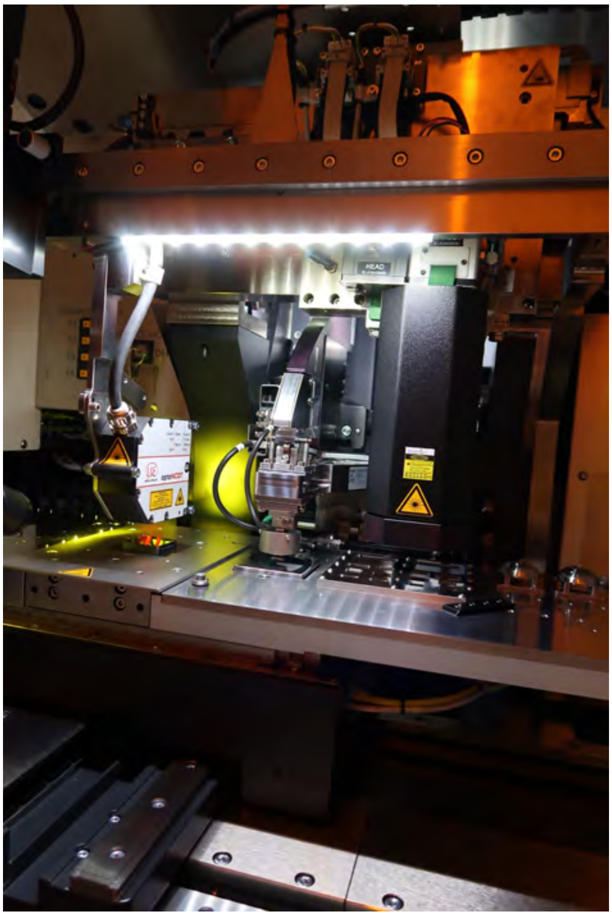

Figure 1: Picture of the FINEPLACER femto 2 die bonder

In flip-chip bonded structures, alignment between the two chips is crucial both horizontally and vertically. For this purpose, the system is equipped with cameras and pattern recognition software, allowing for a horizontal placement accuracy below 0.3 µm. It also includes an adapter plate with flatness below 0.5 µm for improved vertical alignment. Furthermore, after the bonding process, a built-in laser-height module allows us to measure the resulting structure's thickness and study the alignment and tilt.

Finally, the machine is also modulable to meet future needs. Various chip holders, tool bases, and tool tips may be installed. Moreover, process gases, such as nitrogen or formic acid, can be added to the system for cleaner bonding conditions and oxide removal.

[1] This equipment was funded by BMBF program No 13N15 982 (SEQT)

Overview of Fabrication Facilities towards Large-Scale Quantum Processors

L. Södergren, L. Koch, N. Bruckmoser, L. Richard, D. Bunch, T. Luschmann, K. Honasoge, A. Marx, S. Filipp

In the following, an overview of capabilities for fabricating high-coherence superconducting qubits available at the WMI will be introduced. Most of the recently acquired equipment enables us to increase our wafer-scale fabrication capabilities and develop 3D-integration technologies, which are crucial for realizing larger Quantum Processor Units (QPUs).

The institute operates a clean room of roughly 50 m^2 with cleanliness of class 1000. It is equipped with standard facilities for lithography processes such as wet benches, spin coaters, hot plates, and an optical microscope. We currently have two systems for optical lithography (direct laser writing). The PicoMaster 200 with a 0.3 µm resolution is used for high-resolution optical lithography. The other system is a maskless aligner MLA150 from Heidelberg Instruments (installed in 2023), which provides a minimum resolution of 0.6 µm but, more importantly, it provides a significant reduction in the write time. This facilitates the development of new processes, especially on the wafer scale. For smaller structures ($\sim$100 nm) we use our electron beam lithography (EBL) system (NanoBeam nB5, more info in the 2021 annual report). During the qubit fabrication, the EBL system is used to pattern the Josephson junctions.

For pattern transfer, the clean room hosts two reactive ion etchers. The Plasmalab 80 Plus is mainly used for etching niobium. The second system is the recently installed PlasmaPro 100 Cobra system (both systems are from Oxford Instrument Plasma Technology). The Cobra is equipped with an end point detection system and has an excellent etch uniformity on the wafer scale. It supports both Bosch etching and cryogenic deep silicon etching. This enables us to do through-silicon-vias (TSVs), which is an important technology for 3D-integration.

Our UHV deposition system (Plassys MEB 550 S4-I, more info in the 2021 annual report) was set up in 2020 and has since then been vital for our qubit process development. The system consists of a load-lock, sputtering chamber, and evaporation/oxidation chamber. We have restricted the available materials in this system to ensure stable deposition parameters and reduced spread in film properties from run to run. This enables us to carefully study deposition parameters and develop fabrication processes yielding high-coherence qubits. The sputtering chamber is used for depositing the qubit ground plane film (niobium). The Josephson junctions are fabricated in the evaporation/oxidation chamber, which allows for in-situ deposition of the $Al/AlO_x/Al$ stack without breaking the vacuum.

In 2023, we have also installed two additional systems, which give us the capability to develop flip-chip bonding with superconducting indium bumps. The first one is an indium evaporation system (Plassys ME450S-In) used to deposit thick layers ($\sim$10 µm) of indium. Two chips can then be bonded together via indium bumps, creating a galvanic connection between the chips. This is done using the recently installed (in the clean room) flip-chip bonder (Finetech Fineplacer femto 2).

In terms of metrology, the WMI can do surface morphology with our atomic force microscope (NanoSurf CoreAFM) and the recently acquired (in 2023) Profilometer (Bruker DekTak XT). We also have a scanning electron microscope (JEOL JSM-IT800, more info in 2022 annual report) with a resolution down to 0.5 nm. This is a central tool for imaging small structures and facilitating process development. This year, we also installed an automatic wafer probe station (MPI TS2000-IFE), which enables us to do fast initial electrical characterization of circuit components on a wafer scale.

For sample preparation and packaging, we use an automatic dicing saw (DISCO DAD3221) to cut the wafers in to appropriate chip sizes. Before measuring, we use our newly installed automatic wire bonder (F&S Bondtec 5630i) to bond our sample chip to a printed circuit board (PCB). This new bonder allows us to package our chips quickly with high precision and repeatability.

New Cryostats and Control Electronics for Large-Scale Quantum Processing Units and Rapid Small-Scale Sample Characterizations

C.M.F. Schneider, M. Werninghaus, D.C. Bunch, F. Wallner, J. Schirk, N. Glaser, J. Romeiro Alves, G. Huber, I. Tsitsilin, F.X. Haslbeck, A. Marx, S. Filipp [1]

In a significant upgrade to the WMI's infrastructure, two new Bluefors XLD1000 dilution refrigerators have been acquired. The first system, shown in Fig. 2(a), is equipped with 216 coaxial lines and is designed to support up to two 24 generalized flux qubit chips, where each qubit is coupled with tunable couplers. This setup is integral to the WMI MQV project, which is focused on developing a 24 generalized-flux-qubit processor. The second system, shown in Fig. 2(b), hosts the efforts of the WMI within the MUNIQC-SC project, geared towards the fabrication and operation of processors with up to 100 qubits. To meet this goal, the cryostat is equipped with 400 coaxial lines. The necessity for such a high number of coaxial cables arises from the tunable coupler architecture. In this configuration, each qubit requires one drive line, two magnetic flux bias lines for the adjacent tunable couplers, and two lines for readout every five qubits. To effectively manage this extensive network of control lines, we have acquired Bluefors' high-density (HD) wiring solution, as depicted in Fig. 1.

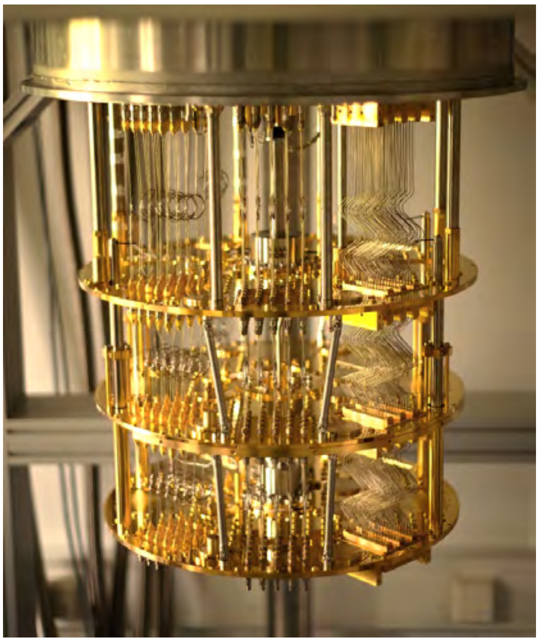

Figure 1: Inside view of a Bluefors XLD1000 cryostat, illustrating its thermal layering and control line capacity. The bottom plate reaches a base temperature of below 10 mK. Supporting sufficient control lines while maintaining low temperatures is essential for operating large-scale systems. Our new systems are equipped with up to 336 Bluefors High-Density coaxial cables for this purpose, as exemplified on the right with a configuration of 72 coaxial cables.

The ability to operate quantum computers of such size requires a substantial amount of microwave electronics. The WMI is working with Zurich Instruments to set up a sufficiently large control infrastructure. These systems are essential for the precise generation, coordination, and routing of microwave and flux pulses, which are key to controlling the qubits in our quantum computing endeavors. In 2023, the WMI has acquired enough instruments to control 56 control channels, 20 readout channels and 64 flux current channels. Due to the modular nature of these systems, this will allow the operation of all small- and medium-size systems that will be on the development roadmap until large-scale systems are reached.

Additionally, we have installed a new L-Type Rapid (L201f) adiabatic demagnetization refrigerator (ADR) from Kiutra, as shown in Fig. 2(c). This addition significantly boosts our ability to rapidly characterize and improve superconducting qubits, resonators, and parametric amplifiers. The cryostat operates without the need for costly ^{3}He and is equipped with 40 DC and 4 microwave lines. Notably, it can cool from room temperature to 100 mK in less than three hours, where it can hold for nine hours in a single shot. Such a rapid turnaround time vastly

[1] This project is part of the Munich Quantum Valley, which is supported by the Bavarian state government with funds from the Hightech Agenda Bayern Plus and has received support by the Munich Quantum Valley Quantum Computer Demonstrators - Superconducting Qubits (MUNIQC-SC; project number: 13N16188).

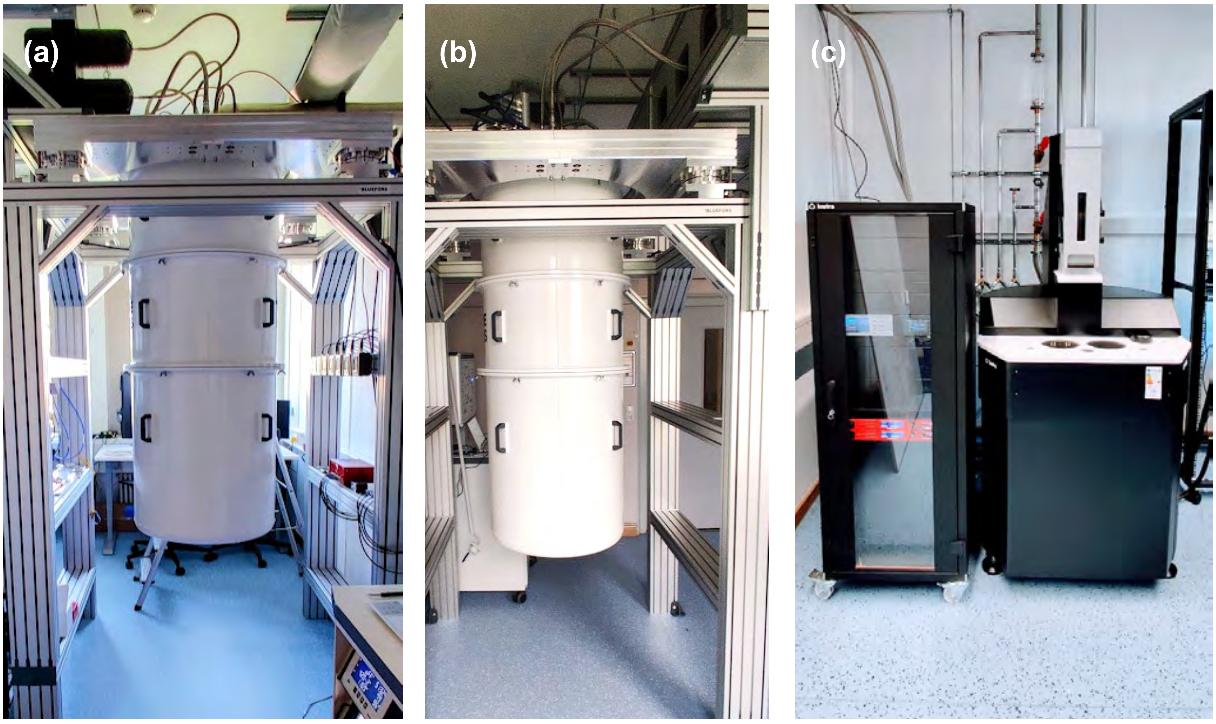

Figure 2: New croystats at the WMI. (a) and (b) show the two new Bluefors XLD1000 cryostats with Bluefors high-density wiring to support large-scale quantum processing units. (c) New adiabatic demagnetization refrigerator from Kiutra for fast small-scale sample characterizations.

increases sample throughput, but also enables quick verification of a research direction, saving even more resources in the long run. It also allows continuous operation between 200 mK and 300 K at any given temperature. This feature is essential to assess the critical temperature of materials and the temperature response of microwave resonators. The cooling mechanism is cryogen-free, and thus avoids the temperature instability of dilution refrigerators around 1 K where the ^{3}He/^{4}He phase separation occurs. Many superconducting materials exhibit critical temperatures around 1 K, so having a cryostat that can produce accurate temperature sweeps in this range is crucial. An easy-to-use python API allows for automated control of the fridge and integration with measurement devices. Incorporating the ADR system into our laboratory underscores our commitment to exploring beyond conventional qubits and technologies in quantum computing.

Integrating the two new large dilution refrigerators, control electronics, and fast-cycling ADR cryostat significantly bolsters our quantum computing research capabilities. They enable the operation of large-scale QPUs and facilitate the fast characterization of small-scale samples, allowing us to undertake more complex and varied quantum computing projects and paving the way for future innovations in the field.

New High-Resolution X-ray Diffraction System for the Characterization of Thin Films and Powder Samples

S. Geprägs, R. Gross, S. Filipp [1]

The structural characterization is of key importance for the fabrication of high-quality thin film samples forming the basis for many research projects at the Walther-Meißner-Institute (WMI). Due to its non-destructive nature, X-ray diffraction (XRD) is one of the most versatile tools to characterize various forms of thin films as well as powder samples. To upgrade to state-of-the-art requirements, we have installed a new high-resolution XRD system at the WMI. The new XRD system, which has been funded by the German federal government within the MUNIQC-SC project, is optimized for the structural characterization of epitaxial thin films, heterostructures and superlattices as well as thin polycrystalline layers and powder samples. In 2022, after a Europe-wide tender a new XRD system D8 Discover (see Fig. 1) was ordered and delivered by the supplier Bruker AXS in May 2023. The core of the system is the vertical, high-accuracy goniometer equipped with a non-coplanar arm for in-plane diffraction measurements. This goniometer thus allows for coplanar as well as non-coplanar diffraction experiments, which offers a large variety of scanning options. In the center of the goniometer, an Euler cradle with a x, y, z-stage, a continuous φ-rotation as well as a ψ-drive are installed. This allows for a precise alignment of the sample and various stage attachments. To mount the sample, different options are available, depending on the size as well as on the alignment purpose of the sample [see Fig. 1(a)-(c)]. Additionally, a temperature stage (TC-dome) allows for measurements from 93 K to 1373 K, see Fig. 1(d).

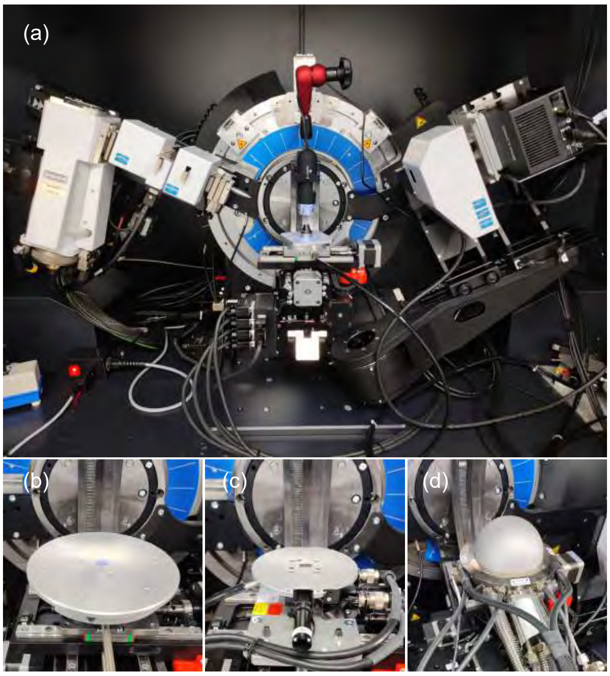

Figure 1: (a) D8 Discover equipped with a vertical, high-accuracy goniometer and a non-coplanar arm for in-plane diffraction. The picture is taken during a diffraction experiment in the coplanar geometry investigating the structural properties of a Hall bar mesa structure using a 0.3 mm collimator. To control the lateral position of the X-ray beam, two crossed laser beams together with a camera have been used. (a)-(d) Various attachments to the centric Euler cradle: (a) holder for small thin film samples, (b) 5-inch vacuum chuck for large wafers, (c) tilt-stage for precise alignment with respect to the azimuthal φ-axis, (d) TC-dome allowing for measurements in the temperature range from 93 K to 1373 K. A powder sample holder with an additional spinner (not shown) is also available.

On the primary side of the diffractometer, the system is equipped with a Cu-X-ray source and a Goebel mirror generating a high-brilliance X-ray beam. For a monochromatic X-ray beam with $Cu_{K\alpha_1}$ radiation 2-bounce or 4-bounce Ge-monochromators with high resolution are available. On the secondary side, the so-called Pathfinder Optics allows to switch between a motorized slit for high flux measurements and a 2-bounce Ge-analyzer crystal for high-resolution experiments without further alignment. Another key component of the X-ray diffractometer is the X-ray detector. The system is equipped with a Dectrics Eiger X-ray detector. The 512×512 pixel array with a pixel size of $(75 \times 75)\,\mu\mathrm{m}^2$ covers a macroscopic area with microscopic resolu-

[1] Supported by the German federal government within the MUNIQC-SC project.

tion. The detector exhibits two independent energy thresholds and a maximum count rate of 7×10^8 photons/s/mm^2. 0D, 1D and 2D operation modes with snapshot, step, continuous or advanced scanning modes are possible. Furthermore, the system allows for variable detector positions with automated calibration. All the components can be exchanged without further alignment by a snap-lock technology, which offers a high flexibility as well as fast and easy changes between different optics and scattering geometries. Furthermore, the system offers real-time component recognition and status display of the installed components.

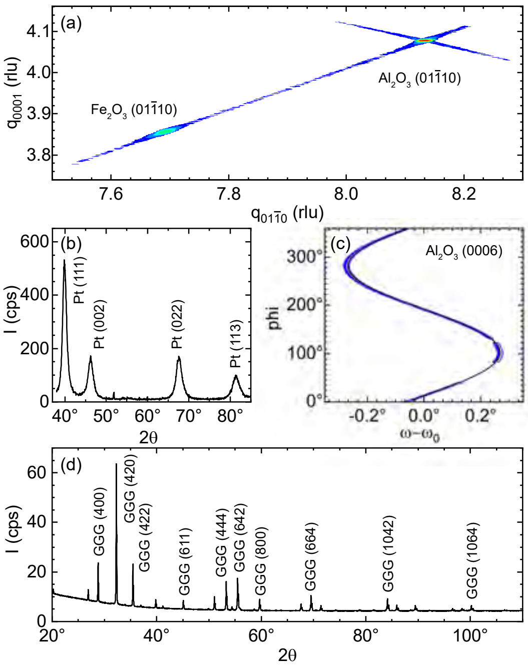

Figure 2: Measurement results of various samples using different scattering geometries: (a) Reciprocal space mapping of a 150 nm thick epitaxial Fe_2O_3 thin film fabricated on a (0001)-oriented Al_2O_3 substrate, (b) grazing incidence diffraction of a 3 nm thick, polycrystalline Pt layer, (c) measurement of the Al_2O_3 substrate miscut angle using the tilting stage shown in Fig. 1(c), and (d) powder diffraction of $Gd_3Ga_5O_{12}$ (GGG) in the Bragg-Brentano geometry. Only the main reflections are indexed.

To demonstrate the capability of the X-ray diffraction system, measurement results on various samples using different scattering geometries are displayed in Fig. 2. Figure 2(a) shows an asymmetric reciprocal space mapping (RSM) carried out on a 150 nm thick, epitaxial Fe_2O_3 thin film fabricated on a (0001)-oriented Al_2O_3 substrate by pulsed-laser deposition (PLD). Taking advantage of the 1D-mode of the Eiger detector, the scan time was greatly reduced from typically 4 hours using a standard scintillation detector to 450 s. The RSM clearly reveals a fully relaxed growth of Fe_2O_3 on Al_2O_3. Grazing incidence diffraction (GID) for the structural characterization of polycrystalline thin film samples is another important application. As an example, the result of a GID measurement on a 3 nm thick, polycrystalline Pt thin film is shown in Fig. 2(b). Despite the small layer thickness, the Pt reflections can be clearly resolved. By using the tilting stage [see Fig. 1(c)], a precise alignment of the sample surface normal with respect to the azimuthal φ-rotation axis can be carried out. This allows for measurements of the substrate miscut of a Al_2O_3 crystal [see Fig. 2(c)]. The miscut value has direct influence on the coupling between a ferromagnetic resonance mode of a ferromagnetic layer and acoustic phonon modes in the substrate material underneath [1]. Finally, powder diffraction data measured on a polycrystalline $Gd_3Ga_5O_{12}$ (GGG) target material for PLD is shown in Fig. 2(d). Due to the snap-lock technology, changes between the parallel X-ray beam configuration and the focusing Bragg-Brentano geometry for powder diffraction can be easily carried out. Furthermore, a motorized divergence slit is used to keep the illuminated area of the sample constant at all 2θ-angles. Figure 2(d) reveals a single-phase GGG garnet structure without any parasitic phases.

In summary, due to its high flexibility, the new high-resolution X-ray system will be of key importance for the characterization of various types of thin film samples and powder materials fabricated at the WMI and, therefore, will improve the materials-oriented research at the WMI.

References

[1] M. Müller, J. Weber, F. Engelhardt, V. A. S. V. Bittencourt, T. Luschmann, M. Cherkasskii, S. T. Goennenwein, S. V. Kusminskiy, S. Geprägs, R. Gross, M. Althammer, and H. Huebl. Chiral phonons and phononic birefringence in ferromagnetic metal - bulk acoustic resonator hybrids. arXiv:2303.08429 (2023).

F&S 5630i Automatic Wire Bonder

N. Bruckmoser, L. Koch, L. Södergren and S. Filipp [1]

An automatic wire bonder is a crucial tool in the field of microelectronics and superconducting quantum circuit manufacturing. This specialized machine plays a critical role in integrating the superconducting chip by bonding thin aluminum wires to a package. Our new system is an automatic wire bonder from F&S Bondtec that delivers high precision, wide tolerances and high throughput. It features a 140 kHz transducer in a wedge-wedge bonding head for bonding of planar topologies. The substrate stage features a 1 µm step resolution and allows a bond placement repetition precision of 3 µm (at 3σ). To maximize the yield of placed wire bonds, the control system allows precise modulation of all relevant parameters such as the bond force during the touchdown of the wedge, the strength and duration of the ultrasonic pulse, as well as the loop form of the bond. Together with the ability to save bond programs for chip layouts, we are now able to consistently package our chips with high precision. In addition, the increased bond speed of 3 bonds per second enables us to measure samples that are exposed to air for a shorter time.

Figure 1: Photograph of the installed automatic wire bonder in the sample preparation room.

Due to its modular setup, the machine can be upgraded with additional bonding heads. It is thus possible to extend the system in the future with a deep access bond head for packages with a non-planar topology, as well as with a pull and shear tester if needed.

Compared with the previous manual wire bonder system, we have gained in the alignment precision, wire bond consistency and reproducibility, bond speed, and reduced operator dependency.

[1] This machine was funded by the BMBF via grant No 13N15982 (SEQT).

Maskless aligner MLA150

N. Bruckmoser, L. Koch, L. Södergren and S. Filipp [1]

The maskless aligner MLA 150 from Heidelberg Instruments is a new addition to our cleanroom facility, designed to significantly reduce exposure time compared to the previously available direct laser lithography tool, Picomaster PM200. The MLA features a spatial light modulator in the form of a digital micromirror device, which projects a two-dimensional pixel array onto the substrate. It operates with a 375 nm laser diode and achieves a minimum feature size of 0.6 µm. This wavelength is compatible with most photoresists, enabling a broader range of processes as compared to the 405 nm laser module installed on the PM200.

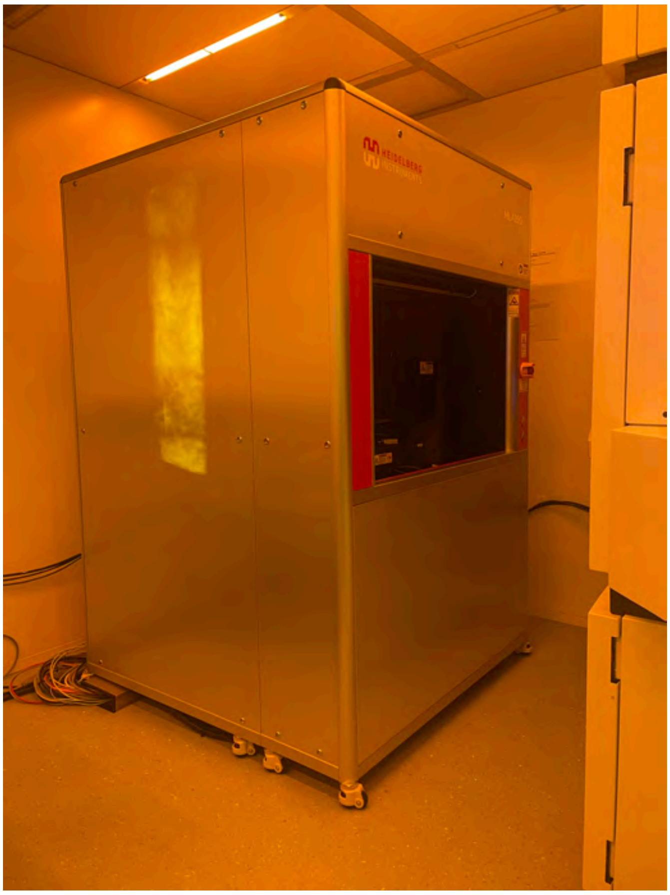

Figure 1: Photograph of the installed MLA150 in the cleanroom.

In addition to accommodating wafers up to 150 mm in diameter, the substrate table supports small substrate sizes down to $3 \times 3\,\text{mm}^2$. Our machine is equipped with two distinct auto-focus mechanisms to focus the laser at the substrate surface. The pneumatic auto-focus is suitable for wafers and large substrates. This is particularly useful for focusing on samples with varying reflection coefficients and topologies, such as air bridges. The optical auto-focus is employed for gaining a higher precision and for focusing on small substrates, where the pneumatic auto-focus does no longer work. Furthermore, the machine is equipped with a backside alignment camera. This allows us to align the backside of the wafer with the top side, which is crucial for trough-substrate vias.

Compared to the PM200, which has an exposure time of $7.7\,\text{mm}^2/\text{min}$, the MLA150 demonstrates a 37-fold speedup with an exposure time of $285\,\text{mm}^2/\text{min}$. This corresponds to an exposure of a 100 mm wafer in less than 35 minutes. The time-wise improvement is crucial due to the growing demand for wafer-scale lithography. It also facilitates prototyping and process optimization by significantly reducing the duration of fabrication cycles.

[1]This machine was funded by the BMBF program No 13N15982 (SEQT).

PLASSYS ME450S-In Indium Evaporator

D. Bunch, L. Richard, L. Koch, N. Bruckmoser, L. Södergren, S. Filipp [1]

In the past years, the WMI has successfully pushed the limits of superconducting qubit fabrication. Our planar thin film architecture is well suited to modestly sized qubit systems, and we have already used this standard process to realize 2x3 qubit grids, multi-qubit couplers, and flux-tunable qubit chains. As we scale up to larger systems with more complicated control schemes, on-chip signal routing becomes challenging in the 2D architecture, requiring networks of crossing control and readout lines with an increasing influence of signal cross-talk. A 3D architecture becomes necessary for continued scale-up, where different circuit elements are fabricated on separate chips and then bonded together. One could, for example, fabricate high-coherence qubits on one chip and control elements on another chip, thus avoiding the signal-routing problem that larger 2D qubit systems would introduce [1]. Developing such a 3D fabrication process also enables research into a wide range of novel configurations. Elements on the two chips can be coupled inductively, capacitively, or galvanically, depending on the desired control properties. Qubit coherence can be increased by isolating the sensitive qubits from the control electronics [2], and fences of superconducting material can be constructed in the gap between chips to reduce cross-talk or even create 3D superconducting cavities [3].

Figure 1: Photograph of the installed PLASSYS Indium Evaporator. The main chamber can be seen on the left, with the load lock on top. The sample stage chiller sits on the table in the center. On the right is the control computer and electronics rack.

To enable the development of a 3D fabrication process, a PLASSYS ME450S-In Indium Evaporator was installed in September 2023 (see Fig. 1). The system heats indium metal in a crucible to over 1000 °C, at which point it evaporates upwards to the sample chamber. The indium vapor condenses into a film on the sample, which can be defined into structures using a lift-off resist mask (see Fig. 2). The ductile indium structures compress during the bonding process to form interconnects between the chips, and become superconducting at cryogenic temperatures.

The Indium Evaporator features a cryo-pumped high vacuum chamber and a sample load-lock for simple sample exchange. Besides the water-cooled indium crucible, the main chamber contains a Kaufman source that provides argon ion milling. The milling removes surface oxides from the samples prior to indium deposition. Exchangeable shields in the chamber protect the chamber walls from excess indium and can be easily cleaned and reused. The sample load-lock can accommodate up to 4 inch wafers on a stage that is temperature controllable

[1] Funding provided by the BMBF through the project No 13N15982 "Skalierbare Einzelphotonendetektoren für Quantentechnologien" (SEQT).

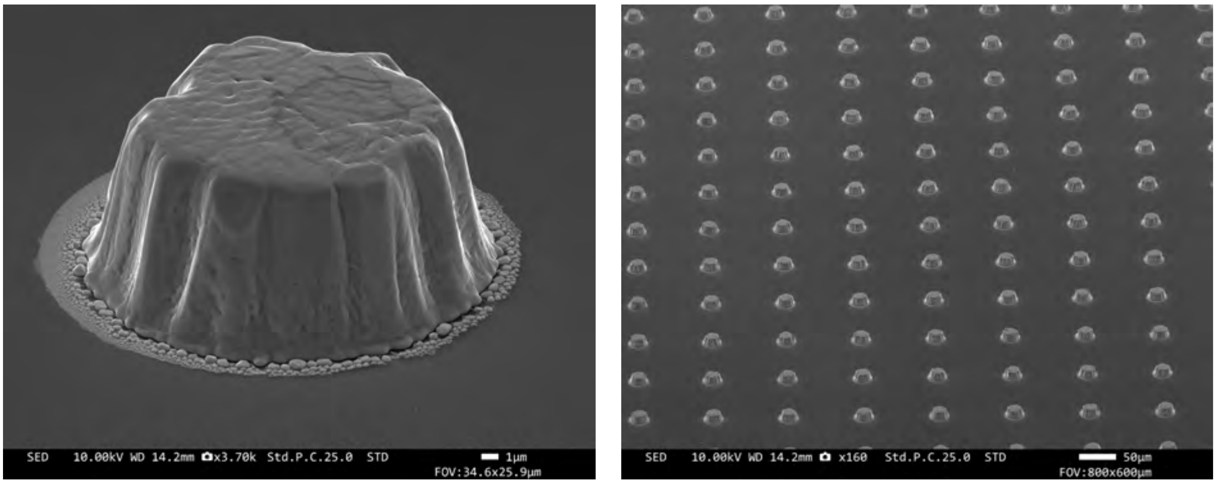

Figure 2: SEM photos of indium bumps on silicon after resist mask lift-off.

from $-40\,°C$ to $100\,°C$ to tune film formation properties. Two quartz crystal monitor systems are located near the sample to measure the film thickness accurately during deposition. The system was shipped with automated control software that supports the creation of custom process recipes that can be repeatedly executed. This tool is a foundational technology for developing a 3D fabrication architecture, which is crucial for our ultimate goal of producing a German quantum computer.

References

[1] D. R. W. Yost, M. E. Schwartz, J. Mallek, D. Rosenberg, C. Stull, J. L. Yoder, G. Calusine, M. Cook, R. Das, A. L. Day, E. B. Golden, D. K. Kim, A. Melville, B. M. Niedzielski, W. Woods, A. J. Kerman, and W. D. Oliver, npj Quantum Inf. **6**, 59 (2020).

[2] X. Pan, Y. Zhou, H. Yuan, L. Nie, W. Wei, L. Zhang, J. Li, S. Liu, Z. H. Jiang, G. Catelani, L. Hu, F. Yan, and D. Yu, Nat. Comm. **13**, 7196 (2022).

[3] C. U. Lei, L. Krayzman, S. Ganjam, L. Frunzio, and R. J. Schoelkopf, Appl. Phys. Lett. **116**, 154002 (2020).

Statistics

Publications

1. **Universal Time-Dependent Control Scheme for Realizing Arbitrary Linear Bosonic Transformations**
   Ze-Liang Xiang, Diego Gonzalez Olivares, Juan Jose Garcia-Ripoll, Peter Rabl
   Physical Review Letters **130**, 5 (2023).

2. **How pressure enhances the critical temperature for high temperature superconductivity in $YBa_2Cu_3O_{6+y}$**
   Michael Jurkutat, Carsten Kattinger, Stefan Tsankov, Richard Reznicek, Andreas Erb, Jürgen Haase
   PNAS (Proceedings of the National Academy of Sciences of the United States of America) **120**, e2215458120 (2023).

3. **Superspin ensembles of oxidized-$Co_xFe_{1-x}S_2$ with embedded magnetic nanoparticles**
   Henrik Gabold, Chinawat Ekwongsa, Pinit Kidkhunthod, Rattikorn Yimnirun, Matthias Opel, Amitesh Paul
   Journal of Materials Research **38**, 867 (2023).

4. **Hybrid magnetization dynamics in Cu_2OSeO_3/NiFe heterostructures**
   Carolina Lüthi, Luis Flacke, Aisha Aqeel, Akashdeep Kamra, Rudolf Gross, Christian Back, Mathias Weiler
   Applied Physics Letters **122**, 12401 (2023).

5. **Dry dilution refrigerator with pulse tube shutoff option**
   Kurt Uhlig
   Cryogenics **130**, 103649 (2023).

6. **Coherent heavy charge carriers in an organic conductor near the bandwidth-controlled Mott transition**
   S. Oberbauer, S. Erkenov, W. Biberacher, N. D. Kushch, R. Gross, M. V. Kartsovnik
   Phys. Rev. B **107**, 075139 (2023).

7. **Controlled-Controlled-Phase Gates for Superconducting Qubits Mediated by a Shared Tunable Coupler**
   Niklas J. Glaser, Federico Roy, Stefan Filipp
   Phys. Rev. Applied **19**, 044001 (2023).

8. **Surface acoustic wave resonators on thin film piezoelectric substrates in the quantum regime**
   Thomas Luschmann, Alexander Jung, Stephan Geprägs, Franz X. Haslbeck, Achim Marx, Stefan Filipp, Simon Gröblacher, Rudolf Gross, Hans Huebl
   Materials for Quantum Technology **3**, 021001 (2023).

9. **Entangling microwaves with light**
   R. Sahu, L. Qiu, W. Hease, G. Arnold, Y. Minoguchi, P. Rabl, J. M. Fink
   Science **380**, 718 (2023).

10. **Quantum behavior of a superconducting Duffing oscillator at the dissipative phase transition**
    Qi-Ming Chen, Michael Fischer, Yuki Nojiri, Michael Renger, Edwar Xie, Matti Partanen, Stefan Pogorzalek, Kirill G. Fedorov, Achim Marx, Frank Deppe, Rudolf Gross
    Nature Communications **14**, 2896 (2023).

11. **Observation of nonreciprocal magnon Hanle effect**
    Janine Gückelhorn, Sebastián de-la-Peña, Matthias Grammer, Monika Scheufele, Matthias Opel, Stephan Geprägs, Juan Carlos Cuevas, Rudolf Gross, Hans Huebl, Akashdeep Kamra, Matthias Althammer
    Physical Review Letters **130**, 216703 (2023).

12. **Can We Observe Nonperturbative Vacuum Shifts in Cavity QED?**
    R. Sáez-Blázquez, D. De Bernardis, J. Feist, P. Rabl
    Physical Review Letters **131**, 013602 (2023).

13. **Geometric and holonomic quantum computation**
    Jiang Zhang, Thi Ha Kyaw, Stefan Filipp, Leong-Chuan Kwek, Erik Sjöqvist, Dianmin Tong
    Physics Reports **1027**, 1–53 (2023).

14. **Optimizing the growth conditions of Al mirrors for superconducting nanowire single-photon detectors**
R. Flaschmann, C. Schmid, L. Zugliani, S. Strohauer, F. Wietschorke, S. Grotowski, B. Jonas, M. Müller, M. Althammer, R. Gross, J.J Finley, and K. Müller
Mater. Quantum. Technol. **3**, 035002 (2023).

15. **Chiral quantum optics in the bulk of photonic quantum Hall systems**
D. De Bernardis, F. Piccioli, P. Rabl, I. Carusotto
PRX Quantum **4**, 030306 (2023).

16. **High-Q Magnetic Levitation and Control of Superconducting Microspheres at Millikelvin Temperatures**
Joachim Hofer, Rudolf Gross, Gerard Higgins, Hans Huebl, Oliver F. Kieler, Reinhold Kleiner, Dieter Koelle, Philip Schmidt, Joshua A. Slater, Michael Trupke, Kevin Uhl, Thomas Weimann, Witlef Wieczorek, Markus Aspelmeyer
Physical Review Letters **131**, 043603 (2023).

17. **Quantum Microwave Parametric Interferometer**
F. Kronowetter, F. Fesquet, M. Renger, K. Honasoge, Y. Nojiri, K. Inomata, Y. Nakamura, A. Marx, R. Gross, K.G. Fedorov
Phys. Rev. Applied **20**, 024049 (2023).

18. **Perspectives of microwave quantum key distribution in open-air**
F. Fesquet, F. Kronowetter, M. Renger, Q. Chen, K. Honasoge, O. Gargiulo, Y. Nojiri, A. Marx, F. Deppe, R. Gross, and K. G. Fedorov
Physical Review A **108**, 032607 (2023).

19. **Impact of magnetic anisotropy on the magnon Hanle effect in α-Fe_2O_3**
Monika Scheufele, Janine Gückelhorn, Matthias Opel, Akashdeep Kamra, Hans Huebl, Rudolf Gross, Stephan Geprägs, Matthias Althammer
APL Materials **11**, 091115 (2023).

20. **Site-Selective Enhancement of Superconducting Nanowire Single-Photon Detectors via Local Helium Ion Irradiation**
S. Strohauer, F. Wietschorke, L. Zugliani, R. Flaschmann, C. Schmid, S. Grotowski, M. Müller, B. Jonas, M. Althammer, R. Gross, K. Müller, and J.J Finley
Advanced Quantum Technologies **6**, 2300139 (2023).

21. **Autonomous distribution of programmable multiqubit entanglement in a dual-rail quantum network**
J. Agustí, X. H. H. Zhang, Y. Minoguchi, P. Rabl,
Physical Review Letters **131**, 250801 (2023).

22. **Electrical detectability of magnon-mediated spin current shot noise**
Luise Siegl, Michaela Lammel, Akashdeep Kamra, Hans Huebl, Wolfgang Belzig, Sebastian T. B. Goennenwein
Physical Review B **108**, 144420 (2023).

23. **Emission of coherent THz magnons in an antiferromagnetic insulator triggered by ultrafast spin–phonon interactions**
E. Rongione, O. Gueckstock, M. Mattern, O. Gomonay, H. Meer, C. Schmitt, R. Ramos, T. Kikkawa, M. Micica, E. Saitoh, J. Sinova, H. Jaffres, J. Mangeney, S.T.B. Goennenwein, S. Geprägs, T. Kampfrath, M. Kläui, M. Bargheer, T.S. Seifert, S. Dhillon, R. Lebrun
Nature Communications **14**, 1818 (2023).

24. **Spin Hall Magnetoresistance (SMR) in Antiferromagnetic Insulators**
Stephan Geprägs, Matthias Opel, Johanna Fischer, Philipp Schwenke, Matthias Althammer, Hans Huebl, Rudolf Gross
2023 IEEE International Magnetic Conference - Short Papers (INTERMAG Short Papers) **1-2**, (2023).

25. **Nonreciprocal Magnon Hanle Effect in Antiferromagnetic α-Fe2O3**
Janine Gückelhorn, Sebastián de-La-Peña, Monika Scheufele, Matthias Grammer, Matthias Opel, Stephan Geprägs, Juan Carlos Cuevas, Rudolf Gross, Hans Huebl, Akashdeep Kamra, Matthias Althammer

2023 IEEE International Magnetic Conference - Short Papers (INTERMAG Short Papers) **1-2** (2023).

26. **Observation of a low energy nuclear recoil peak in the neutron calibration data of the CRESST-III Experiment**
G. Angloher, S. Banik, G. Benato, A. Bento, A. Bertolini, R. Breier, C. Bucci, J. Burkhart, L. Canonica, A. D'Addabbo, S. Di Lorenzo, L. Einfalt, A. Erb, F. v. Feilitzsch, S. Fichtinger, D. Fuchs, A. Garai, V. M. Ghete, P. Gorla, P. V. Guillaumon, S. Gupta, D. Hauff, M. Jeskovsky, J. Jochum, M. Kaznacheeva , A. Kinast, H. Kluck, H. Kraus, S. Kuckuk, A. Langenkämper, M. Mancuso, L. Marini,11, B. Mauri, L. Meyer, V. Mokina, M. Olmi, T. Ortmann, C. Pagliarone, L. Pattavina, F. Petricca1, W. Potzel, P. Povinec, F. Prö bst, F. Pucci, F. Reindl, J. Rothe, K. Schäffner, J. Schieck, S. Schönert, C. Schwertner, M. Stahlberg, L. Stodolsky, C. Strandhagen, R. Strauss, I. Usherov, F. Wagner, M. Willers,V. Zema
Phys. Rev. D **108** 022005 (2023).

27. **Characterisation of low background CaWO4 crystals for CRESST-III**
Angelina Kinast1, G. Angloher, S. Banik, G. Benato, A. Bento, A. Bertolini,R. Breier, C. Bucci, J. Burkhart, L. Canonica, A. D'Addabbo, S. Di Lorenzo,L. Einfalt, A. Erb, F. v. Feilitzsch, N. Ferreiro Iachellini, S. Fichtinger, D. Fuchs,A. Fuss, A. Garai, V. M. Ghete, S. Gerster, P. Gorla, P. V. Guillaumon, S. Gupta,D. Hauff, M. Ješkovský, J. Jochum, M. Kaznacheeva1, H. Kluck, H. Kraus ,A. Langenkämper, M. Mancuso, L. Marini, L. Meyer, Valentyna Mokina, A. Nilima, M. Olmi, T. Ortmann, C. Pagliarone, L. Pattavina, F. Petricca,W. Potzel, P. Povinec, F. Pröbst, F. Pucci, F. Reindl, J. Rothe, K. Schäffner,J. Schieck, D. Schmiedmayer, S. Schönert, C. Schwertner, M. Stahlberg,L. Stodolsky, C. Strandhagen, R. Strauss, I. Usherov, F. Wagner, M. Willers and V. Zema
SciPost Physics Proceedings (2023).

28. **Results on sub-GeV Dark Matter from a 10 eV Threshold CRESST-III Silicon Detector, CRESST Collaboration**
G. Angloher, S. Banik, G. Benato, A. Bento, A. Bertolini, R. Breier, C. Bucci, J. Burkhart, L. Canonica, A. D'Addabbo, S. Di Lorenzo, L. Einfalt, A. Erb, F. v. Feilitzsch, N. Ferreiro Iachellini, S. Fichtinger, D. Fuchs, A. Fuss, A. Garai, V. M. Ghete, S. Gerster, P. Gorla, P. V. Guillaumon, S. Gupta , D. Hauff, M. Jeskovsky, J. Jochum, M. Kaznacheeva, A. Kinast, H. Kluck, H. Kraus, A. Langenkämper, M. Mancuso, L. Marini, L. Meyer, V. Mokina, A. Nilima, M. Olmi, T. Ortmann, C. Pagliarone, L. Pattavina, F. Petricca, W. Potzel, P. Povinec, F. Pröbst, F. Pucci, F. Reindl, J. Rothe, K. Schäffner, J. Schieck, D. Schmiedmayer, S. Schönert, C. Schwertner, M. Stahlberg, L. Stodolsky, C. Strandhagen, R. Strauss, I. Usherov, F. Wagner, M. Willers, and V. Zema
Phys. Rev. D **107**, 122003 (2023).

29. **Secular Equilibrium Assessment in a CaWO4 Target Crystal from the Dark Matter, Experiment CRESST using Bayesian Likelihood Normalisation**
G. Angloher, S. Banik, G. Benato, A. Bento, A. Bertolini, R. Breier, C. Bucci, J. Burkhart, L. Canonica, A. D'Addabbo, S. Di Lorenzo, L. Einfalt, A. Erb, F. v. Feilitzsch, N. Ferreiro Iachellini, S. Fichtinger, D. Fuchs, A. Fuss, A. Garai, V. M. Ghete, P. Gorla, S. Gupta, D. Hauff, M. Ješkovský, J. Jochum , M. Kaznacheeva, A. Kinast, H. Kluck, H. Kraush, A. Langenkämper, M. Mancusoa, L. Marinid,, V. Mokinab, A. Nilimaa, M. Olmid, T. Ortmann,C. Pagliaroned, L. Pattavinad, F. Petricca, W. Potzel, P. Povinec, F. Pröbsta, F. Pucci, F. Reindl, J. Rothe, K. Schäffner, J. Schieckb, D. Schmiedmayer, S. Schönert, C. Schwertner, M. Stahlberg, L. Stodolsky, C. Strandhagen, R. Strauss, I. Usherov, F. Wagner, M. Willers, V. Zema
Applied Radiation and Isotopes **194**, 110670 (2023).

30. **Probing superconducting order in overdoped $Ca_xY_{1-x}Ba_2Cu_3O_7$ by neutron diffraction measurements of the vortex lattice**
A. S. Cameron, E. Campillo, A. Alshemi, M. Bartkowiak, L. Shen, H. Kawano-Furukawa, A. T. Holmes, O. Prokhnenko, A. Gazizulina, J. S. White, R. Cubitt, N. -J. Steinke, C. D. Dewhurst, A. Erb, E. M. Forgan, E. Blackburn
Physical Review B **108**, 14 (2023).

31. **Towards an automated data cleaning with deep learning in CRESST**
G. Angloher, S. Banik, D. Bartolot, G. Benato, A. Bento, A. Bertolini, R. Breier, C. Bucci, J. Burkhart, L. Canonica, A. D'Addabbo, S. Di Lorenzo, L. Einfalt, A. Erb, F. v. Feilitzsch, N. Ferreiro Iachellini, S. Fichtinger, D. Fuchs, A. Fuss, A. Garai, V. M. Ghete, S. Gerster, P. Gorla,

P. V. Guillaumon, S. Gupta, D. Hauff, M. Ješkovský, J. Jochum, M. Kaznacheeva, A. Kinast, H. Kluck, H. Kraus, M. Lackner, A. Langenkämper, M. Mancuso, L. Marini, L. Meyer, V. Mokina, A. Nilima, M. Olmi, T. Ortmann, C. Pagliarone, L. Pattavina, F. Petricca, W. Potzel, P. Povinec, F. Pröbst, F. Pucci, F. Reindl, D. Rizvanovic, J. Rothe, K. Schäffner, J. Schieck, D. Schmiedmayer, S. Schönert, C. Schwertner, M. Stahlberg, L. Stodolsky, C. Strandhagen, R. Strauss, I. Usherov, F. Wagner, M. Willers, V. Zema, W. Waltenberger & CRESST
Eur. Phys. J. Plus **138**, 1100 (2023).

32. **Festkörperphysik. Aufgaben und Lösungen** (3rd revised and extended edition)
Rudolf Gross, Achim Marx, Dietrich Einzel, Stephan Geprägs
De Gruyter Oldenbourg, Berlin/Boston (2023), ISBN: 9783110782356 (hardcover), ISBN: 9783110782530 (eBook) (2023) .

33. **Quantencomputer: Präzise Kontrolle über die Welt der Quanten in 'Chancen und Risiken von Quantentechnologien'**
Stefan Filipp (Eds. Alissa Wilm, Florian Neukart)
Springer-Verlag

34. **Quantenkorrelation verbessert Radartechnik**
F. Kronowetter
Rohde & Schwarz Neues **226**, 24–29 (2023), ISSN 0548-3093.

35. **Quantensensorik und Quantenmetrologie machen gewaltige Fortschritte**
R. Gross, F. Kronowetter
Rohde & Schwarz Neues **226**, 20–23 (2023), ISSN 0548-3093.

36. **Quantencomputing - mit Supraleitung und Spin**
Stefan Filipp, Gian Salis
Physik Journal **22** 1, 42-45 (2023)

37. **The bosonic skin effect: boundary condensation in asymmetric transport**
L. Garbe, Y. Minoguchi, J. Huber, P. Rabl
arXiv:2301.11339, submitted for publication (2023).

38. **Chiral phonons and phononic birefringence in ferromagnetic metal–bulk acoustic resonator hybrids**
M. Müller, J. Weber, F. Engelhardt, V.A.S.V. Bittencourt, T. Luschmann, M. Cherkasskii, M. Opel, S.T.B. Goennenwein, S. Viola Kusminskiy, S. Geprägs, R. Gross, M. Althammer, H. Huebl
arXiv:2303.08429, accepted for publication in Physical Review B (2023).

39. **High-Dimensional Bayesian Likelihood Normalisation for CRESST's Background Model**
G. Angloher, S. Banik, G. Benato, A. Bento, A. Bertolini, R. Breier, C. Bucci, J. Burkhart, L. Canonica, A. D'Addabbo, S. Di Lorenzo, L. Einfalt, A. Erb, F. v. Feilitzsch, S. Fichtinger, D. Fuchs, A. Garai, V. M. Ghete, P. Gorla, P. V. Guillaumon, S. Gupta, D. Hauff, M. Jeskovsky, J. Jochum, M. Kaznacheeva , A. Kinast, H. Kluck, H. Kraus, S. Kuckuk, A. Langenkämper, M. Mancuso, L. Marini,11, B. Mauri, L. Meyer, V. Mokina, M. Olmi, T. Ortmann, C. Pagliarone, L. Pattavina, F. Petricca1, W. Potzel, P. Povinec, F. Pröbst, F. Pucci, F. Reindl, J. Rothe, K. Schäffner, J. Schieck, S. Schönert, C. Schwertner, M. Stahlberg, L. Stodolsky, C. Strandhagen, R. Strauss, I. Usherov, F. Wagner, M. Willers, V. Zema
arXiv:2307.12991, submitted for publication (2023).

40. **Two-Dimensional Planck Spectroscopy**
S. Gandorfer, M. Renger, W. K. Yam, F. Fesquet, A. Marx, R. Gross, K. G. Fedorov
arXiv:2308.02389, submitted for publication (2023).

41. **Imperfect photon detection in quantum illumination**
F. Kronowetter, M. Würth, W. Utschick, R. Gross, K. G. Fedorov
arXiv:2308.02343, accepted for publication in Physical Review Applied (2023)

42. **Cryogenic microwave link for quantum local area networks**
M. Renger, S. Gandorfer, W. Yam, F. Fesquet, M. Handschuh, K. E. Honasoge, F. Kronowetter, Y. Nojiri, M. Partanen, M. Pfeiffer, H. van der Vliet, A. J. Matthews, J. Govenius, R. N. Jabdaraghi, M. Prunnila, A. Marx, F. Deppe, R. Gross, K. G. Fedorov
arXiv:2308.12398, submitted for publication (2023).

43. **Single-crystalline YIG nanoflakes with uniaxial in-plane anisotropy and diverse crystallographic orientations**
Roman Hartmann, Seema, Ivan Soldatov, Michael Lammel, Daphné Lignon, Xianyue Ai, Gillian Kiliani, Rudolf Schäfer, Andreas Erb, Rudolf Gross, Johannes Boneberg, Martina Müller, Sebastian T. B. Goennenwein, Elke Scheer, Angelo Di Bernardo
arXiv:2309.12477, submitted for publication (2023).

44. **Light Dark Matter Search Using a Diamond Cryogenic Detector**
CRESST Collaboration, G. Angloher, S. Banik, G. Benato, A. Bento, A. Bertolini, R. Breier, C. Bucci, J. Burkhart, L. Canonica, A. D'Addabbo, S. Di Lorenzo, L. Einfalt, A. Erb, F. v. Feilitzsch, S. Fichtinger, D. Fuchs, A. Garai, V. M. Ghete, P. Gorla, P. V. Guillaumon, S. Gupta, D. Hauff, M. Ješkovský, J. Jochum , M. Kaznacheeva, A. Kinast, H. Kluck, H. Kraus, S. Kuckuk, A. Langenkämper, M. Mancuso, L. Marini, B. Mauri, L. Meyer, V. Mokina, M. Olmi, T. Ortmann, C. Pagliarone, L. Pattavina, F. Petricca1, W. Potzel, P. Povinec, F. Pröbst, F. Pucci, F. Reindl, J. Rothe, K. Schäffner, J. Schieck, S. Schönert, C. Schwertner, M. Stahlberg, L. Stodolsky, C. Strandhagen, R. Strauss, I. Usherov, F. Wagner, M. Willers, V. Zema
arXiv:2310.05815, submitted for publication (2023).

45. **Slow and Non-Equilibrium Dynamics due to Electronic Ferroelectricity in a Strongly-Correlated Molecular Conductor**
Tatjana Thomas, Yassine Agarmani, Steffi Hartmann, Mark Kartsovnik, Natalia Kushch, Sebastian Schmid, Peter Lunkenheimer, Michael Lang, Jens Müller
arXiv:2310.17242, submitted for publication (2023)

46. **17O enrichment of $CaWO_4$ crystals for spin-dependent DM search**
Angelina Kinast, Andreas Erb, Stefan Schönert, Raimund Strauss, Jürgen Haase
arXiv:2311.0316, submitted for publication (2023).

47. **Electrically induced angular momentum flow between separated ferromagnets**
R. Schlitz, M. Grammer, T. Wimmer, J. Gückelhorn, L. Flacke, S.T.B. Goennenwein, R. Gross, H. Huebl, A. Kamra, M. Althammer
arXiv:2311.05290, submitted for publication (2023).

48. **A Unified Interface Model for Dissipative Transport of Bosons and Fermions**
Y. Minoguchi, J. Huber, L. Garbe, A. Gambassi, P. Rabl
arXiv:2311.10138, submitted for publication (2023).

49. **Demonstration of microwave single-shot quantum key distribution**
F. Fesquet, F. Kronowetter, M. Renger, W. K. Yam, S. Gandorfer, K. Inomata, Y. Nakamura, A. Marx, R. Gross, K. G. Fedorov
arXiv:2311.11069, submitted for publication (2023).

50. **Temperature dependence of the magnon-phonon interaction in high overtone bulk acoustic resonator-ferromagnetic thin film hybrids**
M. Müller, J. Weber, S.T.B. Goennenwein, S. Viola Kusminskiy, R. Gross, M. Althammer, H. Huebl
arXiv:2311.16725, submitted for publication (2023).

51. **Efficient decoupling of a non-linear qubit mode from its environment**
F. Pfeiffer, M. Werninghaus, C. Schweizer, N. Bruckmoser, L. Koch, N. J. Glaser, G. Huber, D. Bunch, F. X. Haslbeck, M. Knudsen, G. Krylov, K. Liegener, A. Marx, L. Richard, J. H. Romeiro, F. Roy, J. Schirk, C. Schneider, M. Singh, L. Södergren, I. Tsitsilin, F. Wallner, C. A. Riofrío, S. Filipp
arXiv:2312.16988, submitted for publication (2023).

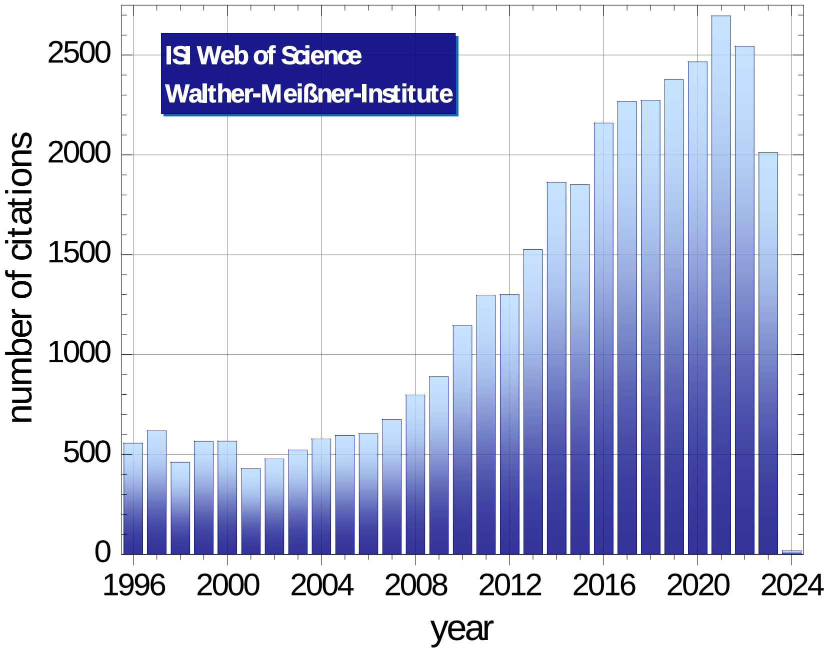

The total number of citations per year of papers published by members of WMI since 1996. This number has almost quadrupled within the last twenty years.

Books

Festkörperphysik. Aufgaben und Lösungen (3rd revised and extended edition)

The extended 3rd edition of the textbook **«Festkörperphysik. Aufgaben und Lösungen»** by Rudolf Gross, Achim Marx, Dietrich Einzel and Stephan Geprägs appeared at De Gruyter Oldenbourg. The book complements the textbook on **«Festkörperphysik»** by Rudolf Gross and Achim Marx, which meanwhile represents a standard textbook on solid-state physics. Both books are well received by university teachers and highly esteemed by the students. Therefore, new editions have to be prepared regularly.

https://doi.org/10.1524/9783486858969

The first, second, and third editions of the textbook on **«Festkörperphysik»** appeared in 2012, 2014, and 2018. The latest fourth edition has become available in November 2022 from De Gruyter Oldenbourg (ISBN: 9783110782349). It is also available as an ebook (ISBN: 9783110782394).

Deepening and extending the understanding of solid-state physics by solving specific problems is highly valuable. Therefore, there has been a supplementary book entitled «Festkörperphysik. Aufgaben und Lösungen» from the beginning. Since this book's 2nd edition was sold out in 2022, an extended and revised follow-up version has been prepared. This third edition of the book appeared in July 2023. It contains more than 100 problems related to the solid-state physics textbook «Festkörperphysik» together with detailed model solutions. By providing the full solutions, the exercise book allows students to consolidate and expand their knowledge and test what they have learned. Compared to the previous editions, the third edition contains seven new problems and solutions on the topic of quantum materials that has not been covered yet in the previous editions. The exercises & solutions book, with many new exercises on topological quantum matter, is ideal for preparing for exams and learning independently.

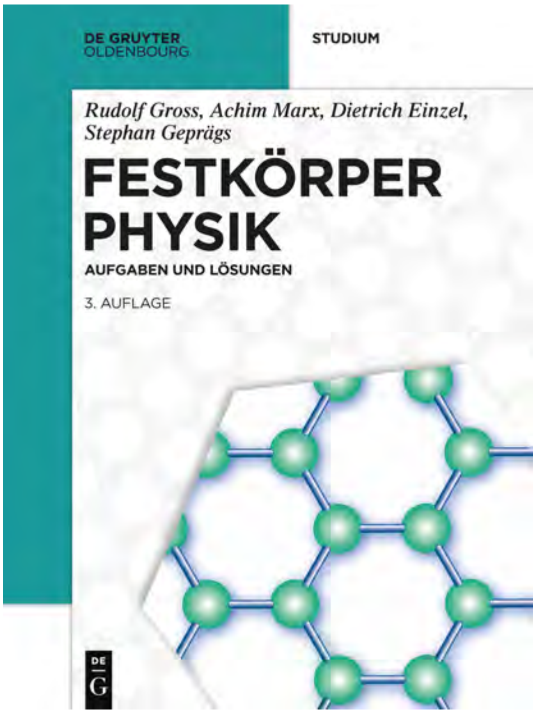

Bachelor, Master, Doctoral, and Habilitation Theses

A. Completed and Ongoing Habilitation Theses

WMI strongly supports habilitation candidates, as fostering young scholars is one of its key concerns. The habilitation process serves as the formal assessment tool ascertaining whether or not a candidate is suitable, from an academic and a pedagogical point of view, to be a professor in a particular field at the university level. Within the past 20 years, 7 research staff members of WMI completed the habilitation procedure and received the **«venia legendi»** of the Technical University of Munich (TUM). The fact that three of them subsequently received W3 professor positions outside of Munich and one a leading position in the industry clearly demonstrates that the habilitation procedure is still a valuable way of fostering young talents and that WMI is quite successful in supporting young talents along this career path.

Regarding the promotion of scientific careers, it is worth noting that 4 research staff members of WMI have become professors outside of Munich (Alff, Erb, Gönnenwein, Weiler), and four adjunct professors at the Technical University of Munich (Einzel, Lerf, Schuberth, Hackl) within the past 20 years.

In 2023, **Matthias Althammer** and **Kirill Fedorov** received the «venia legendi» in experimental physics of TUM after successfully finishing their habilitation process already in the previous year. We heartily congratulate Kirill and Matthias and are very happy that we have two more ambitious young lecturers at WMI who also support the teaching program of the interdisciplinary master course in Quantum Science and Technology. We know that offering high-quality lectures and seminars is key to attracting talented students to WMI.

At present, only **Nadezhda Kukharchyk** is passing through the habilitation procedure at the Technical University of Munich.

Dr. Nadezhda Kukharchyk

Supporting and mentoring talented female scientists in natural sciences and engineering is an important long-term task. This is particularly true for quantum sciences where the share of female scientists is still much too low, particularly at the postdoc and professor levels. Therefore, WMI is happy to have a female group leader who is presently passing the habilitation procedure.

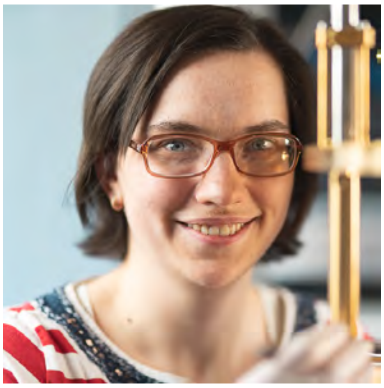

Nadezhda Kukharchyk received one of the prestigious ***START Fellowships*** of the Excellence Cluster MCQST in 2020. Supported by this fellowship, she joined the group of Rudolf Gross at WMI in November 2020 and built up a new research group at WMI focusing on the spectroscopy and applications of spin-based quantum systems. In November 2021, she presented her research field and recent achievements to the Faculty of Physics teaching body within the Solid-State Colloquium. After this formal step, she submitted the required documents to the dean's office and was then accepted as a habilitation candidate by the School of Natural Sciences of TUM early in 2022. Her *Fachmentorat* consists of Rudolf Gross (WMI/BAdW and TUM, chairman), Jonathan Finley (TU Munich/Walter Schottky Institute, member), and Klaus Mølmer (Niels Bohr Institute, University of Copenhagen, Denmark, member).

Nadezhda Kukharchyk studied physics at the Belarussian State University in Minsk, Belarus, and then joined the University of Bochum (group of Prof. Andreas Wieck) as a Ph.D. student in 2011. She finished her thesis entitled *Focused Ion-Beam Implantation of Rare-Earth Ions for Realisation of Spin-Ensemble Systems* in 2015. She then joined Saarland University, where she was setting up a newly established experimental laboratory for optical and microwave spectroscopy of rare-earth doped single crystals at mK temperatures before accepting the MCQST offer and joining the group of Rudolf Gross at WMI. We are very happy to be able to support the scientific career of an ambitious female researcher.

Meanwhile, Nadezhda Kukharchyk already acquired a new BMBF-project on the ***Storage of Microwave Quantum Tokens in Electron and Nuclear Spin Ensembles*** (**QuaMToMe**, grant No. 16 KISQ 036). She is the coordinator of this new project, which started in November 2021. The core objective of QuaMToMe is the realization, investigation, and demonstration of quantum tokens (Q-tokens) in the microwave or GHz frequency range. The quantum tokens will be implemented in the form of quantum keys stored in quantum memories based on spin ensembles. In general, scalable and long-lived quantum memories represent one of the missing elements needed to build local microwave-based quantum networks. Quantum tokens in the form of propagating squeezed states represent a particularly important use case for such quantum networks.

B. Completed and Ongoing Ph.D. Theses

Completed Ph.D. Theses:

1. **Quantum Microwave Communication**
   Michael Renger, Technical University of Munich, November 2023.
2. **Pure Spin Currents in Epitaxial All Oxide Heterostructures**
   Janine Gückelhorn, Technical University of Munich, December 2023.
3. **Coupling Phenomena in Magnonic Hybrid Heterostructures**
   Manuel Müller, Technical University of Munich, December 2023.
4. **Onset of Transmon Ionization in Microwave Single-Photon Detection**
   Yuki Nojiri, Technical University of Munich, December 2023.

Ongoing Ph.D. Theses:

1. **Operation and Modelling of Superconducting Qubit Devices**
   Federico Roy, Saarland University, since September 2018.
2. **Hybrid Solid State Quantum Systems**
   Thomas Luschmann, Technical University of Munich, since September 2019.
3. **Fabrication and Investigation of Superconducting Quantum Processors with Novel Architectures**
   Leon Koch, Technical University of Munich, since July 2020.
4. **Tailoring the Control of Superconducting Qubits to Efficiently Solve Molecular Chemistry Problems**
   Malay Singh, Technical University of Munich, since October 2020.
5. **Multi-Qubit Gates for the Efficient Exploration of Hilbert Space with Superconducting Circuits**
   Ivan Tsitsilin, Technical University of Munich, since October 2020.
6. **A Journey into Quantum Illumination**
   Fabian Kronowetter, Technical University of Munich, since February 2021.
7. **Fabrication and Characterization of Superconducting Parametric Devices**
   Kedar Honasoge, , since February 2021.
8. **Demonstration of Microwave Quantum Key Distribution**
   Florian Fesquet, Technical University of Munich, since February 2021.
9. **Providing external access to a superconducting quantum processor**
   Martin Knudsen, Technical University of Munich, since March 2021.
10. **Implementation of Optical Approaches in Microwave Quantum Memory Systems**
    Ana Strinic, Technical University of Munich, since April 2021.
11. **Josephson Travelling Wave Parametric Amplifier for Multi-qubit Readout**
    Daniil Bazulin, Technical University of Munich, since August 2021.
12. **Evolution of the Charge Carrier Properties and Electronic Correlations in Layered Organic Metals near the Mott Metal-Insulator Transition**
    Shamil Erkenov, Technical University of Munich, since September 2021.
13. **Industry-compatible development of Travelling Wave Parametric Amplifiers**
    Nicolas Arlt, Technical University of Munich, since Oktober 2021.

14. **Hardware-tailored Quantum algorithms with Superconducting Qubits**
Frederik Pfeiffer, Technical University of Munich, since November 2021.
15. **Scalable Multi-Qubit Architectures Based on Superconducting Qubits**
Niklas Glaser, Technical University of Munich, since December 2021.
16. **Design and Application of Multi-Qubit Couplers**
Gerhard Huber, Technical University of Munich, since December 2021.
17. **Scalable quantum processor with novel superconducting qubits**
Florian Wallner, Technical University of Munich, since January 2022.
18. **Experimental Realization of Quantum Memory Based on Phosphorous Donors in Silicon Including Storage and Retrieval of Q-Tokens**
Patricia Oehrl, Technical University of Munich, since February 2022.
19. **Fabrication and Characterization of Thin Films and Heterostructures of Quantum Materials**
Monika Scheufele, Technical University of Munich, since April 2022.
20. **Fabrication and Characterization of Superconducting Single Photon Detectors**
Maria Handschuch, Technical University of Munich, since April 2022.
21. **Towards high-coherence 3D integrated quantum circuits**
Lea Richard, Technical University of Munich, since June 2022.
22. **Fabrication of high-coherence superconducting qubits**
David Bunch, Technical University of Munich, since June 2022.
23. **Scalable Control for Superconducting Qubits**
João Romeiro, Technical University of Munich, since July 2022.
24. **Quantum Information Processing based on Alternative Superconducting Qubits**
Johannes Schirk, Technical University of Munich, since July 2022.
25. **Realization of a Multimode Quantum Memory Based on Rare-Earth Spin Ensembles**
Jianpeng Chen, Technical University of Munich, since August 2022.
26. **Quantum Gravity – Levitated Superconductors and their Position Measurement**
Korbinian Rubenbauer, Technical University of Munich, since October 2022.
27. **Entanglement distribution with continuous and discrete variable systems**
Joan Agustí, Technical University of Munich, since November 2022.
28. **Microwave Quantum Communication over Thermal Channels**
Wun Kwan Yam, Technical University of Munich, since November 2022.
29. **Remote entanglement of superconducting qubits**
Simon Gandorfer, Technical University of Munich, since January 2023.
30. **Tailored Magneto-Mechanical Hybrids for Quantum Transduction**
Matthias Grammer, Technical University of Munich, since March 2023.
31. **Investigating the Origin of Decoherence in Superconducting Qubits**
Niklas Bruckmoser, Technical University of Munich, since April 2023.
32. **Optimal control of quantum communication protocols**
Przemyslaw Zielinski, Technical University of Munich, since April 2023.
33. **Storage of Microwave-Based Quantum Tokens in Rare-Earth Spin Ensembles in $CaWO_4$ Single Crystals**
Georg Mair, Technical University of Munich, since July 2023.
34. **Protected light-matter interfaces in hybrid quantum networks**

Syeda Aliya Batool, Technical University of Munich, since September 2023.

35. **Development of a scalable readout and control system for superconducting qubits**
Kevin Kiener, Technical University of Munich, since September 2023.
36. **Noise informed control of superconducting quantum systems**
Emily Wright, Technical University of Munich, since October 2023.
37. **Waveguide QED systems with interacting photons**
Adrian Misselwitz, Technical University of Munich, since October 2023.
38. **Quantum simulations of lattice gauge theories**
Lucia Valor, Technical University of Munich, since October 2023.
39. **Magnetic Resonance Spectroscopy of Quantum Materials**
Johannes Weber, Technical University of Munich, starts in January 2024.

C. Completed and Ongoing Bachelor and Master Theses

Completed Master Theses:

1. **All-electrical spin transport in Superconductor/Ferromagnetic insulator heterstructures**
   Yuhao Sun, Technical University of Munich, January 2023.
2. **Nano-scale NMR of Pt thin films using quantum sensors in diamond**
   Joachim Leibold, Technical University of Munich, January 2023.
3. **Study of Energy Exchange between Spatially Separated Rare-Earth Electronic Spin Ensembles at Cryogenic Temperatures**
   Owen Thomas Huisman, Technical University of Munich, April 2023.
4. **Unidirectional spin wave propagation in magnetic nanograting/thin film heterostructures**
   Christian Mang, Technical University of Munich, May 2023.
5. **Fabrication of a Superconducting Transmission Line in a Planar Design on a Spin Doped Crystalline Membrane**
   Georg Mair, Technical University of Munich, May 2023.
6. **Superconducting Microwave Resonators for Spin Based Quantum Memories**
   Julian Franz, Technical University of Munich, June 2023.
7. **Microwave Manipulation of Magnon Transport and Spin Pumping**
   Franz Weidenhiller, Technical University of Munich, June 2023.
8. **Advanced calibration of superconducting qubits**
   Catharina Brooks, Technical University of Munich, June 2023.
9. **Generating Small Magnetic Fields Inside an open-End Magnetic Shielding with a Superconducting Solenoid Magnet**
   Lukas Vogl, Technical University of Munich, July 2023.
10. **Growth Optimization and Magnetotransport of GdN hybrid structures**
    Raphael Hoepfl, Technical University of Munich, August 2023.
11. **Thermal History Dependent Electronic Properties of κ-(BEDT-TTF)$_2$Cu[N(CN)$_2$]X (X = Br,Cl) Near the Mott Metal-Insulator Transition**
    Florian Kollmannsberger, Technical University of Munich, September 2023.
12. **Observation of Quantum Switching in Driven-Dissipative Superconducting Oscillators**
    Sebastiano Davide Covone, Technical University of Munich, October 2023.
13. **Coherent Magnetoelastic Coupling in Magnetic Thin Film/Crystalline Substrate Heterostructures**
    Johannes Weber, Technical University of Munich, November 2023.
14. **Simultaneous Electrical and Optical Detection of Zero Effective Magnon Damping in a Magnetic Insulator**
    Maria Sigl, Technical University of Munich, November 2023.
15. **Promising Materials for Unconventional Superconductivity**
    Herman Muzychko, Technical University of Munich, November 2023.
16. **Microwave Cryptography with Propagating Quantum Tokens**
    Valentin Weidemann, Technical University of Munich, December 2023.

Completed Bachelor Theses:

1. **Active Reset of Fluxonium Qubits**
   Petr Ivashkov, Technical University of Munich, July 2023.
2. **Magnon-phonon coupling in symmetric magneto-metallic thin film/bulk acoustic wave resonator heterostructures**
   Keita Takahashi, Technical University of Munich, July 2023.
3. **Magnetometry with NV centers in diamond – implementation of an optically detected magnetic resonance setup**
   Timur Zeisler, Technical University of Munich, July 2023.
4. **Growth and piezoelectric properties of scandium-doped aluminum nitride thin films**
   Luca Schmidt, Technical University of Munich, September 2023.
5. **Nanomechanik mit Niobtitannitrid Nanosaiten und deren mechanischen Eigenschaften bei tiefen Temperaturen**
   Nikita Lyadvinsky, Technical University of Munich, September 2023.
6. **Quench protection of a superconducting magnet**
   Robert Pant, Technical University of Munich, September 2023.
7. **Co_xFe_{1-x} Thin Films for Future Magnonic Devices**
   Otto Graf, Technical University of Munich, October 2023.
8. **Fabrikation und Charakterisierung planarer Mikrowellenresonatoren aus NbTiN bei tiefen Temperaturen**
   Alexander Dolpp, Technical University of Munich, November 2023.

Ongoing Master Theses:

1. **Critically coupled qubit-photon interfaces in waveguide QED**
   Nicolas Jungwirth, Technical University of Munich, since May 2023.
2. **Micromagnetic Simulations of Non-Reciprocal Magnonic Devices**
   Markus Kügle, Technical University of Munich, since June 2023.
3. **Exploring the Potential of Hybrid Classical-Quantum Cloud Computing: Architecture, Protocol, and Performance**
   Maxime Lavocat, Technical University of Munich, since June 2023.
4. **Fabrication of an over-coupled superconducting coplanar transmission line for efficient coupling to rare earth spin ensembles**
   Chiun Fu, Technical University of Munich, since August 2023.
5. **Investigating Decoherence in Fluxonium Qubits**
   Vincent Koch, Technical University of Munich, since October 2023.
6. **Multiple-excitation dynamics in Spin Rings**
   Lukas Vetter, Technical University of Munich, since October 2023.
7. **Alternative qubit readout using multi-mode circuits**
   Rui Wang, Technical University of Munich, since October 2023.
8. **Flip-chip bump bonding optimization towards high coherence 3D integrated quantum circuits**
   Agata Skoczylas, Technical University of Munich, since October 2023.
9. **Analytical models of fluxonium qubits coupled to resonators**
   Longxiang Huang, Technical University of Munich, since October 2023.

10. **Fabrication of impedance-matched parametric amplifiers**
    Diego Contreras, Technical University of Munich, since October 2023.
11. **Magnetic topological insulators**
    Aeneas Leingärtner-Goth, Technical University of Munich, since October 2023.
12. **Semiclassical simulations of dissipative spin systems**
    Aristo Kevin Ardyaneira P, Technical University of Munich, since November 2023.
13. **Improving the signal to noise ratio of multiplexed qubit readout**
    Benedikt Lezius, Technical University of Munich, since November 2023.
14. **Software Communication Interfaces in Superconducting Quantum Computational Environments**
    Teodor Mihaescu, Technical University of Munich, since December 2023.

Research Projects

A large number of our research projects are benefiting from the collaboration with other research institutions and industry in coordinated research projects, as well as from individual collaborations, exchange programs and visitors. Most collaborations are based on joint projects, which are funded by different funding agencies (see list below). A considerable number of collaborations also exists with universities, other research institutions and industry without direct financial support.

A. German Research Foundation: Excellence Initiative & Strategy

Cluster of Excellence Munich Center for Quantum Science and Technology (MCQST)

The new Cluster of Excellence has been granted in September 2018 within Germany's Excellence Strategy and started in January 2019. Together with Immanuel Bloch of LMU Munich and Ignacio Cirac of Max Planck Institute of Quantum Optics, Rudolf Gross of Walther-Meißner-Institute is one of the three spokespersons of MCQST and coordinator of the Research Unit C on Quantum Computing.

1. Research Unit C: *Quantum Computing*
   Principal Investigators: F. Deppe, S. Filipp, R. Gross
   Contributing Researchers: K. Fedorov, A. Marx
2. Research Unit D: *Quantum Communication*
   Principal Investigators: F. Deppe, S. Filipp, R. Gross
   Contributing Researchers: K. Fedorov, A. Marx, N. Kukharchyk
3. Research Unit E: *Quantum Sensing*
   Principal Investigators: F. Deppe, H. Hübl, R. Gross
   Contributing Researchers: K. Fedorov, A. Marx, N. Kukharchyk
4. Research Unit F: *Quantum Matter*
   Principal Investigators: H. Hübl, R. Gross
   Contributing Researchers: M. Althammer, S. Geprägs, M. Opel

B. German Research Foundation: Collaborative Research Centers

Transregional Collaborative Research Center TRR 360: Constrained Quantum Matter

1. Project C3: *Dynamically Driven Quantum Correlations*
   Principal Investigators: H. Hübl, Ch. Pfleiderer, M. Wilde
   project period: 10/2023 – 09/2027

D. German Research Foundation: Research Projects

1. Project: *Shortcuts to Adiabaticity for Quantum Computation and Simulation (STAQS)*, within the QuantERA II ERA-NET Cofund in Quantum Technologies.
   A. Marx, with F. Deppe, K. Fedorov, R. Gross, (Az. DE 3444/1-1)
2. Project: *Evolution of the Charge Carrier Properties and Electronic Correlations in Layered Organic Metals near the Mott Metal-Insulator Transition*.
   M. Kartsovnik, R. Gross (Az. KA 1652/5-1 and GR 1132/19-1)

3. Project: *Multi-qubit Gates for the Efficient Exploration of Hilbert Space with Superconducting Qubit Systems*
   S. Filipp (Az. FI 2549/1-1)
4. Project: *Pure Spin Currents in Oxide-Based Epitaxial Heterostructures*
   M. Althammer, R. Gross (Az. AL 2110/12-1)
5. Project: *Waveguide QED with Interacting Photons*
   P. Rabl, (Az. RA 2138/2-1, Projektnummer: 522216022)

E. European Union

1. EU Collaborative Project (call identifier HORIZON-CL4-2021-Digital-Emerging-02), project title: *Exploring Non-classical States of Center-of-Mass Mechanical Motion with Superconducting Magneto- and Levitomechanics – SuperMeQ*
   H. Hübl, A. Marx, Grant Agreement No. 101080143
   project coordination: Chalmers University of Technology, partners: WMI/BAdW, OeAW, KIT, UAB.
   project period (planned): 10/2022 – 09/2026
2. EU Flagship Specific Grant Agreement (SGA) Project (call identifier HORIZON-CL4-2022-QUANTUM-01-SGA), project title: *Open Superconducting Quantum Computers - OpenSuperQPlus100*
   S. Filipp, H. Hübl, Grant Agreement No. 101113946.
   partners: several European Universities and research facilities.
   project period: (planned) 03/2023 – 09/2026
3. EU Flagship Framework Partnership Agreement (FPA) Project (call identifier HORIZON-CL4-2021-DIGITAL-EMERGING-02-15), project title: *Open Superconducting Quantum Computers - OpenSuperQPlus*
   S. Filipp, H. Hübl, Grant Agreement No. 101080139.
   partners: several European Universities and research facilities.
   project period: 03/2023 – 02/2027
4. EU Collaborative Project (call identifier H2020-FETOPEN-FET H2020-FETOPEN-2018-2020), project title: *Neuromorphic Quantum Computing - Quromorphic*
   S. Filipp, Grant Agreement No. 828826
   partners: several European Universities and research facilities.
   project period: 06/2019 – 02/2023
5. EU Innovative Training Network (call identifier H2020-MSCA-ITN-2020), project title: *MOlecular Quantum Simulations - MOQS*
   S. Filipp, Grant Agreement No. 955479
   partners: several European Universities and research facilities.
   project period: 11/2020 – 10/2024
6. EU MSCA Cofund Action (call identifier H2020-MSCA-COFUND-2018), project title: *Quantum Science and Technologies at the European Campus (QUSTEC)*
   S. Filipp, Grant Agreement 847471
   partners: several European Universities and research facilities.
   project period: 03/2019 – 07/2025
7. EU Collaborative Project (H2020-FETOPEN), project title: *Quantum Local Area Networks with Superconducting Qubits - SuperQuLAN*
   P. Rabl, Grant Agreement No. 899354
   partners: several European Universities and research facilities.
   project period: 09/2020 – 08/2023

F. Bundesministerium für Bildung, Wissenschaft, Forschung und Technologie

1. Project: *Skalierbare Einzelphotonendetektoren für Quantentechnologien (SEQT)*, project number: 13N16188
   project part: *Aufstockungsantrag*
   project coordinator: K. Müller (TUM)
   principal investigators of WMI/TUM: S. Filipp
   project partners: TUM
   project period: 09/2022 – 08/2023
2. Coordinated Project: *Munich Quantum Valley Quantum Computer Demonstrators - Superconducting Qubits (MUNIQC-SC)*, project number: 13N16188
   project part: *Systemoptimierung und -integration*
   project coordinator: S. Filipp (TUM/WMI)
   principal investigators of WMI: .....
   project partners: TUM, Fraunhofer-Gesellschaft, FAU Erlangen-Nürnberg, Infineon Technologies AG, IHP GmbH - Innovations for High Performance Microelectronics/Leibniz-Institut für innovative Mikroelektronik, IQM Germany GmbH, kiutra GmbH, Parity Quantum Computing Germany GmbH, Forschungszentrum Jülich GmbH, Zurich Instruments Germany GmbH.
   project period: 01/2022 – 12/2026
3. Coordinated Project: *Storage of Microwave Quantum Tokens in Electron and Nuclear Spin Ensembles (QuaMToMe)*, project number: 16KISQ036
   project coordinator: N. Kukharchyk (WMI)
   principal investigators of WMI: K. Fedorov, R. Gross, H. Huebl, N. Kukharchyk.
   project period: 11/2021 – 10/2024
4. Coordinated Project: *QUAntenRAdarTEam (QUARATE)*, project number: 13N15380,
   project part: *Superconducting Circuits and Quantum Microwaves for Quantum Radar*,
   project coordinator: Rohde & Schwarz GmbH & Co. KG,
   principal investigators of WMI: F. Deppe, K. Fedorov, S. Filipp, R. Gross, A. Marx),
   project partners: German Aerospace Center (DLR), Technical University of Munich
   project period: 02/2021 – 01/2024
5. Coordinated Project: *German Quantum Computer based on Superconducting Qubits (GeQCoS)*, project number: 13N15680
   project part: *Scaling and Demonstrator*,
   project coordinator: S. Filipp (WMI)
   principal investigators of WMI: F. Deppe, K. Fedorov, R. Gross, A. Marx
   project partners: Forschungszentrum Jülich GmbH, Karlsruher Institut für Technologie, Friedrich-Alexander-Universität Erlangen-Nürnberg, Fraunhofer Gesellschaft zur Forderung der angewandten Forschung e.V, Infineon Technologies AG.
   project period: 02/2021 – 01/2025

G. Free State of Bavaria

1. Munich Quantum Valley e.V. (MQV)
   program: Grundlagenorientierte Leuchtturmprojekte für Forschung, Entwicklung und Anwendungen im Bereich der Quantenwissenschaften und Quantentechnologien
   project part: Networked Quantum Systems (NeQuS)
   Principal Investigators at WMI: R. Gross, S. Filipp, K. Fedorov, A. Marx
   Jointly with research groups at the Technical University of Munich, the LMU Munich, and the Max Planck Institute of Quantum Optics.

project period: 01/2023–12/2025

2. Grundlagenorientierte Leuchtturmprojekte für Forschung, Entwicklung und Anwendungen im Bereich der Quantenwissenschaften und Quantentechnologien
   project part: Integrated Spin Systems for Quantum Sensors (IQSense)
   Principal Investigators at WMI: R. Gross, H. Hübl
   Jointly with research groups at the University of Würzburg and the Technical University of Munich.
   project period: 01/2023–12/2025
3. Munich Quantum Valley e.V. (MQV)
   project part: Quantum Technology Park and Entrepreneurship (QTPE)
   Principal Investigators at WMI: R. Gross (coordination), S. Filipp, K. Fedorov, A. Marx, H. Hübl, Ch. Trummer
   Jointly with research groups at the Technical University of Munich, the LMU Munich, the FAU Erlangen, the Max Planck Institute of Quantum Optics, and the Fraunhofer-Gesellschaft zur Förderung der angewandten Forschung e.V.
   project period: 10/2021–09/2026
4. Munich Quantum Valley e.V. (MQV)
   project part: Superconducting Qubit Quantum Computing (SQQC)
   Principal Investigators at WMI: S. Filipp (coordination), K. Fedorov, R. Gross, A. Marx, H. Hübl
   Jointly with research groups at the Technical University of Munich, the LMU Munich, the FAU Erlangen, the Max Planck Institute of Quantum Optics, and the Fraunhofer-Gesellschaft zur Förderung der angewandten Forschung e.V.
   project period: 10/2021–09/2026

H. Max Planck Society

1. International Max Plank Research School for *Quantum Science and Technology (IMPRS-QST)*, spokesperson: Prof. Dr. J. Ignacio Cirac,
   R. Gross, A. Marx, F. Deppe, K. Fedorov, S. Filipp
   with several partners from the Max Planck Institute of Quantum Optics, the Ludwig-Maximilians-Universität Munich and the Technical University of Munich.
   project period: 03/2016– 02/2028

I. Scientific Instrumentation

1. Heliumverflüssigungsanlage, Vorbuchner VL 100
   (R. Gross, DFG-GZ: INST 95/1637-1 LAGG)

Conferences, Workshops, Public Engagement

Every year, the Walther-Meißner-Institute organizes/co-organizes conferences, workshops, symposia, seminars, and other events. It also participates in several public outreach events aiming at making science accessible to the public.

In previous years, we were reporting in more depth on events, outreach activities, press releases, highlight publications, and other events in our Annual Report. However, meanwhile these topics are well covered by our new web pages and social media accounts. Therefore, we are no longer covering these topics here in depth and refer the interested reader to the news section of our web pages: https://www.wmi.badw.de/news and https://www.linkedin.com/company/49127991.

In the following, we list some highlight outreach activities and public engagement of WMI in the year 2023:

01.01.2023: Lighthouse projects NeQus and IQSense take up work. The Free State of Bavaria is funding five Lighthouse Projects as part of the Munich Quantum Valley e.V.. The WMI contributes to the 3-year projects Networked Quantum Systems (NeQuS) and Integrated Spin Systems for Quantum Sensors (IQSense), which both start in January 2023. In NeQuS, WMI will investigate new approaches to the networking of quantum systems jointly with colleagues from TUM, LMU and MPQ. The project IQSense will develop and demonstrate integrated quantum sensors for a range of application scenarios, including fast screening methods for biological matter. In this project, WMI joins forces with leading Bavarian groups from TUM, LMU, and the University of Würzburg.

08.01.-11.01.2023: WMI organized the 778th Heraeus Seminar on Coping with Errors in Scalable Quantum Computing Systems in Bad Honnef, Germany. Together with colleagues from IBM, Forschungszentrum Jülich, CEA Grenoble and Universität des Saarlandes, researchers from the WMI discussed recent improvements in gate fidelities, error detection and error mitigation technologies.

23.01.2023: WMI welcomed a group of curious high school students from the Rainer-Maria-Rilke Gymnasium Icking. Matthias Opel introduced the local pupils to superconductivity and ultra-low temperature physics. Experiments with liquid nitrogen showed the different properties materials exhibit when cooled down to these temperatures. Particularly spectacular was the demonstration of the Meißner effect of a levitating toy car on a magnetic track. Afterwards, the students had the chance to visit our quantum communication and thin film lab. Michael Renger and Matthias Althammer elaborated on the scientific background of their current research and provided insights into the state-of-the-art quantum communication and thin film technology.

29.03.2023: New students-train-students seminar on fabrication On 23 March, MCQST started its new seminar series on "Practical Top-Down Nanofabrication for Quantum Technologies" directly at the WMI. The seminar is organized by senior PhD students and is specifically designed to prepare Master and PhD students with the crucial skill set to fabricate state-of-the-art quantum devices. For this purpose, the seminar presents lessons on nanofabrication methods such as electron-beam lithography, reactive-ion etching, and thin-film deposition, as well as related topics such as cryogenics and fiber-to-chip coupling.

27.04.2023: Smoking heads, cool experiments: the MQV Dirls'Day. Ten female students aged 14 to 16 took part in Munich Quantum Valley's Girls'Day event. At the Walther Meissner Institute of the Bavarian Academy of Sciences and Humanities, they were able to learn about the profession of (quantum) scientists through a diverse program. Showing experiments with liquid nitrogen, WMI researchers demonstrated how various materials and gases behave at ultracold temperatures. They gave a guided tour of the laboratories, presenting the complex inner workings of cryostats up close, puffing helium pumps in the background. The girls could even hold tiny computer chips in their hand and discover the qubits on them.

12.06.2023: MCQST Award was granted to Andreas Wallraff. Each year, the Excellence Cluster MCQST awards up to two scientists with the MCQST Distinguished Lecturer Award. In 2023, the prize has been awarded to Andreas Wallraff of ETH Zurich during a public event in the Munich Künstlerhaus. "We are very pleased to acknowledge the outstanding scientific achievements of Andreas Wallraff in the field of quantum science and technology, as well as his long-term commitment to communicate his research field to a broader public", Rudolf Gross, WMI director and spokesperson of MCQST, points out when handing over the prize medal.

27.06.2023: Quantum Technologies: Politics & Governance. In a panel discussion on "Quantum Technologies: Politics & Governance" moderated by Ulrich Mans (Quantum Delta NL) within the World of QUANTUM 2023, Petra Wolff (BMBF, Referat 514, QComputing/QTechnologies), Heike Riehl (IBM Research), Marianne Schoerling (GESDA, Open Quantum Institute), and Rudolf Gross (WMI, MCQST, MQV) discussed strategies and measures to promote quantum sciences and technologies in Europe. In particular, they addressed the questions of the EU's position in the global quantum race and what type of European cooperation in QST is needed to achieve long-term technology leadership in Europe.

01.08.2023: Rudolf Gross becomes new MQV Scientific Director. On 1 August 2023, Rudolf Gross becomes Scientific Director of the Munich Quantum Valley (MQV) and Managing Director of the Munich Quantum Valley e.V. association. He takes over the tasks from Rainer Blatt, who hands over the baton to him after about two years. Rudolf Gross has been closely associated with MQV from the very beginning: Together with Immanuel Bloch, Ignacio Cirac, Klaus Blaum and Raoul Klingner, he authored the strategy paper that led to the foundation of MQV. Since 2021, he is member of MQV and coordinates the Quantum Technology Park & Entrepreneurship (QTPE) consortium. He is also PI within the two MQV lighthouse projects NeQuS and IQ-Sense.

29.08.-01.09.2023: Superconducting Qubits and Algorithms conference 2023. The Walther-Meißner-Institute organized this year's Superconducting Qubits and Algorithms (SQA) conference in Munich together with the Technical University of Munich, MQV, and the IQM GmbH. The SQA is Europe's largest conference focusing solely on quantum computing based on superconducting technologies. Over 400 participants came together at the Galileo conference venue in Garching and engaged in fruitful scientific exchange.

23.10.2023: Press Workshop on Quantum Technologies. The Walther-Meißner-Institute supported the press workshop on quantum technologies initiated by the TUM Vice President Global Communication Jeanne Rubner. Rudolf Gross introduced the vision and mission of the Munich Quantum Valley and gave some insights into the present status and potential applications of quantum technologies. The participants could also have a lab tour at WMI to get in direct touch with quantum technologies and the high-tech equipment required for the fabrication of solid-state-based quantum devices. Among the attendees, there have been representatives of CO2FILM, LABORPRAXIS, Konradsblatt, Webedia Deutschland, Redaktionsbüro Medizin/Wissenschaft, Sat1 Bayern, RTL, BR-Hörfunk, Mediengruppe Münchner Merkur tz, B2Bioworld, and the editorial staff of www.gesundheit.com. As a result of the press workshop, the **Münchener Merkur** published an article entitled "Ein Quantum Zukunft" on 25 October 2023, and there will be a focused issue in **TUMcampus** on quantum technologies in January 2024.

Cooperations

The Walther-Meißner-Institute is involved in many collaborations also without any direct project funding. In the following we list the most relevant collaboration partners:

- IBM Research - Zurich, Zurich, Switzerland, A. Fuhrer, D. Egger, G. Salis
- Green Innovation Research Laboratories, NEC Corporation, Japan, J.S. Tsai, K. Inomata, T. Yamamoto
- Forschungszentrum Jülich, Jülich , Germany, P. Bushev, F.K. Wilhelm-Mauch, D. DiVincenzo, G. Bishop, F. Wilhelm
- Fraunhofer Research Institution for Microsystems and Solid State Technologies EMFT, Munich, Germany, Ch. Kutter, K. Bauer
- Fraunhofer Institute for Applied Solid State Physics IAF, Munich, Germany, L. John, S. Chartier, R. Quay
- Fraunhofer Institute for Integrated Circuits IIS, Erlangen, Germany , T. Edelhäuser, T. Thönes, H. Adel
- University of Tokyo, Tokyo, Japan, Y. Nakamura
- ETH-Zurich, Zurich, Switzerland, A. Wallraff, L. Degiorgi, R. Monnier, Dr. M. Lavagnini, Y. Chu, C. Eichler
- Chalmers University of Technology Gothenburg, Sweden, J. Bylander, P. Delsing, G. Wendin, W. Wieczorek
- Instituto de Física Fundamental CSIC, Madrid, Spain, J.J. Garcia-Ripoll, A. Gonzales-Tudela
- University of Tohoku, Sendai, Japan, G.E.W. Bauer
- Kavli Institute for Theoretical Sciences, University of the Chinese Academy of Sciences, Bejing, China, G.E.W. Bauer
- European Synchrotron Radiation Facility, ESRF, Grenoble, France, F. Wilhelm, A. Rogalev
- Lund University , Lund, Sweden, D. Mannix
- Materials Science Research Centre, IIT Madras, India, M.S.R. Rao
- Institute of Solid State Physics, Chernogolovka, Russia, V. Zverev
- Russian Academy of Sciences, Chernogolovka, Russia, N. Kushch, E. Yagubskii
- High Magnetic Field Laboratory, Dresden, Germany, J. Wosnitza, T. Helm
- High-Magnetic-Field Laboratory, Grenoble, France, I. Sheikin, D. LeBoeuf
- Institut Néel, CNRS-UJF, Grenoble, France, M. Enderle, T. Ziman
- CNRS, Grenoble, France, Y. Joly
- Université Grenoble Alpes, CEA, CNRS, Grenoble, France, O. Klein
- European Synchrotron Radiation Facility (ESRF), Grenoble, France, F. Yakkhou-Harris, N. Brookes
- University of Vienna, Wien, Austria, M. Aspelmeyer, S. Rotter, M. Trupke
- Technical University of Vienna, Wien, Austria, A. Pustogow, S. Rotter, T. Pohl
- University of Innsbruck, Innsbruck, Austria, G. Kirchmair
- Kyoto University, Japan, M. Shiraishi
- IFIMAC and Departamento de Física Teórica de la Materia Condensada, Universidad Autónoma de Madrid, Spain, A. Kamra
- Universität Erlangen-Nürnberg, Erlangen, Germany, M. Hartmann, C. Eichler

- University of Wisconsin-Madison, USA, P. Evans
- University of Kent, Canterbury, UK, B. Tomasello
- Karlsruhe Institute of Technology, Karlsruhe, Germany, I. Pop, A. Ustinov, A. Metelmann
- RWTH Aachen, Aachen, Germany, S. Viola-Kusminskiy
- Martin-Luther-Universität Halle, Halle, Germany, G. Woltersdorf, G. Schmidt
- Center for Spinelectronic Materials and Devices, Universität Bielefeld, Bielefeld, Germany, T. Kuschel M. Meinert
- Aalto University, Aalto, Finland, M. Möttönnen, R. Di Candia
- Technical University of Munich, Physics Department, Munich, Germany, Ch. Back, Ch. Pfleiderer, M. Poot, F.C. Simmel, P. Müller-Buschbaum, A. Reiserer
- Technical University of Munich, Walter Schottky Institute, Munich, Germany, J. Finley, M. Stutzmann, M. Brandt, A. Holleitner
- Technical University of Munich, Electrical Engineering Department, Munich, Germany, M. Becherer, W. Utschick, E. Weig
- Technical University of Munich, Heinz Maier-Leibnitz Zentrum, Munich, Germany, J.M. Gomez, R. Dutta, A. Maity
- Technical University of Munich, Chair for Bioseparation Engineering, Munich, Germany, S. Berensmeier
- Technical University of Munich, Chair of Scientific Computing, Munich, Germany, M. Geiger, C. Mendl
- Technical University of Munich, Department of Chemistry, Munich, Germany, L. Van Damme, S. Glaser
- University of Konstanz, AG Quantenmaterialien, Konstanz, Germany, M. Müller
- Jülich Centre for Neutron Science JCNS, Jülich, Germany, S. Pütter
- Goethe University, Frankfurt, Germany, J. Müller, M. Lang
- Johannes-Gutenberg University, Institut für Physik, Mainz, Germany, O. Gomonay, L. Smejkal, J. Sinova, A. Mook
- Institut für Halbleiter- und Festkörperphysik, Johannes-Kepler-Universität Linz , Linz, Austria, A. Ney
- Université de Bourgogne, Bourgogne, France, D. Sugny
- University Stuttgart, Stuttgart, Germany, R. Kolesov
- University of Konstanz, Konstanz, Germany , S. T. B. Goennenwein, W. Belzig, U. Nowak
- The University of Melbourne, Melbourne, Australia, J. McCallum
- TU Delft, Delft, The Netherlands, S. Gröblacher
- Institute for Science and Technology Austria, Klosterneuburg, Austria, J. Fink
- Universidad Autonoma de Madrid, Madrid, Spain, J. Feist
- Universita di Trento, Trento, Italy, J. Carusotto
- Harvard University, Cambridge, USA, M. Loncar, M. Lukin
- Joint Quantum Institute, College Park, USA, M. Hafezi
- University of Palermo, Palermo, Italy, F. Ciccarello
- Weizmann Institute of Science, Rehovot, Isreal, A. Poddubny
- RTPU Kaiserslautern-Landau, Kaiserslautern, Germany, M. Weiler, P. Pirro
- Helmholtz Zentrum Dresden-Rossendorf, Institut für Ionenphysik, Dresden-Rossendorf, Germany, H. Schultheiss, K. Schultheiss

- Institute of Physics of the Czech academy of sciences, Prague, Czech Republic, H. Reichlova, D. Kriegner
- University of the Basque Country, Barrio Sarriena, Spain, Mikel Sanz
- VTT, Espoo, Finland, Joonas Govenius
- Parity QC GmbH, Innsbruck, Austria, P. Aumann, C. Ertler
- Infineon AG, Munich, Germany, F. Brandl, S. Luber
- Zurich Instruments, Zurich, Switzerland, C. Riek, C. Müller
- BMW Group, Munich, Germany, J. Klepsch, A. Luckow, W. Stadlbauer, G. Steinhoff, C. Riofrio
- Attocube, Munich, Germany (K. Karrai, D. Andres, E. Hoffmann)
- Kiutra, Munich, Germany (A. Regnat, F. Rucker)
- Parity Quantum Computing, Innsbruck, Austria (W. Lechner, M. Hauser)
- THEVA Dünnschichttechnik, Ismaning, Germany (W. Prusseit)
- Innovent Technologieentwicklung Jena, Germany (C. Dubs, O. Surzhenko)

Research Stays

Also in 2023, extended research stays of members of the Walther-Meißner-Institute at other national or international laboratories have been significantly reduced reminiscient of the Covid-19 pandemic.

1. **Shamil Erkenov**
   Laboratoire National des Champs Magnétiques Intenses, LNCMI-EMFL, Grenoble, France
   14.10. -23.10.2023
   Dresden High Magnetic Field Laboratory (HLD), Rossendorf, Germany
   10.11. - 18.11.2023 and 10.12. - 22.12.2023
2. **Stephan Geprägs**
   RIXS/REXS workshop, REMEI workshop, Sendai, Japan
   01.08. - 08.08.2023
3. **Mark Kartsovnik**
   Laboratoire National des Champs Magnétiques Intenses, LNCMI-EMFL, Grenoble, France
   14.10. - 23.10.2023
   Dresden High Magnetic Field Laboratory (HLD), Rossendorf, Germany
   11.10. - 18.11.2023
4. **Matthias Opel**
   National Institute for Materials Science (NIMS), Tsukuba, Japan
   22.05. - 24.05.2023

Conference Talks and Seminar Lectures

Joan Agustí

1. **Programmable distribution of multi-qubit entanglement in dual-rail waveguide QED**
   Invited talk, Conference Quantum Science Generation, Trento, Italy
   02. 05. 2023
2. **Programmable distribution of multi-qubit entanglement in dual-rail waveguide QED**
   Invited talk, WACQT Virtual Workshop on Quantum Technology, Chalmers University, Sweden
   27. 04. 2023

Matthias Althammer

1. **Evolution of the magnon Hanle effect**
   Invited talk, Magnetic Frontiers: Quantum Magnetism, Orlando, USA
   17. 04. - 23. 04. 2023
2. **Nonreciprocal Magnon Hanle Effect**
   SPICE-Workshop: Altermagnetism: Emerging Opportunities in a New Magnetic Phase, Ingelheim, Germany
   09. 05. - 11. 05. 2023
3. **All electrical magnon transport experiments in magnetically ordered insulators**
   SPICE and Spin+X Online Seminars, Virtual
   21. 06. 2023
4. **Observation of Nonreciprocal Magnon Hanle Effect**
   Invited talk, Joint European Magnetic Symposium 2023, Madrid, Spain
   27. 08. - 01. 09. 2023
5. **Chiral phonons and phononic birefringence in ferromagnetic metal - bulk acoustic resonator hybrids**
   Invited talk, Solid state physics seminar at the Universidad de Autonoma Madrid, Madrid, Spain
   05. 09. 2023
6. **Observation of the nonreciprocal magnon Hanle effect**
   Invited talk, Zernike group seminar, University of Groningen, Groningen, the Netherlands
   20. 09. 2023
7. **Polycrystalline Metallic Thin Films Coupled to Superconducting Microwave Resonators and Bulk Acoustic Resonators**
   Invited talk, Group seminar at the Helmholtz-Zentrum Dresden-Rossendorf, Dresden-Rossendorf, Germany
   30. 11. 2023
8. **Altermagnetism: Transport, Optics, Excitations**
   Organization of a Focus Session (together with S.T.B Goennenwein, A. Thomas) at the Spring Meeting of the Condensed Matter Section of the German Physical Society, Dresden, Germany
   26. 03. - 31. 03. 2023

Niklas Bruckmoser

1. **Improving Fabrication Methods for Superconducting Qubits**
   Contributed talk, Spring Meeting of the German Physical Society, Dresden, Germany
   26. 03. - 31. 03. 2023

Jianpeng Chen

1. **Quantum memory with rare-earth spin ensembles**
   Contributed talk, Industry advisory board meeting of QuaMToMe project, Garching, Germany
   10. 11. 2023

Shamil Erkenov

1. **Effect of anion substitution on the Mott insulating instability in the organic conductors κ-(BEDT-TTF)$_2$X studied by magnetic quantum oscillations**

Contributed talk, Spring Meeting of the German Physical Society, Dresden, Germany
26. 03. - 31. 03. 2023

Kirill Fedorov

1. **Microwave quantum networks**
   Contributed talk, Munich Conference on Quantum Science and Technology (MCQST2023)
   20. 06 - 23. 06. 2023
2. **Microwave quantum sensing**
   Colloquium talk, MCQST Colloquium, Munich, Germany
   05.12.2023

Noelia Fernandez

1. **From graphene research to superconducting qubits**
   Alumni talk, IMPRS-QST Summer School 2023 / MCQST conference
   19. 06 - 23. 06. 2023

Florian Fesquet

1. **Demonstration of microwave single-shot quantum key distribution**
   In-person Talk, MCQST Colloquium with Tracy Northup
   21. 11. 2023

Stefan Filipp

1. **Parametric interactions between superconducting qubits for versatile quantum operations**
   Invited talk, Symposium on Quantum Computing with Superconducting Qubits
   06.12.2023
2. **Controlling superconducting qubits for quantum computing**
   Invited Talk, Quantum Technologies Symposium of the VIII Leopoldo García-Colín Meeting
   23. 10.2023
3. **Scalable quantum computing platforms with focus on superconducting qubits**
   Invited Talk, World of Quantum 2023, Munich, Germany
   29. 06. 2023
4. **High-coherence superconducting qubits for enhanced quantum gate operations**
   Invited Talk, 5th MCQST Conference
   21. 06. 2023
5. **Beyond standard control of superconducting qubits**
   Invited Talk, WACQT virtual workshop on quantum technology
   26. 04. 2023
6. **Optimized control of superconducting qubits**
   Invited Talk, APS March Meeting, Las Vegas, USA
   08. 03. 2023
7. **A quantum perceptron based on superconducting qubits**
   Invited Talk, Quromorphic Winter Workshop
   15. 02. 2023
8. **Quantum computing with superconducting qubits**
   Invited Talk, Lüscher-Wassermann Seminar – Symposium Quantum Technology
   04. 02. 2023
9. **Efficient Characterization and Control of Quantum Systems**
   Invited Talk, IQM Business Club
   23. 11. 2023
10. **Quantencomputing – Unlösbare Probleme lösbar machen**
    Dinner Talk, Dinner organized by AdvantageAustria
    18. 10. 2023
11. **High-coherence superconducting qubits for enhanced quantum gate operations**
    Colloquium Talk, Physics Colloquium Karlsruhe
    14. 06. 2023

12. **Quantum Computing - efficiently solving hard computational problems**
    Invited Talk, Hannover Re – Science Talks
    16. 05. 2023
13. **Quantencomputer verstehen – Eine Einführung für Laien**
    Invited Talk, TUM Medienseminar
    16. 03. 2023

Stephan Geprägs

1. **Rare-earth iron garnets: A prototype material system for spintronics and magnonics**
   Invited Talk, REMEI workshop, Sendai, Japan
   07. 08. - 08. 08. 2023
2. **Control of magnetic properties in iridate thin films by variation of strain and thin film thickness**
   Contributed Talk, RIXS/REXS workshop, Sendai, Japan
   02. 08. - 04. 08. 2023

Maria-Teresa Handschuh

1. **Large-scale fabrication of Josephson parametric devices**
   Contributed Talk, Kryoelektronische Bauelemente (KRYO 2023), Bad Boll, Germany
   24. 09 - 26. 09. 2023

Kedar Honasoge

1. **Fabrication of low-loss Josephson junction based parametric circuits**
   Contributed Talk, APS March Meeting 2023, Las Vegas, USA
   05. 03 - 10. 03. 2023
2. **Fabrication of low-loss Josephson junction based parametric circuits**
   Contributed Talk, Spring Meeting of the German Physical Society, Dresden, Germany
   26. 03. - 31. 03. 2023

Gerhard Huber

1. **Using ANSYS for the simulation and design of superconducting qubit chips**
   Invited Talk, LRZ Ansys Day
   26. 04. 2023
2. **Coupler-mediated unconditional reset of fixed-frequency superconducting qubits**
   Contributed Talk, APS March Meeting, Las Vegas, USA
   08. 03. 2023

Hans Hübl

1. **Spin-based hybrid systems**
   Online talk, Institutsseminar, Universität Halle Wittenberg
   02. 07. 2023
2. **Let the phonons roll - phonons in bulk acoustic resonators**
   Institute Seminar Masashi Shiraishi, Kyoto University, Kyoto, Japan
   27. 10. 2023
3. **Sensing with quantum hybrid systems**
   RIKEN – Tokyo Institute Seminar Yasunobo Nakamura, Tokyo, Japan
   31. 10. 2023
4. **Hybrid Quantum Systems**
   IQOQI – Seminar Obergurgl – Kirchmair group, Austria
   19. 02. - 21. 02. 2023
5. **Hybrid Quantum Systems Probing Solid-State Excitations**
   Universität Regensburg, Regensburg, Germany
   20. 11. 2023
6. **Sensing with quantum hybrid systems**
   Invited talk, SPIE – Conference, San Diego, USA
   20. 8 – 24. 8. 2023

7. **Hybrid Quantum Systems**
   Lüscher-Wassermann Seminar, Klosters
   04. 02 – 10. 02. 2023
8. **Magnon-mechanics in high-overtone acoustic resonators**
   DPG – Spring Meeting, Dresden
   29. - 31. 03. 2023
9. **Let the phonons roll - phonons in bulk acoustic resonators**
   Spins Waves and Interactions – Workshop Greifswald
   28. - 30. 08. 2023
10. **Strong light-matter coupling in the microwave regime**
    TRR360 – Kick off meeting, Kloster Irrsee
    09. - 10. 10. 2023

Mark Kartsovnik

1. **Evolution of Charge Carriers near the Mott Transition: Theory vs. Experiment in κ-(BEDT-TTF)$_2$X**
   Contributed talk, International Conference on Superconductivity and Magnetism, ICSM2023, Fethiye –Oludeniz, Turkey
   04. 05 – 11. 05. 2023

Fabian Kronowetter

1. **A journey into quantum illumination**
   Invited talk, World of Quantum 2023, Munich, Germany
   28. 06. 2023
2. **Quantum microwave parametric interferometer**
   Contributed Talk, APS March Meeting 2023, Las Vegas, USA
   06. - 10. 03. 2023
3. **Quantum microwave parametric interferometer**
   Talk, Munich conference on Quantum Science and Technology 2023, Sonthofen, Germany
   20. - 23. 06. 2023

Nadezhda Kukharchyk

1. **Addressing the rare-earth spin ensembles with propagating microwaves**
   Invited talk, Grete Hermann Network Workshop, Würzburg, Germany
   31. 07 - 02. 08. 2023
2. **Broadband microwave spectroscopy of rare–earth spin ensembles**
   Contributed Talk, Workshop on Rare Earth Ion Doped Crystals for Quantum Information, Lund, Sweden 27 Sept – 29 Sept 2023
   27. 09. - 29. 09. 2023
3. **QuaMToMe : microwave quantum tokens**
   Invited talk, Q.TOK Workshop, Berlin, Germany
   08. 05. 2023
4. **QuaMToMe : microwave quantum tokens**
   Invited talk, QR.X-Statusseminar, Bad Honnef, Germany
   15. 06 – 16. 06. 2023

Thomas Luschmann

1. **Mechanical frequency control in inductively coupled electromechanical systems**
   Contributed talk, APS March Meeting 2023, Las Vegas, Nevada, USA
   05. 03 - 10. 03. 2023
2. **Surface acoustic wave resonators on thin film piezoelectric substrates in the quantum regime**
   Sektion Kondensierte Materie der DPG-Frühjahrstagung, Dresden
   26. 03 – 31. 03. 2023

Georg Mair

1. **Fabrication of a superconducting transmission line in a planar design on a spin-doped crystalline membrane**
   Contributed talk, Spring Meeting of the German Physical Society, Dresden, Germany
   26.03. - 31.03.2023
2. **Quantum memory with rare-earth spin ensembles**
   Contributed Talk, Industry advisory board meeting of QuaMToMe project, Garching, Germany
   10. 11. 2023

Manuel Müller

1. **Magnon transport in $Y_3Fe_5O_{12}$/Pt nanostructures with reduced effective magnetization**
   Contributed talk, Spin waves and interactions Workshop in Greifswald, Germany
   28. 08 - 30. 08. 2023
2. **Magnon-phonon coupling in polycrystalline metallic thin films**
   Contributed talk, Spring Meeting of the German Physical Society, Dresden, Germany
   26. 03. - 31. 03. 2023

Patricia Oehrl

1. **Quantum state storage in spin ensembles**
   Munich Conference on Quantum Science and Technology, Sonthofen, Germany
   20. 06. 2023
2. **Quantum state storage in spin ensembles**
   Contributed talk, Spring Meeting of the German Physical Society, Dresden, Germany
   26. 03. - 31. 03. 2023
3. **Pulsed electron spin resonance protocols for storing microwave quantum states**
   Silicon Quantum Electronics Workshop, Kyoto, Japan
   01. 11. 2023

Matthias Opel

1. **Tiefe Temperaturen, Supraleitung und Spinelektronik**
   Invited talk, MINT-Berufsinformationstag im Rahmen der "Humboldt Academy of Science and Engineering" (HASE), Humboldt-Gymnasium Vaterstetten, Germany
   17. 02. 2023
2. **Observation of nonreciprocal magnon Hanle effect**
   Contributed talk, Spring Meeting of the German Physical Society, Dresden, Germany
   26. 03. - 31. 03. 2023
3. **Diffusive Transport of Antiferromagnetic Magnons in α-Fe_2O_3**
   Invited talk, 7th International Conference on Nanoscience and Nanotechnology (ICONN-2023, virtual), Chennai, India
   29. 03. 2023
4. **Spin-Hall Magnetoresistance (SMR) in Magnetic Oxide Insulators**
   Invited talk, Seminar of the High Magnetic Field Laboratory, Helmholtz-Zentrum Dresden-Rossendorf (HZDR), Germany
   04. 04. 2023
5. **Nonreciprocal Magnon Hanle Effect in Antiferromagnetic α-Fe_2O_3**
   IEEE International Magnetic Conference (Intermag 2023), Sendai, Japan
   15. 05. 2023

Peter Rabl

1. **Asymmetric Bosonic Transport**
   Seminar talk, Max-Planck Institute for Quantum Optics, Garching, Germany
   01. 03. 2023
2. **Continuous/discrete variable quantum networks**
   Contributed talk, NeQuS Kickoff Meeting, Garching, Germany
   22. 03. 2023

3. **High-fidelity quantum information processing with spins & phonons**
Invited talk, Spring Meeting of the German Physical Society, Dresden, Germany
26. 03. - 31. 03. 2023
4. **Stochastic Simulations of Dissipative Spin Systems**
Invited talk, SPICE "Quantum Spinoptics" Workshop, Ingelheim, Germany
14. 06. 2023
5. **Programmable multi-qubit entanglement in hybrid quantum networks**
Invited talk, MCQST conference, Sonthofen, Germany
23. 06. 2023
6. **Non-perturbative (cavity) QED**
Seminar talk, Colloquium, University of Konstanz, Germany
18. 07. 2023
7. **Phase transitions and universal scaling in bosonic transport**
Invited talk, WE-Heraeus-Seminar, Bad Honnef, Germany
07. 09. 2023
8. **Dissipative bosonic transport**
Invited talk, CALI workshop, Crete, Greece,
04. 10. 2023
9. **Effective models, ground states and the coupling strength in cavity QED**
Invited talk, Int. Conference on Quantum Vacuum in Matter, Rice University, Houston, USA
12. 10. 2023
10. **Dissipative Bosonic Transport**
Seminar talk (online), University of Bari, Italy
05.12.2023
11. **Dissipative Bosonic Transport**
Seminar talk, Physics Colloquium, University of Augsburg, Germany
18. 12. 2023

Frederik Pfeiffer

1. **Purcell protection and crosstalk reduction using multimode superconducting circuits**
Contributed Talk, APS March Meeting 2023, Las Vegas, USA
05. 03 - 10. 03. 2023

Federico Roy

1. **Implementation of Fractional State Transfer on a Superconducting Qubit Chain**
Contributed Talk, APS March Meeting 2023, Las Vegas, USA
05. 03 - 10. 03. 2023

Ana Strinic

1. **Broadband electron spin resonance spectroscopy of rare earth spin ensembles at mK temperatures**
Contributed Talk, Spring Meeting of the German Physical Society, Dresden, Germany
26. 03. - 31. 03. 2023

Christian Schneider

1. **Superconducting Quantum Magnetomechanics**
Contributed Talk, Spring Meeting of the German Physical Society, SAMOP23, Dresden, Germany
26. 03. - 31. 03. 2023

Max Werninghaus

1. **Experimental optimal control of superconducting qubits**
Invited colloquium, LRZ internal colloquium
20. 06. 2023
2. **Experimental optimal control of superconducting qubits**
Invited talk, Superconducting Quantum Computing Workshop, Bilbao, Spain
02. 06. 2023

3. **Control of Superconducting Qubits**
Invited colloquium, Computer Science department, internal colloquium, TUM, Garching, Germany
20. 02. 2023
4. **Black box optimization of computational gates for superconducting qubits**
Invited talk, WE-Heraeus-Seminar, Bad Honnef, Germany
08. 01. - 11. 01. 2023
5. **Einfhrungsvorlesung Quantum Hardware**
Vorlesung, MCQST Summer School, Munich, Germany
03. 08. 2023

Honors and Awards

A. Wun Kwan Yam Receives the MCQST Master's Award

The excellence cluster MCQST annually honors two outstanding Master's theses (theory and experiment) from the MCQST community with the **Master's Award**. The prize highlights and recognizes outstanding master research projects, and it aims to encourage awardees to continue pursuing a further career in science. MCQST considers outstanding theses evaluated with a grade of 1.0 that demonstrate original thought, a unique approach to the chosen topic or field of study, significant personal contribution, and creativity. Only theses from students enrolled in the **Master Course in Quantum Science and Technology**, jointly offered by TUM and LMU, are considered.

In 2023, **Wun Kwan Yam** received the MCQST Master's Award for his Master Thesis entitled **«Microwave Quantum Teleportation Over a Thermal Channel»** which he did at Walther-Meißner-Institute under the supervision of Kirill Fedorov and Rudolf Gross. The award was handed over at the Munich Conference on Quantum Science and Technology 2023 by MCQST spokesperson Rudolf Gross.

The award came with a small prize money kindly donated by **Zurich Instruments AG**. We heartily congratulate Wan Kwan Yam and wish him the same success for his ongoing Ph.D. thesis at WMI.

Membership in Advisory Boards, Committees, etc.

1. **Frank Deppe** is Coordinator of the European Quantum Technology Flagship Project *Quantum Microwaves for Communication and Sensing (QMiCS)*.
2. **Frank Deppe** is a member and principal investigator of the Cluster of Excellence *Munich Center for Quantum Science and Technology (MCQST)*.
3. **Stefan Filipp** is coordinator of the *Munich Quantum Valley (MQV)* consortium *K1 - Superconducting Qubit Quantum Computing*.
4. **Stefan Filipp** is coordinator of the *Munich Quantum Valley Quantumcomputer Demonstrators – Superconducting Qubits* (MUNIQC-SC) project funded by the Federal Ministry of Education and Research (BMBF).
5. **Stefan Filipp** is advisory board member of the *International AIQT Foundation*.
6. **Stefan Filipp** is member of the scientific advisory board of the EU FET Open project *AVAQUS - Annealing based Variational Quantum Processors*.
7. **Stefan Filipp** is member of the executive board of the *Wallenberg Center for Quantum Technology*.
8. **Stefan Filipp** is editorial board member of the IOP multidisciplinary journal *Materials for Quantum Technology*.
9. **Stefan Filipp** is member and principal investigator of the Cluster of Excellence *Munich Center for Quantum Science and Technology (MCQST)*.
10. **Stefan Filipp** is adjoint Member of the Special Research Fund (SFB) *BeyondC* funded by the Austrian Science Fund (FWF).
11. **Stefan Filipp** is member of the *Munich Quantum Center (MQC)*.
12. **Rudolf Gross** is spokesperson (together with Immanuel Bloch and Ignacio Cirac) of the Cluster of Excellence *Munich Center for Quantum Science and Technology (MCQST)* and coordinator of the Research Unit C on *Quantum Computing*.
13. **Rudolf Gross** is initiator and Principal Investigator of *Munich Quantum Valley (MQV)*.
14. **Rudolf Gross** is Scientific Director *Munich Quantum Valley (MQV)* Managing Director of the MQV Association.
15. **Rudolf Gross** is a member of the *Deutsche Akademie der Technikwissenschaften e.V. (acatech)*.
16. **Rudolf Gross** is a member of the *Forum Technologie* of the Bavarian Academy of Sciences and Humanities.
17. **Rudolf Gross** is Co-organizer of the annual *Munich Conference on Quantum Science & Technology*.
18. **Rudolf Gross** is a member of the Advisory Board of the permanent exhibition on *Matter and Light* of the German Science Museum.
19. **Rudolf Gross** is a member of the *Committee for the allocation of Alexander von Humboldt Foundation Research Awards*.
20. **Rudolf Gross** is a member of the *Appointment and Tenure Board* of the Technical Univer-

sity of Munich.

21. **Rudolf Gross** is a member of the *Munich Quantum Center (MQC)*.

22. **Rudolf Gross** is a member of the *Scientific Advisory Board of the Bavarian Research Institute of Experimental Geochemistry and Geophysics (BGI)*, Bayreuth, Germany.

23. **Rudolf Gross** is a member of the *Scientific Advisory Board of the Institut de Ciència de Materials de Barcelona*, Spain.

24. **Hans Hübl** is member and principal investigator of the Cluster of Excellence *Munich Center for Quantum Science and Technology (MCQST)*.

25. **Mark Kartsovnik** is member of the *Selection Committee of EMFL* (European Magnetic Field Laboratories).

26. **Mark Kartsovnik** is member of the *International Advisory Committee of the International Symposium on Crystalline Organic Metals Superconductors and Ferromagnets (ISCOM)*.

27. **Matthias Opel** is one of the four elected members of the *Speaker Council* for the scientists of the Bavarian Academy of Sciences and Humanities.

Teaching

Lectures, Courses and other Teaching Activities

Several members of the Walther-Meißner-Institute give lectures and seminars at the Technical University of Munich.

WS 2022/2023

- WMI Seminar on Current Topics of Low Temperature Solid State Physics (M. Althammer, F. Deppe, K. Fedorov, S. Filipp, R. Gross, S. Geprägs, H. Huebl, N. Kukharchyk, A. Marx, M. Opel)
- Seminar: Spin Currents and Skyrmionics (M. Althammer, H. Huebl, M. Opel, S. Geprägs)
- Seminar: Current Topics in Magneto and Spin Electronics (M. Althammer, M. S. Brandt, H. Huebl, M. Weiler)
- Seminar: Advances in Solid-State Physics (R. Gross with M. Althammer, S. Geprägs, H. Huebl, M. Kartsovnik, A. Marx, N. Kukharchyk, M. Opel)
- Seminar: Superconducting Quantum Circuits (F. Deppe, S. Filipp, R. Gross, A. Marx, K. Fedorov)
- Seminar: Journal Club on Quantum Systems (S. Filipp)
- Lecture: Superconductivity and Low Temperature Physics 1 (R. Gross)
- Problem Session: Superconductivity and Low Temperature Physics I (R. Gross with N.N.)
- Lecture: QST Experiment: Quantum Hardware (S. Filipp)
- Problem Session: QST Experiment: Quantum Hardware (S. Filipp with F. Haslbeck)
- Lecture: Applied Superconductivity 1: from Josephson Effects to RSFQ Logic (K. Fedorov)
- Problem Session: Applied Superconductivity 1: from Josephson Effects to RSFQ Logic (K. Fedorov)
- Lecture: Magnetism (N. Kukharchyk)
- Problem Session: Magnetism (N. Kukharchyk with K. Rubenbauer)
- Lecture: Quantensensorik (M. Brandt, D. Bucher, H.Hübl)
- Colloquium on Solid-State Physics, R. Gross with H. Huebl, M. Opel

SS 2023

- WMI Seminar on Current Topics of Low Temperature Physics (M. Althammer, F. Deppe, K. Fedorov, S. Filipp, R. Gross, S. Geprägs, H. Huebl, N. Kukharchyk, A. Marx, M. Opel, P. Rabl)
- Seminar: Spin Currents and Skyrmionics (M. Althammer, with H. Huebl, M. Opel, S. Geprägs, M. Weiler)
- Seminar: Current Topics in Magneto and Spin Electronics (M. Althammer, M. S. Brandt, S. Geprägs, H. Huebl)
- Seminar: Advances in Solid State Physics (R. Gross with M. Althammer, S. Geprägs, H. Huebl, M. Kartsovnik, A. Marx, N. Kukharchyk, M. Opel)
- Seminar: Superconducting Quantum Circuits (F. Deppe, S. Filipp, R. Gross, A. Marx, K. Fedorov)
- Seminar: Journal Club on Quantum Systems (S. Filipp)
- Lecture: Superconductivity and Low Temperature Physics 2 (R. Gross)
- Problem Session: Superconductivity and Low Temperature Physics 2 (R. Gross with N.N.)
- Lecture: Applied Superconductivity 2: from superconducting circuits to microwave quantum optics (K. Fedorov)
- Problem Session: Exercise to Applied Superconductivity 2: from superconducting circuits to microwave quantum optics (K. Fedorov)
- Lecture: Quantum Computing with Superconducting Qubits (S. Filipp)
- Problem Session: Quantum Computing with Superconducting Qubits (S. Filipp)

- Lecture: Spintronics (N. Kukharchyk)
- Problem Session: Spintronics (N. Kukharchyk with K. Rubenbauer)
- Lecture: Theoretical Quantum Optics (P. Rabl)
- Problem Session: Theoretical Quantum Optics (P. Rabl)
- Seminar: Quantum Optics Theory Seminar (P. Rabl)
- Colloquium on Solid-State Physics, R. Gross with H. Huebl, M. Opel

WS 2023/2024

- WMI Seminar on Current Topics of Low Temperature Solid State Physics (M. Althammer, F. Deppe, K. Fedorov, S. Filipp, R. Gross, S. Geprägs, H. Huebl, N. Kukharchyk, A. Marx, M. Opel, P. Rabl)
- Seminar: Spin Currents and Skyrmionics (M. Althammer, S. Geprägs, H. Hübl, M. Opel)
- Seminar: Novel Topics in Magnetism: quantum hybrid systems, spin dynamics, and angular momentum transport (M. Althammer, H. Huebl, N. Kukharchyk, M. Opel, S. Geprägs)
- Seminar: Advances in Solid-State Physics (R. Gross with M. Althammer, S. Geprägs, H. Huebl, M. Kartsovnik, A. Marx, N. Kukharchyk, M. Opel)
- Seminar: Quantum Science and Technology in Solids: spins, microwaves, and optomechanics (M. Althammer, M. S. Brandt, H. Huebl, S. Geprägs)
- Seminar: Journal Club on Quantum Systems (S. Filipp, C. Schneider)
- Seminar: Superconducting Quantum Circuits (S. Filipp, R. Gross, M. Werninghaus)
- Lecture: Superconductivity and Low Temperature Physics 1 (R. Gross)
- Problem Session: Superconductivity and Low Temperature Physics 1 (R. Gross with N.N.)
- Lecture: QST Experiment: Quantum Hardware (S. Filipp)
- Problem Session: QST Experiment: Quantum Hardware (S. Filipp with G. Krylov)
- Lecture: Applied Superconductivity 1: from Josephson Effects to RSFQ Logic (K. Fedorov)
- Problem Session: Applied Superconductivity 1: from Josephson Effects to RSFQ Logic (K. Fedorov)
- Lecture: Quantensensorik (H. Hübl with M. Brandt, D. Bucher)
- Lecture: Magnetism (M. Althammer)
- Problem Session: Magnetism (M. Althammer with K. Rubenbauer)
- Colloquium on Solid-State Physics, R. Gross with H. Huebl, M. Opel
- Lecture: Theory of Open Quantum Systems (P. Rabl)
- Problem Session: Exercise to Theory of Open Quantum Systems (P. Rabl)
- Seminar: Cavity-, Waveguide- and Circuit QED (P. Rabl)
- Seminar: WMI Theory Seminar (P. Rabl)

Seminars and Colloquia

A. Walther-Meißner-Seminar on Modern Topics in Low Temperature Physics

WS 2022/2023:

1. **InGaAs Nanowire and Quantum Well Devices**
Lasse Södergren, Lund University, Department of Electrical and Information Technology, Lund, Sweden
14.11.2022
2. **Boring phases with interesting features: Helitronic pumps and transport by fluctuations**
Dr. Jan Masell, Institute of Theoretical Solid State Physics (TFP), Karlsruhe Institute of Technology (KIT), Germany
25.11.2022
3. **Tailored High Temperature Superconductors for Power- and Magnet Applications**
Prof. Dr. Bernhard Holzapfel, Karlsruher Institut für Technologie, Institut für Technische Physik (ITEP), Germany
02.12.2022
4. **Two-qubit gates on fluxoniums and transmons**
Ilya Moskalenko, Russian Quantum Center, 143025 Skolkovo, Moscow, Russia
05.12.2022
5. **Dynamics of Transmon Ionization**
Prof. Alexandru Petrescu, Centre Automatique et Systèmes, Ecole des Mines de Paris, France
09.12.2022
6. **THz time-domain spectroscopy of Dirac- and topological materials as well as corresponding circulator geometries**
Johannes Gröbmeyer, Sergey Lavrentyev, and Alexander, Walter Schottky Institute and Physics Department, Technical University of Munich, Germany
16.12.2022
7. **Evaluating the performance of sigmoid quantum perceptrons in quantum neural networks**
Samuel Wilkinson, Friedrich-Alexander-Universität Erlangen-Nürnberg, Institute for Theoretical Physics II, Erlangen, Germany
13.01.2023
8. **Towards a graphene-based superconducting qubit**
Nataliia Zhurbina, Faculty of Science, Université Grenoble Alpes (UGA), 230 rue de la physique, 38400 Saint-Martin-d'Hères, France
24.02.2023
9. **Superconducting flux circuits for quantum annealing: crosstalk calibration and understanding the role of environment**
Xi Dai, University of Waterloo, Canada
24.03.2023
10. **Understanding critical metrology**
Dr. Karol Gietka, Institut für Theoretische Physik, Universität Innsbruck, Innrain 52, 6020 Innsbruck, Austria
31.03.2023

SS 2023:

11. **Towards novel qubits**
Dr. Christian Jünger, Advanced Quantum Testbed, Lawrence Berkeley National Laboratory University of California, USA
21.04.2023
12. **Quantum computing in the presence of errors**
Prof. Dr. Ignacio Cirac, Max Planck Institute for Quantum Optics Garching, Germany
28.04.2023

13. **Application of Quantum Optimal Control to Quantum Technologies**
Prof. Dominique Sugny, Laboratoire Interdisciplinaire Carnot de Bourgogne, Universiteé de Bourgogne, France
26.05.2023
14. **Strong down-conversion regime of cavity/circuit QED**
Prof. Dr. Vladimir Manucharyan, Superconductor Quantum Information Laboratory, EPFL, CH-1015 Lausanne, Switzerland
02.06.2023
15. **Electronic excitations in Josephson weak links for quantum computation**
Lukyi Cheung, Department of Physics, University of Basel, Switzerland
06.06.2023
16. **Quadratic and cubic magneto-optic Kerr effect in magnetic thin films**
Dr. Timo Kuschel, Faculty of Physics, Bielefeld University, Bielefeld, Germany
16.06.2023
17. **Topology in Quasiperiodically Driven Systems**
Dr. David Long, The Department of Physics, Boston University, 590 Commonwealth Avenue, Boston, MA 02215, USA
30.06.2023
18. **Towards Functional Quantum Technologies: The Role of Quantum Control**
Prof. Hugo Ribeiro, Department of Physics and Applied Physics, University of Massachusetts Lowell, Lowell, MA 01854, USA
28.07.2023
19. **Chiral (Directional) Photon Emission and High-Fidelity Two-Qubit Gates with Superconducting Qubits**
Prof. William D. Oliver, Department of Electrical Engineering and Computer Science & Department of Physics, Massachusetts Institute of Technology, Cambridge, MA 02139, USA
28.08.2023
20. **Anisotropic Melting of Frustrated Ising Antiferromagnets**
Dr. Makariy A. Tanatar, Ames National Laboratory, Iowa State University, Ames, Iowa, USA
18.09.2023
21. **Pulse-VQE and leakage in restless measurements**
Dr. Daniel Egger, IBM Research - Zurich, Rueschlikon, Switzerland
05.10.2023

WS 2023/2024:

22. **Quantum criticality of the frustrated transverse-field Ising model on a triangular bilayer using directly evaluated enhanced perturbative continuous unitary transformations**
Lukas Schamriss, Department of Physics, Chair of Theoretical Physics II, FAU Erlangen, Germany
19.10.2023
23. **Effective Negative Mass and Frequency Down-Conversion in Two-Tone Optomechanics**
Nikolaj Aagaard Larsen, Niels Bohr Institute, University of Copenhagen, Jagtvej 155 A, 2200 Copenhagen N., Denmark
20.110.2023
24. **Mesoscopic Non-Hermitian Skin Effect**
Alexander Poddubny, Weizmann Institute of Science, Israel
10.11.2023
25. **2D spin-orbit coupled frustrated magnets**
Vera Bader, University of Augsburg, Germany
22.11.2023
26. **Interfacing with Quantum Information Processors—From Readout to Control**
Benjamin Lienhard, Princeton University, USA
14.12.2023
27. **Tolopogical Spintronics/Orbitronics**
Masashi Shiraishi, Kyoto University, Japan

15.12.2023

B. Topical Seminar on Advances in Solid State Physics

WS 2022/2023:

1. **Preliminary discussion and assignment of topics**
R. Gross, Walther-Meißner-Institute (E23), Technical University of Munich and BAdW
18. 10. 2022 and 25. 10. 2022
2. **Mott-Driven BEC-BCS Crossover in a Doped Spin Liquid Candidate**
Aeneas Leingärtner-Goth, Technical University of Munich
13. 12. 2022
3. **Josephson diode effect from Cooper pair momentum in a topological semimetal**
Tim Bohnen, Technical University of Munich
20. 12. 2022
4. **Emission of Photon Multiplets by a dc-Biased Superconducting Circuit**
Rubek Poudel, Technical University of Munich
10. 01. 2023

SS 2023:

5. **Preliminary discussion and assignment of topics**
R. Gross, Walther-Meißner-Institute (E23), Technical University of Munich and BAdW
18. 04. 2023 and 25. 04. 2023
6. **Electric field–dependent phonon spectrum and heat conduction in ferroelectrics**
Axcel Ordinola, Technical University of Munich
23.05.2023
7. **Giant magnetoresistance of Dirac plasma in high-mobility graphene**
Ivan Volkau, Technical University of Munich
06.06.2023
8. **Topological kagome magnets and superconductors**
Luca Schmidt, Technical University of Munich
20.06.2023
9. **Real-time quantum error correction beyond break-even**
Michael Schmidlechner, Technical University of Munich
27.06.2023
10. **Evidence for spin swapping in an antiferromagnet**
Chongwen Yin, Technical University of Munich
04.07.2023
11. **Superconducting-qubit readout via low-backaction electro-optic transduction**
Andreas Dunaev, Technical University of Munich
11.07.2023

WS 2023/2024:

12. **Preliminary discussion and assignment of topics**
R. Gross, Walther-Meißner-Institute (E23), Technical University of Munich and BAdW
17. 10. 2023 and 24. 10. 2023
13. **Loophole-free Bell inequality violation with superconducting circuits**
Otto Graf, Technical University of Munich
28.11.2023
14. **Single-electron spin resonance detection by microwave photon counting**
Alexander Dolpp, Technical University of Munich
19.12.2023

C. Topical Seminar: Topical Issues in Magneto- and Spin Electronics

WS 2022/2023:

1. **Spin memories based on Paramagnetic Ensembles in Silicon**
   Patricia Oehrl, Technical University of Munich and WMI
   30.11.22
2. **Back-action evasion in Optomechanics: Concepts and Implementations**
   Korbinian Rubenbauer, Technical University of Munich and WMI
   07.12.2022
3. **Unidirectional Spin Waves in Nanoscale Magnetic Gratings**
   Christian Mang, Technical University of Munich and WMI
   21.12.2022
4. **Electron Spin Resonance on Donor Spins in Isotopically Engineered Silicon**
   Niklas Vart, Technical University of Munich
   11.01.2023
5. **Donor Spins in Silicon Under Pressure**
   David Vogl, Technical University of Munich
   18.01.2023
6. **Donor Spins in Silicon Under Pressure - The Real Deal**
   Basak Özcan, Technical University of Munich
   25.01.2023
7. **ESR using Superconducting Reflection Resonators**
   Julian Franz, Technical University of Munich and WMI
   01.02.2023
8. **Spin-Dependent Polaron-Hopping in BiVO**
   Sven Doll, Technical University of Munich
   08.02.2023

SS 2023:

9. **Magnetic Resonance Primer**
   Martin Brandt, Technical University of Munich
   03.05.2023
10. **Historic notes on the electronic g-factor**
    Martin Brandt, Technical University of Munich
    10.05.2023
11. **A bird's eye view on spin-electric effects**
    Matthias Althammer, Technical University of Munich
    17.05.2023
12. **The ST1 center in diamond as an alternative to NV - part I**
    Jonas Wieber, Technical University of Munich
    24.05.2023
13. **The ST1 center in diamond as an alternative to NV - part II**
    Magnus Palenta, Technical University of Munich
    24.05.2023
14. **Qubit memory with a coherence time of 39 minutes - part I**
    Melina Pees, Technical University of Munich
    31.05.2023
15. **Qubit memory with a coherence time of 39 minutes - part II**
    Niklas Vart, Technical University of Munich
    31.05.2023
16. **Quantum "supremacy"**
    Michael Göldl, Technical University of Munich
    07.06.2023
17. **Single electron-spin-resonance detection by microwave photon counting**

Yannick Schoehs, Technical University of Munich
14.06.2023

18. **Spin-Wave Diode and Circulator Based on Unidirectional Coupling**
Ankita Najak, Technical University of Munich
28.06.2023
19. **Entanglement of two NV centers**
Nora Braitsch, Technical University of Munich
05.07.2023
20. **An optically addressable qubit in silicon**
Henry Stock, Technical University of Munich
12.07.2023

C. Topical Seminar: Novel Topics in Magnetism: Quantum Hybrid Systems, Spin Dynamics, and Angular Momentum Transport

WS 2023/2024:

1. **Broadband Electron Spin Resonance Spectroscopy of Rare Earth Spin Ensembles at mK Temperatures**
Ana Strinic, Technical University of Munich and WMI
16.11.2023
2. **Chiral Phonons and Phononic Birefringence**
Manuel Müller, Technical University of Munich and WMI
30.11.2023
3. **Magnetoelastic Coupling in Magnetic Thin Film / Crystalline Substrate Heterostructures**
Johannes Weber, Technical University of Munich and WMI
30.11.2023
4. **Tilted Spin Current Generated by the Collinear Antiferromagnet Ruthenium Dioxide**
Tobias Herrlich, Technical University of Munich
14.12.2023
5. **Superconducting Transmission Lines Coupled to Paramagnetic Spin Ensembles**
Georg Mair, Technical University of Munich and WMI
11.01.2024
6. **Zeeman and Hyperfine Interactions of a Single 167Er^{3+} Ion in Si**
Leevi Lehto, Technical University of Munich
18.01.2024
7. **Advances in the Growth of Magnetic Thin Films**
Monika Scheufele, Technical University of Munich and WMI
25.01.2024
8. **Engineering Phonon-Magnon Coupling by Suspended Structures**
Matthias Grammer, Technical University of Munich and WMI
01.02.2024
9. **Micromagnetic SImulations of Spinwave Propagation in Periodic Thin Film Structures**
Markus Kügle, Technical University of Munich and WMI
08.02.2024

D. Topical Seminar on Superconducting Quantum Circuits

WS 2022/23:

merged with **Topical Seminar on Advances in Solid State Physics**.

SS 2023:

1. **Preliminary discussion and assignment of topics**
F. Deppe, A. Marx, S. Filipp, R. Gross, Walther-Meissner-Institute (E23), Technical University of

Munich and BAdW
18. 04. 2023 and 25. 04. 2023

2. **Random-Access Quantum Memory Using Chirped Pulse Phase Encoding**
   Rafael Dias, Technical University of Munich
   13.06.2023
3. **Suppressing quantum errors by scaling a surface code logical qubit**
   Karolina Weber, Technical University of Munich
   20.06.2023
4. **Microwave quantum local area network**
   Michael Renger, Walther-Meißner-Institut, BAdW
   27.06.2023
5. **Chiral cavity quantum electrodynamics**
   Muhammad Usama Akbar, Technical University of Munich
   11.07.2023
6. **Quantum computing with superconducting qubits in a commercial environment**
   Dr. Frank Deppe, Walther-Meißner-Institut, BAdW, and IQM Germany
   18.07.2023

WS 2023/24:

7. **Preliminary discussion and assignment of topics**
   M. Werninghaus, S. Filipp, R. Gross, Walther-Meissner-Institute, Technical University of Munich (E23) and BAdW
   17. 10. 2023 and 24. 10. 2023
8. **Building Blocks of a Flip-Chip Integrated Superconducting Quantum Processor**
   Agatha Skoczylas, Technical University of Munich and WMI
   28.11.2023
9. **Mechanically Induced Correlated Errors on Superconducting Qubits with Relaxation Times Exceeding 0.4 Milliseconds**
   Apollon Marango, Technical University of Munich
   12.12.2023
10. **Lunch seminar** on **Travelling wave parametric amplification**
    Daniil Bazulin, Walther-Meissner-Institute
11. **Real-time quantum error correction beyond break-even**
    Ludwig Martlmueller, Technical University of Munich
    09.01.2024
12. **Dissipative stabilization of dark quantum dimers via squeezed vacuum**
    Juan Soriano, Technical University of Munich
    16.01.2024
13. **Control and readout of a superconducting qubit using a photonic link**
    Darius Haitsch, Technical University of Munich
    23.01.2024

E. Solid State Colloquium

The WMI has organized the Solid-State Colloquium of the Faculty of Physics in WS 2022/2023, SS 2023, and WS 2023/2024. The detailed program can be found on the WMI webpage: www.wmi.badw.de/teaching/colloquium-on-solid-state-physics.

Staff

Staff of the Walther-Meißner-Institute

ScientificDirectors
Prof. Dr. Stefan Filipp (managing director)
Prof. Dr. Peter Rabl
Prof. Dr. Rudolf Gross

Technical Director
Dr. Achim Marx

The technical director and the elected representative of the scientific staff (Dr. Matthias Opel) are members of the WMI Executive Committee and support the scientific directors in the management of the WMI.

Administration/Secretary's Office
Andrea Person
Carola Siegmayer
Dong Li
Emel Dönertas
Martina Meven

Scientific Staff
Priv.-Doz. Dr. Matthias Althammer
Priv.-Doz. Dr. Frank Deppe
Prof. Dr. Andreas Erb
Priv.-Doz. Dr. Kirill Fedorov
Dr. Noelia Fernandez
Dr. Louis Garbe
Dr. Stephan Geprägs
Priv.-Doz. Dr. Hans Huebl
Dr. Mark Kartsovnik
Dr. Gleb Krylov
Dr. Nadezhda Kukharchyk
Dr. Klaus Liegener
Dr. Jacquelin Luneau
Dr. Matthias Opel
Dr. Christian Schneider
Dr. Lasse Södergren
Dr. Max Werninghaus
Dr. Xin Zhan
M. Sc. Christopher Trummer
M. Sc. Agustí
M. Sc. Nicolas Arlt
M. Sc. Syeda Aliya Batool
M. Sc. Daniil Bazulin
M. Sc. Niklas Bruckmoser
M. Sc. David Bunch
M. Sc. Jianpeng Chen
M. Sc. Shamil Erkenov
M. Sc. Florian Fesquet
M. Sc. Simon Gandorfer
M. Sc. Niklas Glaser
M. Sc. Matthias Grammer
M. Sc. Janine Gückelhorn
M. Sc. Maria-Teresa Handschuh
M. Sc. Kedar Honasoge
M. Sc. Gerhard Huber
M. Sc. Kevin Kiener
M. Sc. Martin Knudsen
M. Sc. Leon Koch
M. Sc. Fabian Kronowetter
M. Sc. Thomas Luschmann
M. Sc. Georg Mair
M. Sc. Adrian Misselwitz
M. Sc. Manuel Müller
M. Sc. Yuki Nojiri
M. Sc. Patricia Oehrl
M. Sc. Frederik Pfeiffer
M. Sc. Michael Renger
M. Sc. Lea Richard
M. Sc. João Henrique Romeiro Alves
M. Sc. Federico Roy

M. Sc. Korbinian Rubenbauer
M. Sc. Monika Scheufele
M. Sc. Johannes Schirk
M. Sc. Malay Singh
M. Sc. Ana Strinic
M. Sc. Ivan Tsitsilin
M. Sc. Lucia Valor
M. Sc. Florian Wallner
M. Sc. Johannes Weber
M. Sc. Emily Wright
M. Sc. Wun Kwan Yam
M. Sc. Przemyslaw Zielinski

Technical Staff

Peter Binkert
M. Sc. Thomas Brenninger,
Julia Gollasch
Dieter Guratzsch
Astrid Habel
Dipl.-Ing. (FH) Josef Höß
Sebastian Kammerer
Jan Naundorf
Georg Nitschke
Mario Nodes
Christian Reichlmeier
Alexander Rößl
Andreas Russo
Harald Schwaiger

Assistants

Sybilla Plöderl
Maria Botta

Guest Researchers

The Walther-Meißner-Institute welcomes a significant number of guests every year to strengthen international collaborations and intensify scientific exchange with leading places internationally. Unfortunately, also in 2023 the number of guests was disappointingly reminiscent of the Covid-19 pandemic.

1. Dr. Werner Biberacher
   permanent guest
2. Prof. Dr. Dietrich Einzel
   permanent guest
3. Dr. Kurt Uhlig
   permanent guest
4. Georg Mair, 3. Physikalisches Institut, University of Stuttgart, Stuttgart, Germany,
   06. 11. – 16. 11. 2023
5. Pablo Garcia, University of the Basque Country, Bilbao, Spain
   8. 10. -19. 11. 2023
6. Dr. Makariy A. Tanatar, Ames National Laboratory, Iowa State University, Ames, Iowa, USA
   17.09. - 22.09.2023

Scientific Advisory Board & Executive Committee

Scientific Advisory Board

According to the statutes of the Bavarian Academy of Sciences and Humanities (BAdW) the Scientific Advisory Board evaluates the quality of the scientific work of Walther-Meißner-Institute (WMI) and gives advice to its Executive Committee to provide scientific quality assurance. The Scientific Advisory Board regularly reports to the Research Committee of the BAdW.

The members of the Scientific Advisory Board include members of BAdW with appropriate scientific background, representatives of the two Munich universities (TUM and LMU), as well as leading national and international scientists. They are appointed by the Section III "Naturwissenschaften, Mathematik, Technikwissenschaften" of BAdW for five years. The scientific directors of WMI are consultive members of the WMI Scientific Advisory Board. The Scientific Advisory Board is headed by a chairperson and deputy chairperson. They are elected by the Section III "Naturwissenschaften, Mathematik, Technikwissenschaften" of BAdW for five years at the suggestion of the members of the WMI Scientific Advisory Board. The chairperson of the Scientific Advisory Board must be a member of BAdW.

The present members of the WMI Scientific Advisory Board are:

- **Vollhardt, Dieter**, chairman (BAdW, University of Augsburg)
- **Bloch, Immanuel**, deputy chairman (BAdW, LMU Munich and Max-Planck-Institute of Quantum Optics)

- **Abstreiter, Gerhard** (BAdW, Technical University of Munich)
- **Bühler-Paschen, Silke** (Technical University of Vienna)
- **Filipp, Stefan**, consultive member (Technical University of Munich)
- **Finley, Jonathan** (Technical University of Munich)
- **Gross, Rudolf**, consultive member (BAdW and Technical University of Munich)
- **Hänsch, Theodor** (BAdW, LMU Munich and Max-Planck-Institute of Quantum Optics)
- **Hartmann, Michael** (FAU Erlangen-Nuremberg)
- **Molenkamp, Laurens** (BAdW and University of Würzburg)
- **Rabl, Peter**, consultive member (Technical University of Munich)
- **Wallraff, Andreas** (ETH Zurich)
- **Weiss, Dieter** (University of Regensburg)

Executive Committee

The Walther-Meißner-Institute is headed by the board of scientific directors which is responsible for the development and implementation of the research program. The scientific directors hold a full professor position at one of the Munich universities (TUM or LMU). They are appointed in a joint process of the respective university and BAdW. The scientific directors are supported by the deputy director, the technical director and an elected representative of the scientific staff. They are appointed by the Section III "Naturwissenschaften, Mathematik, Technikwissenschaften" of BAdW for five years at the suggestion of the members of the WMI Scientific Advisory Board.

The present members of the WMI Executive Committee are:

- **Filipp, Stefan**, scientific director (managing director)
- **Gross, Rudolf**, scientific director
- **Rabl, Peter**, scientific director
- **Hübl, Hans**, deputy director
- **Marx, Achim**, technical director
- **Opel, Matthias**, representative of the scientific staff

Contact:

Walther–Meißner–Institut
Bayerische Akademie der Wissenschaften
Walther–Meißner–Str. 8
D - 85748 Garching
GERMANY

Phone: +49 – (0)89 289 14202
Fax: +49 – (0)89 289 14206
E–mail: Sekretariat@wmi.badw.de

www.wmi.badw.de

Published by:

Walther–Meißner–Institut
Walther–Meißner–Str. 8, D - 85748 Garching
December 2023

Walther-Meißner-Institut
DER BAYERISCHEN AKADEMIE DER WISSENSCHAFTEN